Fluorescent Detection of Chiral Amino Acids: A Micelle Approach

Gengyu Du

Yilong, Sichuan, China

B.S. in Chemistry

University of Science and Technology of China, Hefei, China, 2015

A Dissertation presented to the Graduate Faculty

of the University of Virginia in Candidacy for the Degree of

Doctor of Philosophy

Department of Chemistry

University of Virginia

April 2020

_____

_____

_____

_____

Abstract

Fluorescent Detection of Chiral Amino Acids: A Micelle Approach

1,1'-Bi-2-naphthol (BINOL)-based fluorescent probes have been developed as powerful tools for the molecular recognition of many chiral molecules. High sensitivity and enantioselectivity for chiral amino acids have been achieved in organic media, but the recognition in water media has been limited by their poor solubility in aqueous solution.

By using a diblock copolymer PEG-PLLA, 3,3'-diformyl-BINOL was encapsulated into micelles to form a micelle probe. It allowed the detection of chiral lysine (Lys) both *chemoselectively* and *enantioselectively* in carbonate buffer solution. A limit of detection (LOD) of 848 nM and 2nd order fit of ee detection was obtained for D-Lys. The chemoselectivity was attributed to the selective reaction of Lys's terminal amino groups with the probe.

Series of monoformyl-BINOL with varying substituents were synthesized and engineered into micelle probes. These probes achieved specific detection of chiral tryptophan (Trp) both enantioselectively and chemoselectively in carbonate buffer solution, with LOD of 2.6 μM and 1st order fit of ee detection.

A non-C_2 symmetric molecule, 3,3'-diformyl-tetrahydro-BINOL, was fabricated into a micelle probe. It achieved specific detection of chiral His both enantioselectively and chemoselectively in carbonate buffer solution, with LOD of 107 nM and 2nd order fit of ee detection.

Several copolymers were screened to form various micelle probes with the same 3,3'-diformyl-BINOL core. Among these copolymer-based micelles, the probe made of a triblock copolymer F68 achieved specific detection of chiral Trp both enantioselectively and

chemoselectively in carbonate buffer solution, with LOD of 962 nM and 3rd order fit of ee detection.

This work demonstrates that the micelles made of the block polymers not only allow the use of water insoluble probes for fluorescent detection of amino acids in aqueous solution, but also provide unique microenvironments to tune and enhance the sensitivity and selectivity of these probes in fluorescent recognition. It provides a new strategy for the development of chemoselective as well as enantioselective fluorescent probes for various applications.

Acknowledgements

For the years studying at the beautiful UVA, there are many people that need to be thanked. The kindness and knowledge of my advisor, the chemistry department, and Charlottesville have made it a home to me.

Professor Lin Pu is my adviser, and provided numerous guides on my study. He always came up with plans to deal with puzzles and helped me overcome research difficulties. Lin set himself as a very good example as a hardworking person by maintaining constant office hours and keeping contacted at late nights.

At the first year, Professor Brent Gunnoe taught me inorganic chemistry. Brent intended to introduce many transition metal complexes through molecular orbital theory. As a humorous and nice person, Brent encouraged students to learn via providing an open atmosphere in his classes.

Professor Fraser Cassandra, professor David Cafiso and professor Kelly Dryden have provided lots of help on materials and instruments. Without their help, the studies won't be able to be finished. Professor Ian Harrison and professor Jiang He are thanked for serving as committee members.

Current members and alumni of the Pu lab are greatly appreciated. Dr. Wei Chen, Dr. Jun Ying are particularly mentioned because of their training and guidance both inside and outside the lab. Dr. Shifeng Nian, Dr. Chaoyuan Zeng, Feng Zhao, Yifan Mao are also thanked for in-lab collaborations.

I would also like to thank my collaborators from the Zhang lab, where I've worked with Dr. Xiao Wang, Chang Liu, Yulu Zhang and Dr. Zhiyong Zhang.

Professor Kevin Welch and Dr. Chuck Arrington have been helping on my teaching for years. Their philosophy of teaching is very inspiring.

My friends at the chemistry department have provided abundant information needed for my research and beyond. Dr. Jeff Ellena, Dr. Junqi Chen, Xiaofan Jia, Qian Liang, and Michael Birckhead have provided many different kinds of help.

I am grateful for my wife and family for their support. They help me overcome my own weakness and failures through forgiveness, joy and love.

Table of Contents

List of Figures

List of Schemes

Chapter 1. Introduction to Chiral Recognition of Chiral Molecules

1.1. Importance of Chirality

Chirality is a type of asymmetry that exists in many molecules and ions in nature.[1] The word *chirality* is derived from the Greek word χειρ, meaning *hand*, a simple chiral example where left hand cannot match the right hand. For molecular level, a molecule is chiral when it cannot superpose onto its mirror image. The relationship between such a molecule and its mirror image is called enantiomer. Enantiomers of a chiral molecule have identical physical properties such as solubility, melting temperature, color, et al. And they have the same chemical properties only when they are not treated with chiral reactants.

Amino acids are the fundamental building blocks of peptides and enzymes.[2] In the biological systems, amino acids exist almost exclusively in the left-handed form (L-amino acids).[3] The chirality nature is succeeded from amino acids to proteins. Since enzymes catalyze reactions, they enforce homochirality on a great variety of other chemicals, including hormones, toxins, fragrances and food flavors.[4] When the proteins interact with chiral molecules, the matched and mismatched results will differ. (*S,S)*-Ethambutol is a medication primarily used to treat tuberculosis, which is still prevalent in Southeast Asia. On the other hand, (*R,R)*-ethambutol is reported to cause permanent visual loss.[5,6] Another famous case is the thalidomide disaster caused by the misuse of thalidomide.[7] The (*R*)-enantiomer has

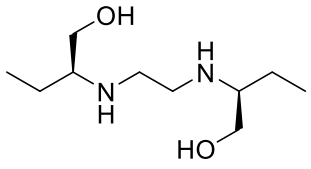

(2S,2'S)-Ethambutol

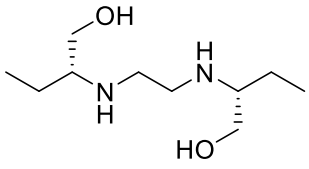

(2R,2'R)-Ethambutol

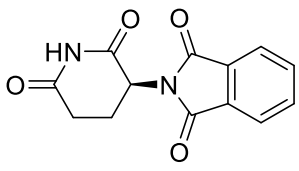

(*S*)-Thalidomide

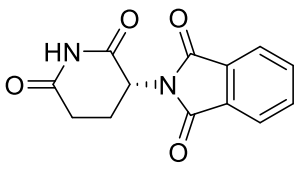

(R)-Thalidomide

sedative effects, whereas the (*S*)-isomer is teratogenic. The drug was marketed as a mild sleeping pill safe for pregnant women. However, it caused more than 10,000 children in 46 countries were born with deformities. Of these babies, about 40% of them did not survive till their first birthday.[8]

Except its importance in pharmaceutical industries, chirality is also important in many other fields such as agriculture and material science. A recent study covered 1693 pesticides, where 30% of 1594 organic pesticides are chiral. The stereoisomers of pesticides can have widely different efficacy, toxicity to nontarget organisms, and metabolic rates in biota.[9] Chiral polymers also possess remarkable properties than regular polymers.[10]

1.2 Traditional Techniques to Determine Chiral Molecules

Enantiomeric excess (ee) is a ratio to quantify relative amount of two enantiomers in a mixture. It is described as, ee = ([*R*]-[*S*])/([*R*]+[*S*]), where [R] and [S] are the respective fraction of two enantiomers in a mixture; or ee = 100 × $[(c_R-c_S)/(c_R+c_S)]$, where c_R and c_S are the concentrations of R- and S-enantiomer. Similarly, enantioselective factor (ef) is the factor to describe how a method favors one enantiomer over the other.

Traditional techniques in detection of chiral molecules includes high-performance liquid chromatography (HPLC)[11], gas chromatography (GC)[12], capillary electrophoresis (CE)[13,14], and nuclear magnetic resonance (NMR)[15]. Despite their abilities to differentiate enantiomers of analytes, those techniques still have drawbacks such as relatively long time for sample preparation, and sophisticated instrumentation. Recently circular dichroism (CD) has been utilized as a powerful tool to detect chiral molecules[16]. But the use is limited by its high cost.

1.3. Fluorescent Method to Detect Chiral Molecules

Optic techniques, especially fluorescence techniques, have received massive attention from current researchers. It advantages in high sensitivity, simple instrumentations, and the possibility

for *in vivo* studies.[17–21] Although biologists were desperate 20 years ago because of the extreme lack of sensors,[22] there is a vast amount of sensors for biologically active molecules nowadays, ranging from inorganic ions[23], organic small molecules[24], and double-stain DNAs[25]. Particularly, during the combat of COVID-19, the most important thing is to accurately detect infected people at early stages. A common strategy used by many labs is to employ a cyanine dye SYBR Green I after polymerase chain reaction (PCR) process to indicate the existence of SARS-COV-2.[26]

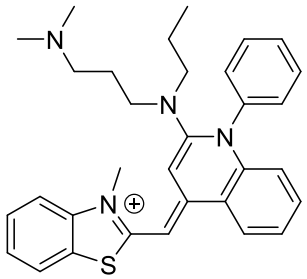

SYBR Green I

Given the large numbers of sensors, very limited of them contains chiral backbones and can be used for the detection of chiral molecules. In the following content, the development of enantioselective fluorescent sensors for biologically important chiral molecules will be briefly described.

1.3.1 Chiral Recognition

Chiral recognition is a chemical interaction, frequently occurring in living systems, by which a given chiral molecule (receptor/host) recognizes a particular stereoisomer (substrate/guest).[27] The term was initially introduced by Donald J. Cram.[28,29] (*S*)-BINOL was used as chiral backbones for chiral crown esters. These chiral crown ethers were complexed with chiral α-phenylethylamine. (*S*,*S*)-**1.3** selected (*R*)-α-phenylethylamine over (*S*)-α-phenylethylamine, with a calculated energy difference of ~266 cal/mol. But we need to notice that Cram did not make use of any fluorescent properties, and his purpose was limited to the optical resolution.

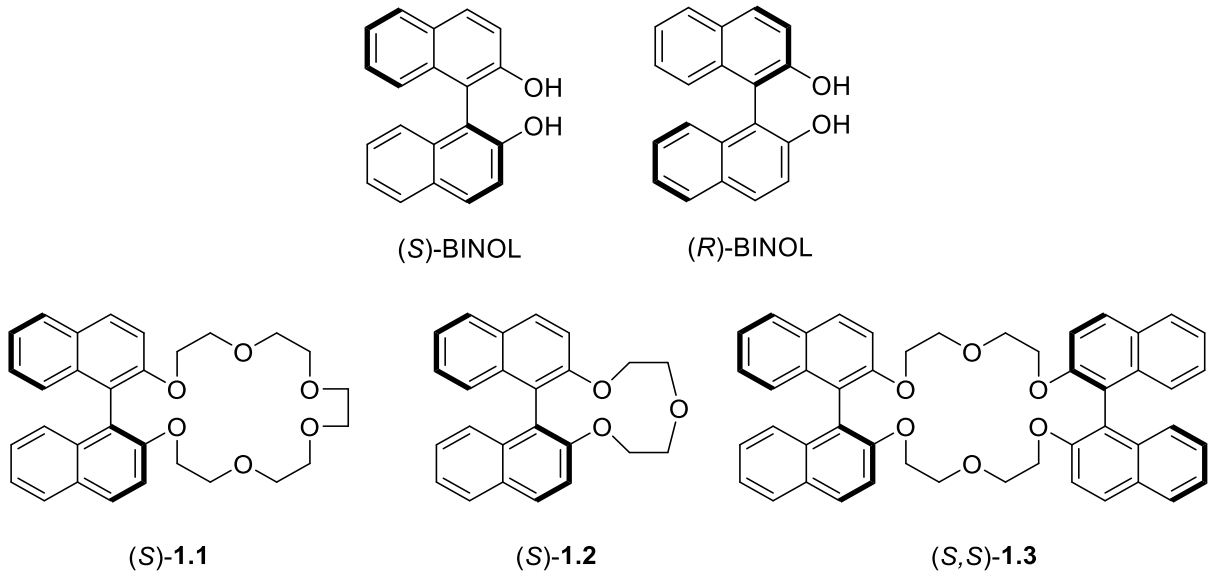

Figure 1. 1 Structures of BINOL and Cram's chiral crown ethers

1.3.2. BINOL-based Fluorescent Probes for Non-Amino Acids Analytes

BINOL compounds are versatile fluorophores and have been actively used as backbones of enantioselective fluorescent probes. It has intrinsic merits including C_2 axial chirality, rigid structure, high energy barrier of racemization, and easily-tuned chemistry. In 1992, Iwanek and coworks reported that the fluorescence of BINOL can be enantioselectively quenched by chiral amines.[30] Later on, numerous probes have been developed on the BINOL core utilizing its amazing structures and properties. The Pu lab pioneered and had done extensive studies to use BINOL in the field of chiral recognition.

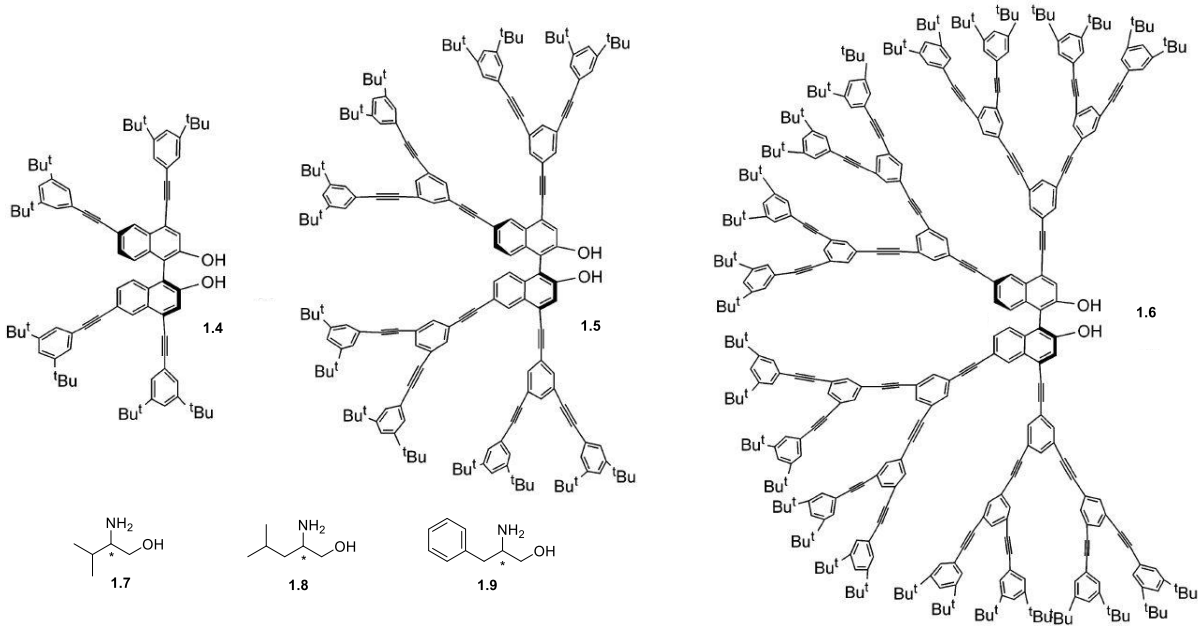

Figure 1. 2 Structures of Pugh's dendrimers and the analytes

In 2000 and 2001, Pugh and coworkers reported BINOL-based dendrimers probes for the chiral recognition of chiral amino alcohols.[31,32] The dendritic materials were believed to facilitate the energy migration from the dendrons to the BINOL core and thus greatly enhanced the fluorescence intensities. The probe **1.6** had about 170 times stronger intensity than simple BINOL cores, and the extremely strong fluorescence signal was enantioselectively quenched by the enantiomers of chiral amino alcohols **1.7-1.9**. The studies were carried out with probe concentrations of 40 nM in organic solvents (bezene:hexane = 20:80). As early studies, those work had drawbacks such as short excitation wavelength at 280 nm, and high analytes loading of mM-scale.

In 2002, Lin and coworkers reported a bisBINOL probe (*S,S*)-**1.10** that could be used for the chiral recognition of mandelic acid **1.11**. The probe was designed with an alkyl amine that quenched the fluorescence of the BINOL core facilitated by the lone pair electrons of the nitrogen atom. After interaction with mandelic acids, three hydrogen bonding between the probe and

analyte were proposed to turn on the fluorescence. This study was carried out with a probe concentration of 95 μM in organic solvents (benzene:dimethoxyethlene = 98:2). The ef value was reported to be 2.49. This strategy of designing this OFF-ON fluorescent probe was succeeded by more other works which we will discuss later.

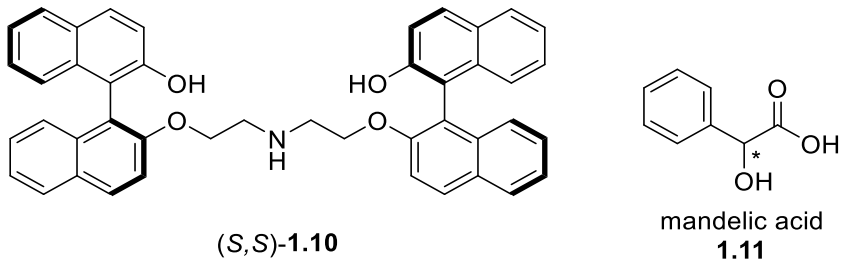

Figure 1. 3 Structures of Lin's bisBINOL probe and the analytes

Similar to their previous work, in 2004, Lin and coworkers reported the use of chiral bisbinaphthyl macrocycle **1.12** for the enantioselective fluorescent recognition of α-amino acid derivatives.[33] The probe **1.12** itself has limited fluorescence intensity. The fluorescence quenching is believed to be due to excited state proton transfer. Carboxylic acid analytes were added to interrupt such a transfer and restored the fluorescence of BINOL systems. Amino acid derivatives (**1.13-1.19**) were studied with probe concentration of 0.1 mM in organic solvents (benzene:dimethoxyethane = 98:2). The ef values are as follows, 5.7 for phenylglycine derivative **1.13**, 2.2 for tryptophan derivative **1.15**, and less than 2 for other analytes.

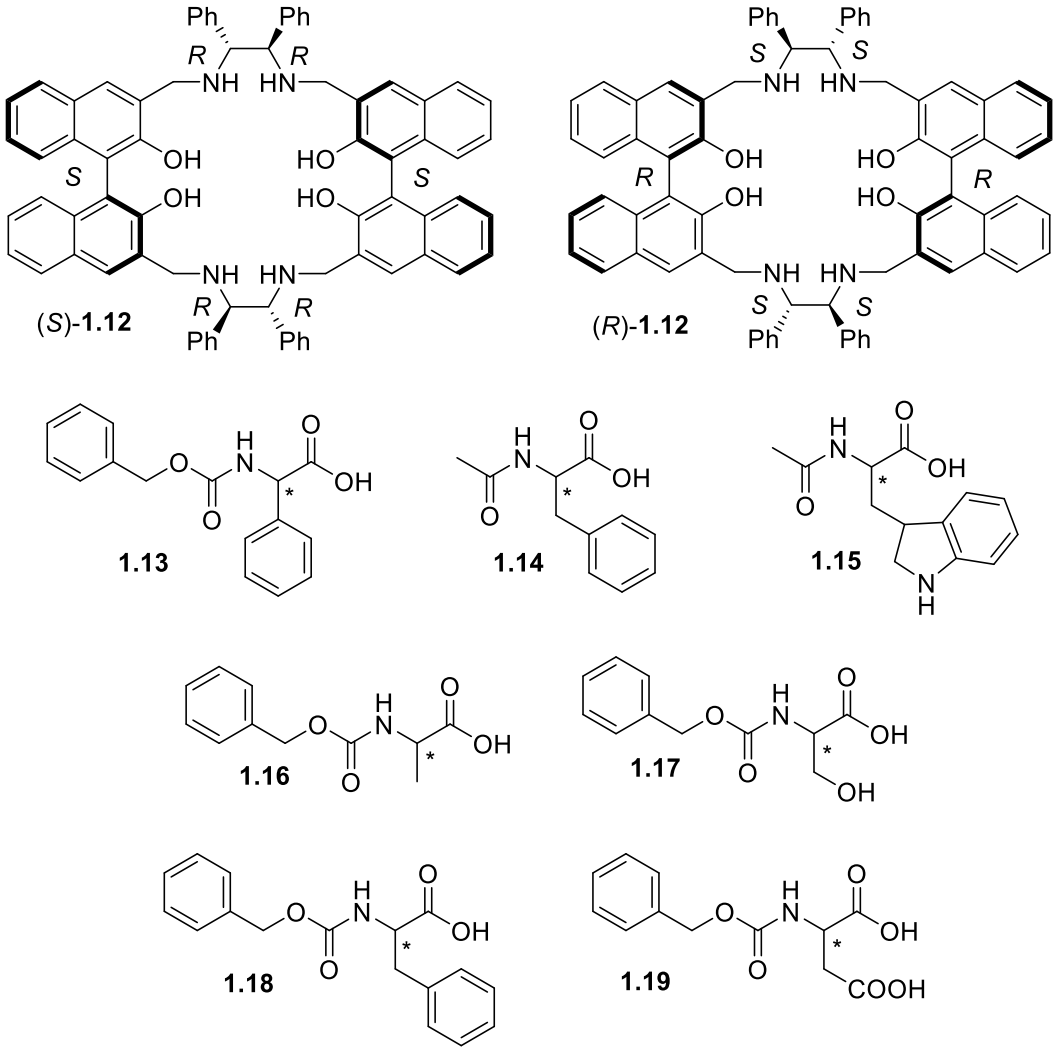

Figure 1. 4 Structures of Lin's bisBINOL macrocycles and the analytes

Similarly, He and coworkers reported the use of molecule **1.20** and **1.21** as fluorescent sensors for N-t-butyloxycarbonyl (N-Boc) amino acids derivatives.[34] The first S- tells the configuration of BINOL, and the latter S- is used to indicate the chirality of the chiral carbons on the 3,3'-postions' sidechains. They had previously use **1.20** and **1.21** in asymmetric catalysis, and studied these molecules as potential probes inspired by the last case mentioned above. The study was conducted in organic solvents (dichloromethane:hexane = 3:7, with 1.2% THF). The ef values are as summarized follows, 10.4 for N-Boc proline **1.22** with probe (*R*,*S*)-**1.20** concentration of 20

mM, 7.9 for N-Boc valine **1.23** with probe (*R*,*S*)-**1.20** concentration of 5 mM, and less than 4 for three other protected amino acids.

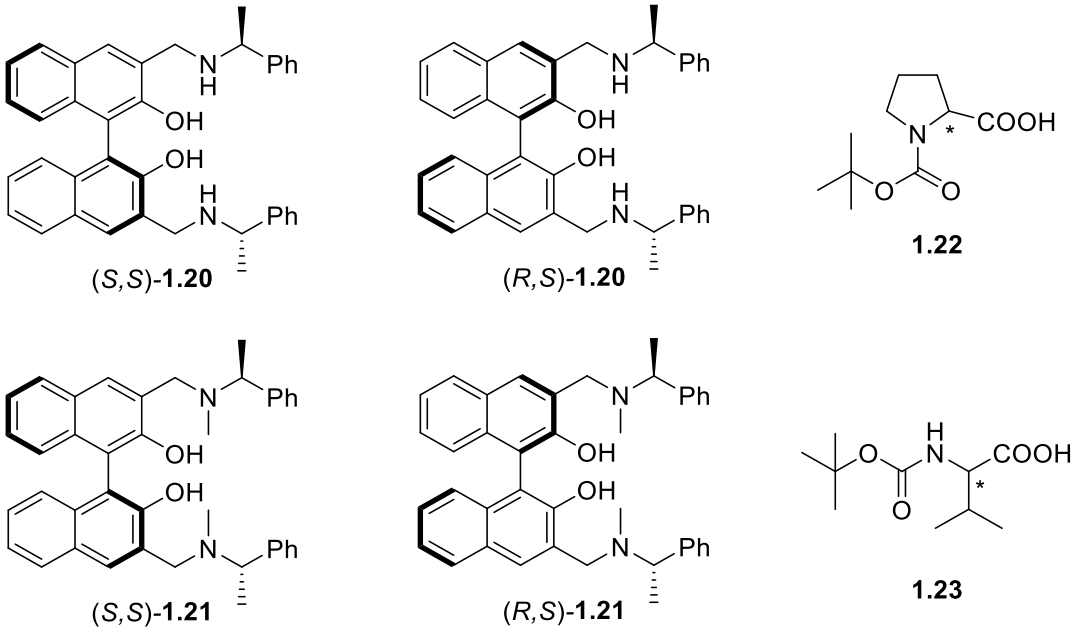

Figure 1. 5 Structures of He's probes and the analytes

Li carefully studied the structures, and found that the acyclic molecule (*S*)-**1.24** could also have fluorescent enhancement but no enantioselectivity for enantiomers of mandelic acid.[35] (*S*)-**1.25** was synthesized as a cyclic analogue that only contained half of the functional groups of (*S*)-**1.12**. Despite its autofluorescence, (*S*)-**1.25** exhibited enantioselective recognition for mandelic acid. This studies was carried out with probe concentration of 100 μM in organic solvents (benzene:dimethoxyethane = 2500:1). The ef was found to be 4, the emission used for recognition was at λ = 370nm.

Later on, Li synthesized more bisBINOL macrocycle based on **1.12**, but with more conjugation on the 6,6'-positions of BINOL.[36] Those new probe (*S*)-**1.26**, (*S*)-**1.27** benefited from extended conjugation and exhibited enhanced fluorescence intensities themselves. This phenomenon allowed lower dose of probe at 2 μM in organic solvents

(dichloromethane:dimethoxyethane = 250:1). The ef value were 2 for both probes. The emission was at redshifted to λ = 400 nm.

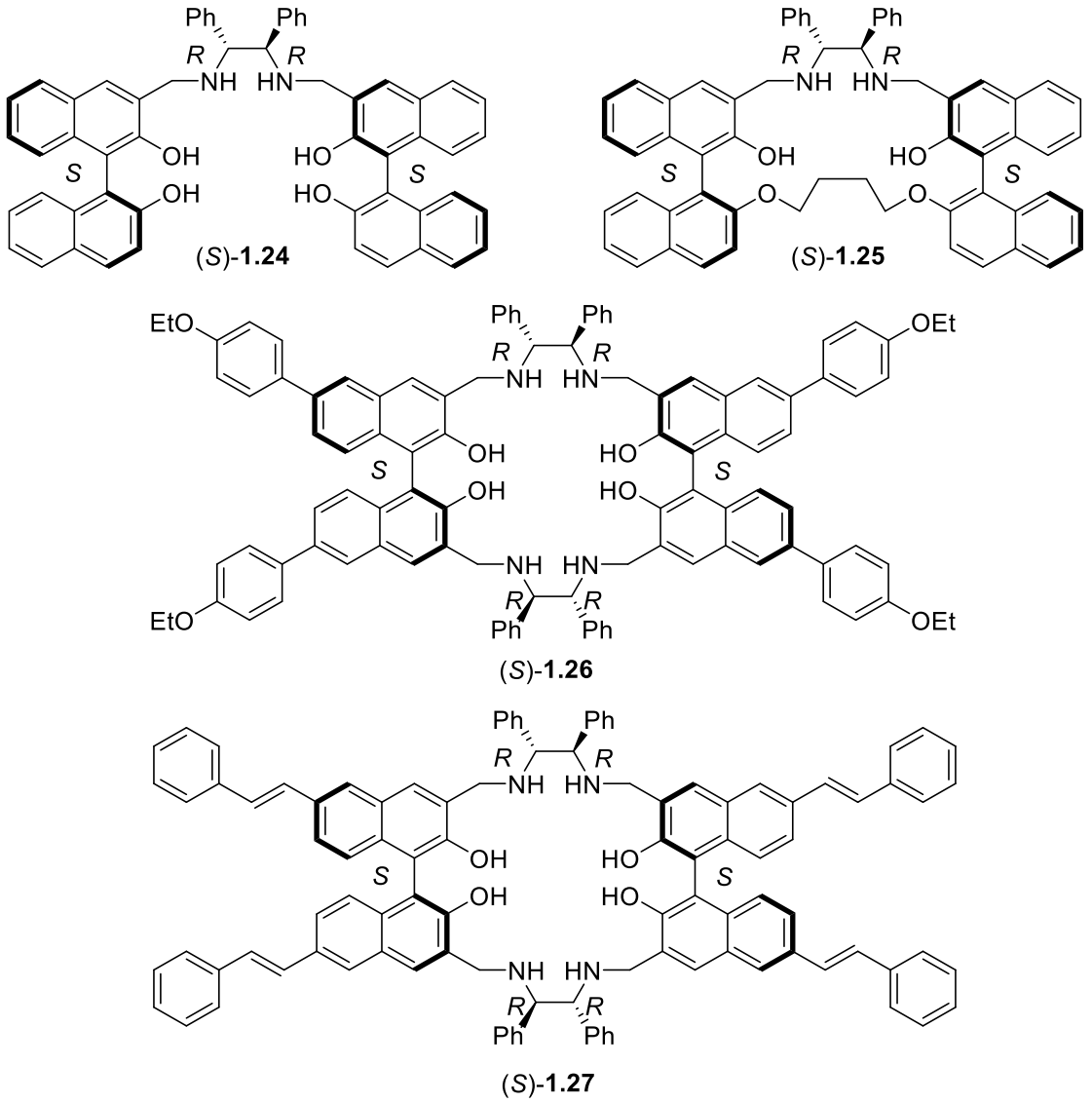

Figure 1. 6 Structures of Li's probes

In 2005, Li and coworkers synthesized a new bisBINOL-based macrocycle **1.28**.[37] They replaced the phenyl substituents into cyclohexane substituents. Unlike the previous macrocycle **1.12**, **1.28** was found to be difficult to purify and always contains 5% impurities. Even though, (*S*)-**1.28** was extremely enantioselective for (*S*)-mandelic acid. The study was carried out with probe

concentration of 10 μM in organic solvents (benzene:dimethoxyethane = 2000:1). The ef value was reported to be 46 and the emission wavelength was at λ = 370 nm.

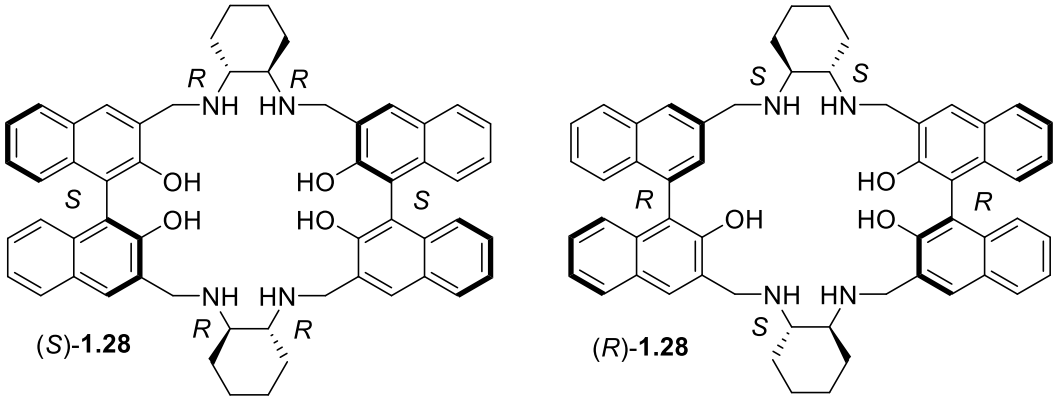

Figure 1. 7 Structures of Li's new macrocycle probes

. In 2010, Yu and her coworkers reported the use of two probes at the same time, to detect both the concentration and enantiomeric composition of mandelic acids.[38] The pseudoenantiomeric pairs (*S*)-**1.29** and (*R*)-**1.30** were mixed together, and used. They have opposite configurations on chiral centers, but (*S*)-**1.29** had a BINOL backbone, while (*R*)-**1.30** contained a partially reduced H_8-BINOL core. Upon interaction with mandelic acid, (*S*)-**1.29** showed the same enantioselective emission at λ = 374 nm as we stated earlier for other probes. (*R*)-**1.30** also exhibited enantioselective emission for mandelic acids at λ = 330 nm, but to a different extent. By combing the data of the two emissions, Yu made a 3D plot of the intensities vs concentration and percentage of (*R*)-mandelic acid. This study was carried out with probe concentration of 100 μM in dichloromethane. Another notable progress they did was the simplicity and lower toxicity of the solvent, from nearly 100% benzene to dichloromethane.

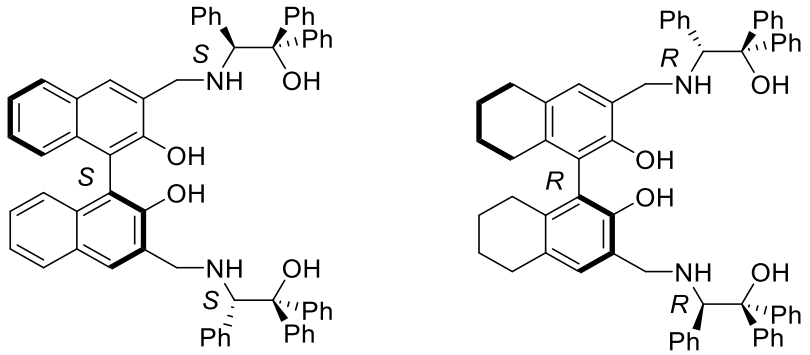

(*S*)-**1.29** (*R*)-**1.30**

Figure 1. 8 Structures of Yu's pseudoenantiomeric pairs

In 2012, Yu and her coworkers reported a single probe (*S*)-**1.31** that could report both concentration and enantiomeric composition of cyclohexyl diamine **1.32**.[39] The synthesis of this probe was much simpler, due to the very simple structures. Because of a possible excited state proton transfer process, this probe again was non-fluorescent. Upon treatments with chiral diamines **1.32**, the fluorescence was turned on. The first emission wavelength at λ_1 = 370 nm was enhanced to approximately the same extent no matter (*R*,*R*)- or (*S*,*S*)-diamine was used. The second emission at λ_2 = 436 nm was enantioselectively enhanced favored the (*R*,*R*)-diamine. The ratio of the I_{370}/I_{436} was independent of concentration but only a function of enantiomeric composition. This interesting phenomenon allowed the accurate detection of a chiral analyte. This study was accomplished with probe concentration of 10 μM in organic solvent dichloromethane.

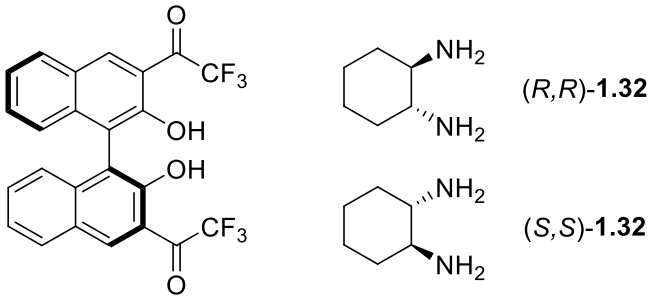

(*S*)-**1.31** (*R*,*R*)-**1.32** (*S*,*S*)-**1.32**

Figure 1. 9 Structures of Yu's ketone probe

In 2015, Wang and his coworkers modified the structures of (*S*)-**1.31**, by elongation of the perfluoroalkyl substituents, and synthesized a new probe (*S*)-**1.33**.[40] The perfluoro chain allowed this probe to be dissolved in perfluoro solvent FC-72. The fluorescence emission at λ = 420 nm could be enantioselectively turned on by (*R*)-**1.34**. The selectivity was proposed to be due to rigid structures of the product with (*R*)-**1.34**, which was evidenced with white insoluble particles forming. This study was finished with probe concentration of 80 μM in dichloromethane:FC-72 = 25:1. Dichloromethane was needed to dissolve analyte **1.34**. This work allowed one step closer for application of probes for asymmetric catalysis, as the perfluoro solvent could extract interesting analyte and exempted the necessity for purification step.

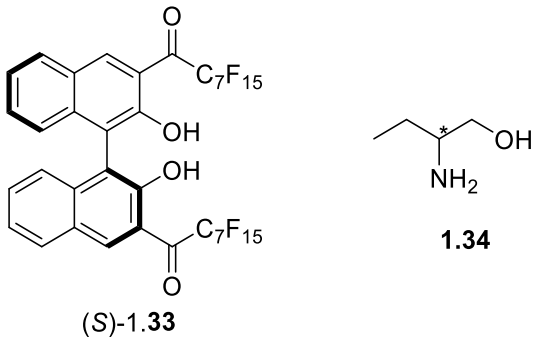

Figure 1. 10 Structures of Wang's ketone probe

1.3.3 BINOL-based Probes for Chiral Amino Acids in Organic Phases

Although BINOL-based probes are very effective for the enantioselective detection of chiral amines and amino alcohols, the detection of free amino acids have been not achieved with probes mentioned above. Previously mentioned probes have three major interaction to detect chiral analytes, these are (i) hydrogen bonding interaction, for simple BINOL and BINOL-based dendrimers; (ii) hydrogen bonding interactions, for macrocycles and chiral amino alcohol-substituted probes aimed for the detection of mandelic acids; (iii) covalent bonding, for perfluoro ketone probes. To detect amino acids, the media will be either water or methanol

(tetrabutylammonium salt is needed). Ion pairs and hydrogen bonding will immediately stumble, as the solvents are much more polar to interrupt these interactions. Perfluoro ketones will also find no use in this area, as they quickly hydrolyzed and lost the probing abilities in these media. To achieve the recognition of amino acids, a novel strategy is needed, besides the solubility issue.

In 2003, Feuster and his coworkers reported a coumarin based probe **1.34**.[41] The aldehyde group on **1.34** could undergo nucleophilic addition and form **1.35**. The hydrogen bonding between the iminium's proton and adjacent ester could effectively turn on the fluorescence signals. In the media of HEPES buffer solution (pH = 7.4), they found 10 μM of **1.34b** could give signals for glycine, aspartate, glutamate, lysine, serine, alanine with 23-45 times stronger emission at λ = 513 nm, a much redshifted signal compared to the probes mentioned earlier.

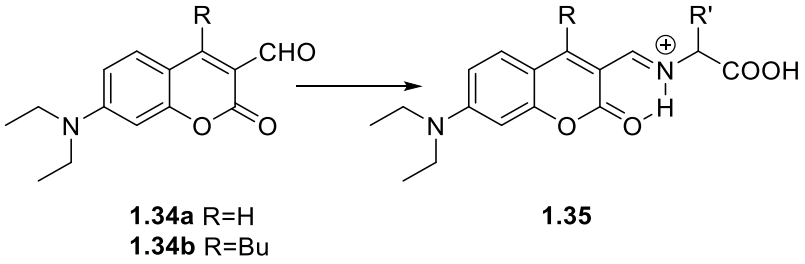

1.34a R=H
1.34b R=Bu

1.35

Figure 1. 11 Structures of Feuster's coumarin probes

Adapted from the aldehyde strategy, Huang and his coworkers investigated (*S*)-**1.36** for the use of a probe in 2014.[42] For a long time, (*S*)-**1.36** had been used as a precursor to construct other asymmetric catalyst or probes, but its ability of probing other molecules had not been explored. With probe concentration of 10 μM in methanol:dichloromethane = 99:1, (*S*)-**1.36** showed dramatically enhanced fluorescence for not only chiral diamines, chiral amino alcohols, but also amino acids with 1 eq. zinc(II) and 10 eq. tetrabutylammonium hydroxide (TBAOH). The emission was at λ = 515 nm for phenylalanine (Phe). This sensor could also be used for the chiral recognition of alanine, histidine, valine, leucine and serine under same conditions. It needs to be

noticed that, (*S*)-**1.36** itself has very limited solubility in methanol, and it needs to be dissolved in dichloromethane and then diluted in methanol for the study. The mechanism was later studied by Song and her coworkers in 2017.[43] Her study highlighted the importance of zinc(II) over other metal ions. Also, mass spectroscopy data and NMR data supported a dimeric structure between zinc(II) and the imine formed between (*S*)-**1.36** with leucenol.

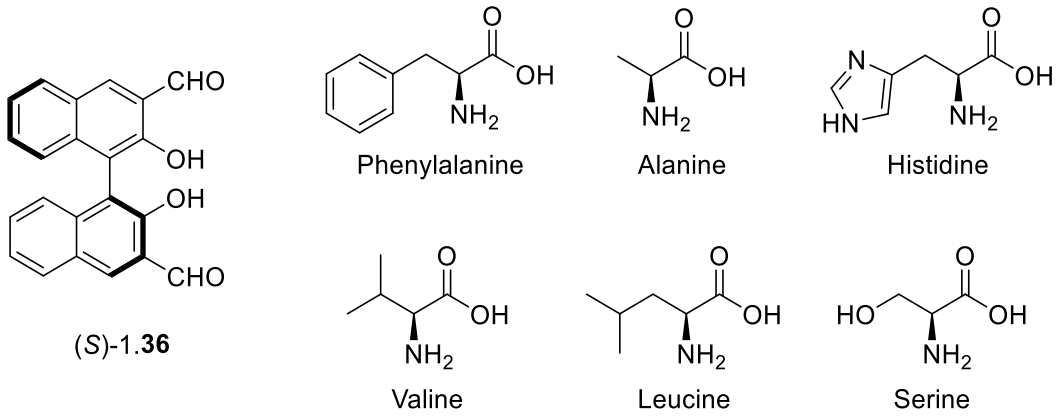

Figure 1. 12 Structures of Huang's diformylBINOL probes

In 2015, Wen and her coworkers synthesized a probe (*S*)-**1.37** for the chiral recognition. (*S*)-**1.37** has nearly no fluorescence, but the fluorescence was turned on after interaction with chiral amines and amino alcohols. The idea was that, chiral amino acids undergo nucleophilic attach on the imine, then displaced the naphthylamine off, and thus formed two fluorophores. The BINOL part fluorophores (*S*)-**1.38** had emission at λ_1 = 509 nm for L-phenylalanine, week fluorescence for D-phenylalanine at λ = 499 nm. By utilizing the fluorescence intensities at 509 nm, the enantiomeric composition of a non-optic pure amino acids could be measured. The naphthylamine had emission at λ_2 = 427 nm, which was only a function of the concentration of amino acids, but not of the enantiomeric composition. That was because both D- and L-amino acids could displace the naphthylamine off from the probe (*S*)-**1.37**. This allowed for direct measurements of the

concentration of amino acids. This study was accomplished with probe concentration of 20 μM, 2eq. Zinc(II) and amino acids-TBA salts in methanol:dichloromethane = 98:2.

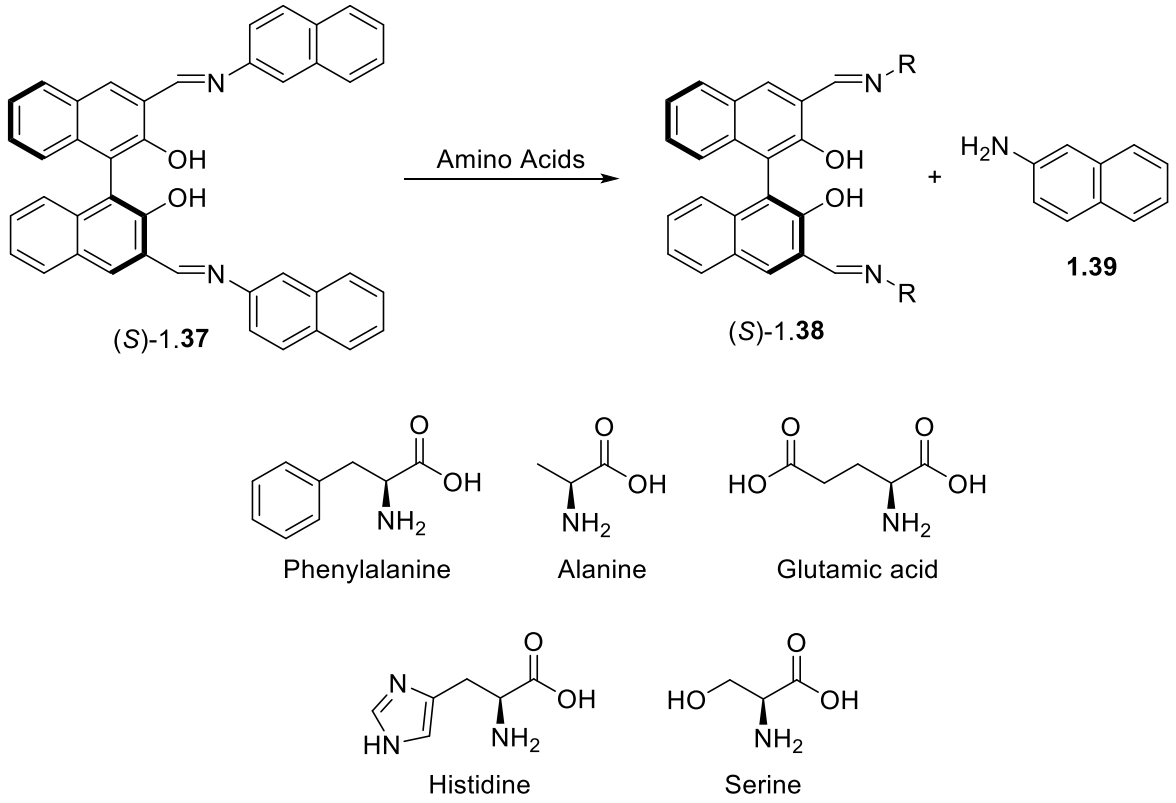

Figure 1. 13 Structures of Wen's probes and analytes

In 2017, Zeng synthesized a SPINOL-based enantioselective probe (*S*)-**1.40** which resembles Huang's diformylBINOL probe mentioned earlier.[44] (*S*)-**1.40** had a SPINOL chiral backbone instead of BINOL, and similar functional groups as well as their relative positions on the aromatic rings. With probe concentration of 20 μM in methanol:dichloromethane = 99:1, 1eq. Zn(II), and 10eq. TBAOH, (*S*)-**1.40** showed enantioselective fluorescence enhancement for D-isomers of valine, leucine, alanine, serine, threonine, phenylalanine, methionine and tryptophan. Particularly, after incubate Hela cells with exogeneous L-valine, Zinc(II) and TBAOH, then the incubation of (*S*)-**1.40**, Zeng achieved in fluorescent imaging of L-valine in living Hela cells. Although there were limitations such as short emission wavelength at $\lambda = 453$ nm, the use of strong

base TBAOH, very pricy starting materials and that the system only detected exogeneous L-valine with exogeneous supplementation of Zin(II), this work was the only enantioselective fluorescent imaging in living cells so far.

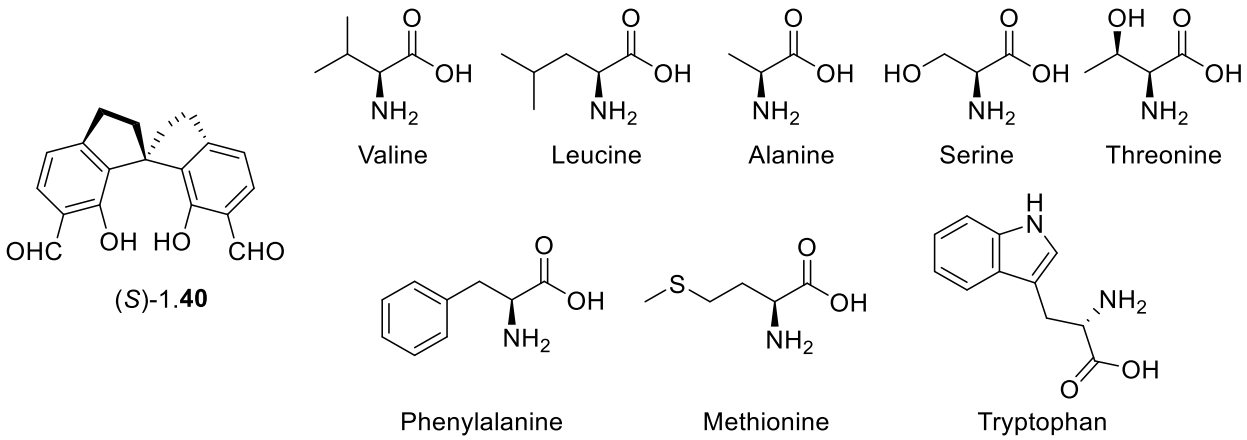

Figure 1. 14 Structures of Zeng's probe and analytes

1.3.3 BINOL-based Probes for Chiral Amino Acids in Water Phase

Current obstacles that prevent more enantioselective fluorescent imaging of amino acids in cell are as follows. First, most of the enantioselective fluorescent probes are built on BINOL structures, which are composed of multiple fused aromatic rings that are hydrophobic. Second, current methods for enantioselective recognition of amino acids utilized aldehyde functional groups, which will later form imine-Zinc(II) complexes that are fluorescent. However, these imine products are very sensitive to moistures, and can very easily hydrolyze back into the initial probes. In short, water solubility and stability are the major problems. What's more, short emission wavelengths and low quantum yields also limited the applications of those probes.

One strategy to render water solubility is to attach hydrophilic substituents. And this issue was firstly answered by Nian and his coworkers in 2017.[45] Amphiphilic polymer poly(N-isopropylacrylamide) (PNIPAM) was introduced to the 6,6'-postions of BINOL to form probe (*S*)-**1.41**. As an amphiphilic polymer, which means it can be dispersed into both water and organic

media, (*S*)-**1.41** allowed the detection to process in both organic media (dichloromethane) and water (BICINE buffer solution or HEPES buffer solution), or even in between the two media. (*S*)-**1.41** was able to floating in between dichloromethane and water layer, the tiny film could be used for fluorescence measurements after filtration and dissolution into one single solvent again. PNIPAM has interesting properties such as lower critical solution temperature (LCST), which allows the polymer to aggregate into insoluble particles at slightly higher temperature. Nian heated the reaction mixture of probe, zinc(II), and amino acids to 45°C to let the (*S*)-**1.41** precipitate, which also allowed fluorescence measurements. This probe could serve as a powerful tool in a relatively complicated situation. It was also believed that PNIPAM provided a relatively hydrophobic pocket to stabilize the imine product. The optimal condition was probe concentration of 1.0 mM in BICINE buffer solution (pH~8), 2 eq. Zinc(II). The emission wavelength was at λ = 504 nm.

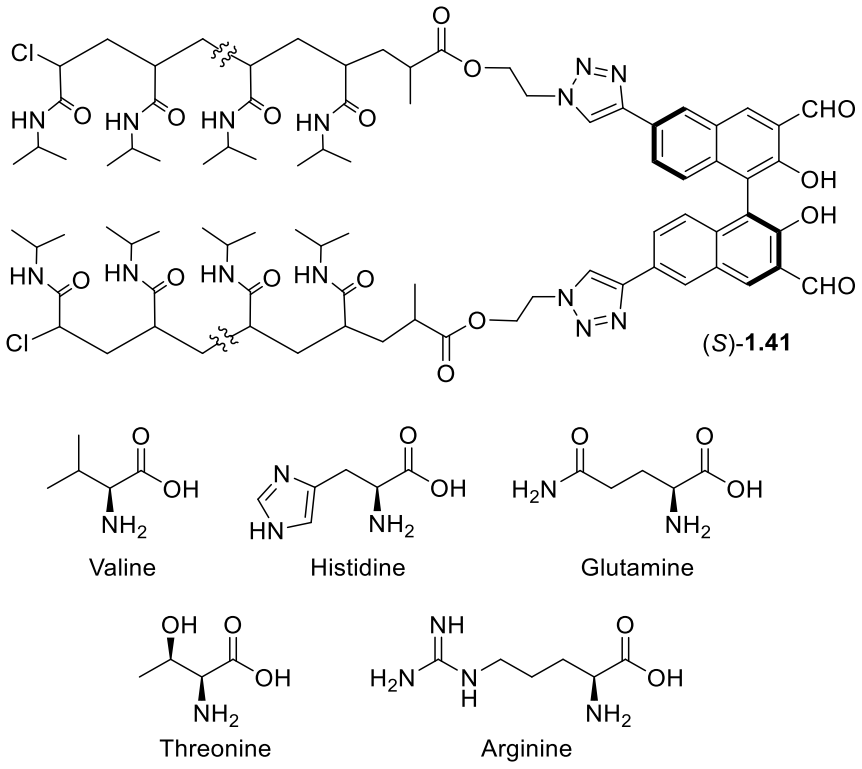

Figure 1. 15 Structures of Nian's probe and analytes

Zhao came up with a second answer to the water solubility question in 2018.[46] Polyethylene glycol oligomer containing three monomer units (PEG_3) was introduced to 6,6'-postions of BINOL via Suzuki reaction to form probe (*S*)-**1.42**. However, the PEG length was too short that it still needed to be dissolved in THF firstly, and then used for the recognition in HEPES buffer solution (pH = 7.4). With probe concentration of 10 μM, and 2eq. zinc(II), the ef values were 13.7 for phenylalanine, 7.0 for methionine, 24.2 for threonine, 12.6 for leucine, and 12.9 for serine with emission wavelength at λ = 510-525 nm.

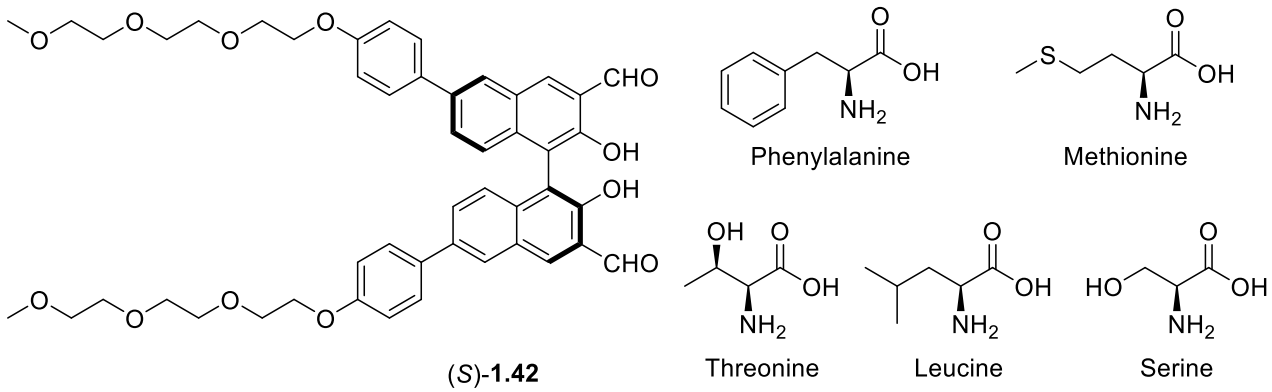

Figure 1. 16 Structures of Zhao's probe and analytes

Although no common strategy to solve the solubility issue was used, Iqbal found that tetrabromo-diformylBINOL could be dissolved in dimethyl sulfoxide and then dispersed into water in 2019.[47] In the presence of 1 eq. zinc(II), the fluorescence signal of (*S*)-**1.43** could be enantioselectively turned on by valine-TBA salt. Tryptophan was then covalently linked to (*R*)-**1.43** through condensation with one of the two aldehydes, and to form probe (*R*)-**1.44** in situ. Similar to Wen's strategy mentioned earlier, **1.44** would release one additional fluorophore tryptophan after interaction with amino acids. And the fluorescence of tryptophan at λ_1 = 350 nm could be used to tell the concentrations of amino acids. The BINOL part had emission at around λ_2 = 500 nm which could report the enantiomeric compositions. This study was finished in water media (HEPES buffer solution, pH = 7.4) with 1% DMSO needed to dissolve the probe. The ef

values were 244.5 for glutamic acid, 18.8 for leucine, 80.2 for methionine, 93.5 for tyrosine, 24.8 for valine, 22.9 for phenylalanine, 93.2 for threonine.

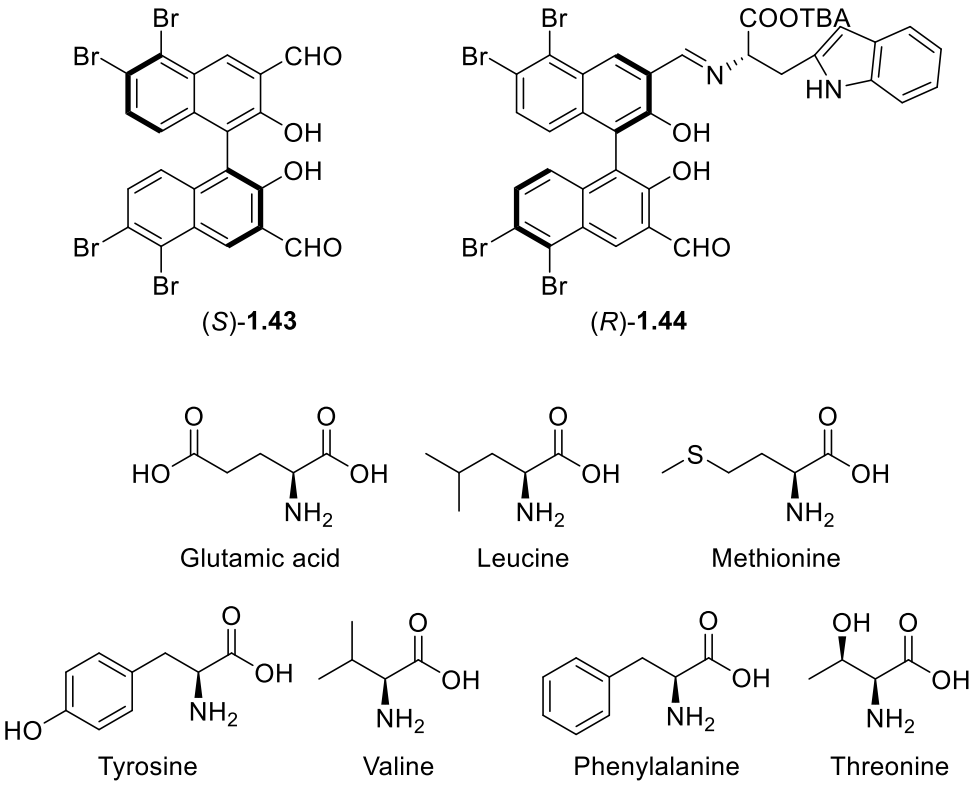

Figure 1. 17 Structures of Iqbal's probe and analytes

At the same year, Zhu reported a bisBINOL-based probe (*S*,*S*)-**1.45** for the chiral recognition of amino acids.[48] The bisBINOL structures were believed to make the chiral pocket more rigid and lead to improved enantioselectivity than regular BINOL-based probes. Despite the very slow reaction process, (*S*,*S*)-**1.45** had emission at λ ~ 520 nm and ef values as follows, 177 for valine, 199 for methionine, 186 for phenylalanine, 118 for leucine, 89 for alanine, 38 for tryptophan, 29 for glutamine, 25 for tyrosine, 18 for asparagine, 10 for threonine and 8 for serine. However, this work was done in predominantly organic solvents acetonitrile. The structure was adapted from Zeng's probe (*S*,*S*)-**1.46**,[49] and the difference in their structures were pyridinyl linker vs alkyl linker. It was a pity that Zeng did not investigated the use of (*S*,*S*)-**1.46** for the recognition

of amino acids, as the two probes are structurally similar and it will be very useful to guide the design of novel probes.

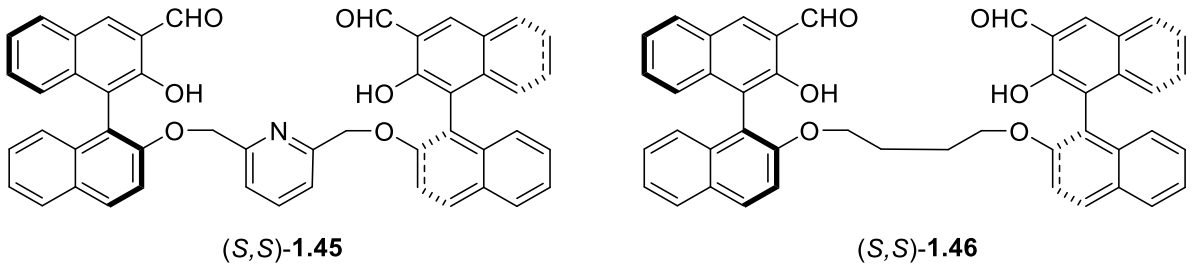

Figure 1. 18 Structures of Zhu's and Zeng's bisBINOL probe

1.4 Other Probes for Chiral Recognition of Amino Acids

1.4.1 Molecular Imprinted Polymers

Molecularly imprinted polymers (MIPs) are a class of polymers synthesized with special molecular templates. The templates often have covalent or non-covalent interactions with the functional monomers, so that the polymerization can be processed via a more controlled way. After the polymerization has been finished, the templates are extracted out to leave complementary cavities in the polymer matrix, which highly resembles the original templates. The resulted MIPs have strong and specific affinity for the templates, and have been applied as molecular sensors.[50,51] While at the same time, MIPs sensors disadvantage in aspects such as the needs of specific synthesis, lack of a scope of analytes, and lack of fluorophores which limited their applications. Although in some research, MIPs sensors were very selective and sensitive, the limit of detection and other analytic criteria strongly relied on the detection techniques. In this section, several representative MIPs sensors will be introduced.

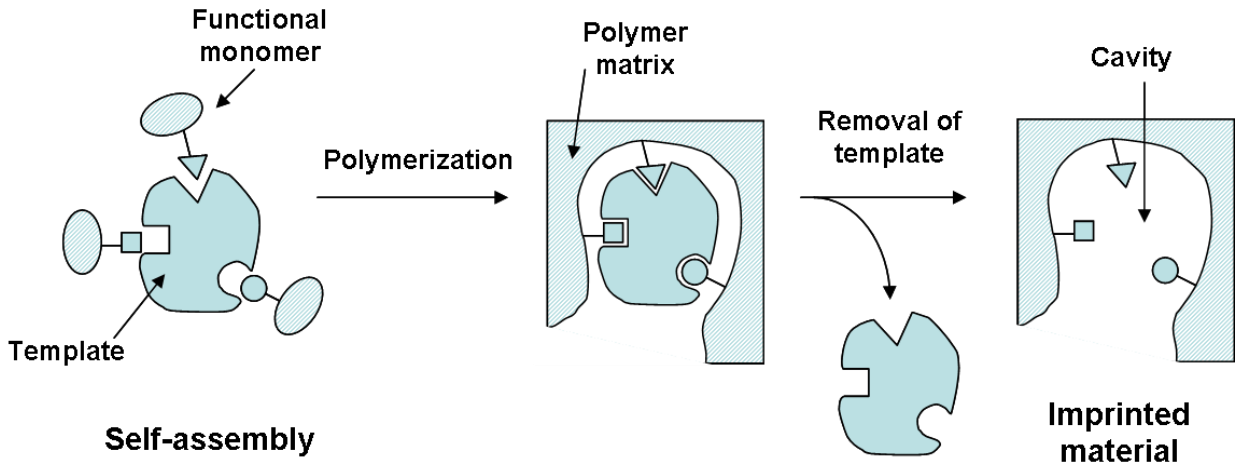

Figure 1. 19 General ideas of MIPs. (Molecularly imprinted polymer. (2020, April 12). In *Wikipedia*. Retrieved from https://en.wikipedia.org/wiki/Molecularly_imprinted_polymer#cite_note-1)

In 2002, Chen reported the L-phenylalanine anilide (L-PAA)-templated molecular imprinted polymer L-MIP **1.50** and its use in probing the enantiomeric composition of PAA.[52] This polymer **1.50** was synthesized via the copolymerization of methacrylic acid (MAA) **1.48** and ethylene glycol dimethacrylate (EGDMA) **1.49**. Although no chiral monomers were used and the chiral template L-PAA was removed, the L-MIP **1.50** exhibited enantioselectivity among D- and L-PAA. In this study, equilibrated L-MIP **1.50** with 1.2 mM PAA was used in organic solvent acetonitrile. UV-vis spectroscopy was used for the monitoring of analytes.

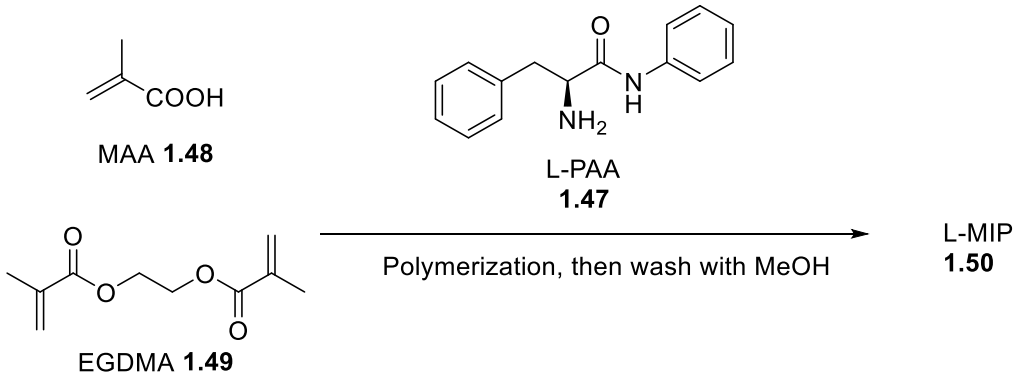

Figure 1. 20 Synthesis of Chen's L-MIP

In 2006, Liu and his coworkers reported MIPs for the chiral recognition of chiral tryptophan.[53] Acrylamide **1.51** and a cross-linker **1.52** was polymerized with a template L-tryptophan **1.53** to form a series of MIPs **1.54**. A quartz crystal microbalance (QCM) electrode was then coated with **1.54** so that the change in the current frequency could be used to detect the chiral tryptophan analytes. The frequency changes were about six times different upon interaction with the enantiomers of tryptophan, and the lowest detection limit (three times of noise standard deviation over the calibration curve slope) was found to be 8.8 μM for L-Trp, and 44 μM for D-Trp. The electrode could also be used to detect the enantiomeric composition of tryptophan mixtures. The media was citric acid buffer solution for this study. No other amino acids substrates were tested.

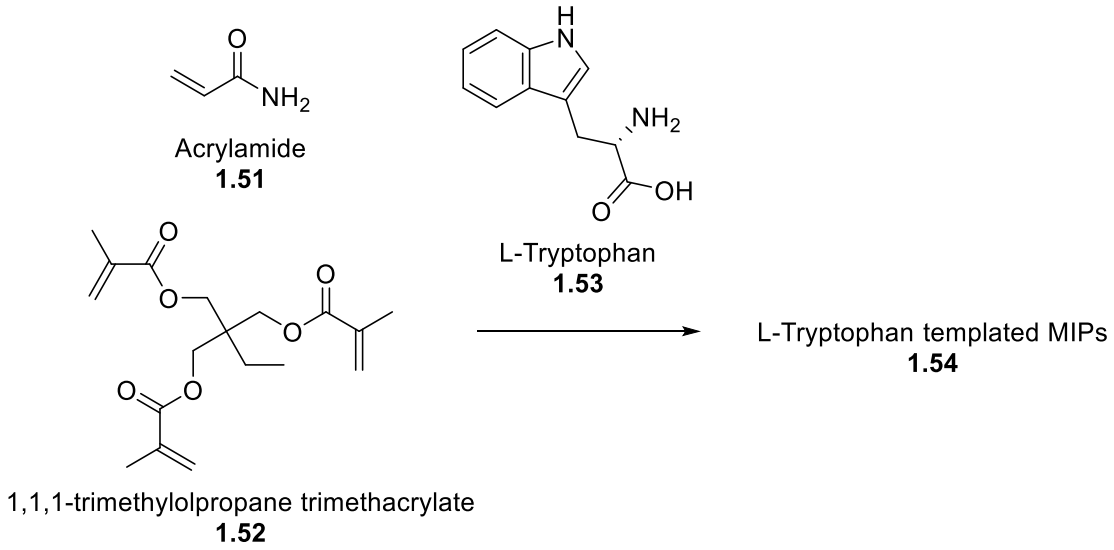

Figure 1. 21 Synthesis of Liu's MIPs

In 1999, Liao and his coworkers incorporated a fluorescent dye dansyl chloride into their monomer, and successfully synthesized a fluorescent MIP **1.56**.[54] The fluorescence of MIP **1.56** could be quenched by a quencher p-nitrobenzaldehyde **1.57**. Then upon addition of L-tryptophan, the quencher **1.57** was displaced off from the cavities of the MIP by L-Trp due their stronger interactions. Thus, the fluorescence was turned back on. Meanwhile, the opposite enantiomer D-

Trp had much weaker interaction and binding affinity to the cavities, and had weaker fluorescence than the L-isomer. The D-Trp had fluorescence intensity about 70% of that of L-Trp. At the same time, L-Phe, and L-Ala had much smaller change on the fluorescence intensities than L-Trp as well. This study was finished with MIP probe **1.56** concentration of 10 mg/ml, quencher concentration of 3 mM in chloroform, and amino acids in citric acid buffer. The fluorescence emission wavelengths were at $\lambda = 485$ nm.

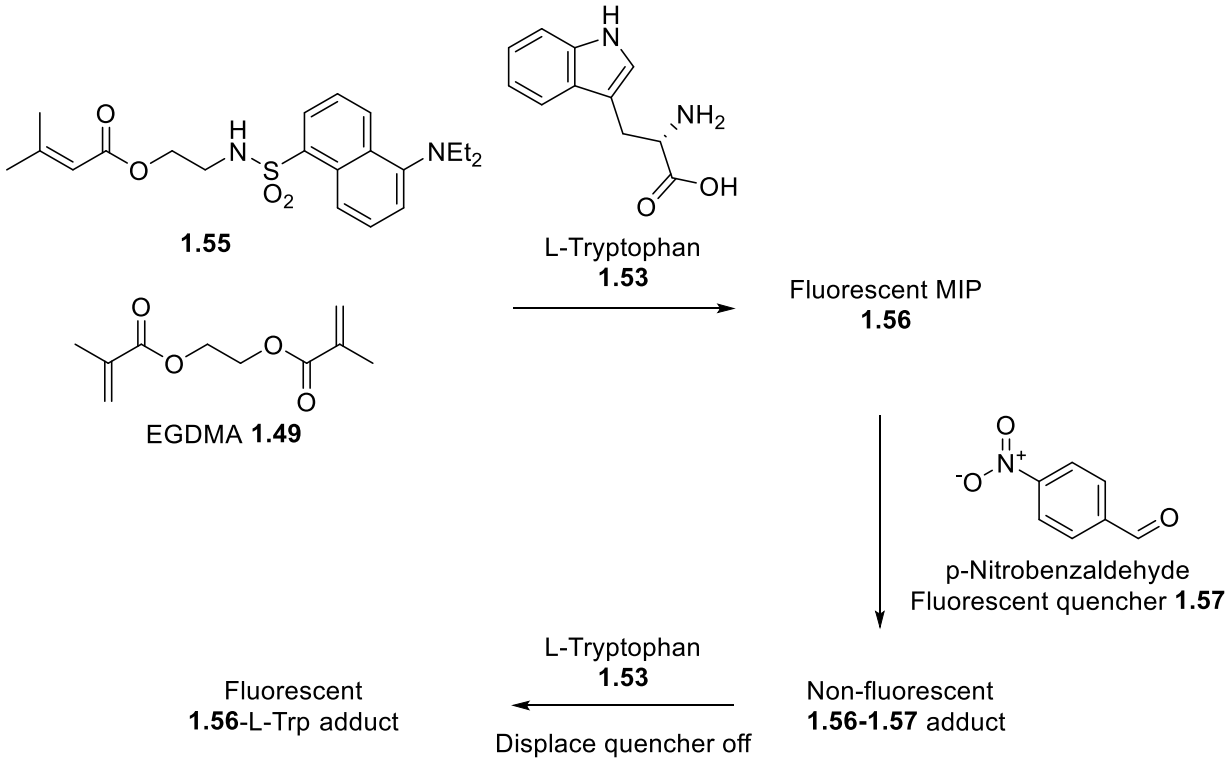

Figure 1. 22 Liao's strategy to detect L-Trp

Iskierko reported MIP **1.61** for the chiral recognition of L-phenylalanine **1.60** in 2017.[55] **1.58** was used as the functional monomer and **1.59** was used as the cross-linker. They calculated the interaction energy of pre-polymerization complexes of **1.58** and **1.60**. The free Gibbs energy change ΔG was remarkable, -119 kJ/mol, indicating very strong complexation for the template phenylalanine **1.60**. Upon coating on electrodes, the MIP-electrode showed enantioselective

current change for L-phenylalanine over its D-isomer when dipping into amino acid solutions. The limit of detection was calculated to be 13 μM for the templates.

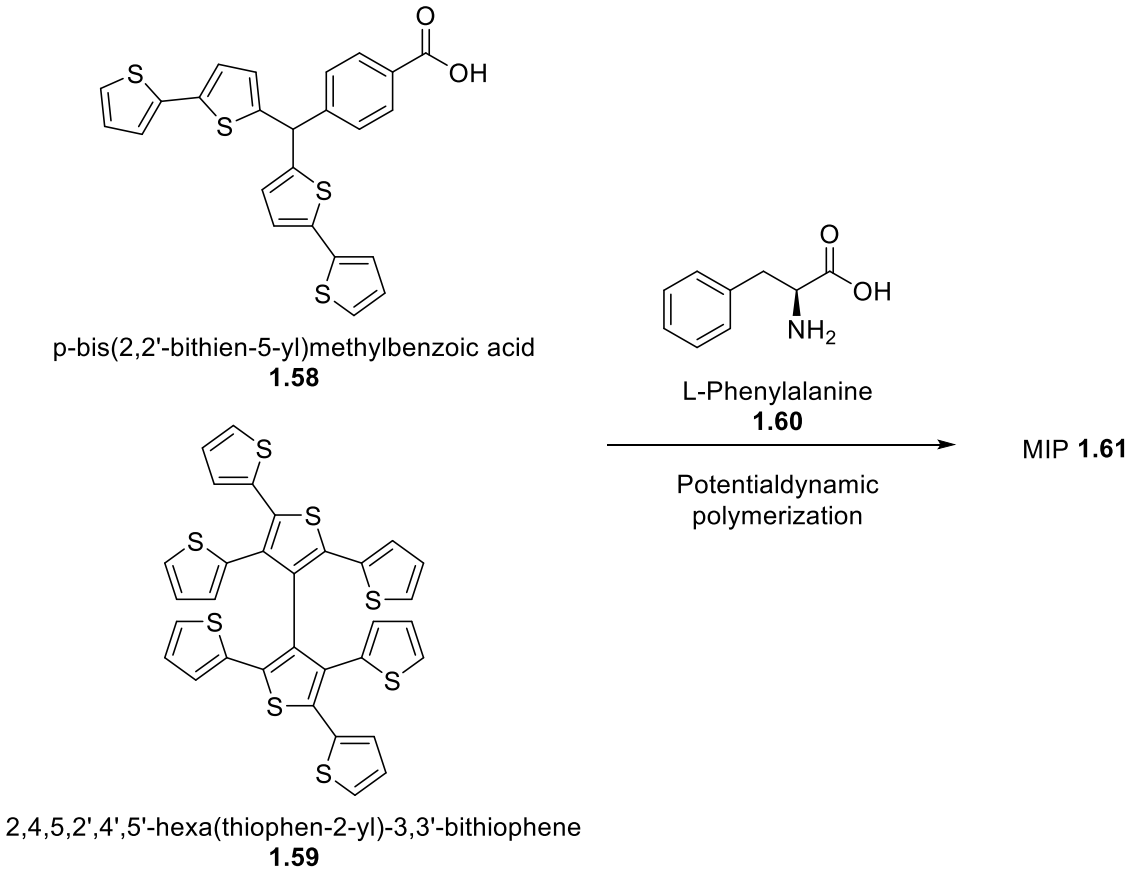

Figure 1. 23 Iskierko's strategy to detect L-Phe

1.4.2 β-Cyclodextrin-based Fluorescent Probes

Cyclodextrins (CDs) are a family of cyclic oligosaccharides, which have macrocyclic structures of glucose via α-1,4 glycosidic bonds. Depending on the numbers of glucose, they are classified into α-CD (6 glucose subunits), β-CD (7 glucose subunits), γ-CD (8 glucose subunits). Among those three types of CDs, β-CD received more attention especially in the area of chiral recognition. 18 hydroxyl groups in total make the exterior of β-CD hydrophilic, while the interior is considered hydrophobic. Given the fact that β-CD can be easily accessed naturally and that the

many hydroxyl groups enable multiple functionalization, β-CD has been widely used as carriers in drug delivery and beyond.[56] Recently it has also been used as a chiral backbone for the recognition for chiral amino acids. However, it needs to be noticed that, since the enantiomeric analogues of β-CD-based probes are very challenging to synthesize, those enantioselective probes can often only recognize one particular enantiomer of their analytes. Another issue is that β-CD has no conjugated systems, so extra fluorophores are needed for the use of fluorescent recognition. Otherwise the more sophisticated techniques will be required as reported by early research in 1991.[57]

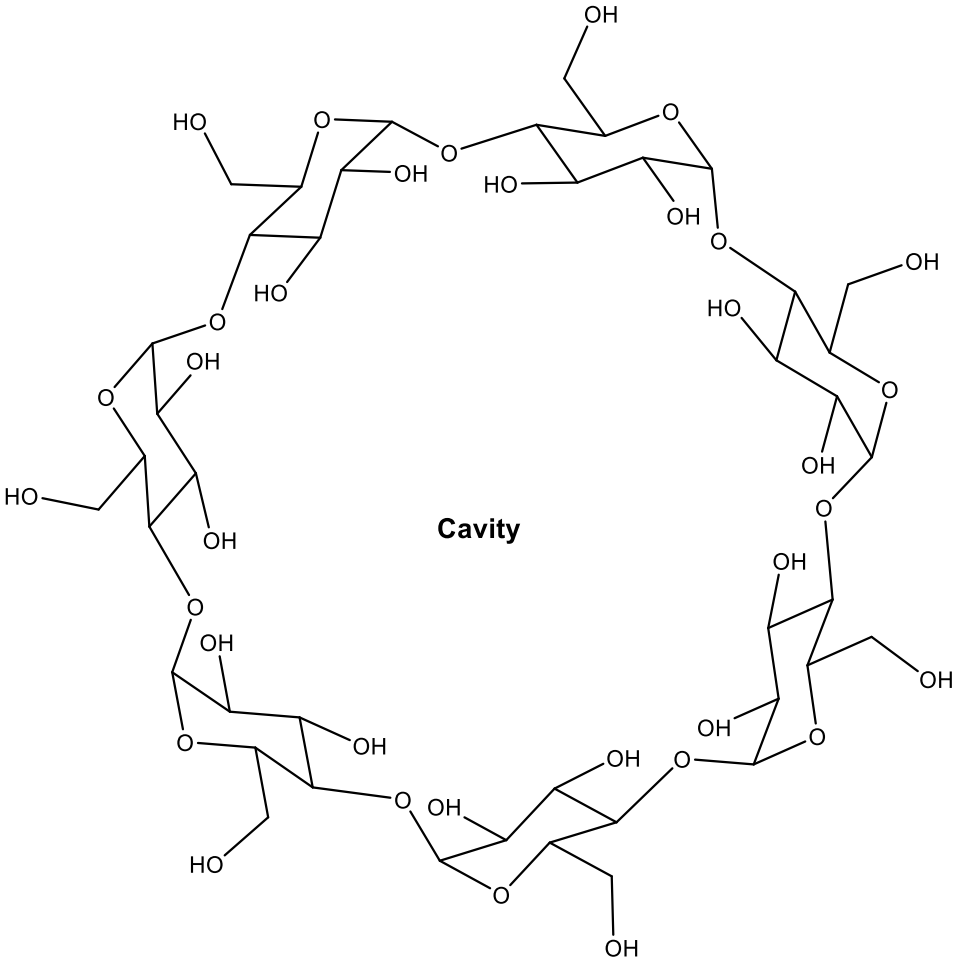

Figure 1. 24 Structure of β-CD

In 2000, Pagliari at his coworkers reported a β-CD-based enantioselective probe **1.63** for the chiral recognition of multiple amino acids.[58] **1.63** consisted of three major units, β-CD as the backcone, R- or S-phenylalanineamide for binding with copper (II), and dansyl as the additional fluorophore. Copper(II) was found to efficiently quench the fluorescence of adjacent dansyl. Upon interaction with amino acids, the fluorescence was switched on enantioselectively. Among four chiral amino acids pairs studied, **1.63a** was found to have better enantioselectivity over the **1.63b.** This study was finished with probe concentration of 60 μM in tetraborate buffer (pH = 7.3). The best ef value obtained was 3.89 for proline and 0.33 for phenylalanine when **1.63a** was used, and the emission wavelength was at λ = 516 nm. The ef values for other amino were very limited, and histidine leaded to very strong fluorescence which could interfere any detections.

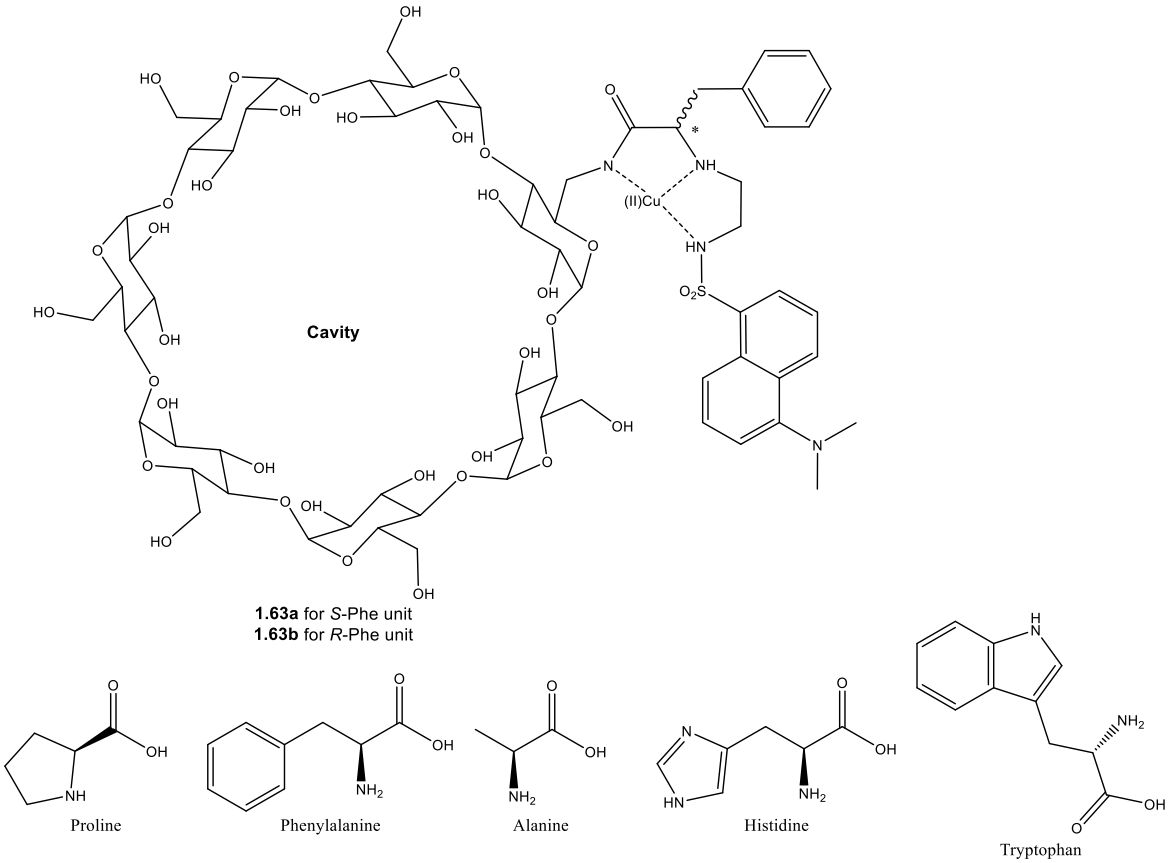

Figure 1. 25 Structure of Pagliari's probes and analytes

As follow-up studies, Corradini and his coworkers replaced the L-Phe unit in the probe into several other chiral ligand including L-phenylglycine (L-Phg), D-Phg, L-Pro, hydrogenated L-Phg.[59,60] Addition of copper(II)(proline/valine)$_2$ enantioselectively quenched the fluorescence of the probe. Similar to Pagliari's, this study was finished with probe concentration of 60 μM in tetraborate buffer (pH = 7.3).

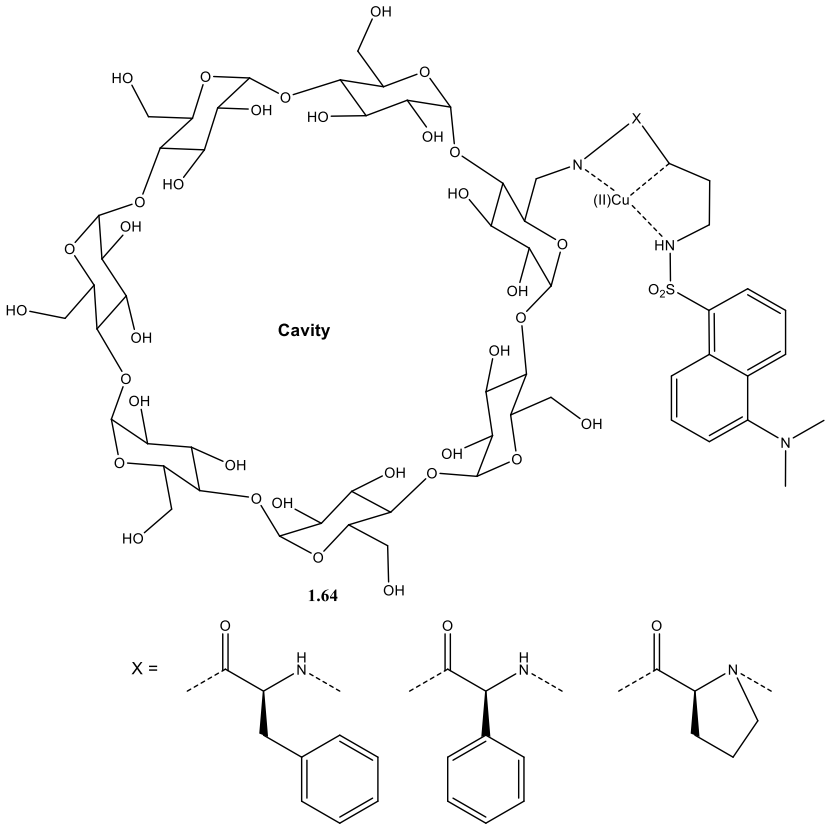

Figure 1. 26 Structure of Corradini's probes

1.4.3 Probes for Chemoselective Detection of Amino Acids

In order to chemoselectively detect certain amino acids while remain signal off for the others, the probes are expected to have much stronger interaction for expected amino acids over the rest of all. For several amino acids such as basic amino acids and cysteine, chemoselective amino acids have been achieved in many different approaches. While there are still blank for many

other amino acids considering the big family (20 amino acids). In this section, several common strategies will be introduced.

Basic amino acids including histidine, arginine and lysine. Compared to other amino acids, they have basic functionalities which do not just make them basic, but also endure Lewis-basicity for strong binding affinities to metal ions. Minami at his coworkers reported polycyclic structural probes **1.65** and **1.66**.[61] Eu^{3+} ion was added to the probe to quench the fluorescence upon binding with C=O moieties. This fluorescence quenching was due to energy transfer from naphthalene to the metal ion. Basic amino acids were believed to bind with the probes via cation-π or hydrophobic interaction and displace Eu^{3+} to turn on the fluorescence signal. With probe **1.65** concentration of 3 μM with Eu^{3+} concentration of 300 μM in neutral water, lysine turned on fluorescence at multiple peaks at λ = 320-370 nm, while arginine showed fluorescence enhancement at one single peak at λ ~ 370 nm. After linear discrimination analysis (LDA), all species of basic amino acids were identified.

Cysteine's thiol functional group can very easily undergo nucleophilic addition to acrylates to form 1,4-thiazepines.[62] This well known reaction was used by Yang for the design of cysteine/homocysteine-specific probe **1.67**.[63] The probe itself had no fluorescence initially. After nucleophilic addition, enol-like product **1.68** was firstly formed to show fluorescence emission at λ = 377 nm. The amino acids' amino groups then underwent another nucleophilic addition followed by cleavage of ester bond on the probe to form product **1.69** and **1.70**. This later step would turn on fluorescence emission at λ = 487 nm. The reaction rate of the later step varies between Cys and Hcy, which allowed speciation of the two thiols. This study was accomplished with probe concentration of 20 μM in ethanol:PBS buffer = 2:8. The Limit of detection of Cys was 0.11 μM and 0.18 μM respectively.

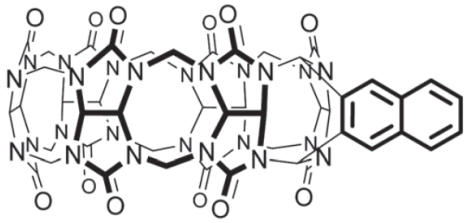

1.65

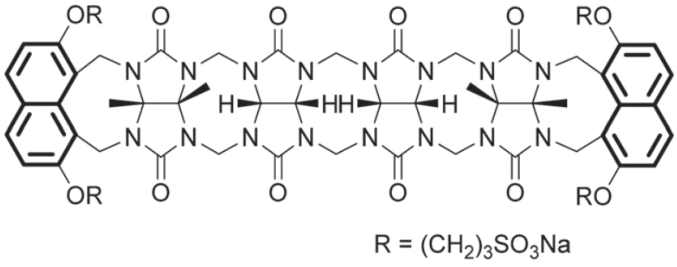

1.66

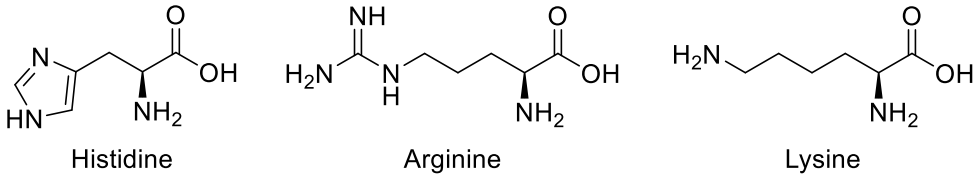

Figure 1. 27 Structure of Minami's probes and basic amino acids

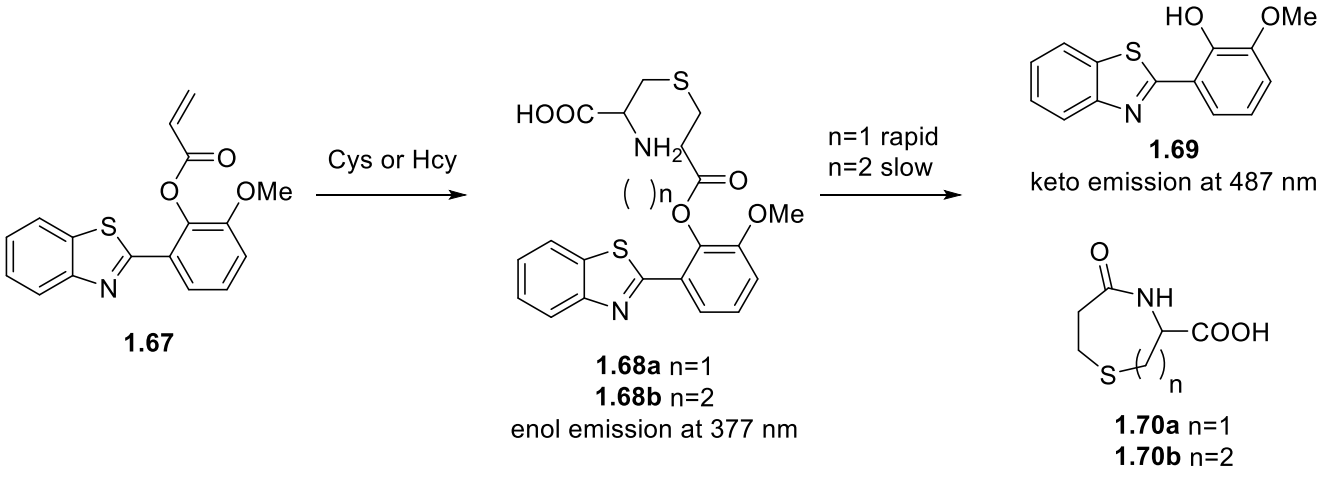

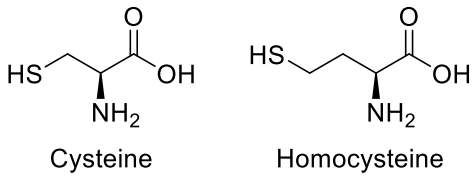

Figure 1. 28 Mechanism for cysteine probing

In 2012, Huang and his coworkers reported a simple terpyridine probe $TpyCuCl_2$ **1.71** could be used for the chemoselective detection for histidine.[64] As a classical coordination complex firstly prepared in 1937,[65] TpyCu2+ had been studied including its complexation with histidine in water media.[66] In Huang's work, **1.71** was found to be non-fluorescent and the fluorescence could be turned on to 1004 fold upon addition of histidine. This study was finished with probe concentration of 20 μM in HEPES buffer solution (pH = 6.35). The emission wavelength was at λ = 352 nm. However, a strong interference from cysteine was observed probably due to strong thiol-copper complexation.

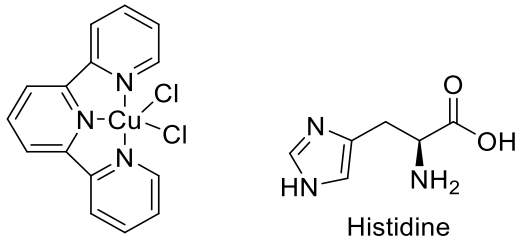

1.71

Figure 1. 29 Structures of Huang's probe and analyte

1.5 The Use of Micelles to Render Water Solubility

Micelles are aggregates or supramolecular assemblies that formed by surfactants in liquid colloid. Typically, micelles in aqueous solution are formed with the hydrophilic part stretching out in contact with water media., while forcing the hydrophobic part in the center area.[67,68] This particular property has made micelles excellent carriers for drug delivery. Compared with surfactants, block copolymers received more attention for novel carrier systems recently, due to their high drug-loading capacity and unique disposition characteristics in the body. Because of the space limitations, several block copolymers will be introduced in this section.

Chen and his coworkers studied the use of enantiomeric poly(ethylene-glycol)-poly(lactide) (PEG-PLA) for the drug delivery of rifampin *in vitro*.[69] Poly(ethylene-glycol)-poly(L-lactide)

(PEG-PLLA) **1.74** and poly(ethylene-glycol)-poly(D-lactide) (PEG-PLLA) **1.75** were synthesized through ring opening polymerization of $mPEG_{5k}$ and D-/L-lactide **1.73**/**1.74** respectively with stannous octoate catalyst. The resulted block dipolymers had 14-70 lactide units, with M_w/M_n value of 1.14-1.37. The micelles were obtained by self-assembly in water with critical micelle concentration of 0.8-4.8 mg/L and hydrodynamic diameters of 40-120 nm. Rifampin was encapsulated into the micelles, and the drug release in vitro could be controlled by molecular weight of the polymers and morphology of the micelles.

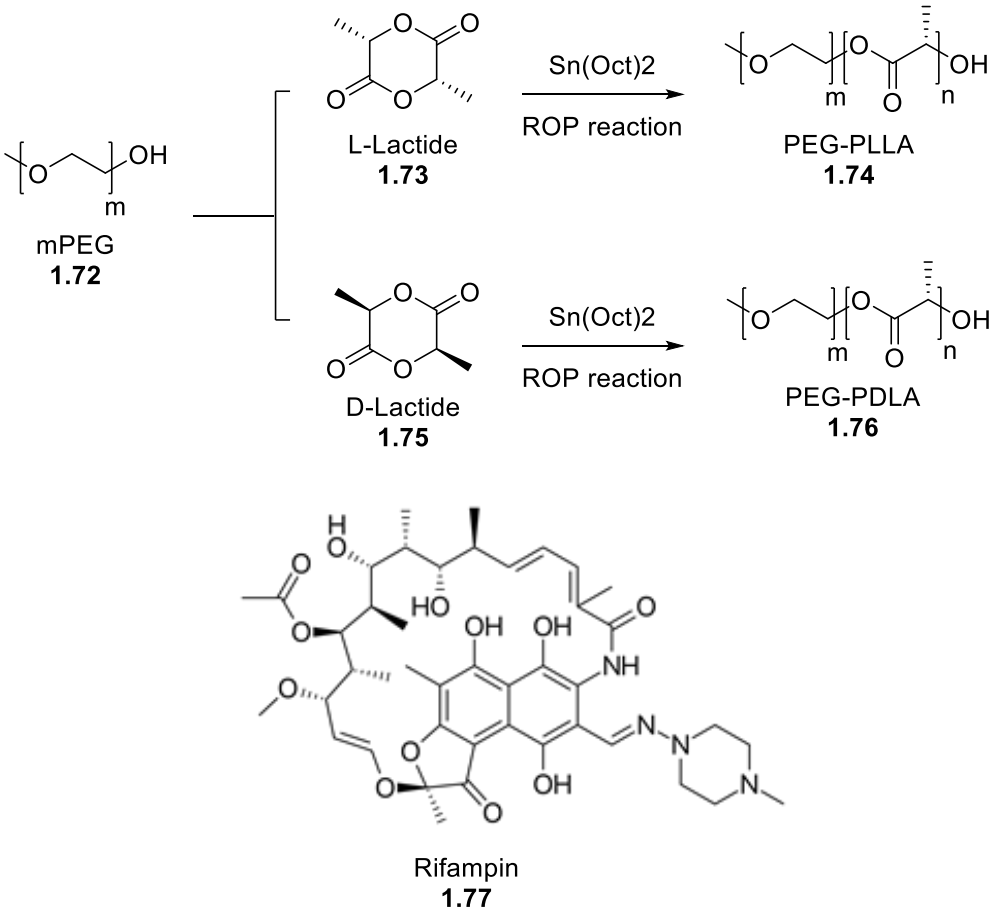

Figure 1. 30 Synthesis of PEG-PLAs and Structure of Rifampin

Shao and his coworkers reported the use of poly(ethylene)-poly(ethylene-glycol) (PE-PEG) based micelles for the drug-delivery of amphotericin B to the brain.[70] Amphotericin B was an antibiotic with very limited water solubility. It had been used for the treatment of fungal infections

of the central nervous system. In this study, Shao found PE-PEG based micelle could efficiently deliver amphotericin B to the brain with limited toxicity to mammalian cells.

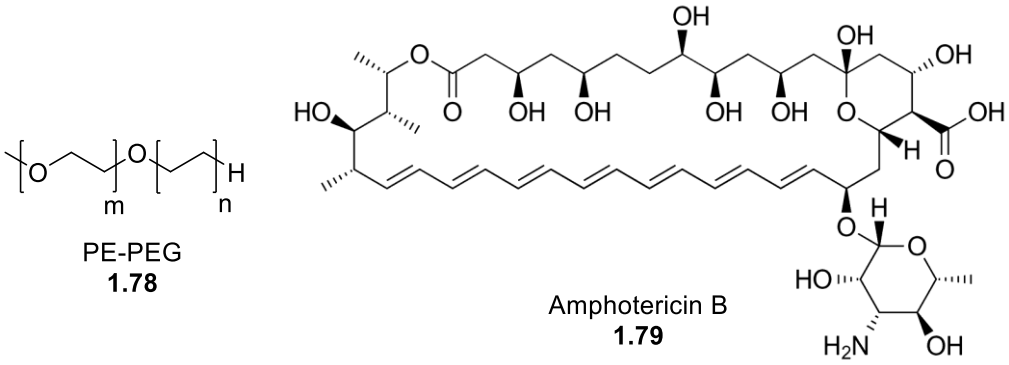

Figure 1. 31 Structure of PE-PEG and Amphotericin B

Poloxamers and Pluronics are the brand name of poly(ethylene oxide)-block-poly(propylene oxide)-block-poly(ethylene oxide) (PEO-PPO-PEO or PEG-PPO-PEG).[71] These triblock copolymers with centered hydrophobic part and two outstretching hydrophilic part, have customized critical micelle concentration and critical micelle temperature. A recent study reported the use of Pluronic F127/F68 for ocular drug delivery and how they could improve drug residence.[72]

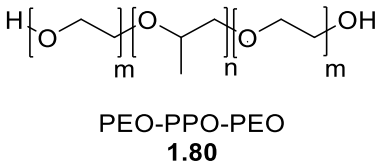

Figure 1. 32 Structure of triblock copolymer PEO-PPO-PEO

The last copolymer introduced here is poly(ethylene glycol)-poly(ε-caprolactone) copolymers (PEG-PCL) **1.81**. PEG-PCL has characteristics such as high biocompatibility and biodegradability. The micelles formed by PEG-PCL were reported to be able to enhance the drug accumulation on the site of action and avoid off-target effect.[73]

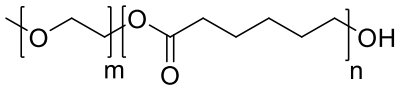

PEG-PCL
1.81

Figure 1. 33 Structure of block copolymer PEG-PCL

1.6 Summary

Compared to other chiral backbones of enantioselective probes, BINOL is favored due to axial chirality, easily-tuned chemistry and high enantioselectivity. BINOL-based probes are very efficient to detect chiral amines, chiral amino alcohols, chiral amino acids through multiple strategies. However, most of those probes are used in organic media, which are not optimal for the detection of amino acids. The probes designed for the detection of chiral amino acids in aqueous media needs rather sophisticated synthesis. As an alternate answer to solve the solubility issue, micelles have been widely used for the drug delivery of many insoluble molecules. But the use of micelles for dispersing probes in water media has not been fully investigated.

Chemoselective detection of amino acids have been briefly introduced. Histidine, cysteine, and basic amino acids have been chemoselectively detected in water media. However, expect ambiguity in the analysis of other amino acids, there are still many amino acids that are not selectively distinguished. Combined those together, the specific detection, in the ways of both enantioselective and chemoselective, will be much more challenging.

1.7 References

(1) Lord Kelvin, William Thomson, Baron. *The molecular tactics of a crystal;*Clarendon Press: Oxford, 1984.

(2) National Research Council (US). *Recommended Dietary Allowances*; National Academies Press: Washington (DC), 1989.

(3) Zubay, G. L. *Origins of Life on the Earth and in the Cosmos*; Academic Press, 2000.

(4) Seckbach, J. *Cellular Origin, Life in Extreme Habitats and Astrobiology.*

(5) Chhabra, N.; Aseri, M. L.; Padmanabhan, D. A Review of Drug Isomerism and Its Significance. *Int. J. Appl. Basic Med. Res.* **2013**, *3(1)*, 16-18.

(6) Lim, S. A. Ethambutol-Associated Optic Neuropathy. *Ann. Acad. Med. Singapore* **2006**, *35* (4), 274–278.

(7) Lenz, W. A Short History of Thalidomide Embryopathy. *Teratology* **1988**, *38* (3), 203–215.

(8) Nippert, I.; Edler, B.; Schmidt-Herterich, C. 40 Years Later: The Health Related Quality of Life of Women Affected by Thalidomide. *Public Health Genomics* **2002**, *5* (4), 209–216.

(9) Ulrich, E. M.; Morrison, C. N.; Goldsmith, M. R.; Foreman, W. T. Chiral Pesticides: Identification, Description, and Environmental Implications. *Rev Environ Contam Toxicol*. **2012**, *217*, pp 1–74.

(10) Kane-Maguire, L. A. P.; Wallace, G. G. Chiral Conducting Polymers. *Chem. Soc. Rev.*, **2010**, *39*, 2545-2576.

(11) Ilisz, I.; Berkecz, R.; Péter, A. Application of Chiral Derivatizing Agents in the High-Performance Liquid Chromatographic Separation of Amino Acid Enantiomers: A Review. *J Pharm Biomed Anal*. **2008**, *47(1)*, pp 1–15.

(12) Schurig, V. Practice and Theory of Enantioselective Complexation Gas Chromatography. *J*

Chromatogr A. **2002**, *965*, pp 315–356.

(13) Simó, C.; Barbas, C.; Cifuentes, A. Chiral Electromigration Methods in Food Analysis. *Electrophoresis* **2003**, *24* (15), 2431–2441.

(14) Prokhorova, A. F.; Shapovalova, E. N.; Shpigun, O. A. Chiral Analysis of Pharmaceuticals by Capillary Electrophoresis Using Antibiotics as Chiral Selectors. *J Pharm Biomed Anal*.. **2010**, *53*, pp 1170–1179.

(15) Evans, M. A.; Morken, J. P. Isotopically Chiral Probes for in Situ High-Throughput Asymmetric Reaction Analysis. *J. Am. Chem. Soc.* **2002**, *124* (31), 9020–9021.

(16) Meierhenrich, U. J.; Filippi, J.-J.; Meinert, C.; Bredehöft, J. H.; Takahashi, J.; Nahon, L.; Jones, N. C.; Hoffmann, S. V. Circular Dichroism of Amino Acids in the Vacuum-Ultraviolet Region. *Angew. Chemie Int. Ed.* **2010**, *49* (42), 7799–7802.

(17) Martínez-Máñez, R.; Sancenón, F. Fluorogenic and Chromogenic Chemosensors and Reagents for Anions. *Chem. Rev.* **2003**, *103* (11), 4419–4476.

(18) Conrad, R. M.; Berg, C. P. The optical inversion of d-histidine in the animal body. *J Biol Chem*, **1937**, *117*, 351-363.

(19) Kim, J. S.; Quang, D. T. Calixarene-Derived Fluorescent Probes. *Chem Rev*. 2007, *107*, 9, pp 3780–3799.

(20) Ueno, T.; Nagano, T. Fluorescent Probes for Sensing and Imaging. *Nat Methods*. **2011**, *8*, pp 642–645.

(21) Ghoroghchian, P. P.; Therien, M. J.; Hammer, D. A. In Vivo Fluorescence Imaging: A Personal Perspective. *Nanomed Nanobiotechnolo* **2009**, *1* (2), 156–167.

(22) Czarnik, A. W. Desperately Seeking Sensors. *Chem. Biol.* **1995**, *2* (7), 423–428.

(23) Chan, J.; Dodani, S. C.; Chang, C. J. Reaction-Based Small-Molecule Fluorescent Probes

for Chemoselective Bioimaging. *Nat. Chem.* **2012**, *4*, 973-984.

(24) Zhang, X.; Yin, J.; Yoon, J. Recent Advances in Development of Chiral Fluorescent and Colorimetric Sensors. *Chem. Rev.* **2014**, *114*, 9, 4918-4959.

(25) Bolger, R.; Lenoch, F.; Allen, E.; Meiklejohn, B.; Burke, T. Fluorescent Dye Assay for Detection of DNA in Recombinant Protein Products. *Biotechniques* **1997**, *23* (3), 532–537.

(26) Lamb, L. E.; Bartolone, S. N.; Ward, E.; Chancellor, M. B. Rapid Detection of Novel Coronavirus (COVID19) by Reverse Transcription-Loop-Mediated Isothermal Amplification. In: *medRxiv* (2020).

(27) Pappalardo, S.; Parisi, M. F. Ten-Membered Rings or Larger with One or More Oxygen Atoms. *Comprehensive Heterocyclic Chemistry III* **2008**, *14*, pp 667–749.

(28) Kyba, E. B.; Koga, K.; Sousa, L. R.; Siegel, M. G.; Cram, D. J. Chiral Recognition in Molecular Complexing. *J. Am. Chem. Soc.* **1973**, *95* (8), 2692–2693.

(29) Peacock, S. S.; Walva, D. M.; Gaeta, F. C. A.; Helgeson, R. C.; Cram, D. C. Host-guest complexation. 22. Reciprocal chiral recognition between amino acids and dilocular systems. *J. Am. Chem. Soc.* **1980**, *102*, 6, 2043-2052.

(30) Iwanek, W.; Mattay, J. Ground State and Excited State Association: Chiral Recognition between 2,2′-Dihydroxy-1,1′-Binaphthyl and Amines. *J. Photochem. Photobiol. A Chem.* **1992**, *67* (2), 209–226.

(31) Pugh, V. J.; Hu, Q.; Pu, L. The First Dendrimer-Based Enantioselective Fluorescent Sensor for the Recognition of Chiral Amino Alcohols. *Angew. Chemie Int. Ed.* **2000**, *39* (20), 3638–3641.

(32) Pugh, V. J.; Hu, Q.-S.; Zuo, X.; Lewis, F. D.; Pu, L. Optically Active BINOL Core-Based Phenyleneethynylene Dendrimers for the Enantioselective Fluorescent Recognition of

Amino Alcohols. *J. Org. Chem.* **2001**, *66*, 18, 6136-6140.

(33) Lin, J.; Li, Z. B.; Zhang, H. C.; Pu, L. Highly Enantioselective Fluorescent Recognition of α-Amino Acid Derivatives. *Tetrahedron Lett.* **2004**, *45* (1), 103–106.

(34) He, X.; Cui, X.; Li, M.; Lin, L.; Liu, X.; Feng, X. Highly Enantioselective Fluorescent Sensor for Chiral Recognition of Amino Acid Derivatives. *Tetrahedron Lett.* **2009**, *50* (42), 5853–5856.

(35) Li, Z.-B.; Pu, L. Synthesis of a New Bisbinaphthyl Macrocycle for Enantioselective Fluorescent Recognition. *J. Mater. Chem.*, **2005**, *15*, 2860–2864.

(36) Li, Z.-B.; Lin, J.; Zhang, H.-C.; Sabat, M.; Hyacinth, M.; Pu, L. Macrocyclic Bisbinaphthyl Fluorophores and Their Acyclic Analogues: Signal Amplification and Chiral Recognition. *J. Org. Chem.* **2004**, *69*, 19, 6284-6293.

(37) Li, Z.-B.; Lin, J.; Pu, L. A Cyclohexyl-1,2-Diamine-Derived Bis(Binaphthyl) Macrocycle: Enhanced Sensitivity and Enantioselectivity in the Fluorescent Recognition of Mandelic Acid. *Angew. Chemie Int. Ed.* **2005**, *44* (11), 1690–1693.

(38) Yu, S.; Pu, L. Pseudoenantiomeric Fluorescent Sensors in a Chiral Assay. *J. Am. Chem. Soc.* **2010**, *132* (50), 17698–17700.

(39) Yu, S.; Plunkett, W.; Kim, M.; Pu, L. Simultaneous Determination of Both the Enantiomeric Composition and Concentration of a Chiral Substrate with One Fluorescent Sensor. *J. Am. Chem. Soc.* **2012**, *134*, 50, 20282-20285.

(40) Wang, C.; Wu, E.; Wu, X.; Xu, X.; Zhang, G.; Pu, L. Enantioselective Fluorescent Recognition in the Fluorous Phase: Enhanced Reactivity and Expanded Chiral Recognition. *J. Am. Chem. Soc.* **2015**, *137*, 11, 3747-3750.

(41) Feuster, E. K.; Glass, T. E. Detection of Amines and Unprotected Amino Acids in Aqueous

Conditions by Formation of Highly Fluorescent Iminium Ions. *J. Am. Chem. Soc.* **2003**, *125*, 16174–16175.

(42) Huang, Z.; Yu, S.; Wen, K.; Yu, X.; Pu, L. Zn(Ii) Promoted Dramatic Enhancement in the Enantioselective Fluorescent Recognition of Functional Chiral Amines by a Chiral Aldehyde. *Chem. Sci.* **2014**, *5* (9), 3457–3462.

(43) Song, T.; Cao, Y.; Zhao, G.; Pu, L. Fluorescent Recognition of Zn 2+ by Two Diastereomeric Salicylaldimines: Dramatically Different Responses and Spectroscopic Investigation. *Inorg. Chem* **2017**, *56*, 8, 4395-4399.

(44) Zeng, C.; Zhang, X.; Pu, L. Enantioselective Fluorescent Imaging of Free Amino Acids in Living Cells. *Chem. - A Eur. J.* **2017**, *23* (10), 2432–2438.

(45) Nian, S.; Pu, L. Amphiphilic Polymer-Based Fluorescent Probe for Enantioselective Recognition of Amino Acids in Immiscible Water and Organic Phases. *Chem. - A Eur. J.* **2017**, *23* (71), 18066–18073.

(46) Zhao, F.; Du, Y.; Tian, J.; Shi, D.; Wang, Y.; Hu, L.; Yu, S.; Yu, X.; Pu, L. Enantioselective Fluorescent Recognition of Amino Acids in Aqueous Solution by Using a Chiral Aldehyde Probe. *European J. Org. Chem.* **2018**, *2018* (16), 1891–1895.

(47) Iqbal, S.; Yu, S.; Jiang, L.; Wang, X.; Chen, Y.; Wang, Y.; Yu, X.; Pu, L. Simultaneous Determination of Concentration and Enantiomeric Composition of Amino Acids in Aqueous Solution by Using a Tetrabromobinaphthyl Dialdehyde Probe. *Chem. – A Eur. J.* **2019**, *25* (42), 9967–9972.

(48) Zhu, Y.-Y.; Wu, X.-D.; Gu, S.-X.; Pu, L. Free Amino Acid Recognition: A Bisbinaphthyl-Based Fluorescent Probe with High Enantioselectivity. *J. Am. Chem. Soc.* **2019**, *141*, 1, 175-181.

(49) Zeng, C.; Zhang, X.; Pu, L. Enhanced Enantioselectivity in the Fluorescent Recognition of a Chiral Diamine by Using a Bisbinaphthyl Dialdehyde. *ACS Omega* **2018**, *3* (10), 12545–12548.

(50) Haupt, K.; Mosbach, K. Molecularly Imprinted Polymers and Their Use in Biomimetic Sensors. *Chem. Rev.* **2000**, *100* (7), 2495–2504.

(51) Tiwari, M. P.; Prasad, A. Molecularly Imprinted Polymer Based Enantioselective Sensing Devices: A Review. *Anal. Chim. Acta* **2015**, *853* (1), 1–18.

(52) Chen, Y.; Shimizu, K. D.; Angew, A. H.; Angew, D. Measurement of Enantiomeric Excess Using Molecularly Imprinted Polymers4) (A. *c). Chem., Int. Ed. Engl* **2001**, *40* (2), 37.

(53) Liu, F.; Liu, X.; Ng, S. C.; Chan, H. S. O. Enantioselective Molecular Imprinting Polymer Coated QCM for the Recognition of L-Tryptophan. *Sensors Actuators, B Chem.* **2006**, *113* (1), 234–240.

(54) Liao, Y.; Wang, W.; Wang, B. Building Fluorescent Sensors by Template Polymerization: The Preparation of a Fluorescent Sensor for L-Tryptophan. *Bioorg. Chem.* **1999**, *27* (6), 463–476.

(55) Iskierko, Z.; Checinska, A.; Sharma, P. S.; Golebiewska, K.; Noworyta, K.; Borowicz, P.; Fronc, K.; Bandi, V.; D'souza, F.; Kutner, W. Molecularly Imprinted Polymer Based Extended-Gate Field-Effect Transistor Chemosensors for Phenylalanine Enantioselective Sensing †. *J. Mater. Chem. C* **2017**, *5*, 969.

(56) Uekama, K.; Hirayama, F.; Irie, T. Cyclodextrin Drug Carrier Systems. *Chem. Rev.* **1998**, *98* (5), 2045–2076.

(57) Impellizzeri, G.; Maccarrone, G.; Rizzarelli, E.; Vecchio, G.; Corradini, R.; Marchelli, R. 6-Deoxy-6-N-Histamino-β-Cyclodextrin Copper(II) Complex, a New Enantioselective

Receptor for Aromatic Amino Acids. *Angew. Chemie Int. Ed.* **1991**, *30* (10), 1348–1349.

(58) Pagliari, S.; Corradini, R.; Galaverna, G.; Sforza, S.; Dossena, A.; Marchelli, R. Enantioselective Sensing of Amino Acids by Copper(II) Complexes of Phenylalanine-Based Fluorescent β-Cyclodextrins. *Tetrahedron Lett.* **2000**, *41* (19), 3691–3695.

(59) Corradini, R.; Paganuzzi, C.; Marchelli, R.; Pagliari, S.; Sforza, S.; Dossena, A.; Galaverna, G.; Duchateau, A. Design and Synthesis of Fluorescent ?-Cyclodextrins for the Enantioselective Sensing of ?-Amino Acids. *Chirality* **2003**, *15* (S1), S30–S39.

(60) Corradini, R.; Paganuzzi, C.; Marchelli, R.; Pagliari, S.; Sforza, S.; Dossena, A.; Galaverna, G.; Duchateau, A. Fast Parallel Enantiomeric Analysis of Unmodified Amino Acids by Sensing with Fluorescent β-Cyclodextrins. *J. Mater. Chem.* **2005**, *15*, pp 2741–2746.

(61) Minami, T.; Esipenko, N. A.; Zhang, B.; Isaacs, L.; Anzenbacher, P. "'Turn-on'" Fluorescent Sensor Array for Basic Amino Acids in Water †. *Chem. Comm*, **2014**, *50*, 61.

(62) Leonard, N. J.; Ning, R. Y. The Synthesis and Stereochemistry of Substituted 1,4-Thiazepines Related to the Penicillins. *J. Org. Chem.* **1966**, *31* (12), 3928–3935.

(63) Yang, X.; Guo, Y.; Strongin, R. M. Conjugate Addition/Cyclization Sequence Enables Selective and Simultaneous Fluorescence Detection of Cysteine and Homocysteine. *Angew. Chemie Int. Ed.* **2011**, *50* (45), 10690–10693.

(64) Huang, Z.; Du, J.; Zhang, J.; Yu, X.-Q.; Pu, L. A Simple and Efficient Fluorescent Sensor for Histidine. *Chem. Commun* **2012**, *48*, 3412-3414.

(65) Morgan, G.; Burstall, F. H. Researches on Residual Affinity and Co-Ordination. Part XXXVII. Complex Metallic Salts Containing 2:6-Di-2′-Pyridylpyridine (2:2′:2″-Tripyridyl). *J. Chem. Soc.* **1937**, *0* (0), 1649–1655.

(66) Barlow, C. K.; Moran, D.; Radom, L.; McFadyen, W. D.; O'Hair, R. A. J. Metal-Mediated

Formation of Gas-Phase Amino Acid Radical Cations. *J. Phys. Chem. A* **2006**, *110* (27), 8304–8315.

(67) Rubingh, D. N. Mixed Micelle Solutions. In *Solution Chemistry of Surfactants*; Springer New York, 1979; pp 337–354.

(68) Owen, S. C.; Chan, D. P. Y.; Shoichet, M. S. Polymeric Micelle Stability. *Nano Today*. 2012, *7* (1), pp 53–65.

(69) Chen, L.; Xie, Z.; Hu, J.; Chen, X.; Jing, X. Enantiomeric PLA-PEG Block Copolymers and Their Stereocomplex Micelles Used as Rifampin Delivery. *J Nanopart Res*, **2007**, *9*, 777-785.

(70) Shao, K.; Huang, R.; Li, J.; Han, L.; Ye, L.; Lou, J.; Jiang, C. Angiopep-2 Modified PE-PEG Based Polymeric Micelles for Amphotericin B Delivery Targeted to the Brain. *J. Control. Release* **2010**, *147* (1), 118–126.

(71) Alexandridis, P.; Hatton, T. A. Poly(ethylene oxide)-poly(propylene oxide)-poly(ethylene oxide) block copolymer surfactants in aqueous solutions and at interfaces: thermodynamics, structure, dynamics, and modeling. *Colloids Surf. A Physicochem. Eng. Asp.* **1995**, *96*, 1-46.

(72) Al Khateb, K.; Ozhmukhametova, E. K.; Mussin, M. N.; Seilkhanov, S. K.; Rakhypbekov, T. K.; Lau, W. M.; Khutoryanskiy, V. V. In Situ Gelling Systems Based on Pluronic F127/Pluronic F68 Formulations for Ocular Drug Delivery. *Int. J. Pharm.* **2016**, *502* (1–2), 70–79.

(73) Grossen, P.; Witzigmann, D.; Sieber, S.; Huwyler, J. PEG-PCL-Based Nanomedicines: A Biodegradable Drug Delivery System and Its Application. *J. Control. Release*. **2017**, 260, pp 46–60.

Chapter 2. Micelle-Encapsulated Fluorescent Probe: Chemoselective and Enantioselective Recognition of Lysine in Aqueous Solution

2.1 Introduction

2.1.1 Importance of D-Amino Acids

L-Amino acids are the fundamental building blocks in protein construction, and they also play important biological roles in metabolism, immune responses, and reproduction and neuroendocrine regulation.[1–3] D-Amino acids, though much less common in comparison with their L-enantiomers, have also been identified in live organisms, and more and more research has uncovered their biological significance.[4] For example, D-Serine, is an agonist of N-methyl-D-aspartate receptor, whose disorder is related to diseases including Schizophrenia, ischemia, neurodegenerative disorders.[5–8]

2.1.2 Fluorescent Methods for the Detection of Chiral Amino Acids

Chemoselective detection of amino acids have been actively investigated by either single-receptor fashions or array-based approaches,[9–11] and recent progress has also been made for the enantioselective detection of L- and D-amino acids.[9] However, development of fluorescent probes to carry out both chemoselective as well as enantioselective detection of amino acids still remains a big challenge in this area.

In 2014, we reported the use of the 1,1'-bi-2-naphthol (BINOL)-based compound (*S*)-**2.1** as a fluorescent probe for amino acids.[12a] It was found that (*S*)-**2.1** in combination with Zn(II) exhibits enantioselective fluorescent enhancement in the presence of a few amino acids in methanol solution. However, this fluorescent recognition of amino acids cannot be conducted in

aqueous solution because of the insolubility of (*S*)-**2.1** in water. In addition, the aldimine products formed from the condensation of (*S*)-**2.1** with the tetrabutyl ammonium salts of amino acids in methanol solution quickly undergo hydrolysis in water driven by the precipitation of (*S*)-**2.1**. In order to carry out the enantioselective fluorescent recognition of amino acids in aqueous media for potential biological application, we have covalently linked (*S*)-**2.1** with water soluble poly(N-isopropylacrylamide)s or polyethyleneglycol oligomers at the 6,6'-positions of the BINOL unit.[12b,c] Because additional synthetic steps are required to prepare those water-soluble materials, additional strategy for water solubility is needed.

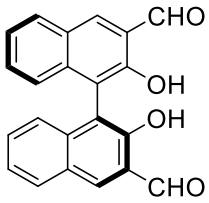

(*S*)-**2.1**

2.1.3 Block Copolymers for Micelle Encapsulation

Block copolymers are known to readily undergo microphase separation in selected solvents to form micelles.[13,14] Particularly, block copolymers consisting of both hydrophilic and hydrophobic segments can encapsulate small organic molecules into micelles and solubilize them in aqueous environments.[15,16] Representative examples of such block copolymers including polyethylene glycol–polylactic acid (PEG–PLA)[15], polyethylene glycol–polycaprolactone (PEG–PCL)[17], and triblock polymers such as PLA–PEG–PLA.[18] PEG–PLA block copolymer and its derivatives can enhance the hydrophobic drug loading, reduce the burst effect, avoid being engulfed by phagocytes, increase the circulation time of drugs in blood, improve bioavailability, and accumulate in inflammation or target locations.[15] The biodegradable polyethylene glycol–poly L-lactic acid (mPEG–PLLA) as shown below is a material often used due to its excellent biocompatibility.[19–21] Previously, polymer-based micelles were used for the fluorescent

recognition of chiral compounds but the difference between the fluorescence responses of the two enantiomers of the substrates in the micelles was small.[22] We propose to use the micelles formed by the diblock copolymer mPEG–PLLA to encapsulate (*S*)-**2.1** in water to carry out the fluorescent recognition of amino acids. We have demonstrated that such micelle encapsulated (*S*)-**2.1** shows both high chemoselectivity as well as high enantioselectivity in the fluorescent recognition of lysine (Lys) in aqueous media.[23] Herein, these results are reported.

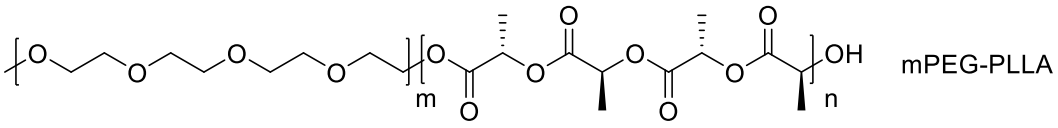

2.2 Results and Discussion

2.2.1 Block Copolymer Synthesis

We prepared a diblock copolymer from mPEG and L-lactide (LLA) following the literature procedure[24] (Scheme 2.1). This process generated a polymer with very narrow polydispersity: M_n (GPC/MALS) = 6500, polydispersity index (PDI) = 1.08. The enantiomer D-lactide (DLA) was also polymerized under the same conditions to give mPEG-PDLA: M_n = 7300 and PDI = 1.04.

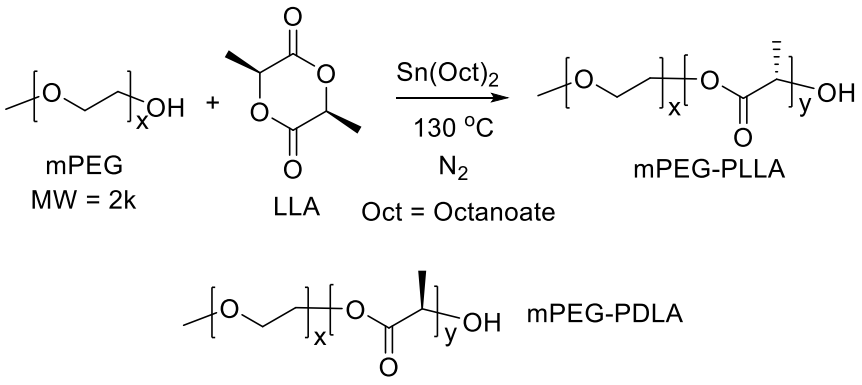

Scheme 2. 1 Synthesis of mPEG-PLLA.

2.2.2 Micelle Probe Preparation

We studied the use of mPEG-PLLA to encapsulate (*S*)-**2.1** by a nano precipitation method.[25] A solution of (*S*)-**2.1** and mPEG-PLLA in DMF was added to a vortex of water at rate

of 1 mL/min. After addition, the vortex was extended for 30 min which was dialyzed with Spectra/Por 4 Dialysis Tubing in water to form a micelle solution containing 2.0 x 10^{-5} M (*S*)-**2.1**, represented as ML-*S*1 [or (*S*)-**2.1**@PEG-PLLA]. It was found that this method gave micelles with smaller sizes than the cosolvent evaporation method (Figure S2.1). In the same way, a MD-*R*1 [or (*S*)-**2.1**@PEG-PDLA] solution was prepared from the interaction of (*S*)-**2.1** with mPEG-PDLA as an analog of the enantiomer of ML-*S*1.

2.2.3 Fluorescence Studies

2.2.3.1 Amino Acids Screening

The ML-*S*1 solution in carbonate buffer (CBS, pH = 10.1) was used to interact with various amino acids at room temperature in the presence of $Zn(OAc)_2$ [2.0 equiv vs (*S*)-**2.1**]. We found that the fluorescence of the micelle probe solution can be turned on by D-Lys and the fluorescence intensity increased continuously over time. This indicates that the reaction of (*S*)-**2.1**with the amino acid in the presence of $Zn(OAc)_2$ progressed continuously at room temperature. In order to carry out more stable fluorescence measurement, we allowed the reaction of ML-*S*1+Zn(II) with all the amino acids to proceed at room temperature for 3 h and then stop the reaction with an ice-water bath. The fluorescence was then measured at 5 ^{o}C. This gave stable fluorescence measurement, indicating the reaction in micelle was effectively quenched at the low temperature.

As the results summarized in Figure 2.1 shown, among all the D- and L-amino acids (10 equiv) tested, only D-Lys greatly enhanced the fluorescence of ML-*S*1 at λ = 528 nm with high enantioselectivity. Trp and Arg showed much smaller increase and all the other amino acids do not cause significant fluorescence response. Thus, ML-*S*1 has exhibited both high chemoselectivity and enantioselectivity in the fluorescent recognition of Lys. L-Lys is an essential amino acid whose analysis has been extensively studied[23a] but little study was conducted on

developing fluorescent probe for both chemoselective and enantioselective recognition of Lys.[23b,c] The diblock copolymer-based micelles have provided the chemoselectivity in aqueous solution very different from (*S*)-**2.1** which shows enantioselective fluorescence enhancement with many functional amines in methanol solution.[12a]

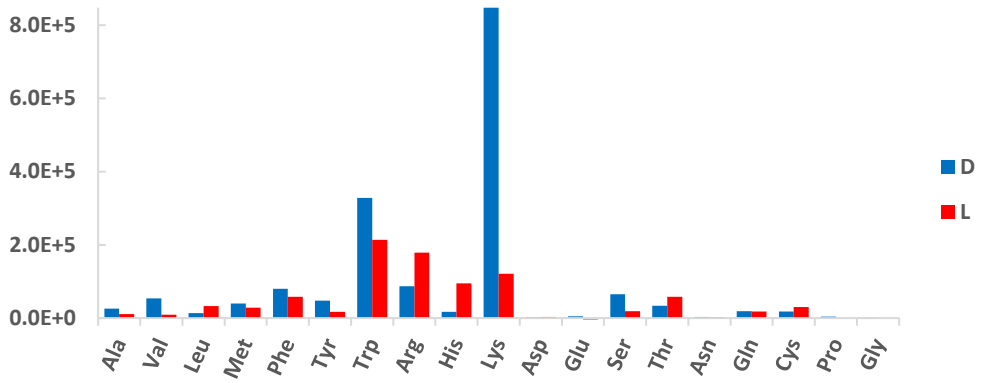

Figure 2. 1 Fluorescence intensity of micelle M*L*-*S***1** [1.0 x 10^{-5} M (*S*)-**2.1**] with $Zn(OAc)_2$ (2.0 equiv) and D-/L-amino acids (10 equiv) in carbonate buffer solutions (pH = 10.1). Peak intensities at 528 nm were recorded at 5 °C after mixed at rt for 3 h and quenched with ice-water bath (λ_{exc}= 407 nm, slit 3/3 nm, int time 0.3 s. Y axis: fluorescence intensity minus that of M*L*-*S***1**+Zn(II)/arbitrary unit.).

2.2.3.2 Concentration Detection

Figure 2a gives the fluorescence spectra of ML-*S*1 [2.0 x 10^{-5} M of (*S*)-**2.1**, 1.0 mL], CBS buffer (1.0 mL, pH = 10.1) with $Zn(OAc)_2$ (2.0 equiv, 10 µL of the 4 mM stock solution) upon addition of D-/L-Lys (10.0 equiv, 10 µL of 20 mM stock solution). It shows that D-Lys greatly enhanced the fluorescence of ML-*S*1+Zn(II) at 528 nm by 9.4 fold and L-Lys gave much weaker fluorescence enhancement at 550 nm. The enantioselective fluorescence enhancement ratio [ef = $(I_D-I_0)/(I_L-I_0)$. I_D, I_L and I_0: fluorescence intensity at 528 nm with and without D-/L-Lys respectively.] was found to be 6.6, representing a high enantioselectivity. The fluorescence intensity of ML-S1 at λ= 528 nm versus the stoichiometry of D- and L-Lys is plotted in Figure 2b. It shows that when D-Lys was increased from 1 to 10 equiv, the fluorescence of ML-*S*1 increased

greatly. When D-Lys was larger than 10 equiv, the fluorescence enhancement became small. When L-Lys was used, only very small fluorescence enhancement was observed.

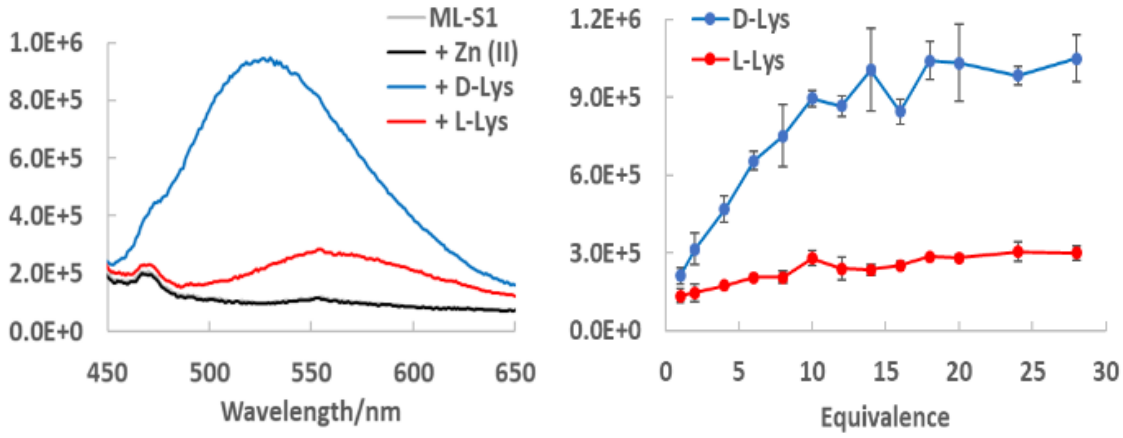

Figure 2. 2 (a) Left, Fluorescence spectra of M*L*-*S***1** [2.0 x 10^{-5} M of (*S*)-**2.1**)] with $Zn(OAc)_2$ (2.0 equiv), Lys (10.0 equiv) in carbonate buffer solutions (using 20 mM Lys stock solution). Spectra were recorded at 5 °C after mixing at rt for 3 h. (b) Right, Fluorescence intensity at λ = 528 nm versus equivalency of D- and L-Lys. (The error bars were obtained by 3 independent measurements. λ_{exc}= 407 nm, slit 3/3 nm, int time 0.3 s. Y axis: intensity/arbitrary unit)

2.2.3.3 ee Detection

MD-*R*1, the enantiomeric analog of ML-*S*1, was also used to interact with $Zn(OAc)_2$ and D-/L-Lys. Under the same conditions, the fluorescence responses of MD-*R*1+Zn(II) toward D-/L-Lys are close to a mirror image relationship with those when ML-*S*1 was used (Figure S2.5). This confirms the chiral recognition process in this fluorescent detection of Lys.

We then studied the fluorescence response of ML-*S*1 and MD-*R*1 toward Lys at various enantiomeric excess (ee = [D-L]/[D+L]). As shown in Figure 2.3, the fluorescence enhancements at 528 nm for ML-*S*1 and MD-*R*1 resemble a mirror image relationship. The small deviation from an exact mirror image fluorescence response between ML-*S*1 and MD-*R*1 could be attributed to the random conformations of the block copolymers in the micelles and the distributions of the micelle sizes.

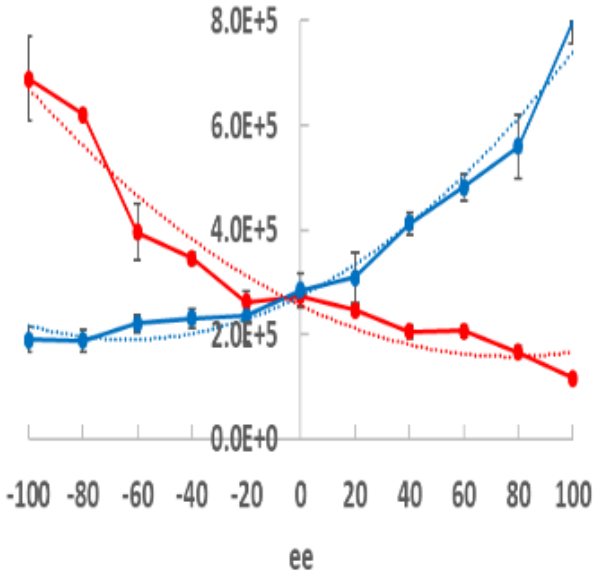

Figure 2. 3 Fluorescence intensity at λ = 528 nm versus ee of Lys for the reaction of ML-*S***1** (red) or MD-*R***1** (blue) with $Zn(OAc)_2$ (2.0 equiv) and Lys (10.0 equiv, from L-Lys to D-Lys: -100 to 100% ee) in CBS. Spectra were recorded at 5 °C after mixing at rt for 3 h (λ_{exc} = 407 nm, slit 3/3 nm, int time 0.3 s. X axis: ee %. Y axis: intensity/arbitrary unit).

2.2.4 Characterization of Micelles

The size of ML-S1 was characterized by dynamic light scattering (DLS) and transmission electron cryomicroscopy (cryo-TEM). DLS results (Figure S2.2) of ML-*S*1 had a narrow distribution with the size close to 10 nm. After interaction with either D- or L-Lys, the sizes of micelles inflated to 30-100 nm and had broader PDI. ML-*S*1 and MD-*R*1 did not have the exact same behaviors when observed by DLS which could be attributed to a result of intrinsic differences of the block polymer mPEG-PLLA and mPEG-PDLA, as they had slight variations on molecular weight and PDI.

The micelle structures were directly visualized through cryo-TEM. Cryo-TEM images showed that ML-*S*1 always maintained a size of around 10 to 30 nm, regardless whether it was treated with Lys analytes or not. This is quite different from that measured by DLS. The difference between the two techniques could be due to the fact that, not just sizes but also the shapes would

influence the DLS results.[26] The sensing reaction required Zn(II) and Lys to travel inside the micelles, and the shape of the micelles would be varied along the reaction process.

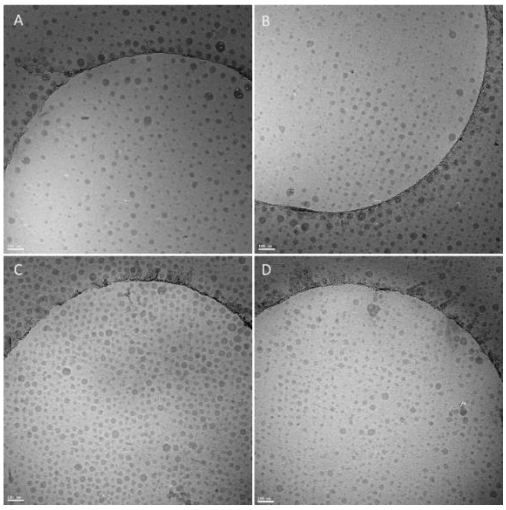

Figure 2. 4 Cryo-TEM imaging. A. M*L*-*S***1**; B. M*L*-*S***1** with 2 equiv $Zn(OAc)_2$ in carbonate buffer solutions; C. M*L*-*S***1** with 2 equiv $Zn(OAc)_2$ and 10 equiv of D-Lys in carbonate buffer solutions; D. M*D*-*R***1** with 2 equiv $Zn(OAc)_2$ and 10 equiv of L-Lys in carbonate buffer solutions. Concentration: M*L*-*S***1** 100 μM, M*D*-*R***1** 100 μM, $Zn(OAc)_2$ 200 μM, Lys 1 mM, PEG-PLLA/PEG-PDLA 5 mg/mL. Scale bar: 100 nm.

2.2.5 Mechanistic Studies

We studied the reaction of (*S*)-**2.1**+Zn(II) with Lys in DMSO-d_6/D_2O by ^1H NMR spectroscopic analysis because of the difficulty to directly study the reaction of ML-*S*1+Zn(II) with Lys (10.0 equiv) in the micelle solution by NMR. The reaction between (*S*)-**2.1** and Lys finished within 15 min with either D- (Figure S2.9a) or L-Lys (Figure S2.9b). As shown in Figure S2.10, when a mixture of (*S*)-**2.1** (2.0 mM) with Zn(II) (2.0 equiv) in DMSO-d_6 was treated with D-Lys (1 – 14 equiv in D_2O) within 30 min, the aldehyde peak of (*S*)-**2.1** at $\delta = 10.24$ (s) completely disappeared when > 6 equiv D- or L-Lys was used. A new product formed with 5 aromatic signals suggesting a symmetric product with an imine proton signal observed at $\delta = 8.76$ (s). Our NMR analyses including NOESY, HSQC, HMBC (Figure S2.11) support the condensation of the terminal amino groups of Lys with the aldehyde groups of (*S*)-**2.1** to form the aldimine product

2.2. Thus, the high chemoselectivity of ML-*S*1 for the fluorescent recognition of Lys over other amino acids could be attributed to the chemoselective reaction of the terminal amine group of Lys with (*S*)-**2.1**.

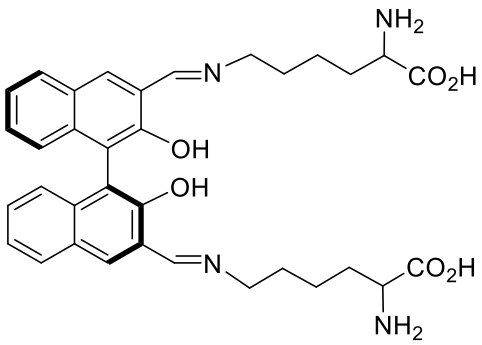

2.2

The structure of **2.2** and its Zn(II) complex are also supported by mass spectroscopic analyses. Mass spectrum (ES) of the reaction mixture of (*S*)-**2.1** (2.0 mM), Zn(OAc)2 (2 equiv), D-Lys (10.0 equiv) in DMSO-d_6:D_2O = 5:1 was obtained. As shown in Figure S2.12a, a peak at m/z = 659.3 was observed for the Zn(II) complex of **2.2** (calculated for [**2.2**+Zn-3H]: 659.2), and a peak at m/z = 597.2716 was observed for **2.2** (calculated for [**2.2**-H]: 597.2713) (Figure S2.12d). Under the same conditions, when L-Lys was used, the mass spectrum does not give the signal for the Zn(II) complex of **2.2** although the same peak at m/z = 597.2716 was observed for **2.2**. This indicates that the Zn(II) complex of **2.2** derived from D-Lys might be more stable than that from L-Lys. Previously, we have demonstrated that coordination of aldimine compounds like **2.2** with Zn(II) leads fluorescence enhancement at $\lambda > 500$ nm.[12a] The stability difference between the Zn(II) complex of **2.2** derived from D-Lys and that from L-Lys might have contributed to the observed highly enantioselective fluorescence response.

2.3 Conclusion

In conclusion, by using a diblock copolymer-based micelle, we have discovered that an amino acid can be discriminated by a fluorescence probe in water solution with both high chemoselectivity and high enantioselectivity. The use of the micelle strategy avoids the synthesis of the water-soluble fluorescent probe and has potential to be generally applicable in the development of enantioselective fluorescent sensors in aqueous media. The structure of the micelle was characterized by DLS and Cryo-TEM. On the basis of NMR and mass spectroscopic study, it is proposed that the high chemoselectivity of the fluorescence probe in the recognition of Lys could be due to the chemoselective reaction of the terminal amine group of Lys with the aldehyde group of the probe and the high enantioselectivity due to the different stability of the Zn(II) complexes of the aldimine products formed from the D- and L-enantiomers of the amino acid.

2.4 Experimental

2.4.1 General information

All amino acids and other chemicals were purchased from Sigma Aldrich Chemical Co. or Alfa Aesar, and used without further purification. ^{1}H NMR spectra were recorded on Varian-600 MHz spectrometer. 2D NMR recorded on Bruker-800 MHz spectrometer. Chemical shifts for ^{1}H NMR and 2D NMR were reported in parts per million relative to a singlet at 2.50 ppm for deuterated DMSO. Steady-state fluorescence emission spectra were recorded on Horiba FluoroMax-4 spectrofluorometer. Low-temperature fluorescence emission spectra were recorded on Horiba FluoroMax-3 spectrofluorometer. Nanoparticle sizes and polydispersity were analyzed via dynamic light scattering (DLS, Wyatt, DynaPro). Cryo-TEM images were recorded on a

Tecnai F20 TEM system. For cryoTEM, nanoparticles were concentrated by centrifugation at 8000 rpm for 6 min in a cellulose filter tube (Amicon, Ultra-15, 30000 Da MW cutoff). High-resolution mass spectra were obtained from the University of Illinois at Urbana-Champaign (UIUC) Mass Spectrometry Facility. Deionized water was used for all the experiments.

Nano precipitation to prepare the micelle encapsulated probe. (*S*)-**2.1** (0.272 mL, 1.0 mg/mL in DMF) was combined with the block copolymer mPEG-PLLA (20.0 mg) (mPEG-PDLA for (*R*)-**2.1**). Additional DMF was added to dissolve the block copolymer and the volume was calibrated to 2.0 mL. The solution was sonicated for 10 min and added dropwise to a vortex of water (18 mL) at a rate of 1.0 mL/min. After the addition of the DMF solution, the vortex was allowed to last 30 more min. The final mixture was dialyzed in deionized water to form a micelle solution containing 20 μM (*S*)-**2.1**.

Cosolvent evaporation to prepare the micelle encapsulated probe. (*S*)-**2.1** (0.272 mg) and the block copolymer (20.0 mg) were dissolved in acetone and sonicated for 30 min. After the acetone was evaporated, deionized water (20 mL) was added and the mixture was sonicated for another 30 min. Buffer salt was then added into the mixture to create a micelle solution in buffer.

2.4.2. Dynamic Light Scattering Results

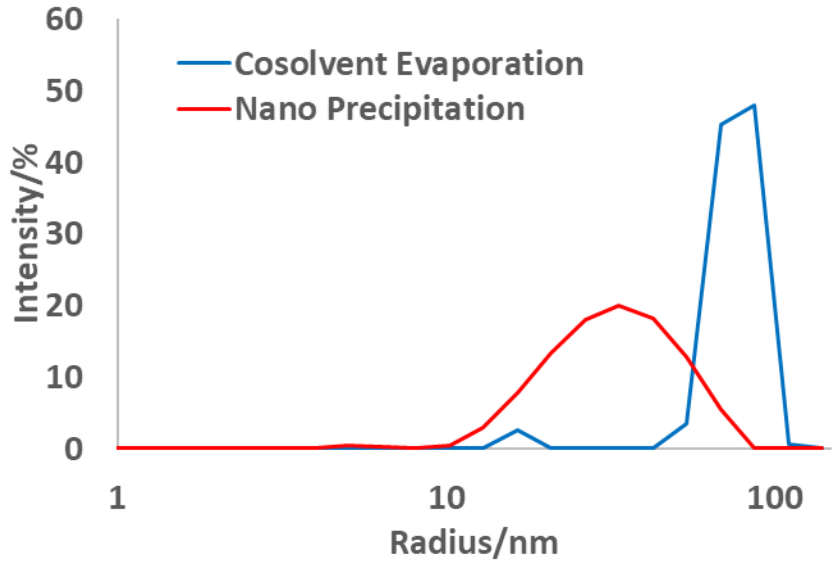

Figure S2. 1 DLS of M*L*-*S***1** prepared through the cosolvent evaporation method and nano precipitation method. (*S*)-**2.1** (2.0×10^{-5} M), PEG-PLLA (1.0 mg/mL).

(a)

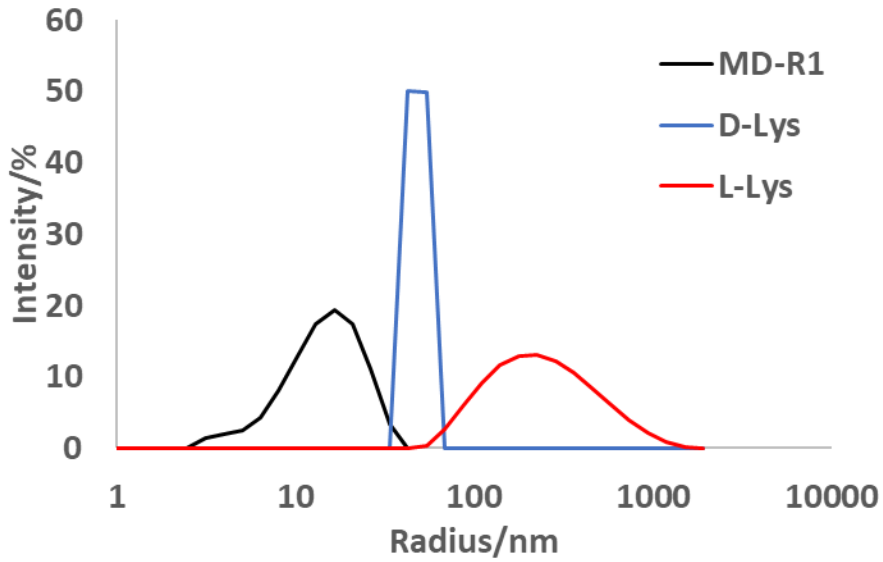

(b)

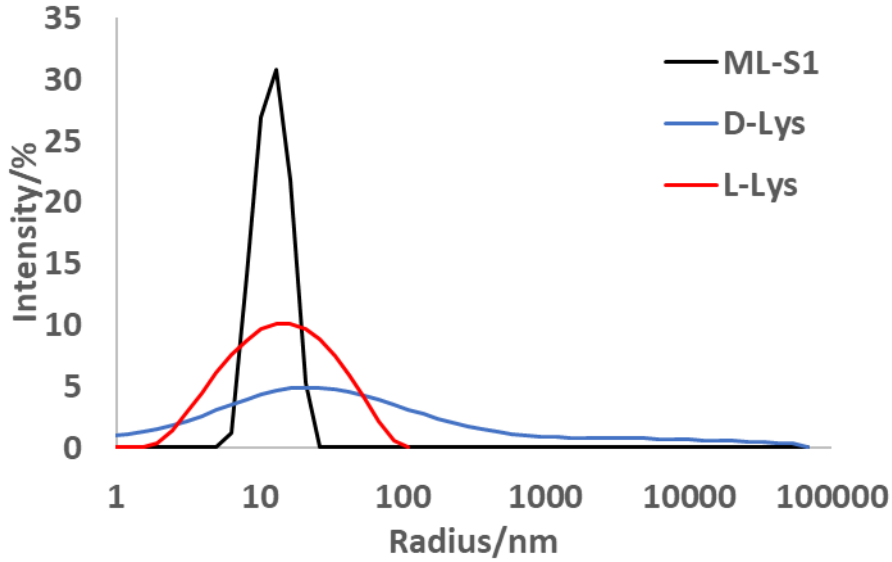

Figure S2. 2 DLS studies of (a) M*D*-*R***1** with $Zn(OAc)_2$ (2.0 equiv) and Lys (10.0 equiv) in carbonate buffer solutions; (b) M*L*-*S***1** with $Zn(OAc)_2$ (2.0 equiv) and Lys (10.0 equiv) in carbonate buffer solutions.

2.4.3. Fluorescence Spectra

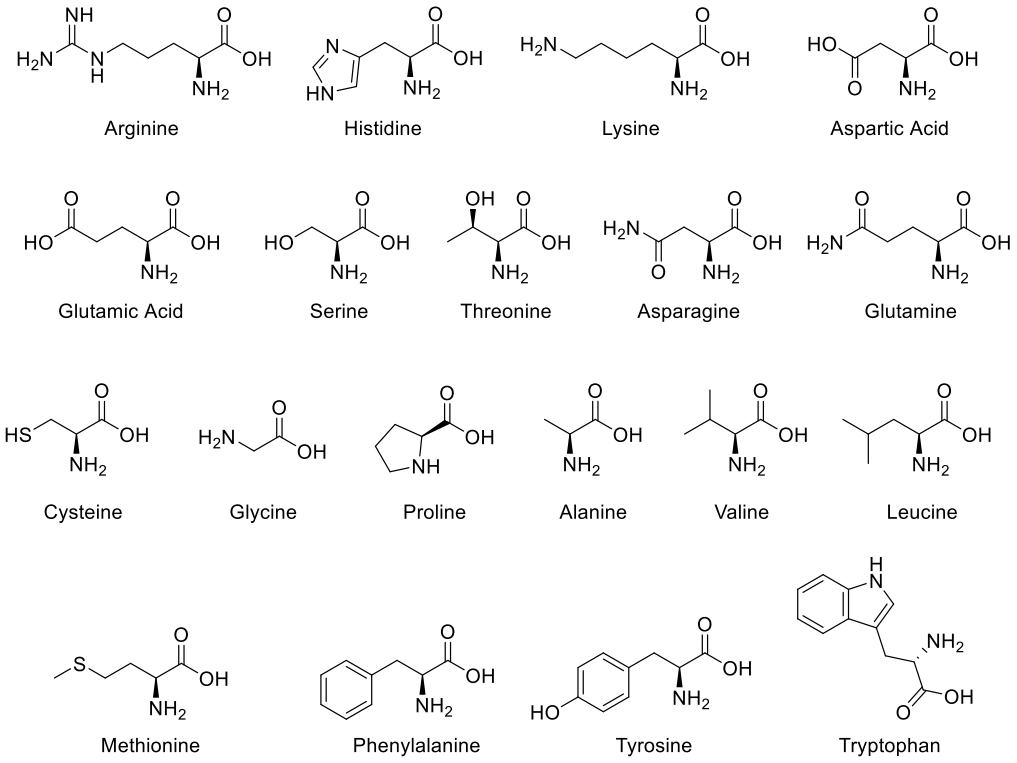

Figure S2. 3 Structure of Chiral Substrates

Low-temperature fluorescence study: To a suspension of the probe M*L*-*S***1** (1 mL, 20 μM) in CBS buffer (1.0 mL) were added an amino acid (10 μL, 20.0 mM in water) and $Zn(OAc)_2$ (10 μL, 4 mM in water). After the mixture was allowed to stand at rt for 3 h, it was chilled with an ice bath, and its fluorescence was measured with FluoroMax3 at 5 ^{o}C with a continuous nitrogen flow. (Slit = 3/3 nm, int time = 0.3 s.)

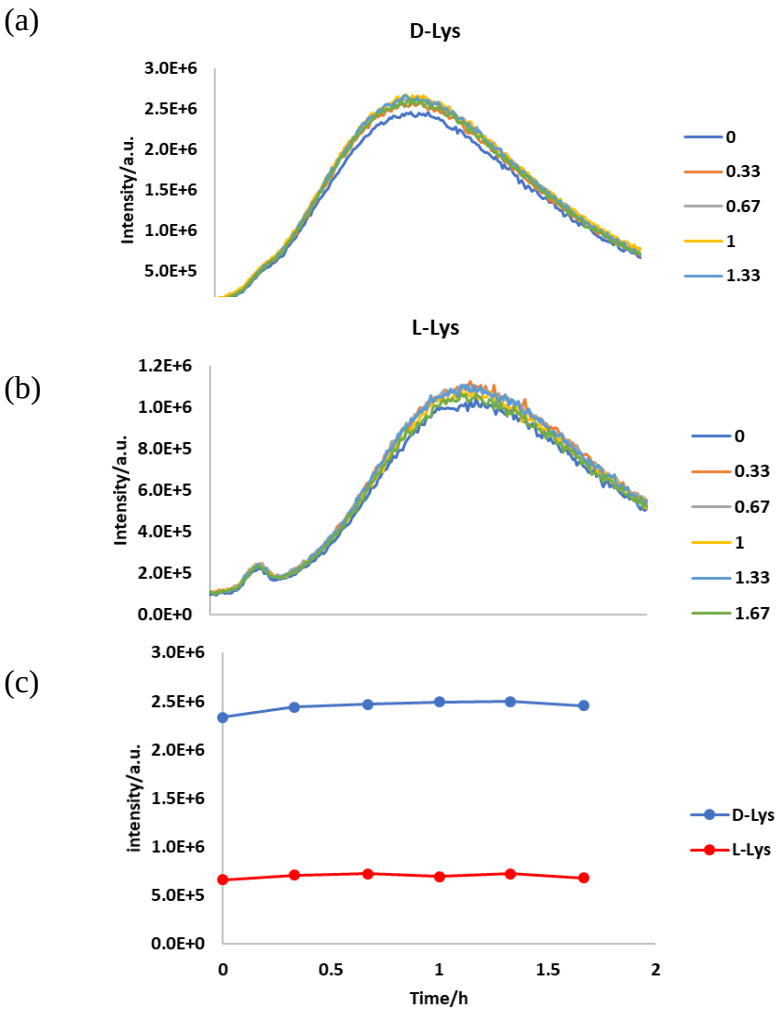

Figure S2. 4 Fluorescence spectra of M*L*-*S***1** with $Zn(OAc)_2$, (2.0 equiv) and 10.0 equiv (a) D-Lys; (b) L-Lys in carbonate buffer solutions. (c) peak intensity at 528 nm was plotted. Spectra were recorded at 5 ^{o}C after mixing at rt for 3 h. (λ_{exc} = 407 nm, slit 3/3 nm, int time 0.3 s.

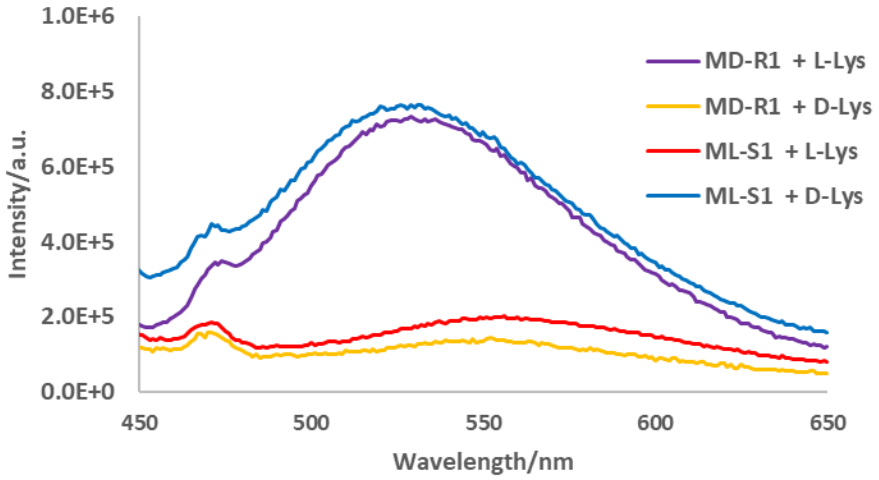

Figure S2. 5 Fluorescence spectra of M*L*-*S***1** and M*D*-*R***1** with $Zn(OAc)_2$ (2.0 equiv) and Lys (10.0 equiv) in carbonate buffer solutions. Spectra were recorded at 5 ^{o}C after mixing at rt for 3 h. (λ_{exc} = 407 nm, slit 3/3 nm, int time 0.3 s.)

(a)

(b)

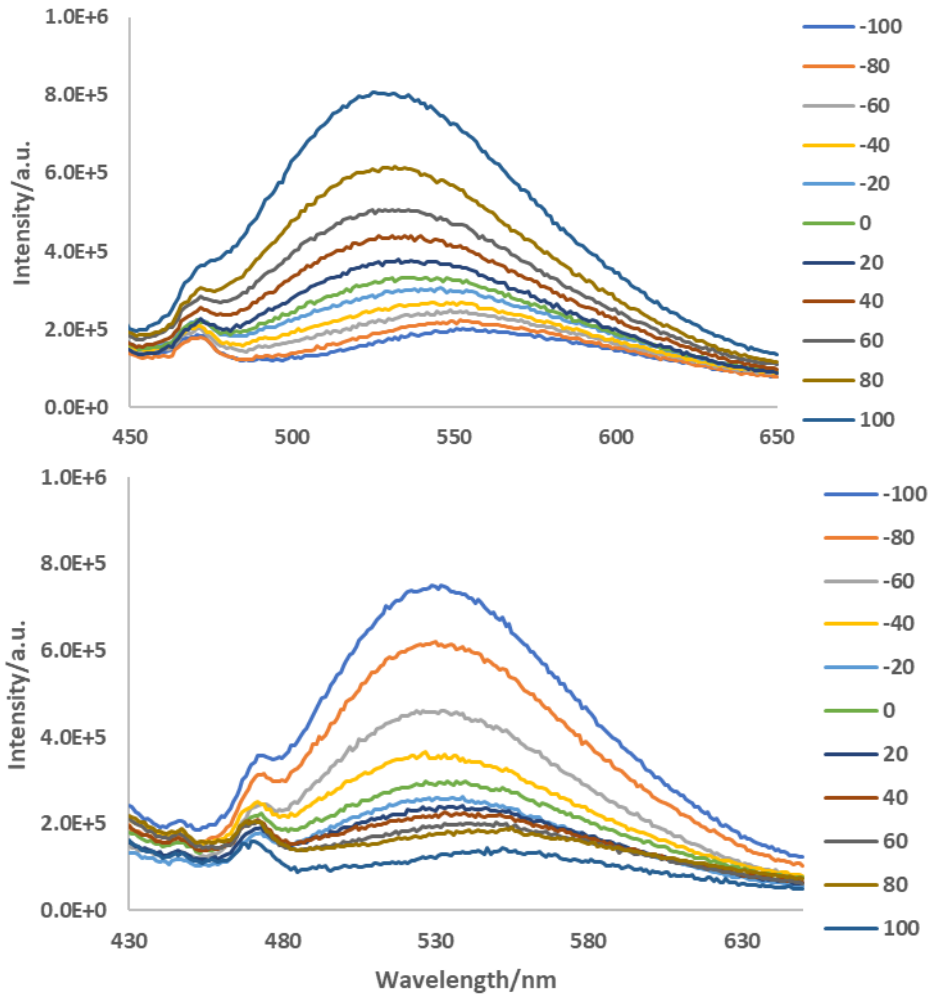

Figure S2. 6 Fluorescence spectra of (a) M*L*-*S***1** and (b) M*D*-*R***1** [1.0 x 10^{-5} M (*S*)- or (*R*)-**1**] towards -100 (L-) to 100 (D-) ee% of Lys (10.0 equiv) with $Zn(OAc)_2$, (2.0 equiv) in carbonate buffer solutions. Spectra were recorded at 5 ^{o}C after mixing at rt for 3 h. (λ_{exc} = 407 nm, slit 3/3 nm, int time 0.3 s.)

(a)

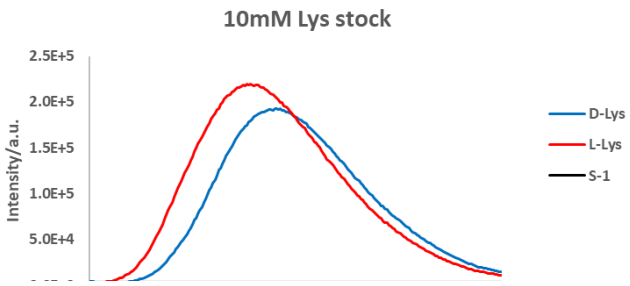

(b)

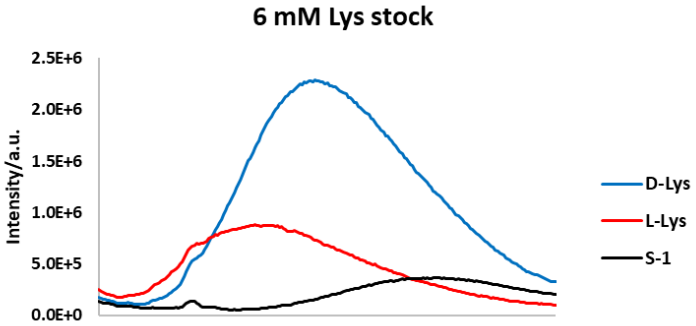

(c)

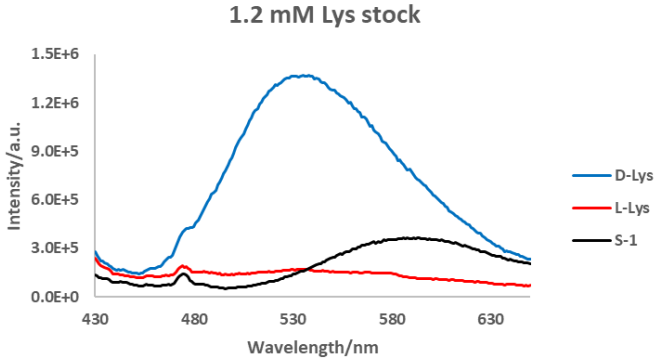

Figure S2. 7 Fluorescence spectra of (*S*)-**1** (20.0 μM) with $Zn(OAc)_2$ (2.0 equiv) and Lys (10.0 equiv) and TBAOH (10.0 equiv) in CH_2Cl_2/MeOH (1:99). (a) 10 mM Lys stock solution in water was used. Spectra were recorded at 5 °C after mixing 3 h at rt. (b) 1.2 mM Lys stock solution in water was used. Spectra were recorded at rt after mixing for 1.5 h at rt. (c) 6 mM Lys stock solution in water was used. Spectra were recorded after 1.5 h and at room temperature. λ_{exc} = 407 nm, slit 3/3 nm, int time 0.3 s. Reference: Huang, Z.; Yu, S.; Wen, K.; Yu, X.; Pu, L. *Chem. Sci.*, **2014**, *5 (9)*, 3457-3462).

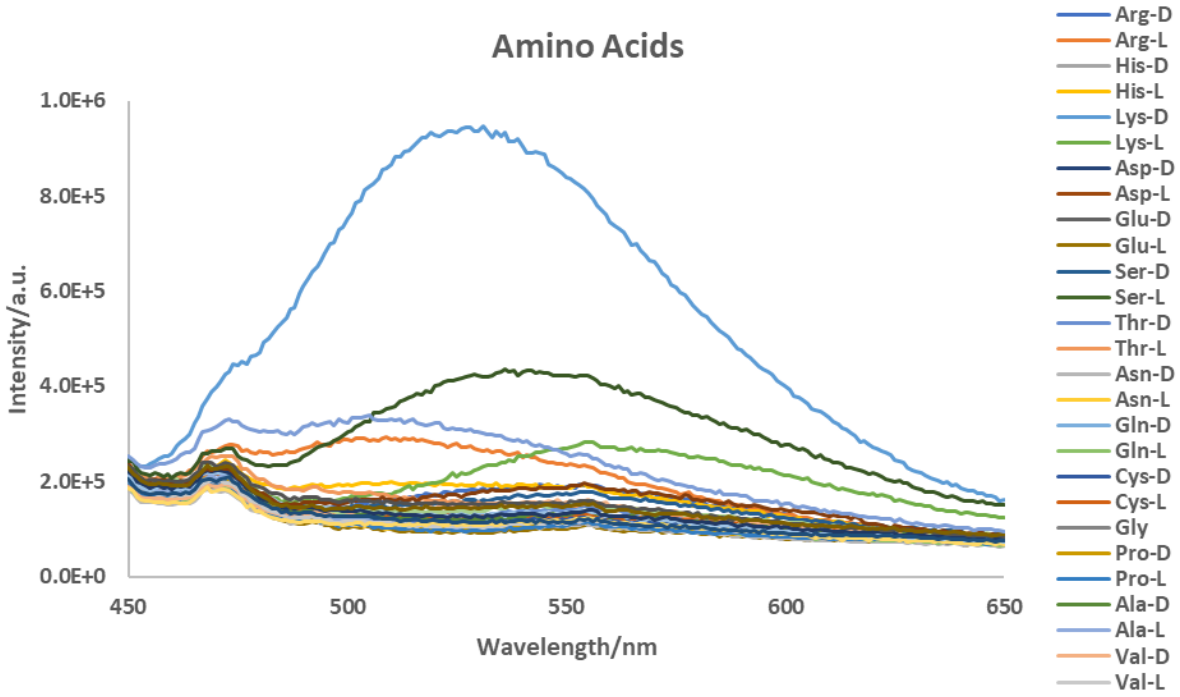

Figure S2. 8 Fluorescence spectra of micelle M*L*-*S***1** with $Zn(OAc)_2$, (2.0 equiv), amino acids (10.0 equiv) in carbonate buffer solutions. Spectra were recorded at 5 ^{o}C after mixing at rt for 3 h. (λ_{exc} = 407 nm, slit 3/3 nm, int time 0.3 s.)

2.4.3. NMR studies for the reaction of (*S*)-2.1 with Lysine

(a)

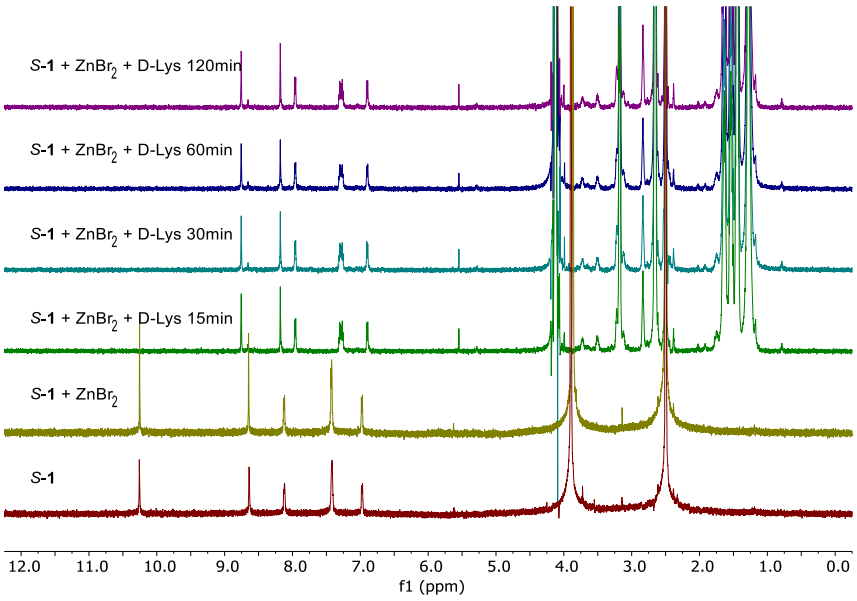

(b)

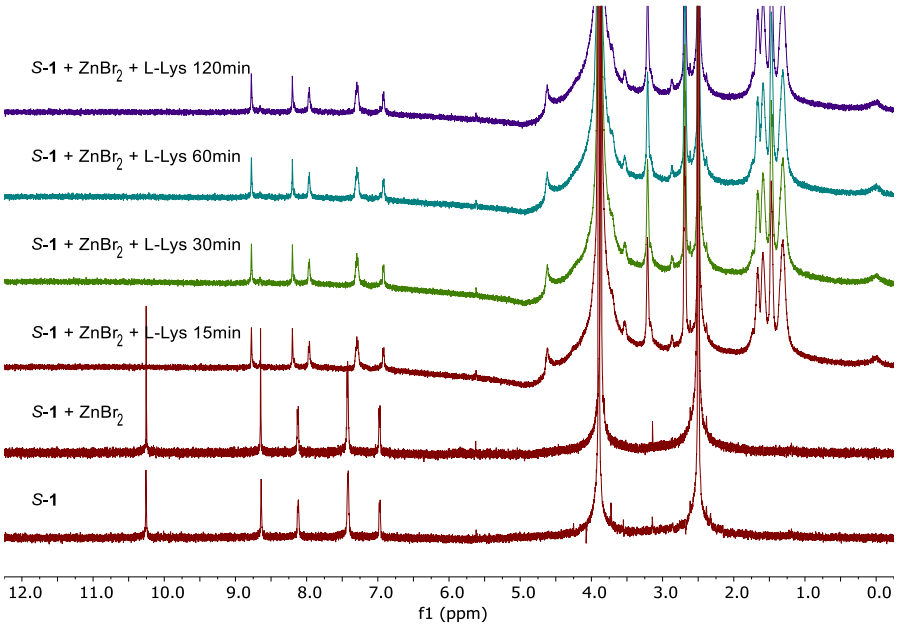

Figure S2. 9 ^{1}H NMR spectra of (*S*)-**2.1** (2.0 mM), Zn(II) (2.0 equiv), (a) D-Lys (10 equiv); (b) L-Lys (10 equiv) in DMSO-d_6:D_2O (5:1) at various reaction time. [$ZnBr_2$ was used for Zn(II)].

(a)

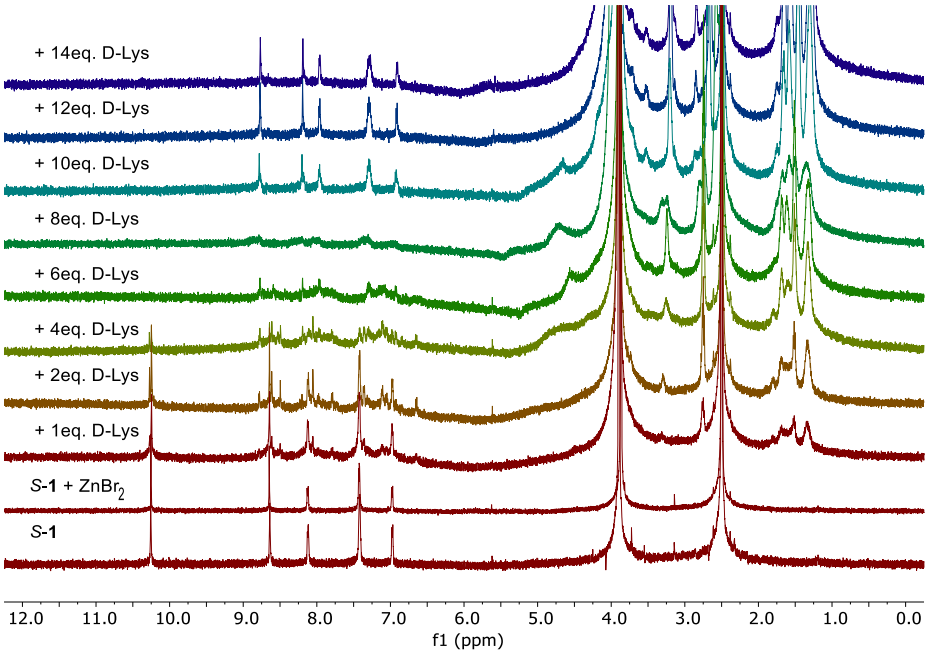

(b)

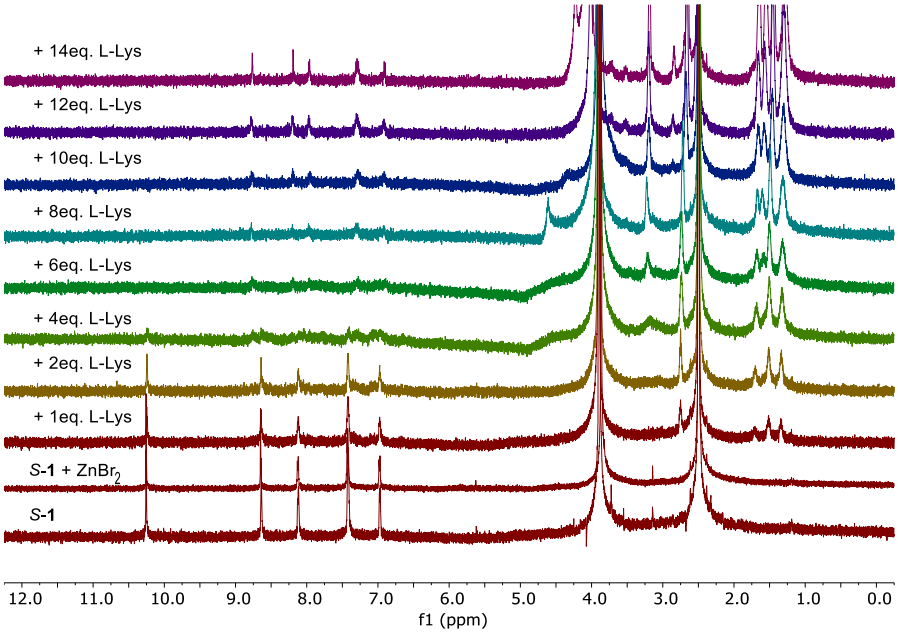

Figure S2. 10 ^{1}H NMR spectra of (*S*)-**2.1** (2.0 mM), Zn(II) (2.0 equiv), and (a) D-; (b) L-Lys (1 – 14 equiv) in DMSO-d_6:D_2O (5:1). (Reaction time = 0.5 h).

In order to identify which one of the two amino groups of Lys reacted with the aldehyde groups of (*S*)-**2.1**, we obtained a NOESY spectrum for the reaction mixture of (*S*)-**2.1** with 10 equiv of L-Lys. It shows cross peaks between the imine proton signal at δ = 8.77 ppm and two proton signals at δ = 3.56 and 3.65 ppm of the $NH_2C\underline{H}_2$- group which supports the condensation of the terminal amino groups of Lys with the aldehyde groups of (*S*)- **2.1** to form the aldimine product **2.2**. HSQC (Figure S2.11b) shows the two proton signals at δ = 3.56 and 3.65 ppm are the two diastereotopic protons of the $=NC\underline{H}_2$- group in the L-Lys unit which are connected to one carbon at δ = 58.8 ppm. Further evidence from HMBC (Figure S2.11c) indicates the correlation between the carbon signal of the $=N\underline{C}H_2$- group at δ = 58.8 ppm and the imine proton signal of the $Ar\underline{C}H{=}N$- group at δ = 8.77 ppm.

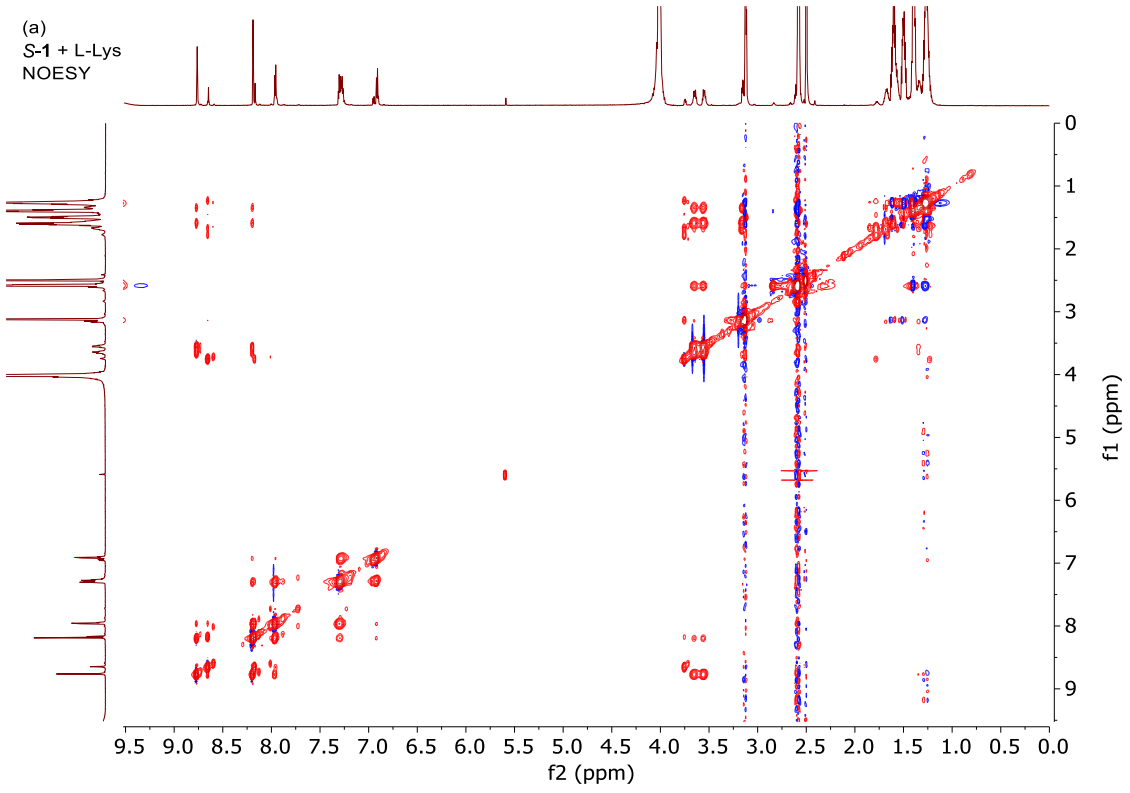

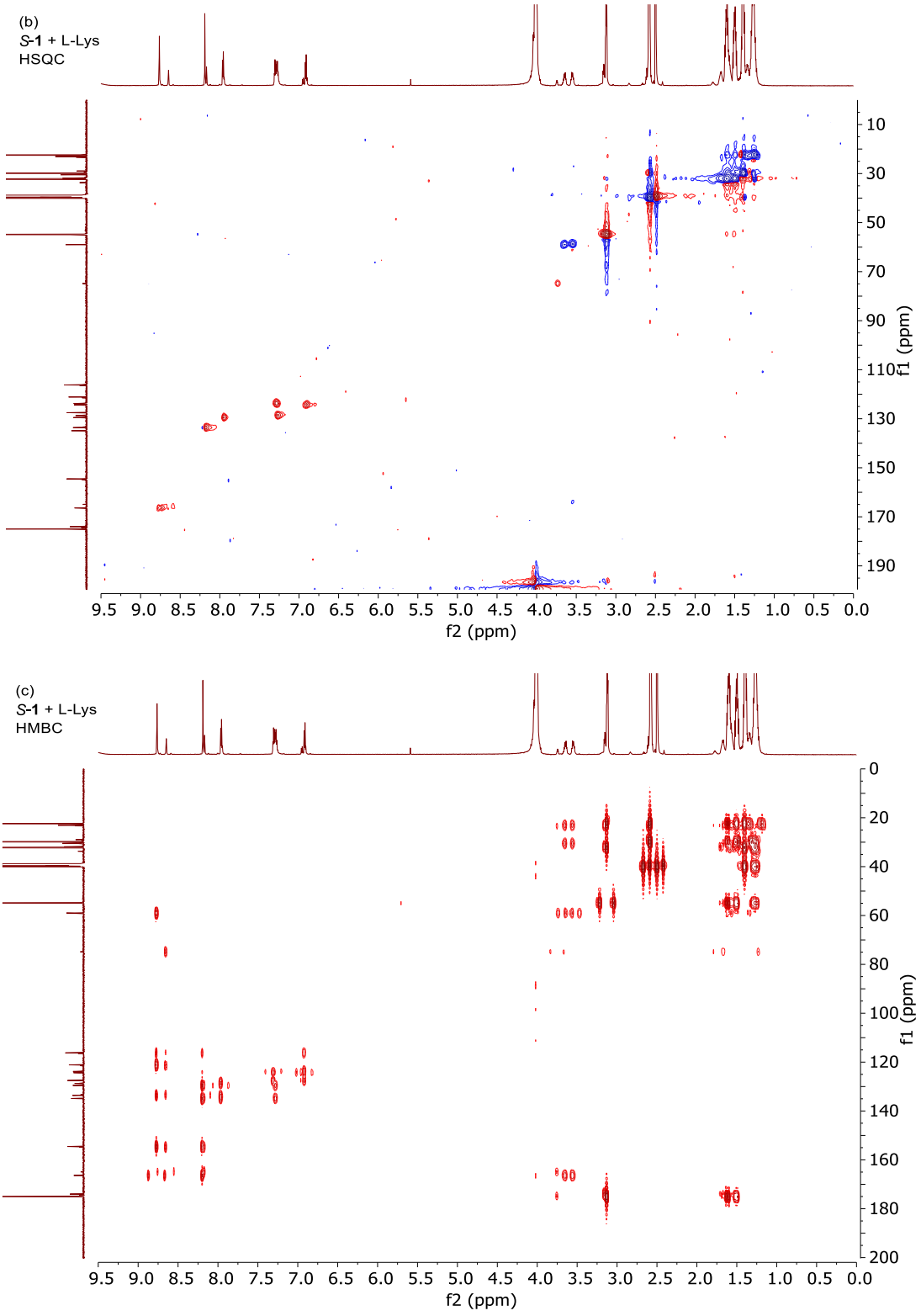

Figure S2. 11 2D NMR of 7.5 mM of (*S*)-**1**, 10 eq. L-Lys in DMSO-d_6:D_2O = 3:1. (a) NOESY with presaturation of water (4.02 ppm); (b) HSQC; (c) HMBC.

2.4.4. Mass Spectra

(a)

(b)

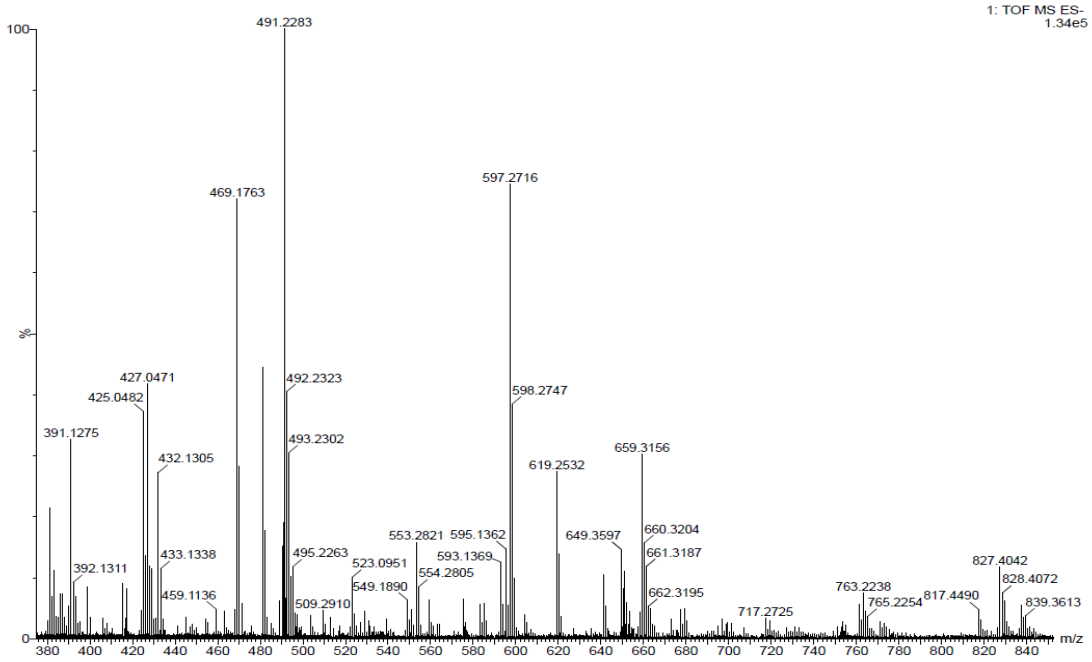

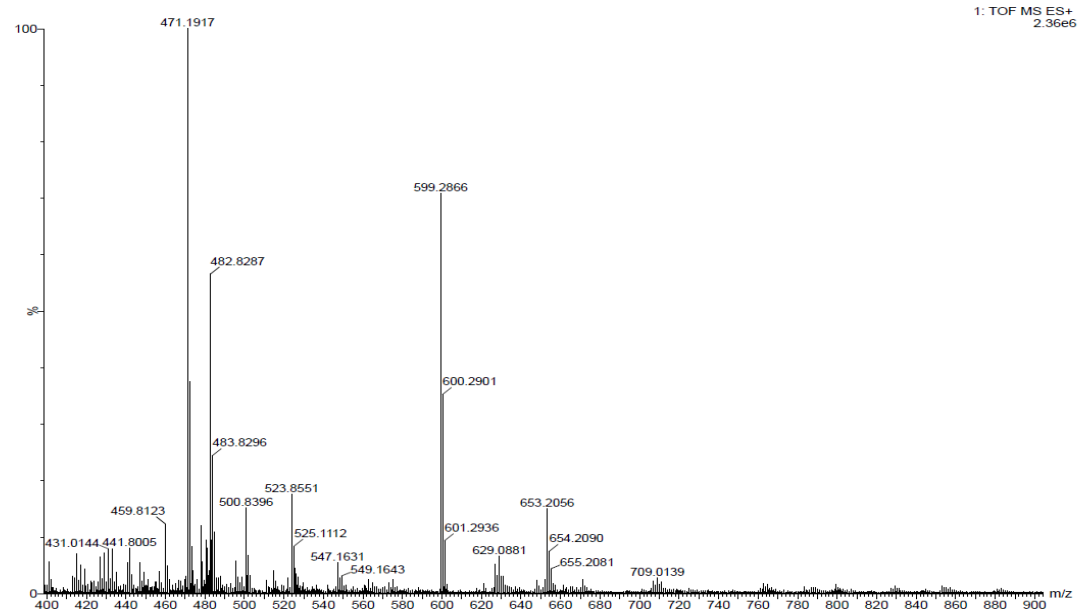

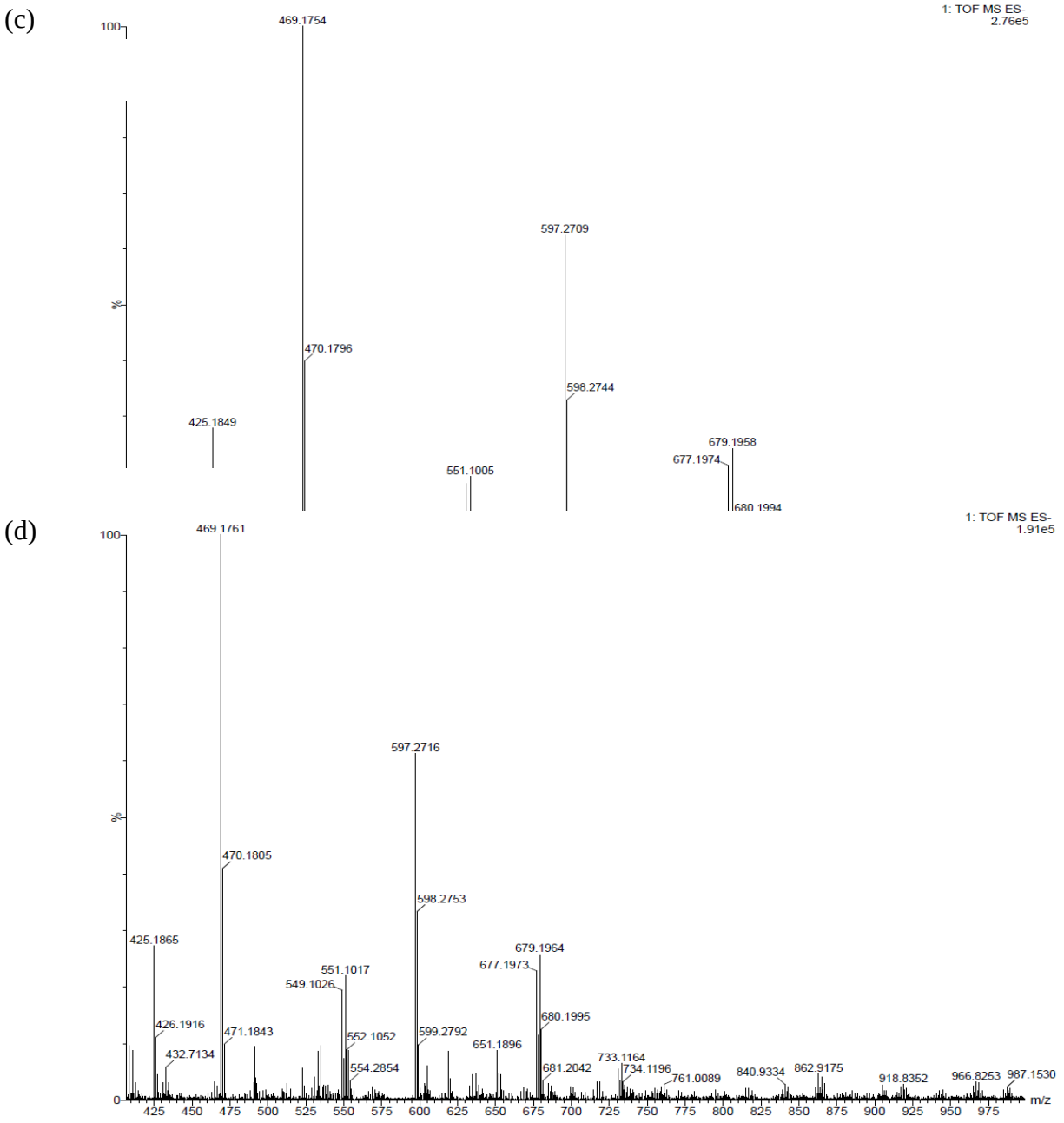

Figure S2. 12 Mass spectra of (*S*)-**2.1** (5.0 mM), $Zn(OAc)_2$ (2.0 equiv) and Lys (10 equiv) in DMSO-d_6:D_2O (5:1). (a) D-Lys, ES negative ionization source; (a) D-Lys, ES positive ionization source; (c) L-Lys, ES negative ionization source; (d) L-Lys, ES positive ionization source.

2.5 References

(1) Holden, J. T. *Amino Acid Pools. Distribution, formation and function of free amino acids.* Elsevier, Amsterdam. 1962.

(2) Lubec, C. *Amino Acids (Chemistry, Biology, Medicine)*. Escom New York. 1990.

(3) Nefyodov L. *Amino Acids and Their Derivatives (chemistry, biochemistry, pharmacology, medicine*). Proc of Internat. Symp; Grodno. 1996.

(4) (a) Konno, R.; Brückner, H.; D'Aniello, A.; Fisher, G.; Fujii, N.; Homma, H. (Eds) *D-Amino Acids: A New Frontier in Amino Acids and Protein Research - Practical Methods and Protocols*. Nova Science, New York, 2007. (b) Weatherly, C. A.; Du, S.; Parpia, C.; Santos, P. T.; Hartman, A. L.; Armstrong, D. W. *ACS Chem. Neurosci.* **2017**, *8*, 1251–1261.

(5) Burnet, P. W. J.; Eastwood, S. L.; Bristow, G. C.; Godlewska, B. R.; Sikka, P.; Walker, M.; Harrison, P. J. *Mol. Psychiatry* **2008**, *13*, 658–660.

(6) Verrall, L.; Burnet, P. W. J.; Betts, J. F.; Harrison, P. J. *Mol. Psychiatry* **2010**, *15*, 122–137.

(7) Shapira, R.; Austin, G. E.; Mirra, S. S. *J. Neurochem.* **1988**, *50*, 69–74.

(8) Cedazo-Minguez, A.; Winblad, B. *Exp. Gerontol.* **2010**, *45*, 5–14.

(9) Zhou, Y.; Yoon, J. *Chem. Soc. Rev* **2012**, *41*, 52–67.

(10) Mutihac, L.; Hong Lee, J.; Seung Kim, J.; Vicens, J. *Chem. Soc. Rev* **2011**, *40*, 2777–2796.

(11) Buryak, A.; Severin, K. *J. Am. Chem. Soc.*, **2005**, *127*, pp 3700–3701.

(12) (a) Huang, Z.; Yu, S.; Wen, K.; Yu, X.; Pu, L. *Chem. Sci.*, **2014**, *5 (9)*, 3457-3462. (b) S.; Pu, L. *Chem. Eur. J.* **2017**, 23, 18066-18073. (c) Zhao, F.; Du, Y.; Tian, J.; Shi, D.; Wang, Y.; Hu, L.; Yu, S.; Yu, X.; Pu, L. *Eur. J. Org. Chem*. **2018**, 1891-1895.

(13) Moughton, A. O.; Hillmyer, M. A.; Lodge, T. P. *Macromolecules*, **2012**, *45*, 2–19

(14) Kataoka, K.; Harada, A.; Nagasaki, Y. *Adv. Drug Deliv. Rev.* **2012**, *64*, 37–48.

(15) Xiao, R. Z.; Zeng, Z. W.; Zhou, G. L.; Wang, J. J.; Li, F. Z.; Wang, A. M. *Int. J. Nanomedicine* **2010**, *5*, 1057–1065.

(16) Rao, J. P.; Geckeler, K. E. *Prog. Polym. Sci.* **2011**, *36*, 887–913.

(17) Ahmed, F.; Discher, D. E. *J. Control. Release* **2004**, *96*, 37–53.

(18) Venkatraman, S. S.; Jie, P.; Min, F.; Freddy, B. Y. C.; Leong-Huat, G. *Int. J. Pharm.* **2005**, *298*, 219–232.

(19) Nguyen, T. H.; Petchsuk, A.; Tangboriboonrat, P.; Opaprakasit, M.; Sharp, A.; Opaprakasit, P. *Adv. Mater. Res.* **2010**, *93–94*, 198–201.

(20) Wan, Y.; Chen, W.; Yang, J.; Bei, J.; Wang, S. *Biomaterials* **2003**, *24*, 2195–2203.

(21) C. Hiemstra, Z.Y. Zhong, X. Jiang, W.E. Hennink, P.J. Dijkstra, J. F. *J. Control. Release* **2006**, *116*, e17–e19.

(22) Williams, A. A.; Fakayode, S. O.; Alptürk, O.; Jones, C. M.; Lowry, M.; Strongin, R. M.; Warner, I. M. *J Fluoresc*, **2008**, *18*, 285–296.

(23) (a) Various biosensors for L-Lys are summarized: Bóka, B.; Korózs, M.; Nánási, M.; Adányi, N. *Electroanalysis* **2015**, *27*, 817–824, and references therein. (b) Carbon quantum dots modified with L-cysteine were recently found to show enantioselective photoluminescence enhancement with Lys: F. Copur, F.; Nisa Bekar, N.; Erhan Zor, E.; Sabri Alpaydin, S.; Haluk Bingol, H. *Sens. Actuat. B: Chem.* **2019**, *279*, 305-312. (c) Copper nanoclusters were recently found to show chemoselective photoluminescence enhancement with L-Lys: Zhang, M.; Qiao, J.; Zhang, S.; Qi, L. *Talanta* **2018**, *182*, 595-599.

(24) Kersey, F. R.; Zhang, G.; Palmer, G. M.; Dewhirst, M. W.; Fraser, C. L. *ACS Nano* **2010**, *4*, 4989–4996.

(25) Pfister, A.; Zhang, G.; Zareno, J.; Horwitz, A. F.; Fraser, C. L. *ACS Nano* **2008**, *2*, 1252–

1258.

(26) Stetefeld, J.; Mckenna, S. A.; Patel, T. R. *Biophys Rev,* **2016**, *8*, 409–427.

Chapter 3. Fluorescent Recognition of L- and D-Tryptophan in Water

3.1 Introduction

3.1.1 Importance of Trp

Chemoselective and enantioselective fluorescent detections of free amino acids are potentially useful because both enantiomers of amino acids are found to play diverse roles in biological systems.[1-4] Tryptophan is an essential amino acid and is important in many metabolic functions.[5-10] The level of tryptophan can be used to diagnose various metabolic disorders and associated diseases. Supplementation with this amino acid is considered in the treatment of depression and sleep disorders. While most related studies focused on L-tryptophan,[5-10] the importance of D-tryptophan has also been realized in cancer cell, bacteria and mice.[11-14] For example, D-tryptophan was recently found in the blood samples of patients with gastric cancer but not in those of healthy people.[11] It may be used as a biomarker for gastric cancer and probably other cancers.

3.1.2. Relevant Probes

In 2011, Tang and coworkers reported that the 1,1'-bi-2-naphthol (BINOL)-based compound **3.1** showed good chemo- and enantioselectivity in the fluorescent recognition of tryptophan in ethanol solution.[15] However, this probe was not reported to be able to conduct selective detection of tryptophan in aqueous solution. Recently, we reported that in the presence of the biodegradable diblock copolymer polyethylene glycol–poly L-lactic acid (PEG–PLLA),[16] a water insoluble probe can be used to conduct fluorescent recognition of lysine in aqueous solution.[17] The polymer PEG-PLLA forms micelles in aqueous solution which can encapsulate

the water insoluble probe in its hydrophobic core to allow the interaction of the probe with the substrate to generate the desired fluorescent response.

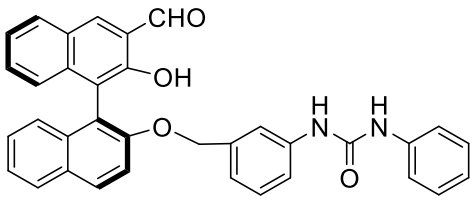

3.1

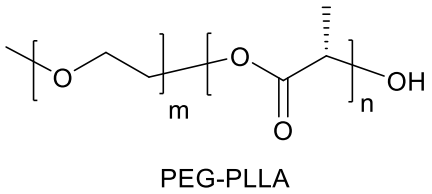

PEG-PLLA

3.1.3. Design of New Probes

In order to develop fluorescent probes for *chemo*- and *enantioselective* recognition of tryptophan in aqueous solution have, we designed a new type of fluorescent probe as represented by **3.2** (Scheme 3.1). Unlike **3.1** which contains a uryl-based hydrogen bonding donor, the probes **3.2** contain a Lewis basic site as a hydrogen bonding acceptor. These compounds are expected to be insoluble in water. They should have weak fluorescence because of the excited state proton transfer between the hydroxyl and the aldehyde groups.[18] In the presence of PEG-PLLA, they can be encapsulated inside the hydrophobic core of the micelles generated from this diblock copolymer. Condensation of **3.2** with tryptophan inside the micelles should form the imine product **3.3** in which the Lewis basic site can form an intramolecular hydrogen bonding interaction with the indole N-H hydrogen in the hydrophobic environment of the micelle core. An energy minimized molecular modeling structure of **3.3**, where B = NEt_2 and tryptophan configuration is L, obtained by semi-empirical calculation by using Spartan (PM3) program is shown in Scheme 3.1 which features a hydrogen bonding interaction between the amine nitrogen and the indole N-H group. On the basis of our previous studies on the BINOL-aldehyde-based fluorescent probes,[18] we expect that the fluorescence intensity of **3.3** should not be strong because of both the excited state proton transfer between the hydroxyl group and the imine nitrogen and the excited state isomerization of the imine C=N bond. However, in the presence of Zn^{2+}, a complex like **3.4** could

be generated with greatly enhanced fluorescence because Zn^{2+} coordination can inhibit the fluorescence quenching processes.[18] Herein, our synthesis and study of several derivatives of **3.2** is reported. We have discovered that in the presence of PEG-PLLA, chemoselective as well as enantioselective fluorescent recognition of tryptophan in aqueous solution by using these probes can be achieved.

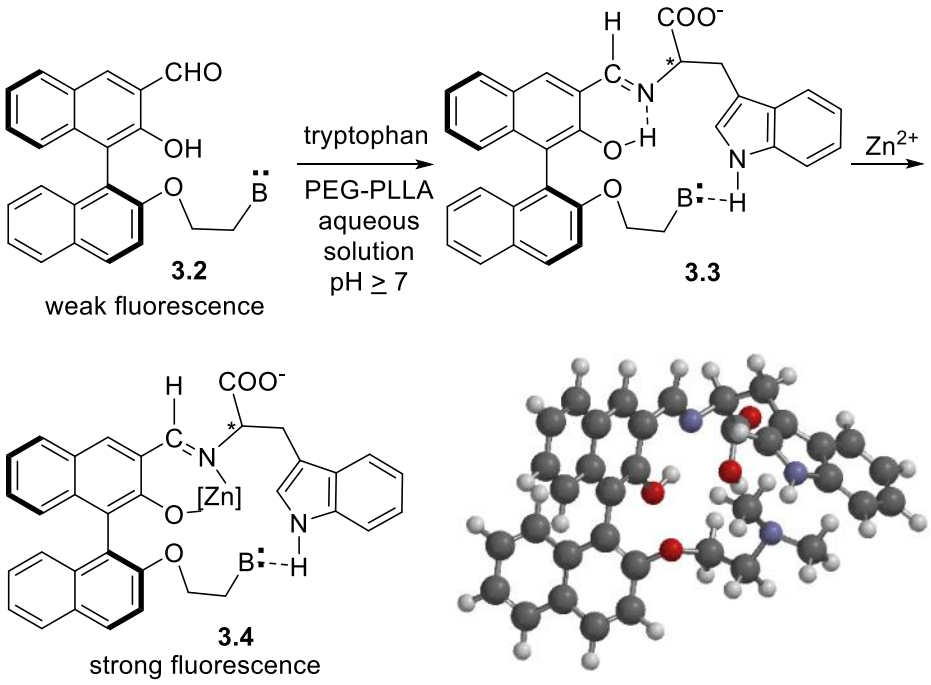

Scheme 3. 1 Design of the fluorescent probes **3.2** for the selective recognition of tryptophan

3.2 Results and Discussion

3.2.1 Synthesis

Scheme 3.2 shows an efficient synthesis of the BINOL-based probes (*S*)-**2a-d**. Treatment of (*S*)-BINOL with 1 equiv MOMBr (MOM = CH_3OCH_2) in the presence of a base gave a monoMOM protected BINOL which upon deprotonation with excess nBuLi and reaction with DMF gave the monoaldehyde product (*S*)-**3.5** in 62% yield after acidic workup.[19] Reaction of (*S*)-**3.5** with an alkyl halide RX in the presence of K_2CO_3 gave (*S*)-**3.6** whose MOM group was removed by treatment with trifluoroacetic acid to give the desired products (*S*)-**3.2a-d** in 40 – 92%

yields. Among these products, compounds (*S*)-**3.2a** and (*S*)-**3.2b** contain nitrogen-based Lewis base sites and compounds (*S*)-**3.2c** and (*S*)-**3.2d** contain oxygen-based Lewis base sites. All these compounds gave two singlets at δ = 10.2 – 10.6 for the proton signals of their aldehyde groups as well as the adjacent hydroxyl groups, indicating strong intramolecular hydrogen bonding interaction. No fast exchange of the naphthyl hydroxyl proton was observed even in the presence of the Lewis base sites such as the tertiary amine and pyridine units. These compounds can be dissolved in common organic solvents but are insoluble in water.

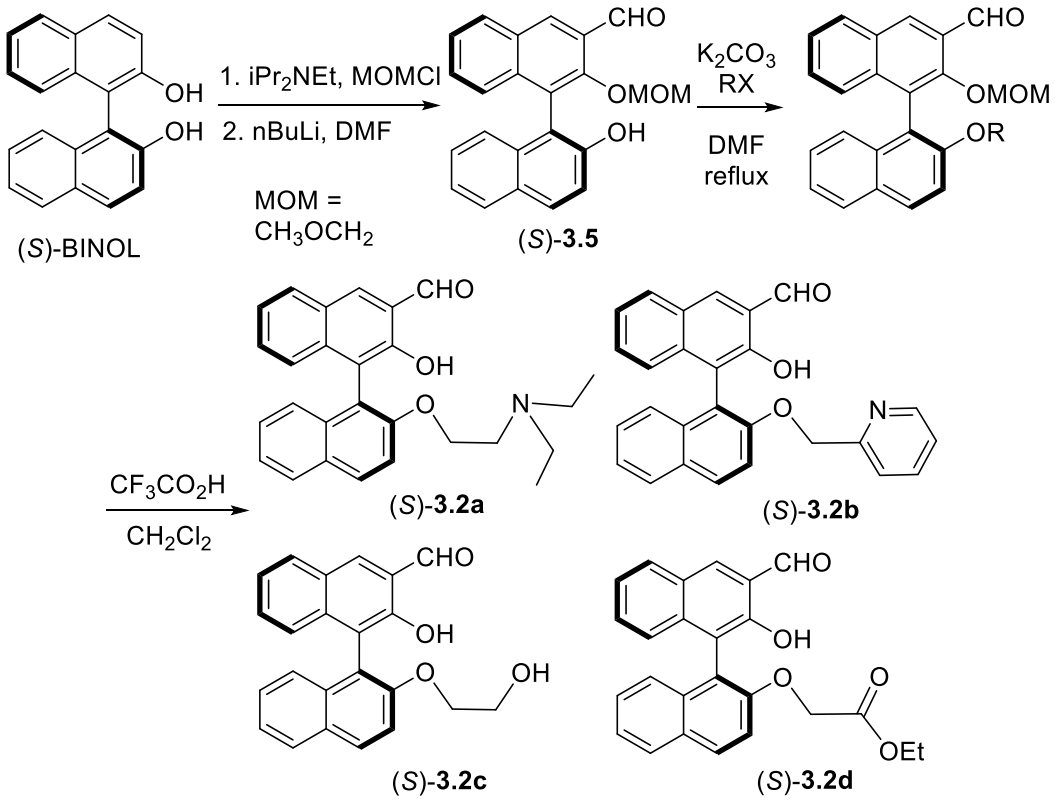

Scheme 3. 2 Synthesis of the fluorescent probes (*S*)-**3.2a-d**

3.2.2 Fluorescence Studies

3.2.2.1 Amino Acids Screening

In order to use compounds (*S*)-**3.2a-d** to conduct fluorescent recognition of amino acids, we encapsulated them into PEG-PLLA to make (*S*)-**3.2a-d**@PEG-PLLA micelle solutions (2.0 x

10^{-5} M) (see Experimental). The fluorescence responses of the (*S*)-**3.2a-d**@PEG-PLLA micelle solutions toward the two enantiomers of 19 amino acids in the presence of $Zn(OAc)_2$ (2.0 equiv) were investigated. For each measurement, 1 mL of a (*S*)-**3.2a-d**@PEG-PLLA solution was mixed with 1 mL carbonate buffer (CBS 25mM), 10 equiv amino acid (10 □L, 20 mM in water) and 2.0 equiv $Zn(OAc)_2$ (10 □L, 4 mM in water) which was allowed to stand at room temperature for 3 h. The final concentration of the probes in the solutions was 1.0 x 10^{-5} M with pH = 10.1. Figure 3.1 gives an example of the fluorescence spectra of (*S*)-**3.2a**@PEG-PLLA in the presence of the enantiomers of 19 amino acids. The micelle solution (*S*)-**3.2a**@PEG-PLLA showed very weak fluorescence upon excitation at 430 nm. When it was treated with most of the amino acids, only very small fluorescence enhancement was observed. However, both D-tryptophan (Figure 3.1a) and L-tryptophan (Figure 3.1b) greatly enhanced the fluorescence at λ = 545 nm. The fluorescence intensity with L-tryptophan was found to be 60% greater than that with D-tryptophan.

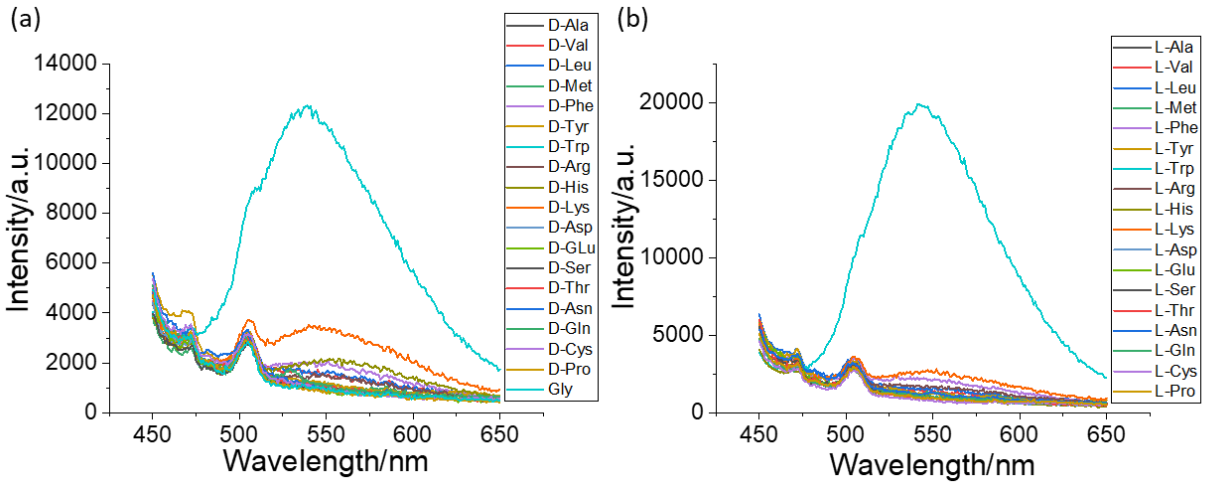

Figure 3. 1 (*S*)-**3.2c**@PEG-PLLA responses for various (a) D-amino acids; (b) L-amino acids. (*S*)-**2c** concentration = 10 μM, with 2 equiv $Zn(OAc)_2$, 10 equiv amino acids. Excited at 430 nm, slit = 3/3 nm, integration time = 0.1 s.

Figure 3.2 summarizes the fluorescence responses of all the micelle solutions (*S*)-**3.2a-d**@PEG-PLLA toward the two enantiomers of 19 amino acids under the same conditions. It shows that among the four probes, (*S*)-**3.2a**@PEG-PLLA and (*S*)-**3.2c**@PEG-PLLA exhibited better chemoselectivities than (*S*)-**3.2b**@PEG-PLLA and (*S*)-**3.2d**@PEG-PLLA, and the chemoselectivity and enantioselectivity of (*S*)-**3.2c**@PEG-PLLA is slightly better than (*S*)-**3.2a**@PEG-PLLA.

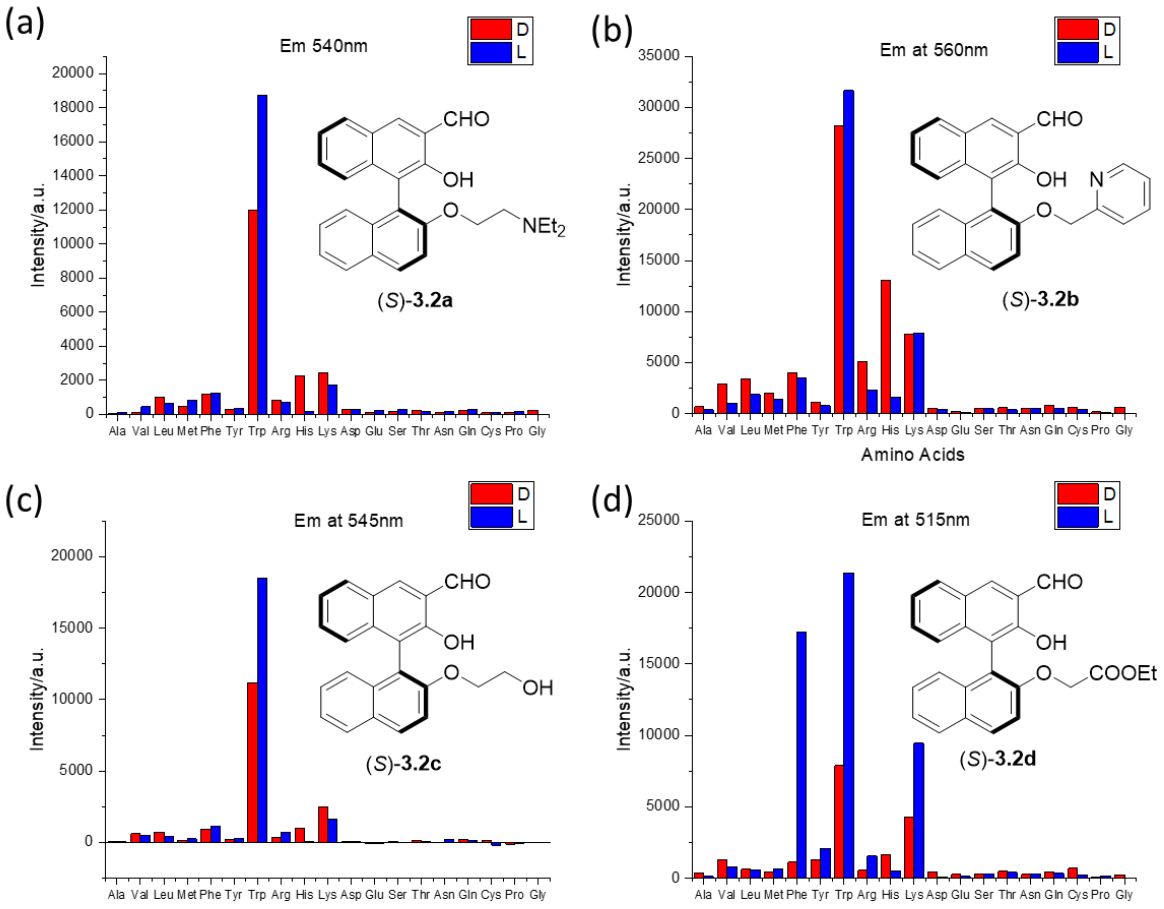

Figure 3. 2 Fluorescence response of the micelle probes (*S*)-**3.2a**@PEG-PLLA, (*S*)-**3.2b**@PEG-PLLA, (*S*)-**3.2c**@PEG-PLLA and (*S*)-**3.2d**@PEG-PLLA towards various amino acids (Conditions: 10 μM micelle probe, 2 equiv $Zn(OAc)_2$, and 10 equiv amino acids in carbonate buffer solution. Peak intensities were used. Spectra were taken after 3 h of reaction at rt. Excited at 430 nm for (*S*)-**3.2a**, (*S*)-**3.2b**, and (*S*)-**3.2c**, and at 400 nm for (*S*)-**3.2d**. slit = 3/3 nm, integration time = 0.1s.)

In the presence of (*S*)-**3.2c**@PEG-PLLA, L-tryptophan generated 19.6 fold fluorescence enhancement at λ = 545 nm and D-tryptophan generated 12.3 fold fluorescence enhancement, that is the enantioselective fluorescence enhancement ratio *ef* = 1.65 [$ef = (I_L-I_0)/(I_D-I_0)$, where I_0 is the fluorescence of the probe without the amino acid]. (*S*)-**3.2d**@PEG-PLLA also showed good enantioselective fluorescent response toward phenylalanine, tryptophan and lysin, and (*S*)-**3.2b**@PEG-PLLA showed good enantioselective fluorescent response toward histidine.

3.2.2.2 Concentration Detection

We then studied the effect of the concentration of tryptophan on the fluorescence response of (*S*)-**3.2c**@PEG-PLLA. As shown in Figure 3.3a, the fluorescence intensity increased with increasing tryptophan concentration until 20 equiv. L- or D-tryptophan at which the fluorescence enhancement was saturated. In the range of 0.5 to 10 equiv. of either D- or L-tryptophan, first-order linear fit was applied and R square value more than 0.99 was found (Figure 3.3b). The limit of detection (LOD) was thus determined to be 5.68 μM for D-tryptophan and 2.60 μM for L-tryptophan (LOD = 3*SD/k. SD, standard deviation of noise. k, slope of calibration curve). With a tryptophan detection concentration range of 5 to 400 μM, (*S*)-**3.2c**@PEG-PLLA is potentially useful to measure the tryptophan concentrations in biological systems such as human serum, where the concentration of tryptophan was found to be 67.2±10.2 μM.[20]

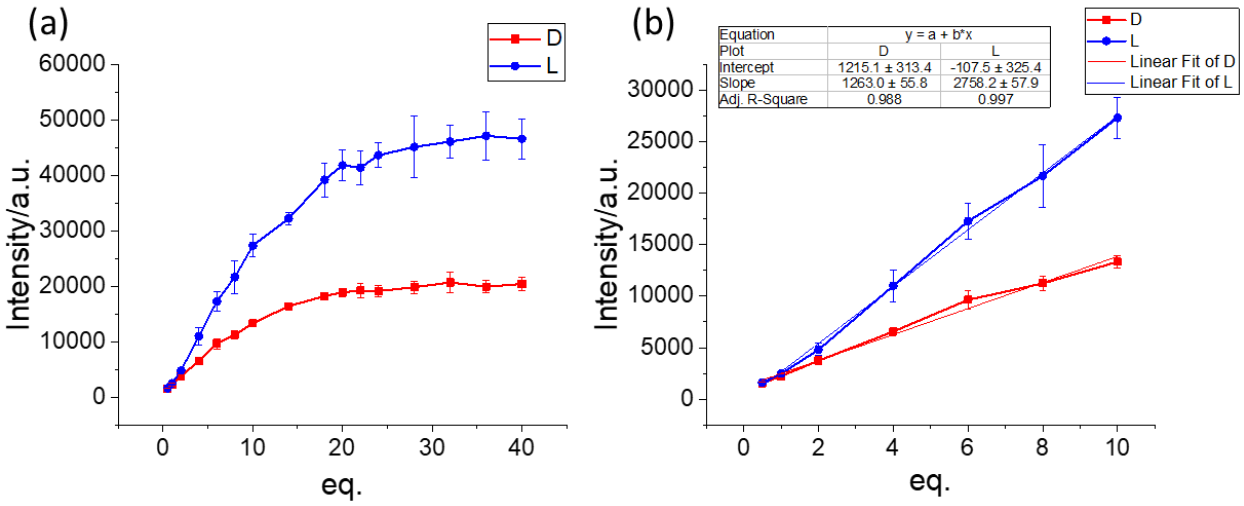

Figure 3. 3 (a) Fluorescence intensity of (*S*)-**3.2c**@PEG-PLLA (10 μM) and $Zn(OAc)_2$ (2 equiv) at λ = 545 nm versus the stoichiometry of tryptophan. (b) Expanded view of 0.5 to 10 equiv tryptophan. (Excited at 430 nm, slit = 3/3 nm, integration time = 0.1 s).

3.2.2.3 ee Detection

(*R*)-**3.2c**, the enantiomer of (*S*)-**3.2c**, was synthesized by starting from (*R*)-BINOL. The diblock copolymer PEG-PDLA was also obtained from the D-lactic acid monomer. We thus prepared (*R*)-**3.2c**@PEG-PDLA as the enantiomeric analog of (*S*)-**3.2c**@PEG-PLLA and studied the fluorescence responses of this pair of enantiomeric probes at various enantiomeric excesses of tryptophan (*ee* = [D-L]/[D+L]). As shown in Figure 3.4, the fluorescence responses of (*R*)-**3.2c**@PEG-PDLA and (*S*)-**3.2c**@PEG-PLLA exhibit a close to mirror image relationship which confirms the observed enantioselective recognition. The imperfect matches are attributed to the intrinsic differences of the micelles, the random conformations of the polymers and their variable molecular weight distributions, and experimental errors.

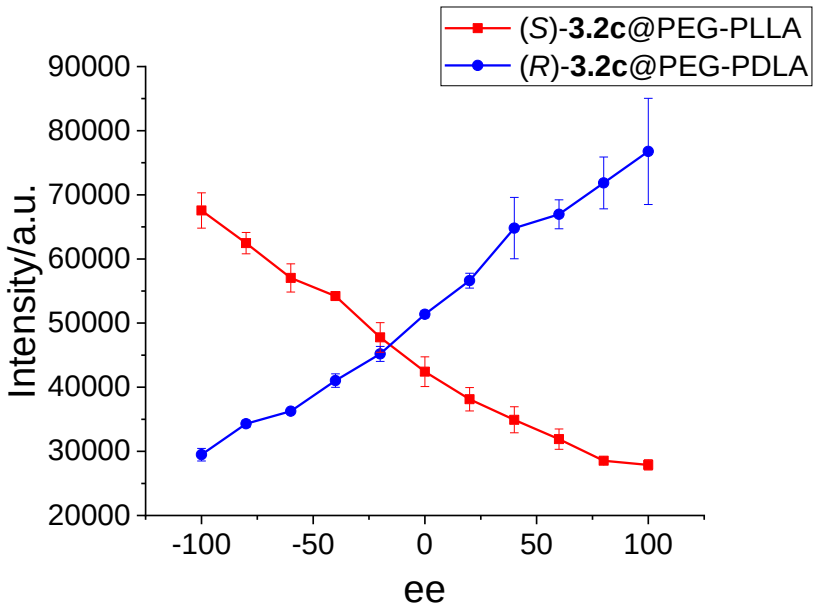

Figure 3. 4 Fluorescence intensity of (*S*)-**3.2c**@PEG-PLLA/(*R*)-**3.2c**@PEG-PDLA (10 μM), $Zn(OAc)_2$ (2 equiv.) and tryptophan (40 equiv.) at λ = 545 nm versus the ee of tryptophan (Excited at 430 nm, slit = 3/3 nm, integration time = 0.1 s).

3.2.3 Characterization of Micelles

When (*S*)-**3,2c**@PEG-PLLA+Zn^{2+} was treated with D- and L-Trp, the UV-vis spectra only showed the increased signals of the added tryptophan but no change in the absorption of the probe (see Figure S3.13) This indicates that there was only a very small degree of reaction between the probe and the amino acid under this condition which however has led to the dramatically enhanced fluorescence in aqueous solution. We also found that in the absence of PEG-PLLA when these probes are used to interact with tryptophan in an organic solvent methanol, there was much weaker and nonselective fluorescent enhancement. Thus, the polymer-based micelles not only allow the detection of tryptophan to be conducted in water, but also greatly enhance the fluorescence sensitivity and selectivity.

The sizes of (*S*)-**3.2c**@PEG-PLLA were characterized by using both dynamic light scattering (DLS) (See Fig S3.14) and transmission electron cryomicroscopy (cryo-TEM), shown in Figure 3.5c, (*S*)-**2c**@PEG-PLLA forms nanoscale spherical structures. Although DLS results

showed more structural changes after interaction with amino acids, cryo-TEM images supported that the micelle structures were mostly maintained after treated with either D-Trp or L-Trp. through the microscopy, meaning a large portion of the micelle was degraded during the reaction.

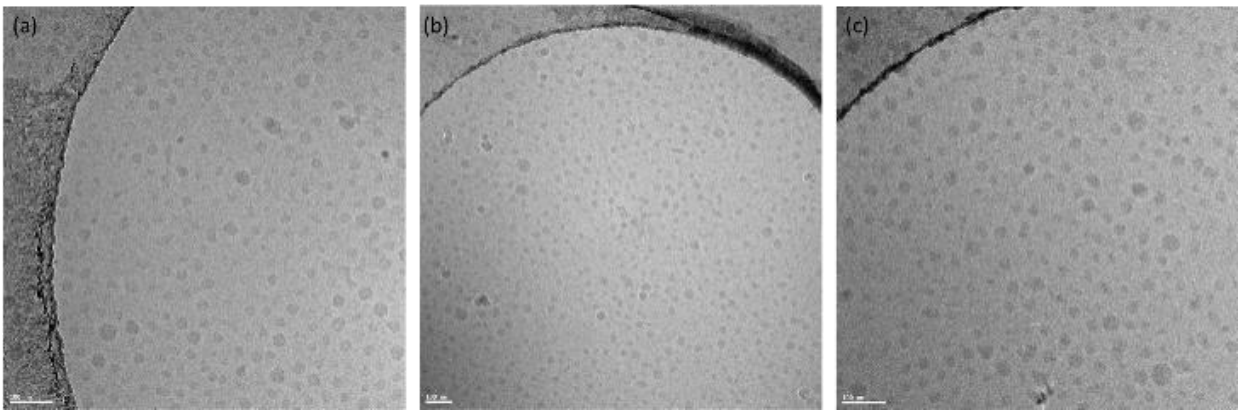

Figure 3. 5 Cryo-TEM of micelle structures. (a) (*S*)-**3.2c**@PEG-PLLA; (b) (*S*)-**3.2c**@PEG-PLLA + D-Trp; (c) (*S*)-**3.2c**@PEG-PLLA + L-Trp.

3.2.4 Mechanistic Studies

Because of the interferences of the polymeric micelles, the ^{1}H NMR spectrum of (*S*)-**3.2c**@PEG-PLLA cannot be directly studied. We thus studied the reaction of (*S*)-**3.2c** with D- and L-Trp in methanol. ^{1}H NMR spectroscopic analyses of the reaction showed that both D- and L-Trp reacted with (*S*)-**3.2c** quickly in methanol to form the corresponding imine products with the disappearance of the aldehyde signal as well as the appearance of a new singlet at $\delta \sim 8.20$ for the imine proton (See Figure S3.10 & S3.11 in SI). Mass spectroscopic analyses of the reaction mixture also supported the imine formation (See Figure S3.19 & S3.20).

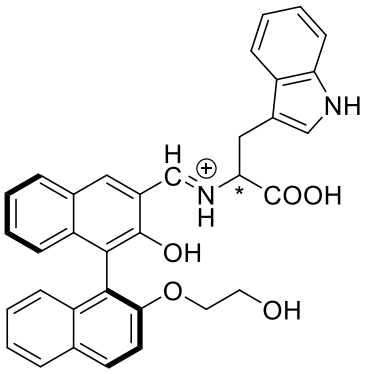

HR mass calculated (M+H): 545.2076
D-Trp found: 545.2092
L-Trp found: 545.2072

3.3 Conclusion

In conclusion, a new class of molecular probes has been designed for the fluorescent recognition of tryptophan in aqueous solution. These probes can be synthesized in four steps from the optically active BINOL. In the presence of the diblock copolymer PEG-PLLA and Zn^{2+}, compounds (*S*)-**3.2a** and (*S*)-**3.2c** have shown excellent chemoselectivity for the fluorescent recognition of tryptophan in aqueous solution. In addition, the chirality of these probes has also made them enantioselective in their fluorescent response toward this amino acid. The micelle structure of the diblock copolymer not only allows the interaction of the water insoluble fluorescent probes with the amino acid to be conducted in aqueous solution, but also provides a hydrophobic interior to greatly enhance the fluorescence sensitivity and selectivity of the probes.

3.4 Experimental

3.4.1 General experimental methods

All amino acids and other chemicals were purchased from Sigma Aldrich Chemical Co. or Alfa Aesar, and used without further purification. NMR spectra were recorded on Varian-600 MHz spectrometer or Bruker-800 MHz spectrometer. Chemical shifts for ^{1}H NMR were reported in parts per million relative to a singlet at 7.26 ppm for deuterated chloroform and 2.50 ppm for

deuterated DMSO. Chemical shifts for ^{13}C NMR were reported in parts per million relative to a triplet at 77.16 ppm for deuterated chloroform. Steady-state fluorescence emission spectra were recorded on Horiba FluoroMax-4 spectrofluorometer. Low-temperature fluorescence emission spectra were recorded on Horiba FluoroMax-3 spectrofluorometer. Nanoparticle sizes and polydispersities were analyzed via dynamic light scattering (DLS, Wyatt, DynaPro). Cryo-TEM images were recorded on a Tecnai F20 TEM system. For cryoTEM, nanoparticles were concentrated by centrifugation at 8000 rpm for 6 min in a cellulose filter tube (Amicon, Ultra-15, 30000 Da MW cutoff). High-resolution mass spectra were obtained from the University of Illinois at Urbana-Champaign (UIUC) Mass Spectrometry Facility. Deionized water was used for all the experiments.

Nano precipitation to prepare the micelle encapsulated probe 1.6 μmol of (*S*)-organic sensor cores (1mg/ml in DMF) were added to 80 mg coblock polymer mPEG-PLLA (mPEG-PDLA for (*R*)-cores). More DMF was added to dissolve the coblock polymer and the volume was calibrated to 8 ml. The solution was sonicated for 10 minutes and added dropwise to a vortex of 72 ml water at a rate of 1 ml/min. The vortex was allowed to last 30 more minutes after the addition of DMF solution. The final mixture was dialyzed in DI water to form micelle solutions containing 20 μM corresponding organic cores.

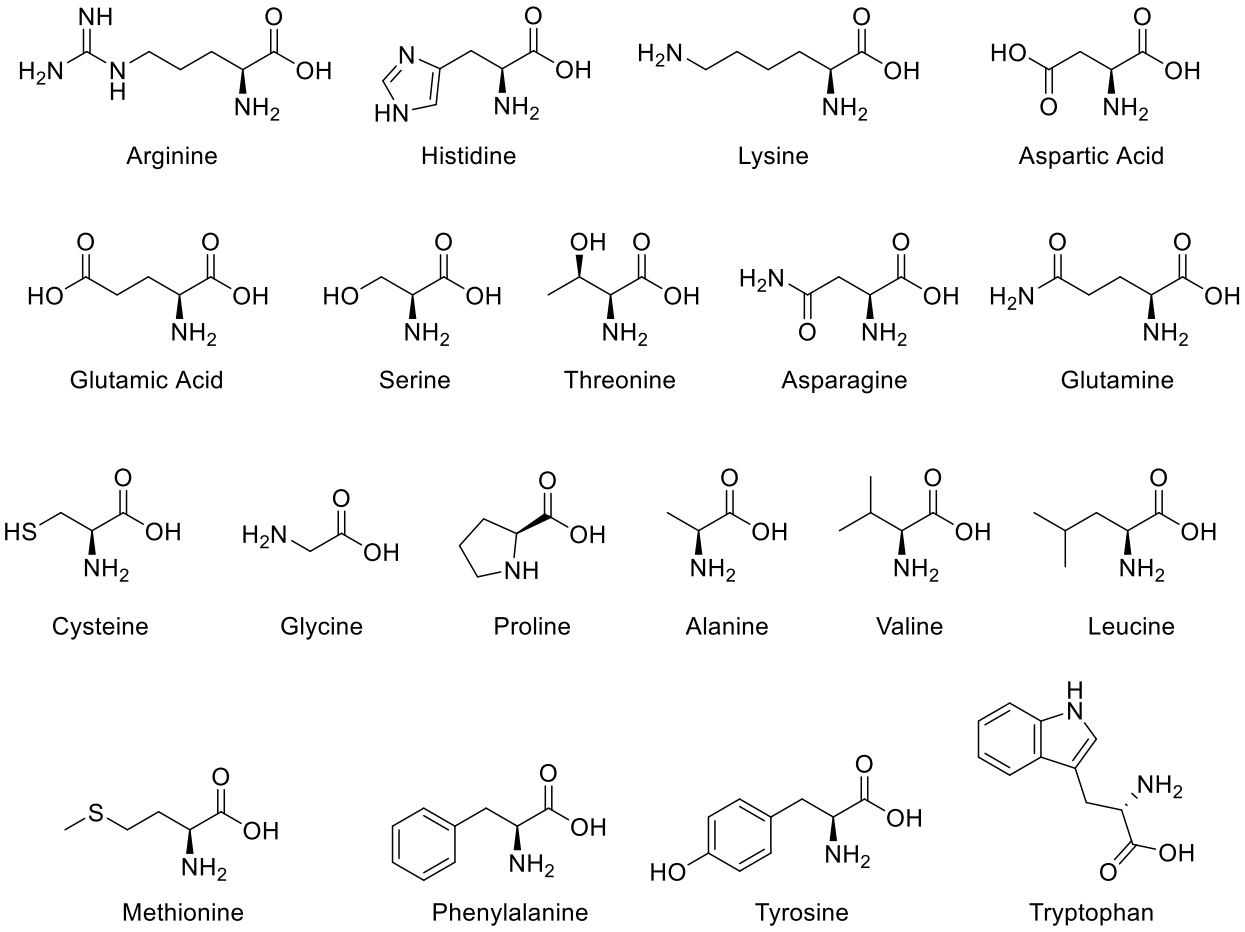

Figure S3. 1 Structure of Chiral Substrates

3.4.2 Synthesis and characterization data

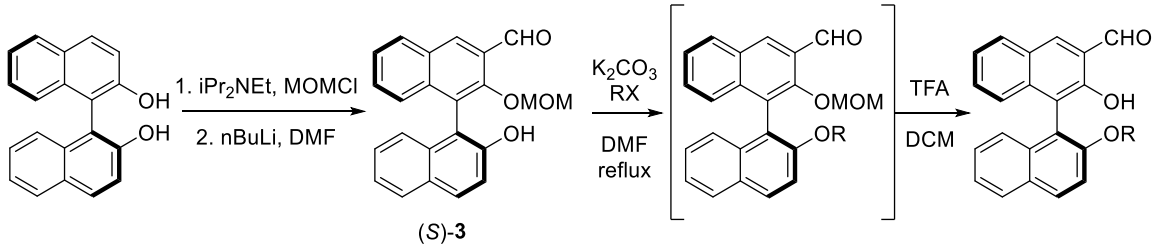

(*S*)-**3**

General Procedures:

After pumping off air and refilling with nitrogen gas three times, the mixture of 200mg of (*S*)-**3.3**, 4eq. of potassium carbonate, and 2.5eq. of alkyl halide (RX) was heated to 100°C for 8 hours in dimethylformamide. The reaction mixture was neutralized with 2M HCl, extracted with ethyl acetate, dried with sodium sulfate. The concentrated mixture was dissolved in dichloromethane and added with 1ml trifluoroacetic acid at 0°C, after which the mixture was allowed to warm up to room temperature. After 40 minutes, the reaction mixture was neutralized with sodium bicarbonate, extracted with dichloromethane, dried with sodium sulfate. The concentrated mixture was purified by column chromatography to afford the products.

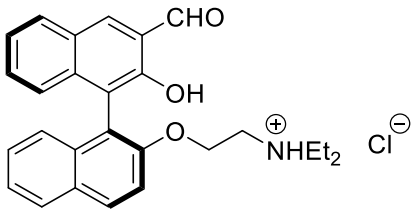

(*S*)-**3.2a** HCl

(*S*)-2'-(2-(diethylamino)ethoxy)-2-hydroxy-[1,1'-binaphthalene]-3-carbaldehyde hydrochloride (*S*)-**3.2a**·HCl :

2-Bromo-N,N-diethylethylamine hydrobromide was used as RX. After the reaction mixture was treated with trifluoroacetic acid, the mixture was neutralized with sodium bicarbonate, acidified with 2M HCl, dried with sodium sulfate. The concentrated mixture was purified by column

chromatography (DCM/MeOH) to afford the products. Yield 57%, yellow oil. ^{1}H NMR (600 MHz, CDCl3), δ: 12.04 (s, 1H), 10.44 (s, 1H), 10.21 (s, 1H), 8.33 (s, 1H), 8.04 (d, J=9.2Hz, 1H), 8.00 (dd, J_1=3.2Hz, J_2=6.3Hz, 1H), 7.91 (d, J=8.2Hz, 1H), 7.41 (m, 4H), 7.28 (t, J=7.6Hz, 1H), 7.1 (d, J= 8.8Hz, 2H), 4.58 (m, 1H), 4.47 (m, 1H), 3.16 (m, 2H), 2.72 (m, 2H), 2.58 (m, 2H), 1.07 (t, J=7.3Hz, 3H), 0.71 (t, J=7.2Hz, 3H). ^{13}C NMR (201 MHz, $CDCl_3$) δ: 196.84, 153.49, 152.92, 137.92, 137.89, 133.57, 130.99, 130.87, 129.97, 129.93, 128.50, 127.65, 127.32, 125.23, 124.91, 124.87, 124.67, 122.14, 118.57, 117.86, 113.96, 77.32, 77.16, 77.00, 63.76, 49.84, 47.27, 46.60, 8.97, 8.10.

Mass calculated ($M+H^+$) 414.2069, found 414.2062.

$[\alpha]_D^{20}$ = -62.233 (c= 1mg/ml $CHCl_3$)

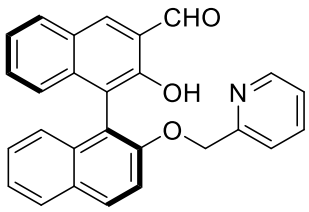

(*S*)-**3.2b**

(*S*)-2-hydroxy-2'-(pyridin-2-ylmethoxy)-[1,1'-binaphthalene]-3-carbaldehyde (*S*)-**3.2b**:

2-(Bromomethyl)pyridine hydrobromide was used as RX, product yield 76%, yellow solid. ^{1}H NMR (600 MHz, CDCl3), δ: 10.48 (s, 1H), 10.22 (s, 1H), 8.47 (d, J=4.1Hz, 1H), 8.34 (s, 1H), 8.00 (m, 1H), 7.95 (d, J=9.1Hz, 1H), 7.87 (d, J=8.2Hz, 1H), 7.42 (d, J=9.0Hz, 2H), 7.38 (m, 2H), 7.35 (t, J=7.6Hz, 1H), 7.27 (t, 8.2Hz, 2H), 7.20 (two d, J_1=10Hz, J_2=9.0Hz, 2H), 7.10 (m, 1H), 6.92 (d, J=7.6Hz, 1H), 5.30 (d, J=14.0Hz, 1H), 5.24 (d, J=14.0Hz, 1H). ^{13}C NMR (201 MHz, $CDCl_3$), δ: 196.89, 156.67, 153.61, 153.46, 146.53, 139.05, 138.01, 133.76, 130.63, 130.54, 129.92, 129.76,

128.42, 127.70, 127.05, 125.52, 125.00, 124.56, 124.32, 123.15, 122.28, 122.06, 118.61, 118.19, 114.89, 69.95.

Mass calculated ($M+H^+$) 406.1443, found 406.1441.

$[\alpha]_D^{20}$ = -104.13 (c= 1mg/ml $CHCl_3$)

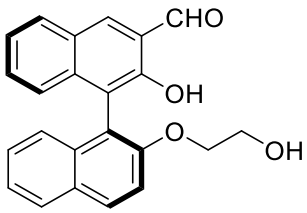

(*S*)-**3.2c**

(*S*)-2-hydroxy-2'-(2-hydroxyethoxy)-[1,1'-binaphthalene]-3-carbaldehyde (*S*)-**3.2c**:

2-Chloroethanol was used as RX, product yield 40%, yellow solid. ^{1}H NMR (600 MHz, CDCl3), δ: 10.58 (s, 1H), 10.20 (s, 1H), 8.33 (s, 1H), 8.00 (m, 2H), 7.89 (d, J=8.5Hz, 1H), 7.45 (d, J=9.0Hz, 1H), 7.40 (m, 2H), 7.37 (t, J=7.4Hz, 1H), 7.27 (t, J=7.4Hz, 1H), 7.17 (m, 2H), 4.24 (m, 1H), 4.11 (m, 1H), 3.64 (m, 1H), 3.57 (m, 1H). ^{13}C NMR (201 MHz, $CDCl_3$) δ: 188.87, 155.13, 152.10, 131.88, 131.55, 131.52, 131.35, 130.36, 129.79, 129.42, 129.31, 128.44, 126.65, 125.80, 125.57, 125.54, 124.93, 121.71, 121.30, 118.53, 113.00, 29.85, 0.12.

Mass calculated ($M+H^+$) 358.1283, found 359.1281.

(*S*)-**2c** $[\alpha]_D^{20}$ = -62.133 (c= 1mg/ml $CHCl_3$)

(*R*)-**2c** $[\alpha]_D^{20}$ = 62.833 (c= 1mg/ml $CHCl_3$)

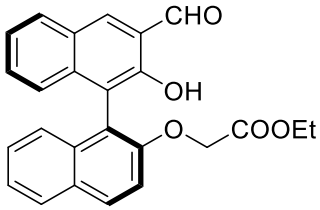

(*S*)-**3.2d**

Ethyl (*S*)-2-((3'-formyl-2'-hydroxy-[1,1'-binaphthalen]-2-yl)oxy)acetate (*S*)-**2d**:

Ethyl bromoacetate was used as RX, product yield 92%, yellow solid. ^{1}HNMR (600MHz, $CDCl_3$), δ: 10.38 (s, 1H), 10.21 (s, 1H), 8.32 (s, 1H), 7.98 (m, 2H), 7.89 (d, J=8.3Hz, 1H), 7.37 (m, 4H), 7.27 (m, 1H), 7.23 (m, 1H), 7,17 (d, J=8.6Hz, 1H), 4.62 (d, J=17Hz, 1H), 4.55 (d, J=17Hz, 1H), 4.11 (q, J=7.1Hz, 2H), 1.16 (t, J=7.1Hz, 3H). ^{13}CNMR (150MHz, $CDCl_3$), δ: 196.78, 169.34, 154.04, 153.59, 137.96, 133.77, 130.46, 130.36, 130.08, 129.85, 128.35, 127.74, 126.99, 125.70, 125.17, 124.48, 124.45, 122.30, 118.91, 118.29, 115.48, 67.31, 61.25, 14.19.

Mass calculated ($M+H^+$) 401.1389, found 401.1395.

$[\alpha]_D^{20}$ = -91.533 (c= 1mg/ml $CHCl_3$)

3.4.3 Fluorescence Spectra

Fluorescent measurement at room temperature:

To a suspension of 1 mL of 2.0 x 10^{-5} M Probe and 1ml carbonate buffer solution (CBS, 25mM of sodium carbonate with 25mM of sodium bicarbonate, pH=10.1), were added with 10 µL of 20 mM amino acids (in CBS) and 10 µL of 4 mM $Zn(OAc)_2$ (in water). After let them stand for 3 hours, the mixtures were tested for fluorescence. Slit=3/3nm, int time =0.1s. Fluorescence emission spectra were recorded on Horiba FluoroMax-4 spectrofluorometer.

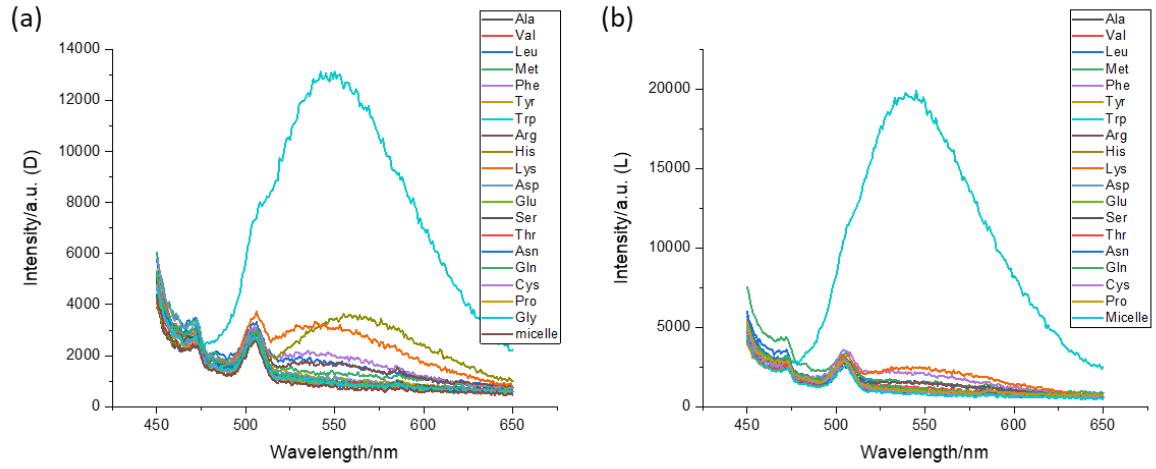

Figure S3. 2 (*S*)-**3.2a**@PEG-PLLA responses for various (a) D-amino acids; (b) L-amino acids. Corresponding organic sensor concentration = 10 µM, with 2eq. zinc acetate, 10eq. amino acids. Excited at 430nm, slit=3/3nm, integration time=0.1s.

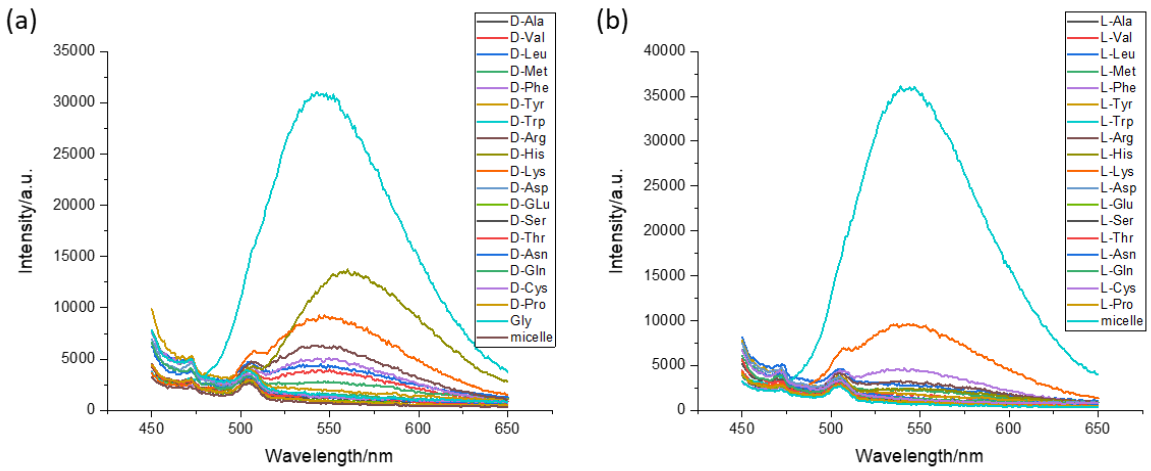

Figure S3. 3 (*S*)-**3.2b**@PEG-PLLA responses for various (a) D-amino acids; (b) L-amino acids. Corresponding organic sensor concentration = 10 μM, with 2eq. zinc acetate, 10eq. amino acids. Excited at 430nm, slit=3/3nm, integration time=0.1s.

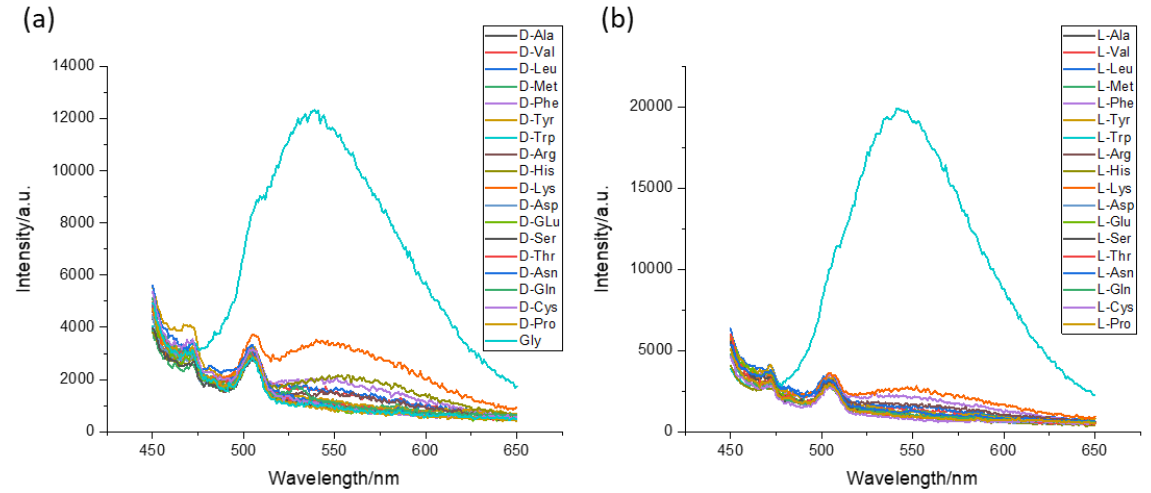

Figure S3. 4 (*S*)-**3.2c**@PEG-PLLA responses for various (a) D-amino acids; (b) L-amino acids. Corresponding organic sensor concentration = 10 μM, with 2eq. zinc acetate, 10eq. amino acids. Excited at 430nm, slit=3/3nm, integration time=0.1s.

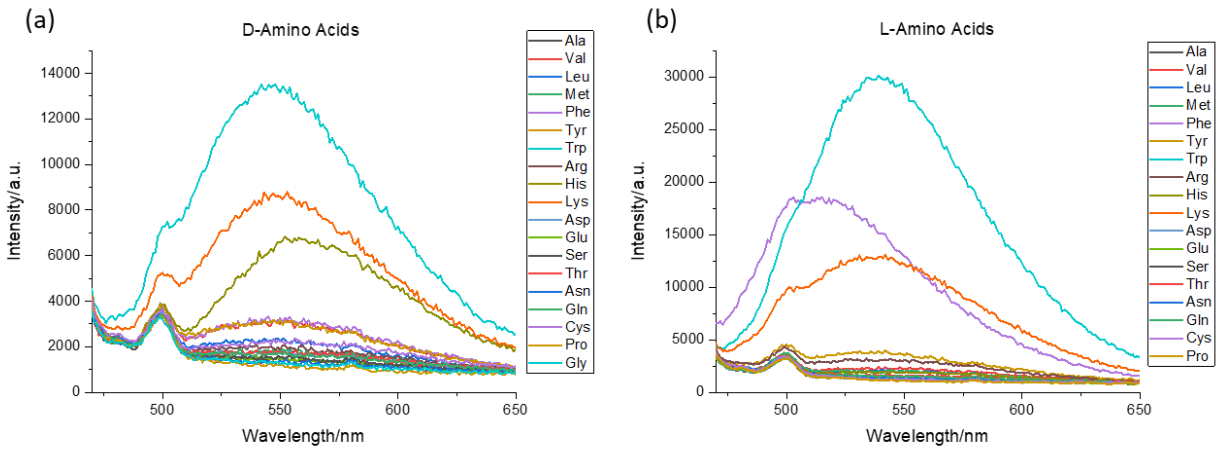

Figure S3. 5 (*S*)-**3.2d**@PEG-PLLA responses for various (a) D-amino acids; (b) L-amino acids. Corresponding organic sensor concentration = 10 μM, with 2eq. zinc acetate, 10eq. amino acids. Excited at 430nm, slit=3/3nm, integration time=0.1s.

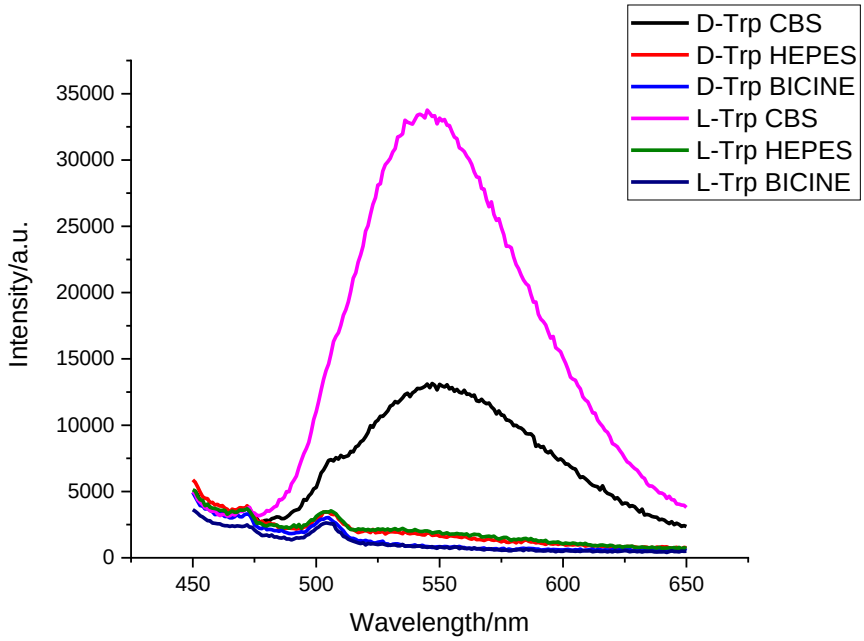

Figure S3. 6 (*S*)-**3.2c**@PEG-PLLA, buffer test. Corresponding organic sensor concentration = 10 μM, with 2eq. zinc acetate, 10eq. amino acids. Excited at 430nm, slit=3/3nm, integration time=0.1s.

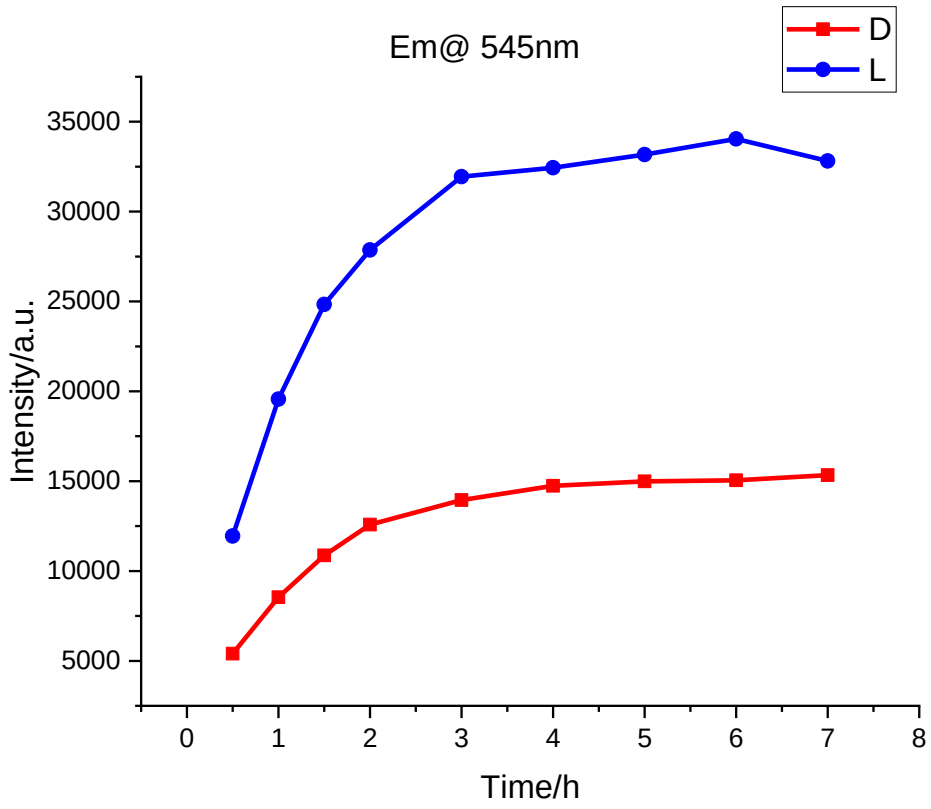

Figure S3. 7 (*S*)-**3.2c**@PEG-PLLA, time course at room temperature. The intensities stabilized at around 5h.

Low-temperature fluorescence study:

To a suspension of 1mL of 20 µM Probe and 1ml CBS buffer, were added with 10 µL of 20 mM AA (in water) and 10 uL of 4 mM $Zn(OAc)_2$ (in water). After let them stand for 3 hours, the mixtures were chilled in an ice bath, and tested for fluorescence with FluoroMax3 at a temperature of 5 degree Celsius with a continuous nitrogen flow. Slit=3/3nm, int time =0.3s.

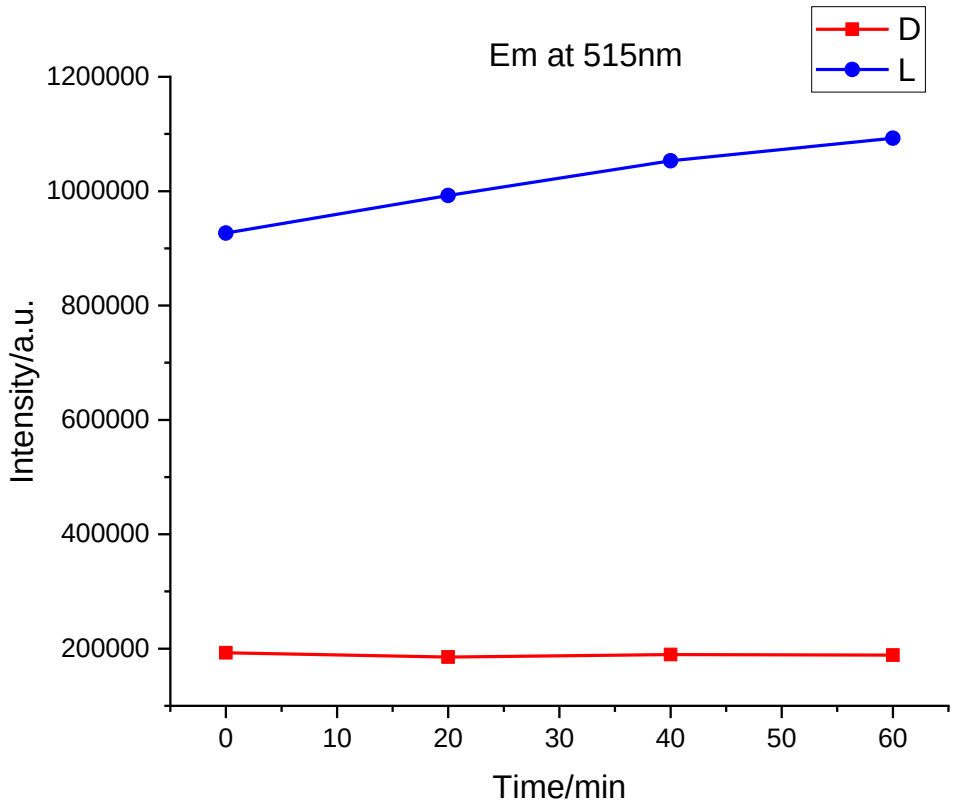

Figure S3. 8 Instability of (*S*)-**3.2d**@PEG-PLLA. The intensity changed 17% within an hour. 10uM of corresponding (*S*)-**3.2d**, 2eq. Zn. 10eq. phenylalanine, in carbonate buffer. Cooled with an ice water bath after 3h reaction at room temperature, and measured at 5 ^{o}C. Ex 430nm, slit=3/3nm, int time=0.1s.

3.4.4 NMR studies for the reaction of (*S*)-3.2c with tryptophan

General conditions: 2mM of (*S*)-**3.2c** in d_6-MeOH, 5eq. of Trp-TBA salt in d_6-MeOH.

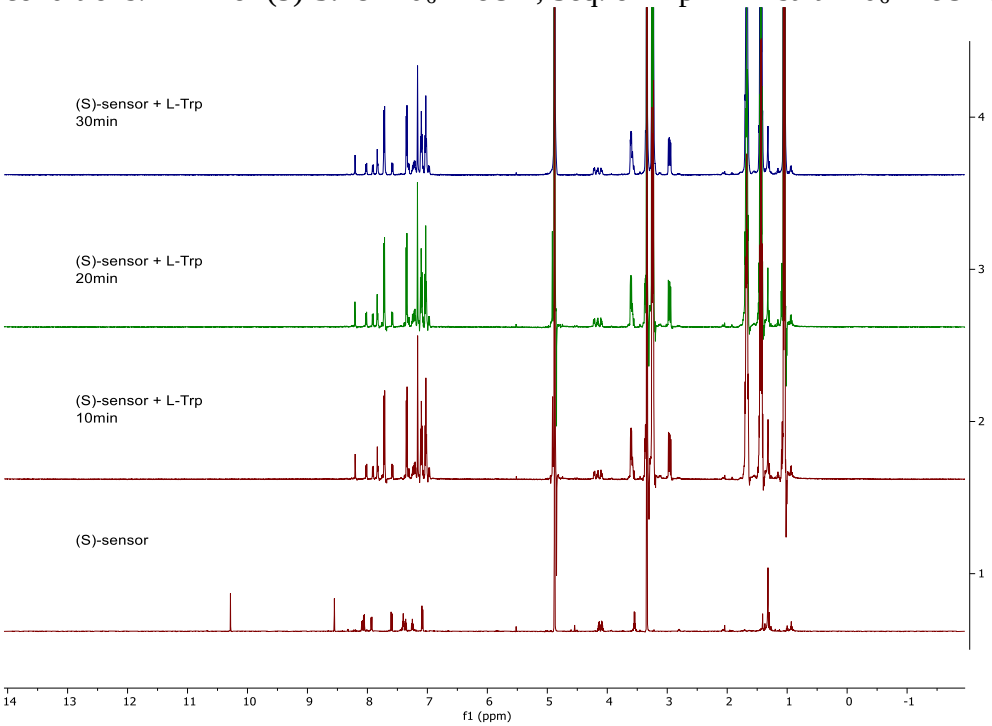

Figure S3. 9 Kinetic studies of the reaction between (*S*)-**3.2c** and L-Trp.

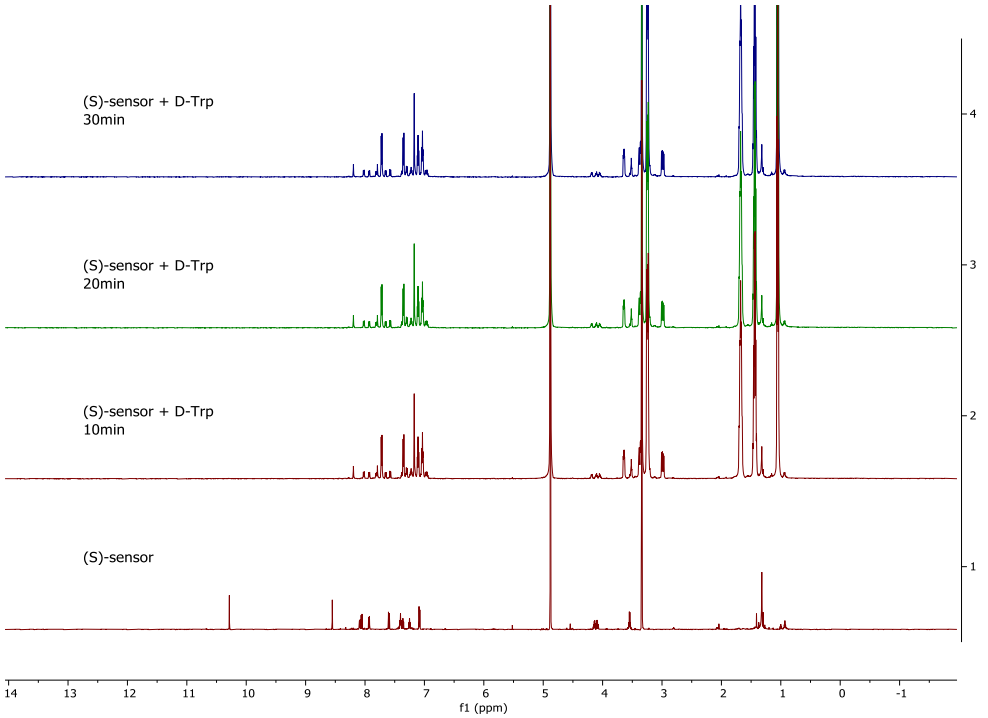

Figure S3. 10 Kinetic studies of the reaction between (*S*)-**3.2c** and D-Trp.

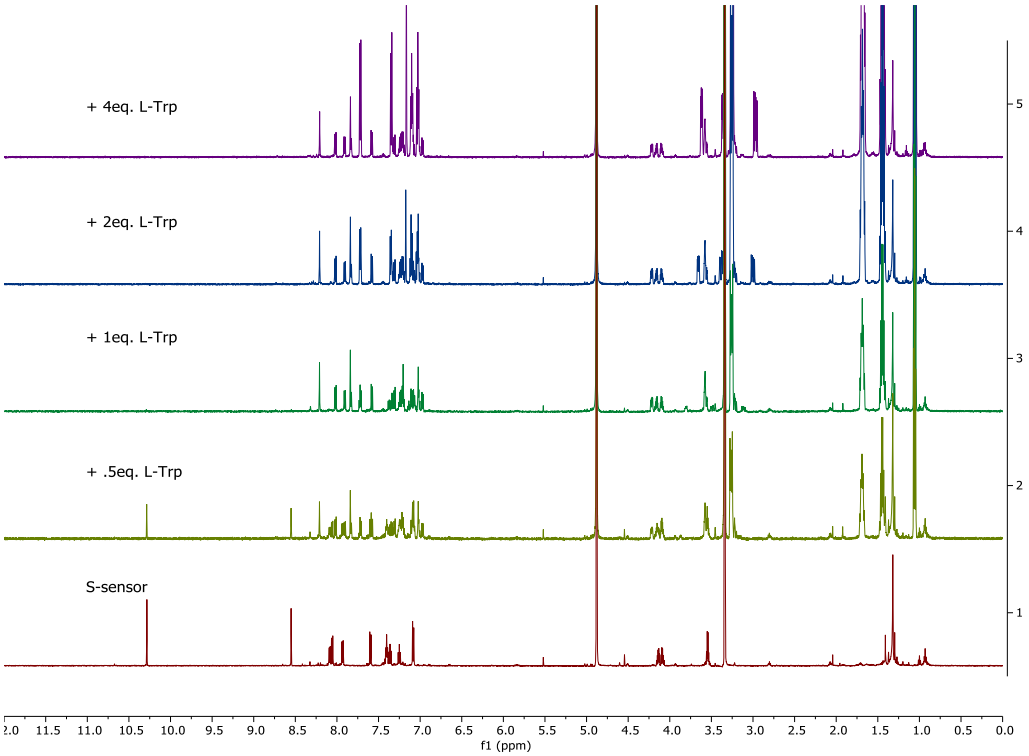

Figure S3. 11 Stoichiometric studies of the reaction between (*S*)-**3.2c** and L-Trp.

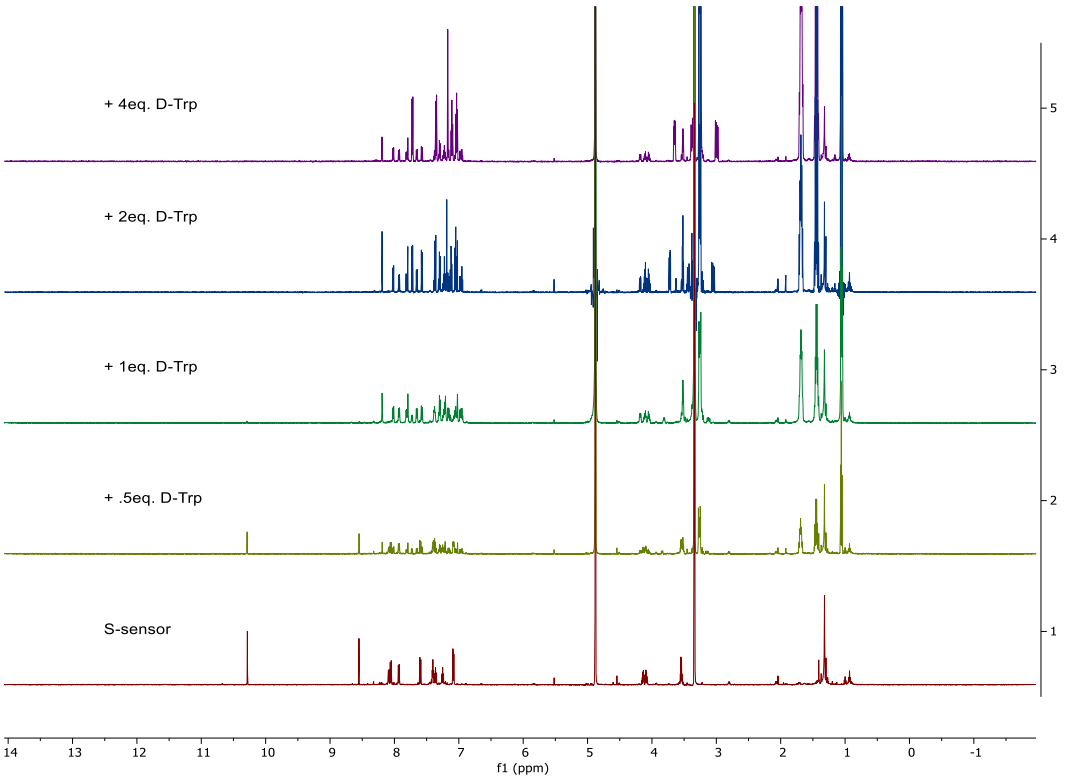

Figure S3. 12 Stoichiometric studies of the reaction between (*S*)-**3.2c** and D-Trp.

3.4.5 UV-vis spectra of (*S*)-3.2c with tryptophan

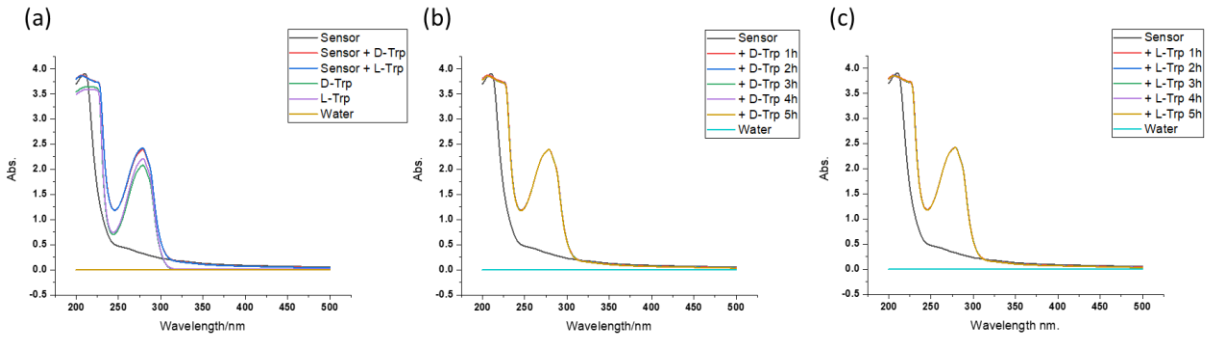

Figure S3. 13 (a) Overview; (b) Time course with D-Trp; (c) Time course with L-Trp. Corresponding concentration = 10μM, 2eq. zinc acetate, 10eq. trp.

3.4.6. DLS studies of (*S*)-2c@PEG-PLLA with tryptophan

Prodecures: To a suspension of 1mL of 20 μM Probe and 1ml CBS buffer, were added with 40 μL of 20 mM AA (in water) and 10 uL of 4 mM $Zn(OAc)_2$ (in water). After let them stand for 3 hours, the mixtures were analyzed via dynamic light scattering (DLS, Wyatt, DynaPro).

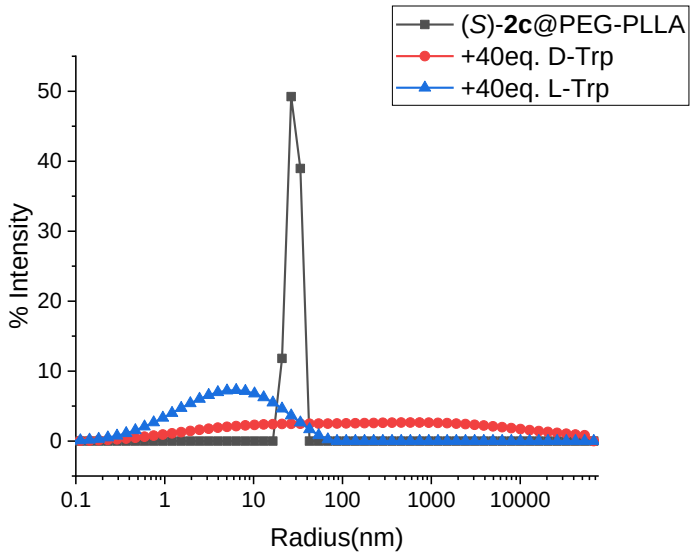

Figure S3. 14 DLS studies.

3.4.7. NMR spectra

^{1}H-NMR (600MHz), $CDCl_3$

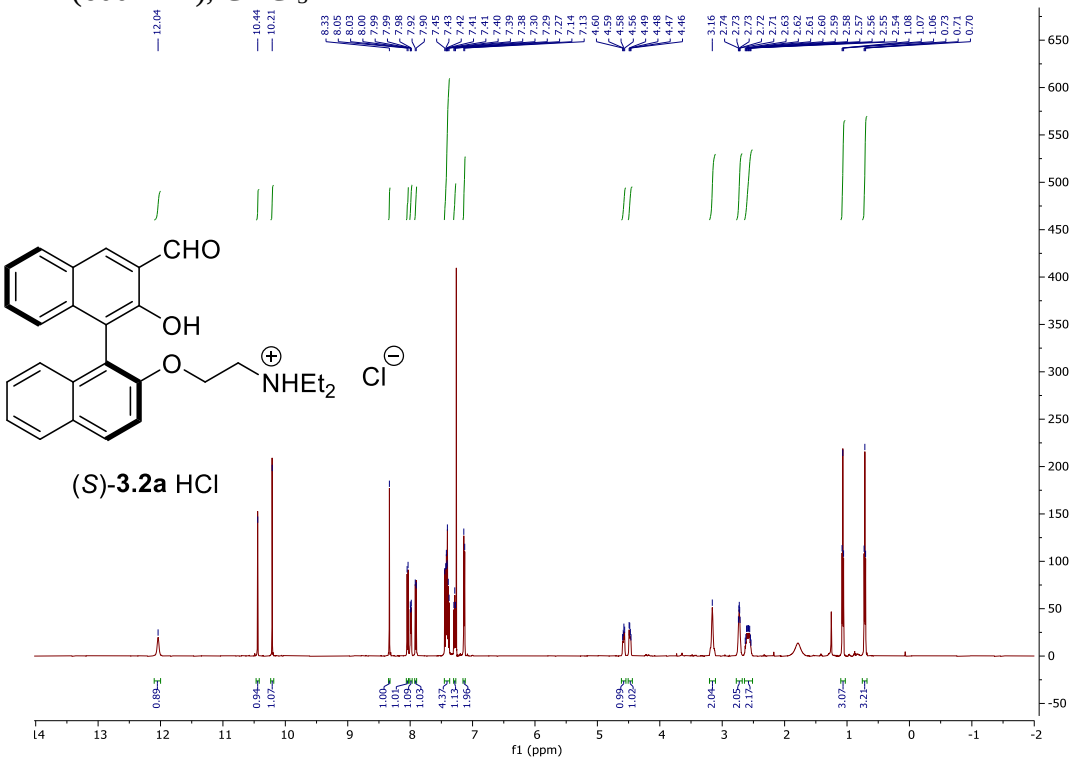

^{13}C-NMR (201MHz), $CDCl_3$

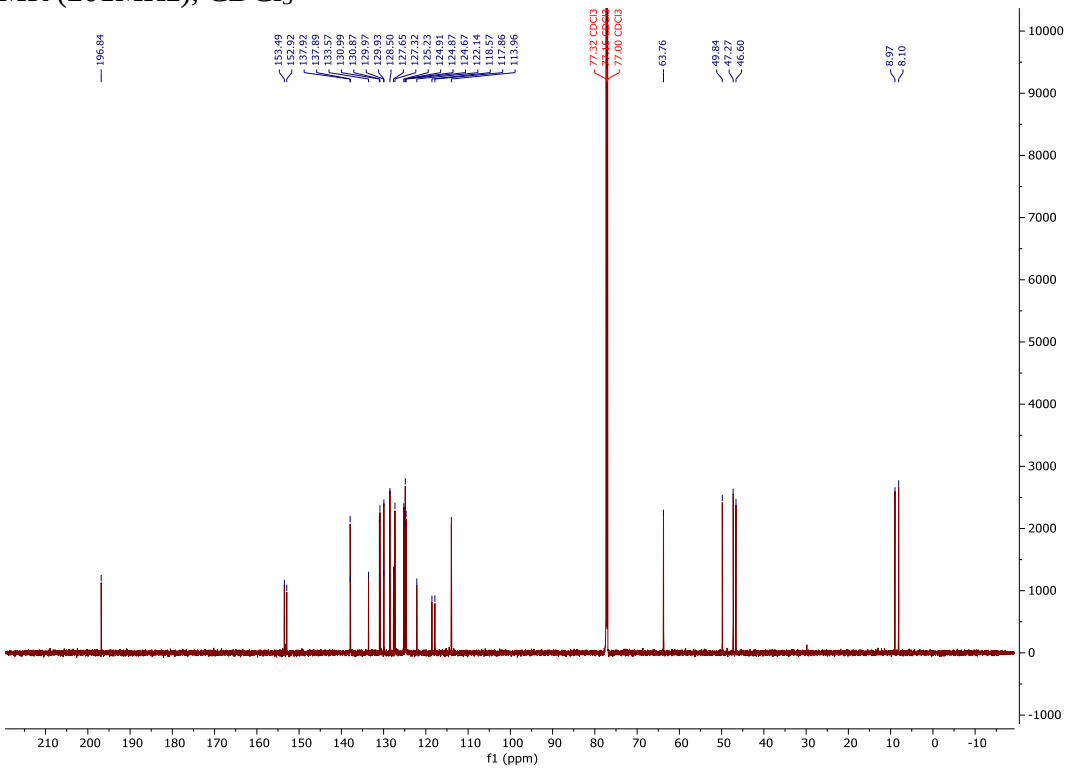

^{1}H-NMR (600MHz), $CDCl_3$

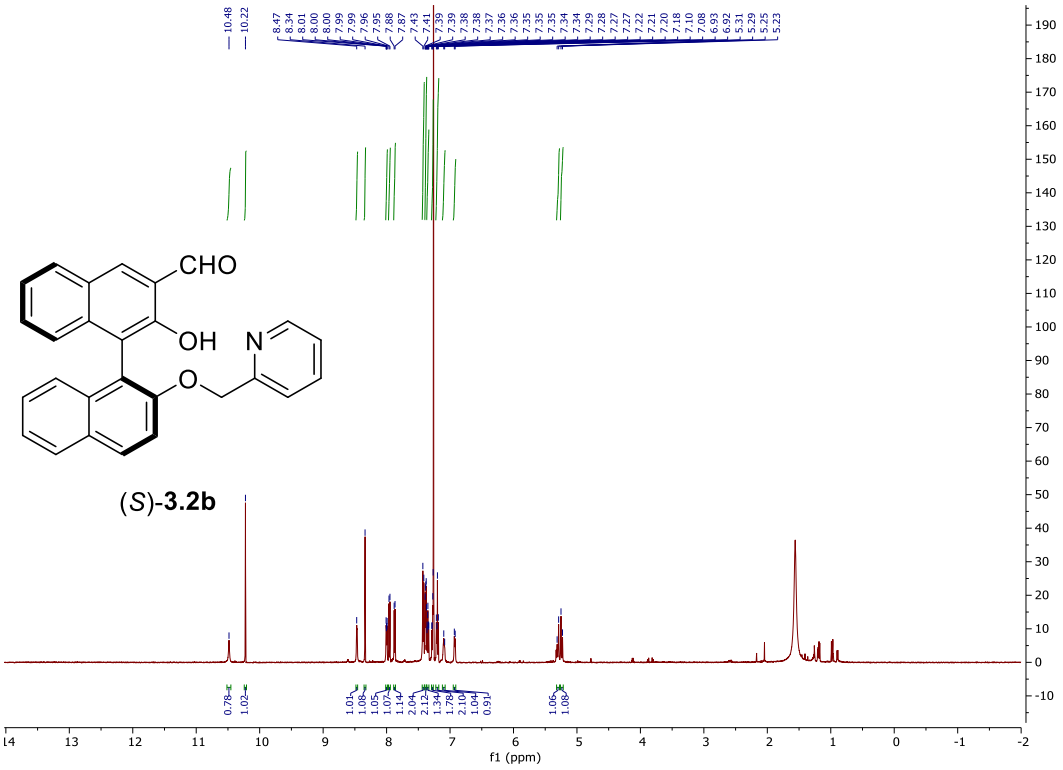

^{13}C-NMR (201MHz), $CDCl_3$

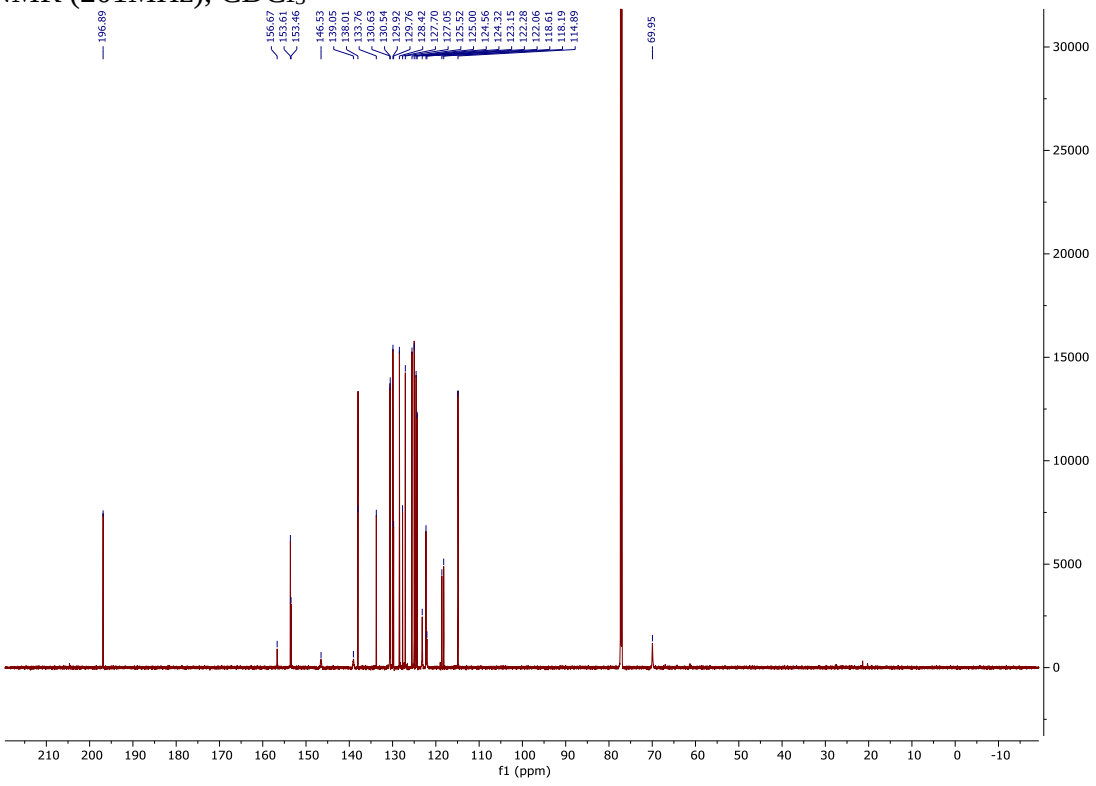

^{1}H-NMR (600MHz), $CDCl_3$

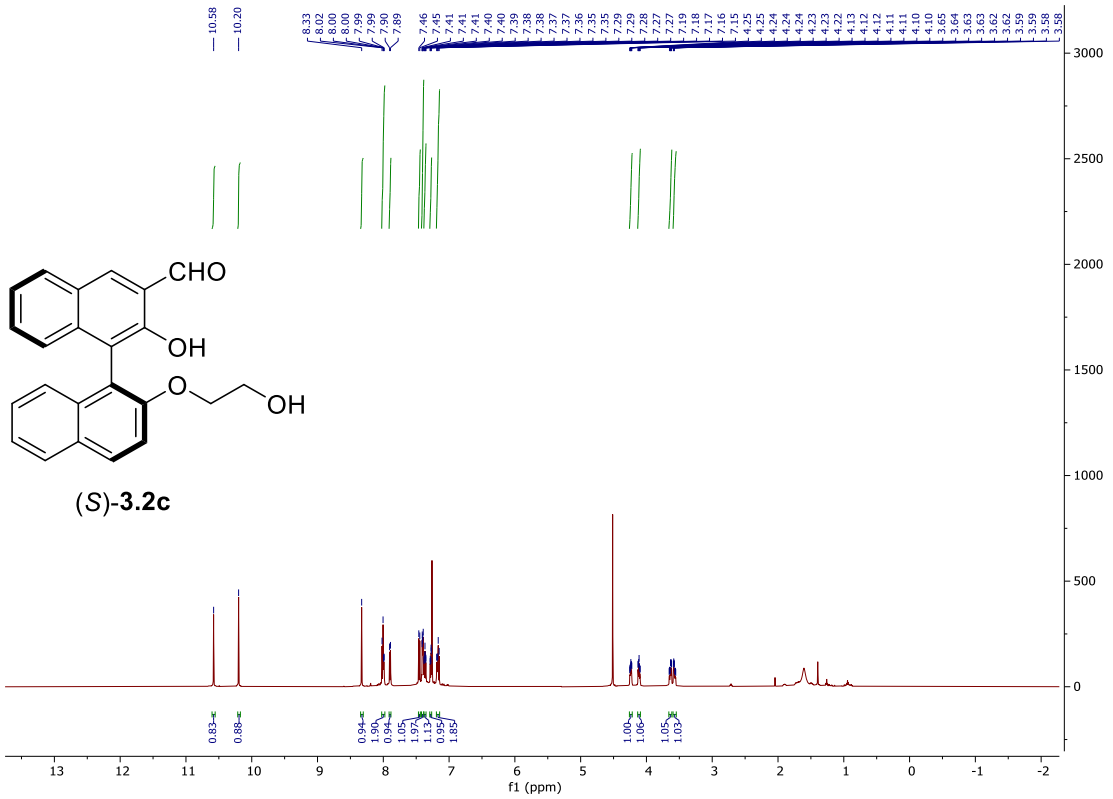

(*S*)-**3.2c**

^{13}C-NMR (201MHz), $CDCl_3$

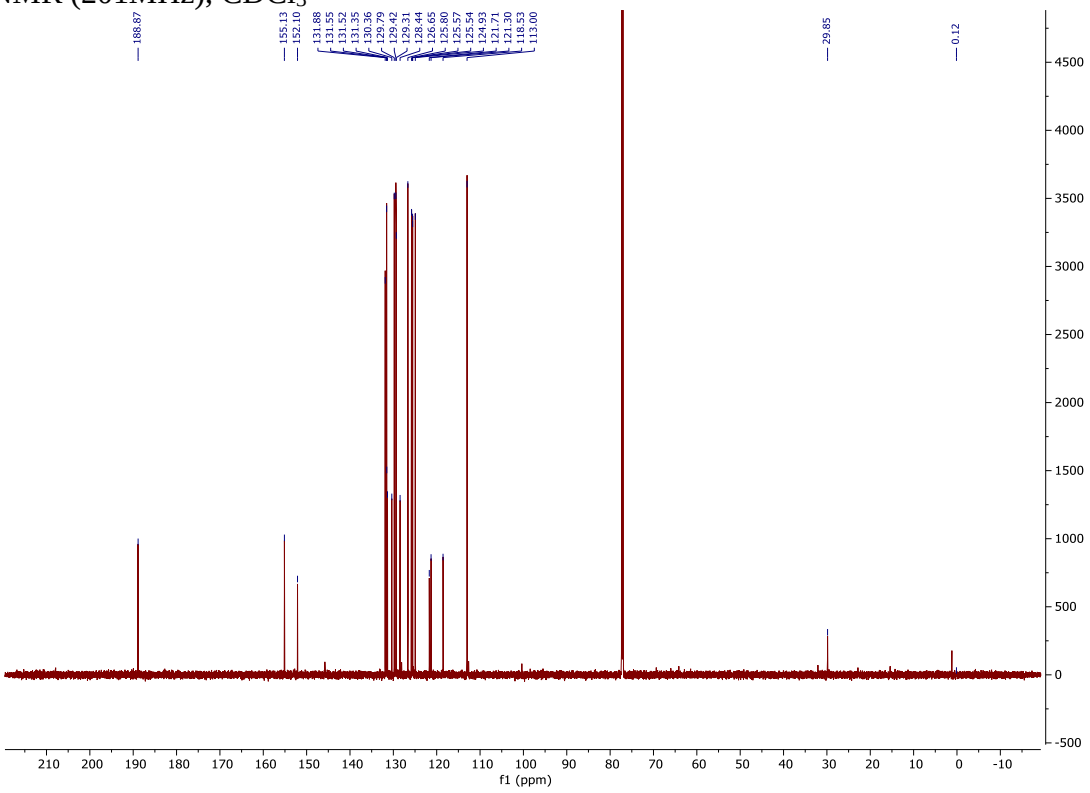

^{1}H-NMR (600MHz), $CDCl_3$

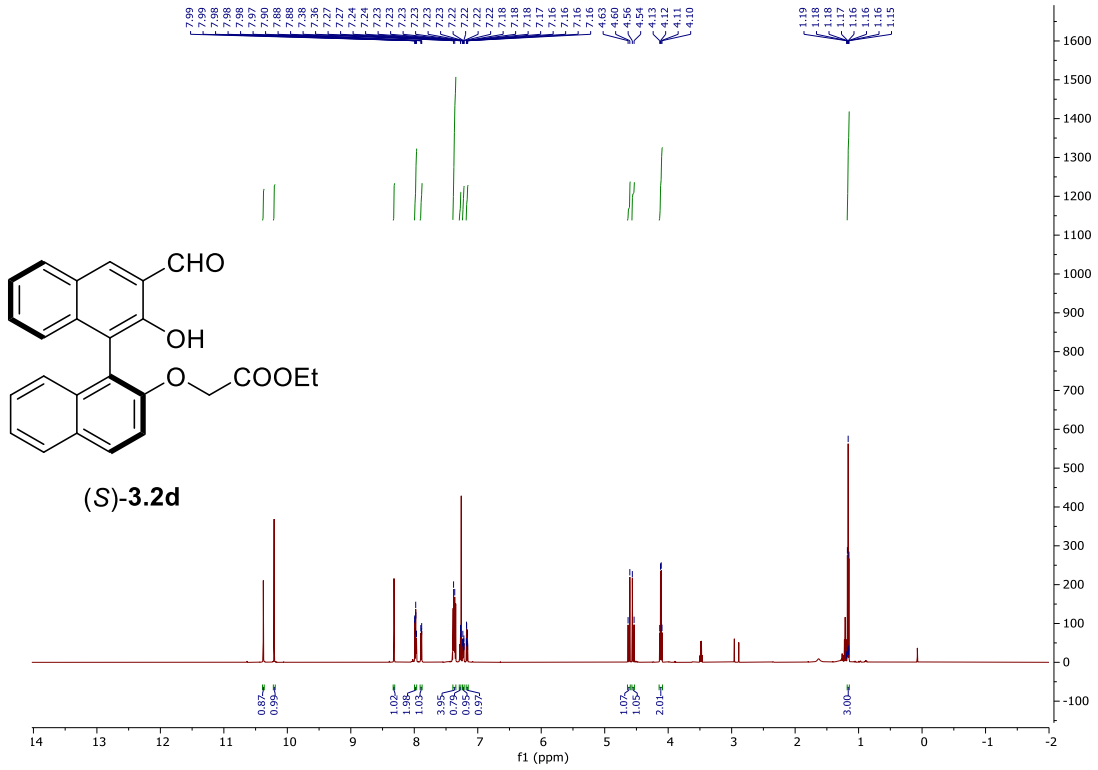

(*S*)-**3.2d**

^{13}C-NMR (201MHz), $CDCl_3$

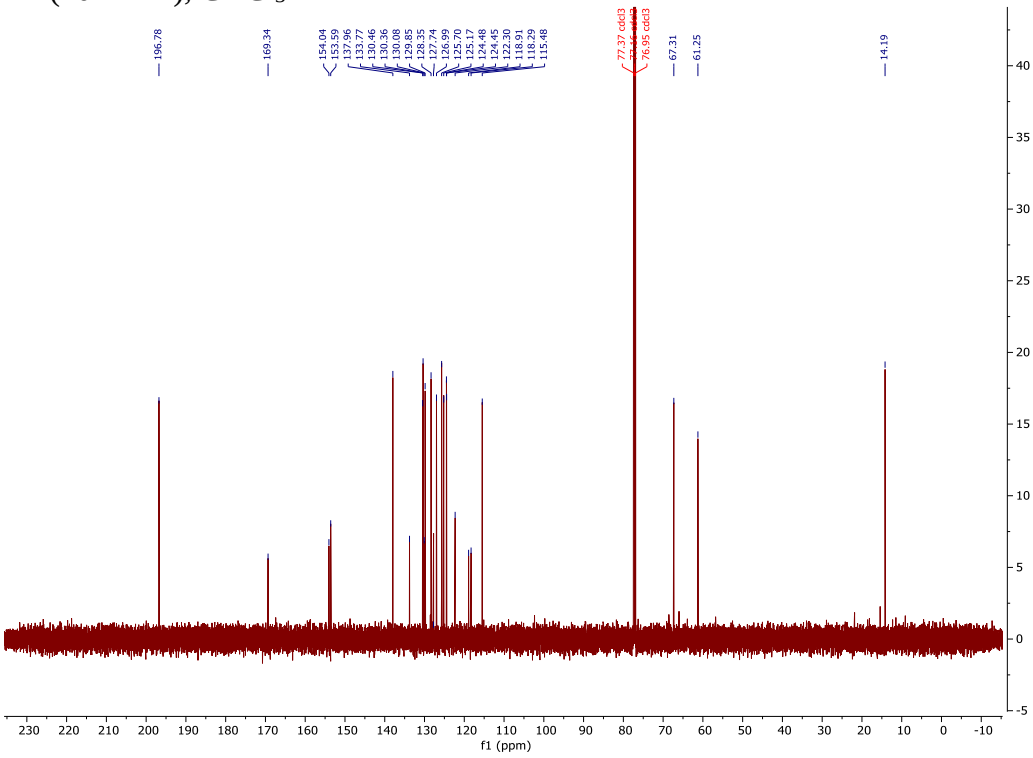

3.4.8. Mass Spectra

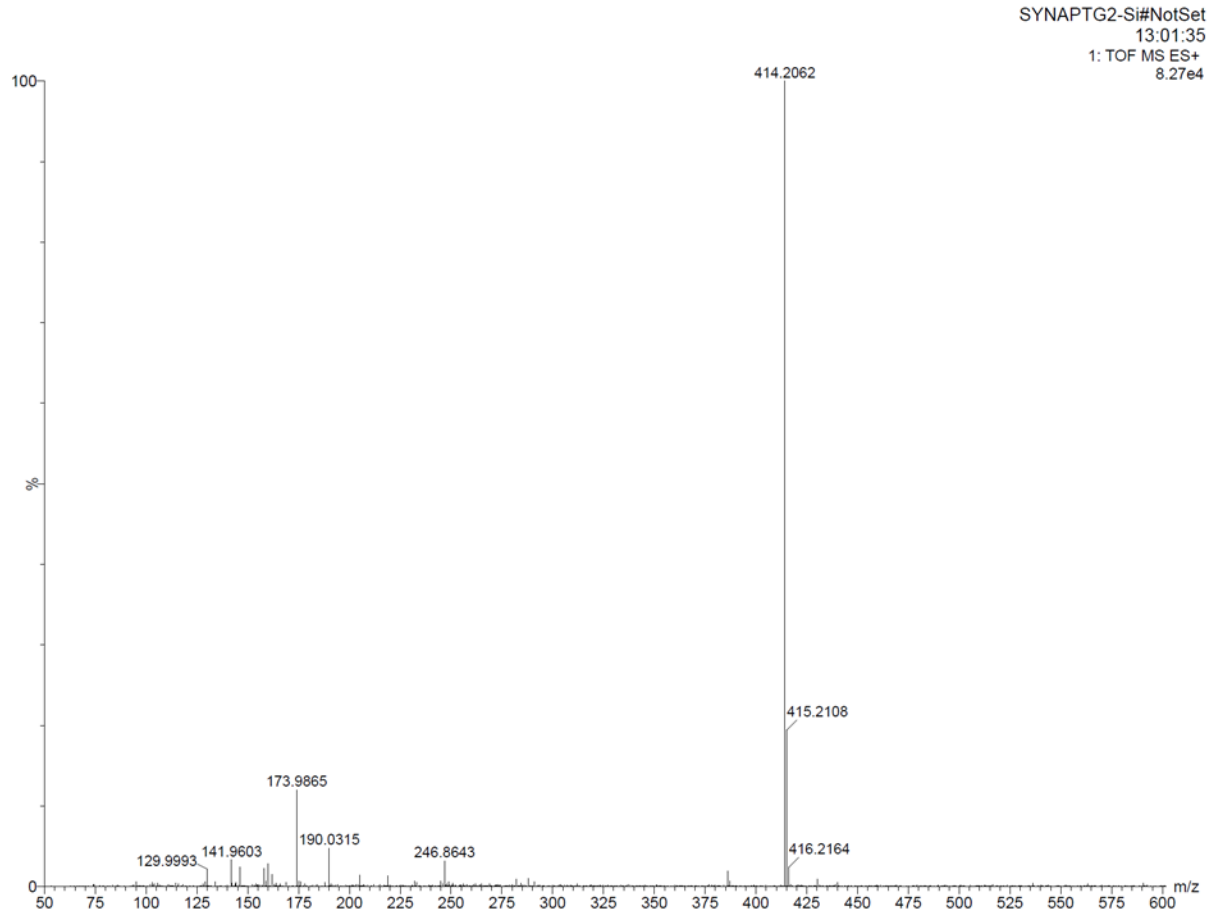

Figure S3. 15 Mass spectrum of (*S*)-**3.2a**.

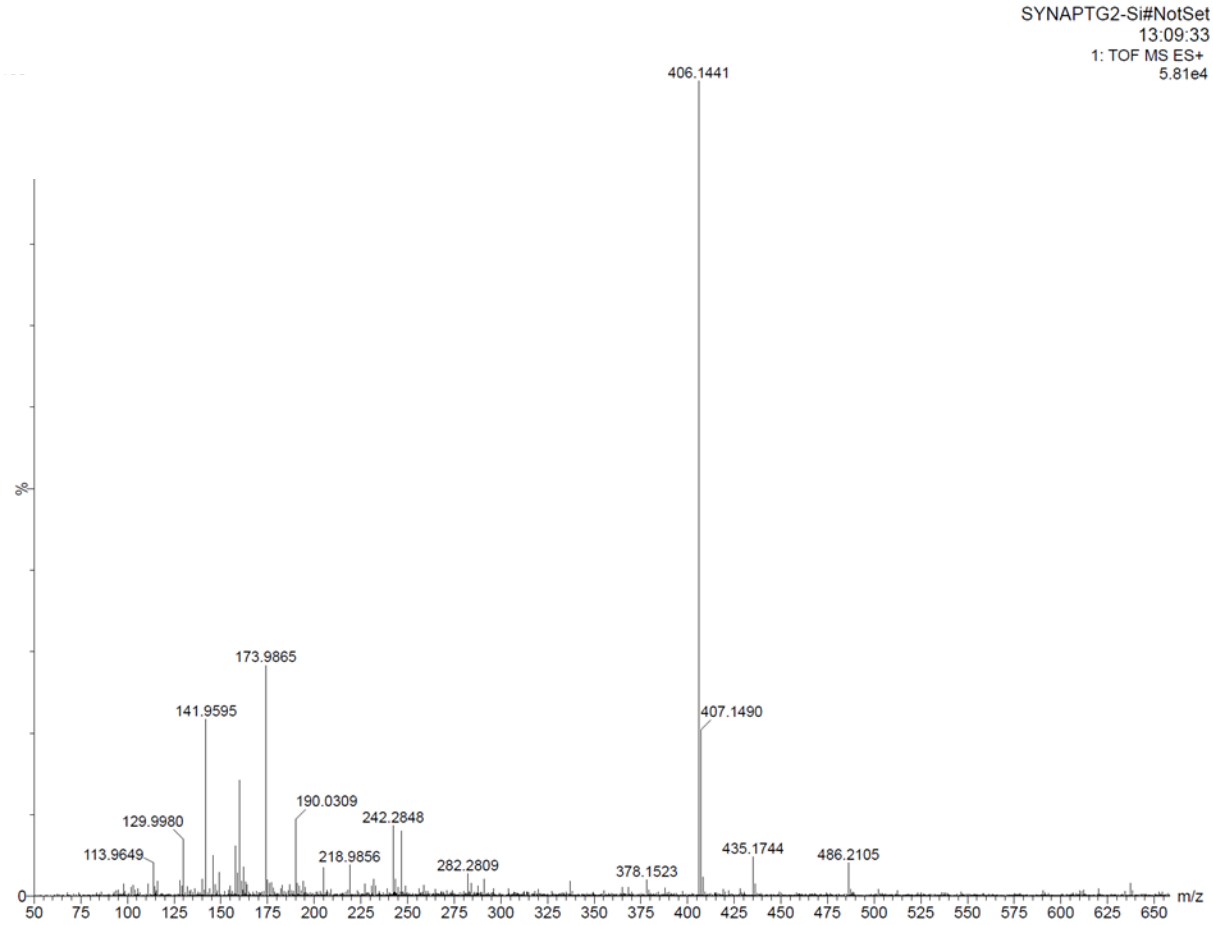

Figure S3. 16 Mass spectrum of (*S*)-**3.2b**.

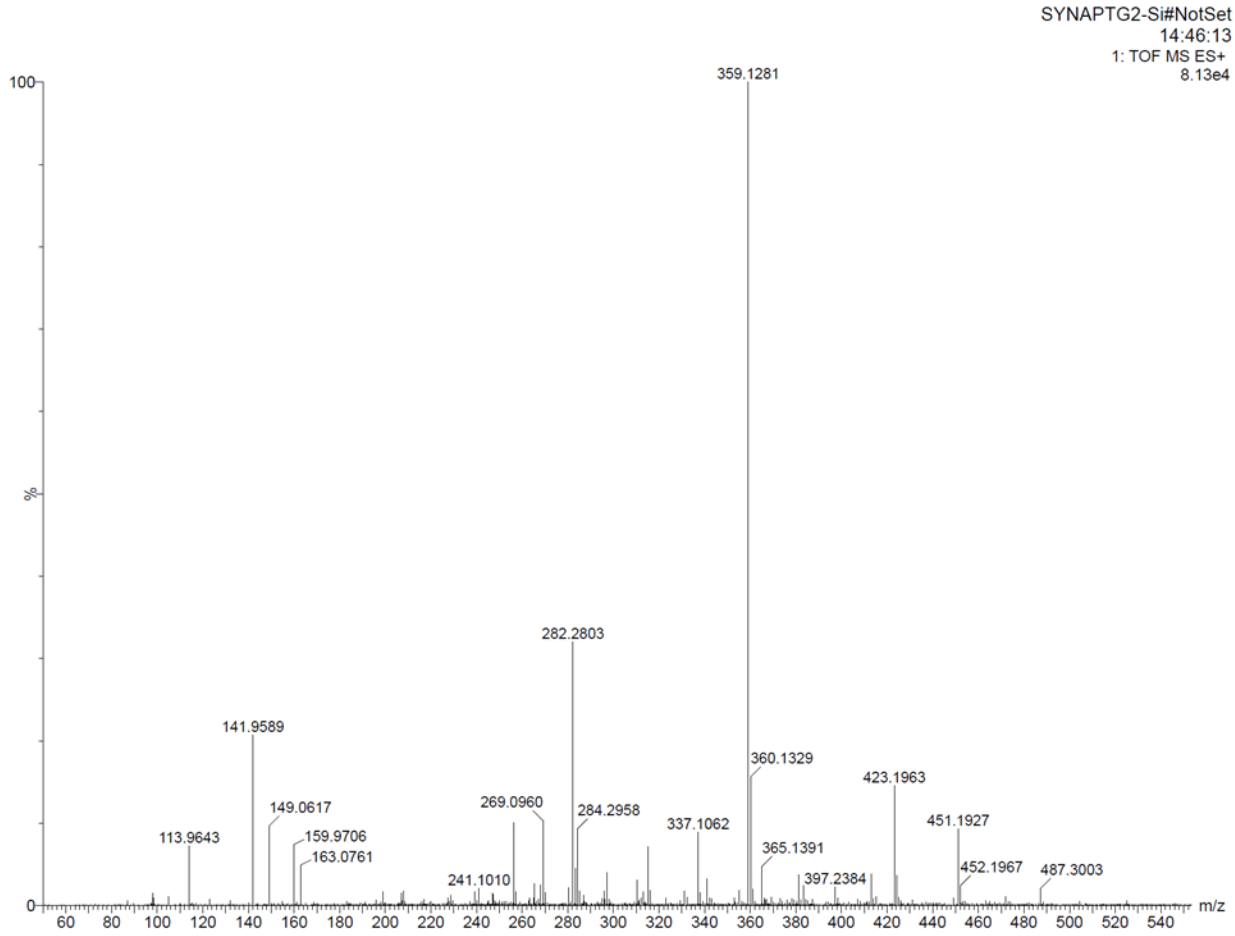

Figure S3. 17 Mass spectrum of (*S*)-**3.2c**.

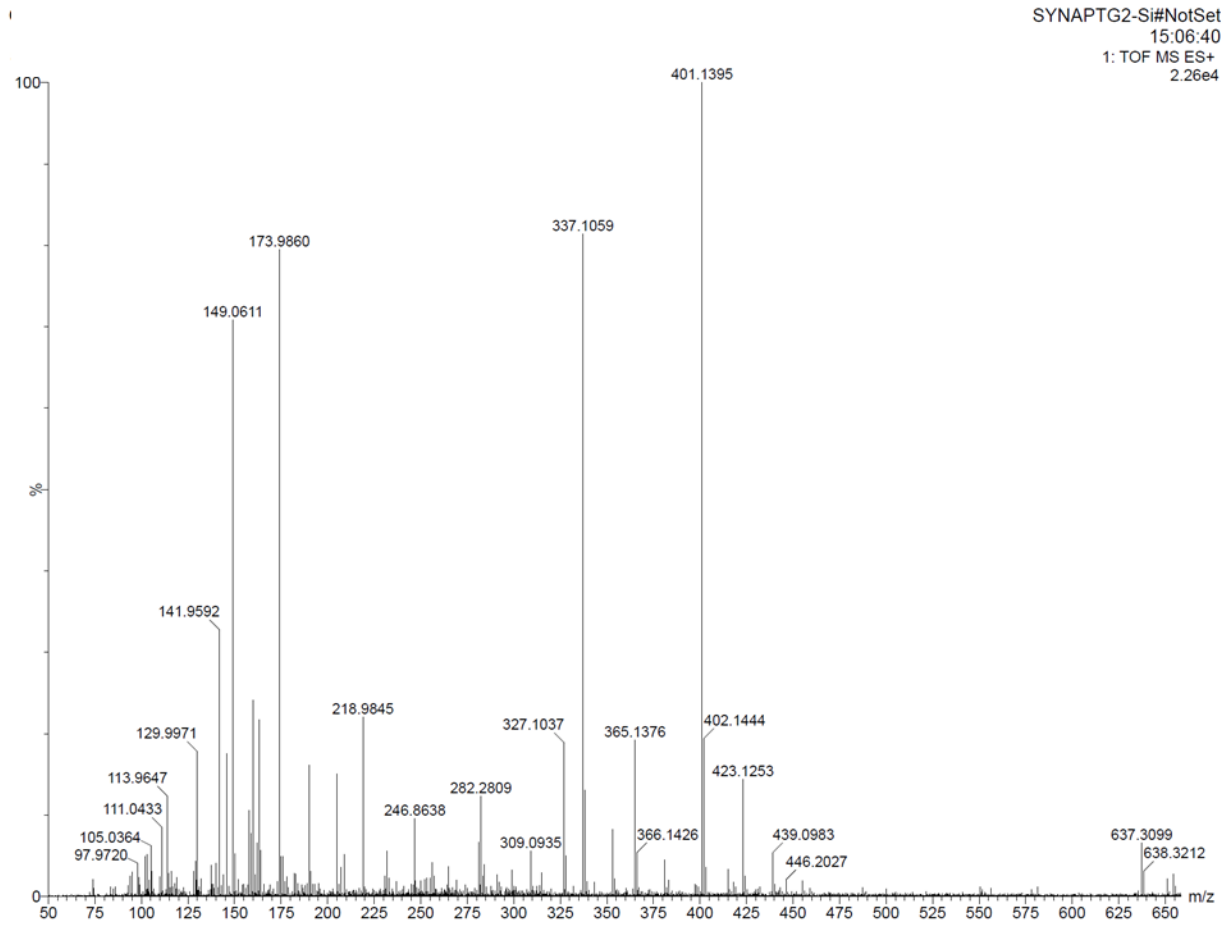

Figure S3. 18 Mass spectrum of (*S*)-**3.2d**.

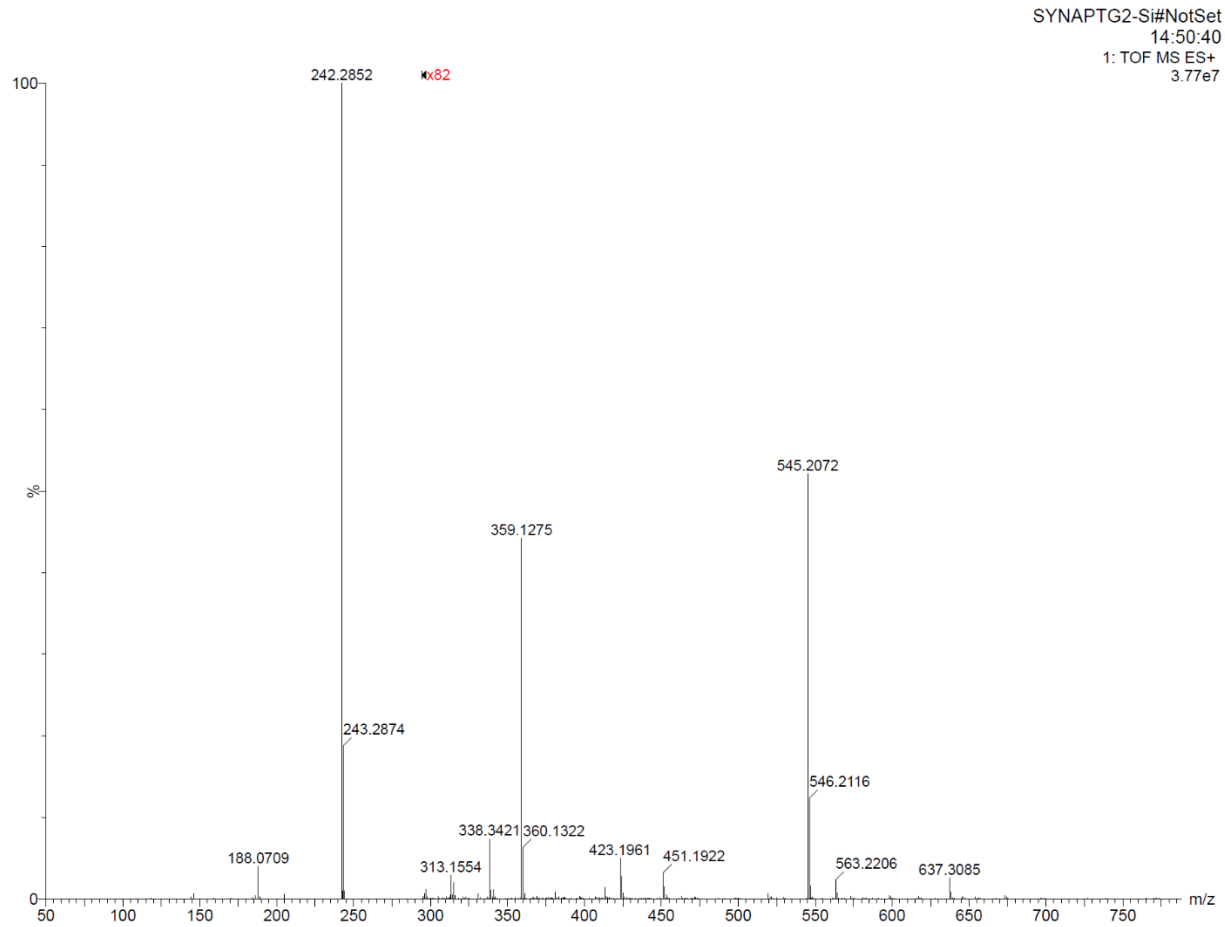

Figure S3. 19 Mass spectrum of the mixture of (*S*)-**3.2c** with 4eq. of L-Trp (TBA salt form).

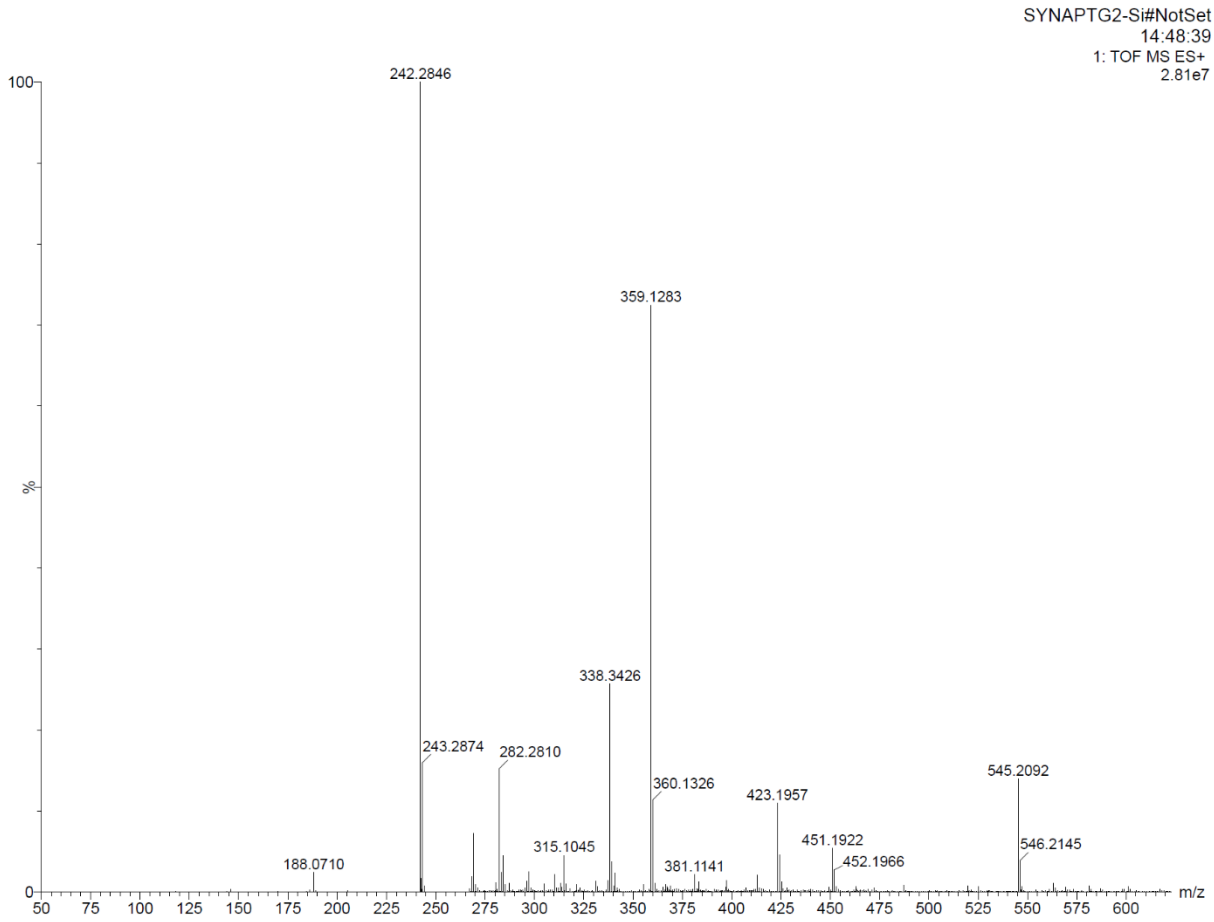

Figure S3. 20 Mass spectrum of the mixture of (*S*)-**3.2c** with 4eq. of D-Trp (TBA salt form).

3.5 References

(1) Selected reports on enantioselective fluorescent recognition of free amino acids: (a) S. Pagliari, R. Corradini, G. Galaverna, S. Sforza, A. Dossena, M. Montalti, L. Prodi, N. Zaccheroni, R. Marchelli, Enantioselective Fluorescence Sensing of Amino Acids by Modified Cyclodextrins: Role of the Cavity and Sensing Mechanism. *Chem. - Eur. J.* **2004**, 10, 2749-2758. (b) H. T. Feng, X. Zhang, Y. S. Zheng, Fluorescence Turn-on Enantioselective Recognition of Both Chiral Acidic Compounds and *α*-Amino Acids by a Chiral Tetraphenylethylene Macrocycle Amine. *J. Org. Chem*. **2015**, 80, 8096-8101. (c) Y. Y. Zhu, X. D. Wu, S. X. Gu, L. Pu, Free Amino Acid Recognition: A Bisbinaphthyl-Based Fluorescent Probe with High Enantioselectivity. *J. Am. Chem. Soc*. **2019**, 141, 175-181.

(2) Reviews on fluorescent detection of amino acids without enantioselective recognition: (a) Zhou, Y.; Yoon, J. Recent Progress in Fluorescent and Colorimetric Chemosensors for Detection of Amino Acids. *Chem. Soc. Rev*. **2012**, *41*, 52–67. (b) Wang, J.; Liu, H.-B.; Tong, Z.; Ha, C.-S. Fluorescent/ Luminescent Detection of Natural Amino Acids by Organometallic Systems. *Coord. Chem. Rev*. **2015**, *303*, 139-184.

(3) (a) C. Lubec, Amino Acids (Chemistry, Biology, Medicine), Escom, New York, **1990**. (b) L. Nefyodov, Amino Acids and Their Derivatives (Chemistry, Biochemistry, Pharmacology, Medicine), Proceeding of the International Symposium, Grodno, **1996**.

(4) (a) R. Konno, H. Breckner, A. D'Aniello, G. Fisher, N. Fujii, H. Homma (Eds) D-Amino Acids: A New Frontier in Amino Acids and Protein Research: Practical Methods and Protocols, Nova Science New York, **2007**; (b) C. A. Weatherly, S. Du, C. Parpia, P. T. Santos, A. L. Hartman, D. W. Armstrong, *ACS Chem. Neurosci*. **2017**, 8, 1251-1261.

(5) Kałużna-Czaplińska, J.; Gątarek, P.; Chirumbolo, S.; Chartrand, M. S.; Bjørklund, G. How

Important Is Tryptophan in Human Health? *Critical Reviews in Food Science and Nutrition*. 2019, 59, 72–88.

(6) Friedman, M. Analysis, Nutrition, and Health Benefits of Tryptophan. *International Journal of Tryptophan Research*. 2018, 11, 1-12.

(7) Peters JC. Tryptophan nutrition and metabolism: an overview. *Adv Exp Med Biol*. **1991**, *294*, 345-358.

(8). Keszthelyi D, Troost FJ, Masclee AAM. Understanding the role of tryptophan and serotonin metabolism in gastrointestinal function *Neurogastroenterol Motil* **2009**, *21*, 1239–1249.

(9) Friedman M, Cuq JL. Chemistry, analysis, nutritional value, and toxicology of tryptophan in food. A review. *J Agric Food Chem*. **1988**, *36*, 1079–1093.

(10) Molnár-Perl I. Tryptophan analysis in peptides and proteins, mainly by liquid chromatography. *J Chromatogr*. **1997**, *763*, 1–10.

(11) Ilie-Mihai, R.-M.; Staden, R.-I. S.-v.; Magerusan, L.; Coros, M.; Pruneanu, S. Enantioanalysis of Tryptophan in whole blood samples using stochastic sensors—A screening test for gastric cancer. *Chirality*. **2020**, *32*, 215–222.

(12) Kakizoe, T.; Komatsu, H.; Honma, Y.; Niijima, T.; Sugimura, T. Detection of Amino Acids as Possible Promoters of Bladder Cancer in Rats by Measuring Their Enhancement of Agglutination of Bladder Cells by Concanavalin A. *Gan* **1982**, *73* (6), 870–873.

(13) (a) Chen, J.; Kudo, H.; Kan, K.; Kawamura, S.; Koseki, S.; Dudley, E. G. Growth-Inhibitory Effect of D-Tryptophan on Vibrio Spp. in Shucked and Live Oysters. *App. Environ. Microbio*. **2018**, *84*, e01543-18.. (b) Ghosh, S.; Qureshi, A.; Purohit, H. D-Tryptophan Governs Biofilm Formation Rates and Bacterial Interaction in P. Mendocina and S. Aureus. *J. Biosci.* **2019**, *44* (1).

(14) Kobayashi, K.; Maezawa, T.; Tanaka, H.; Onuki, H.; Horiguchi, Y.; Hirota, H.; Ishida, T.;

Horiike, K.; Agata, Y.; Aoki, M.; et al. The Identification of D-Tryptophan as a Bioactive Substance for Postembryonic Ovarian Development in the Planarian Dugesia Ryukyuensis *Sci. Rep.* **2017**, *7*, 45175.

(15) L. Tang, G. Wei, R. Nandhakumar, Z. Guo, Facile Synthesis of the Uryl Pendant Binaphthol Aldehyde and Its Selective Fluorescent Recognition of Tryptophan. *Bull. Korean Chem. Soc*. **2011**, 32, 3367-3371.

(16) Kersey, F. R.; Zhang, G.; Palmer, G. M.; Dewhirst, M. W.; Fraser, C. L. *ACS Nano* **2010**, *4*, 4989–4996.

(17) Du, G.; Pu, L. Micelle-Encapsulated Fluorescent Probe: Chemoselective and Enantioselective Recognition of Lysine in Aqueous Solution. *Org. Lett*. **2019**, *21*, 4777-4781.

(18) Huang, Z.; Yu, S.; Wen, K.; Yu, X.; Pu, L. Zn(II) Promoted Dramatic Enhancement in the Enantioselective Fluorescent Recognition of Chiral Amines by a Chiral Aldehyde. *Chem. Sci.*, **2014**, *5 (9)*, 3457-3462.

(19) Zeng, C.; Zhang,X.; Pu, L. Enhanced Enantioselectivity in the Fluorescent Recognition of a Chiral Diamine by Using a Bisbinaphthyl Dialdehyde. *ACS Omega* **2018**, *3*, 12545−12548.

(20) Gostner, J. M.; Geisler, S.; Becker, K.; Fuchs, D.; Mayersbach, P.; Schennach, H. Serum Tryptophan, Kynurenine, Phenylalanine, Tyrosine and Neopterin Concentrations in 100 Healthy Blood Donors. *Pteridines* **2015**, *26*, 31–36.

Chapter 4. Ultrasensitive, Enantioselective and Chemoselective Detection of Chiral Histidine in Water Media

4.1 Introduction

4.1.1 Importance of Histidine

L-histidine is an essential amino acid, and is not synthesized *de novo* in humans. Besides its biofunctions such as key building blocks of proteins, L-histidine is also found to be a source for other biologically active amines, and participates in the tricarboxylic acid cycle (TCA).[1,2] The other enantiomer, D-histidine, has also been realized in agricultural products, foods and human bodies.[3–5] Levels of histidine has been reported to be lower in rheumatoid arthritis (RA) patients, and supplementation of L-histidine has been used to treat RA disease.[6–9] It will be very useful to construct more probes to further interrogate and elucidate the biofunctions of both enantiomers of this amino acids.

4.1.2. Relevant Probes

A common strategy for the non-*enantioselective* detection of basic amino acids, including Histidine, Lysine, and Arginine, is the use of polycyclic compounds, such as calixarenes, cucurbiturils, or pillararenes.[10–15] However, the specific recognition of one particular amino acid among these basic amino acids are very challenging. Most polycyclic structures-based probes experienced a hard time to distinguish the three basic amino acids, due to their comparable binding affinities.[13] Series of terpyridinyl-based probes have also been reported for the *chemoselective* detection of histidine.[16–18] The lack of amino acid screening, and calculations of limit of detection, makes related studies less persuasive and applicable.

Although recent studies have demonstrated many powerful techniques to detect lysine with decent sensitivity,[19,20] the specific recognition of amino acids, in the ways of both *chemoselectively*

and *enantioselectively*, is still challenging in the field of molecular recognition. We recently reported the specific detection of chiral lysine in water media by the micelle probe (*S*)-**4.1**@PEG-PLLA.[21] The *enantioselectivity* is endured by the chiral backbone of 1,1'-bi-2-naphthol (BINOL). And the *chemoselectivity* is attributed to the selective imine formation of terminal amino group of lysine, visualized by 2D-NMR techniques. The lack of water solubility has always been an issue for the BINOL-based *enantioselective* probes, as the fused aromatic rings favor organic phase. In that work, we make use of the micelle encapsulation strategy, with the biocompatible coblock dipolymer PEG-PLLA. The resulted micelle probes enhanced not only sensitivity but also selectivity.

4.1.2. H_4-BINOL

Like BINOL, the partially hydrogenated BINOLs such as octahydro-BINOL (H_8-BINOL) tetrahydro-BINOL (H_4-BINOL) and their derivatives, have been used as catalysts or catalyst precursors for asymmetric catalysts.[22–25] In a number of cases, the partially hydrogenated BINOLs have shown enhanced enantioselectivity over BINOLs due to their increased steric bulkiness and modified electronic environment. Although the BINOL-based carbaldehyde (*S*)-**4.1** and its derivatives have been proven to be powerful probes for *enantioselective* fluorescent detection,[26] the corresponding H_4-BINOL- and H_8-BINOL-based moleculeshave not been examined. Therefore, we have explored the use of the micelle-encapseulated partially hydrogenated BINOL-based carbaldehydes for the fluorescent recognition of amino acids. Herein, we report that the H_4-BINOL-based micelle probe (*S*)-**4.2**@PEG-PLLA is able to conduct selective fluorescent detection of chiral histidine.

4.2 Results and Discussion

4.2.1 Synthesis

As shown in Scheme 4.1., (*S*)-**4.2** were synthesized similarly according to the procedures reported to synthesize the BINOLdicarbaldehyde (*S*)-**1**and H_8-BINOLdicarbaldehyde (*S*)-**3** by three steps. The first step was deprotonation by sodium hydride and protection of the hydroxyl by MOMCl (MOM- = CH_3OCH_2-) in THF. The second step was deprotonation at the 3,3' positions by n-butyl lithium which was followed by reaction with DMF to yield carbaldehydes. The last step was the deprotection of MOM promoted by a strong acid, trifluoroacetic acid (TFA), in DCM. The overall reaction gave a yellow solid in 42% yield. The 1H NMR of S-4.2 in $CDCl_3$ solvent showed four singlets δ = 10.93, 10.55, 10.15, 9.90 representing 2 -O<u>H</u> and 2-C<u>H</u>O protons.

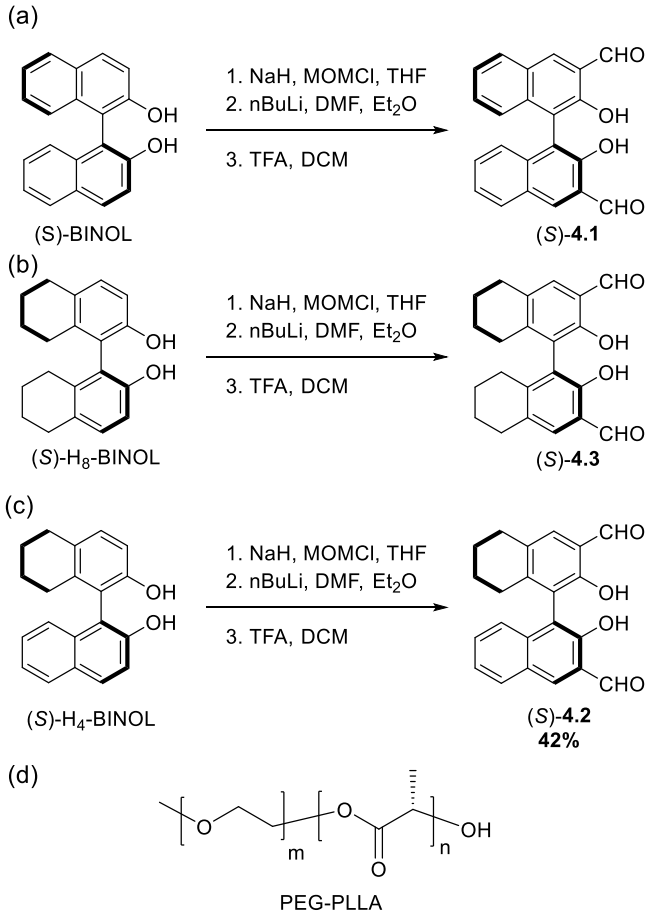

Scheme 4. 1 (a) Synthesis of diformylBINOL (*S*)-**4.1**; (b) Synthesis of diformyl-H_8-BINOL (*S*)-**4.3**; (c) Synthesis of diformyl-H_4-BINOL (*S*)-**4.2**; (d) Structure of PEG-PLLA

4.2.2 Fluorescence Studies

4.2.2.1 Amino Acids Screening

The micelle fabrication was conducted by nanoprecipitation of (*S*)-**4.2** in DMF to DI water (see SI for detailed experiments) according to the procedures for the preparation of (*S*)-**4.1**@PEG-PLLA. PEG-PLLA was used to encapsulate (*S*)-**4.2** to make (*S*)-**4.2**@PEG-PLLA micelle solutions (2.0×10^{-5}M). The fluorescence responses of the (*S*)-**4.2**@PEG-PLLA micelle solutions toward 19 amino acids, including their both enantiomers, were investigated in the presence of $Zn(OAc)_2$ (2.0 equiv). For each measurement, 1 mL of a (*S*)-**4.2@**PEG-PLLA solution was mixed with 1 mL carbonate buffer (CBS 25mM), 4 equiv amino acid (8 μL, 10 mM in water) and 2.0 equiv $Zn(OAc)_2$ (10 mL, 4 mM in water) which was allowed to stand at room temperature for 3 h. Then the mixtures were placed into an ice-water bath to quench the reaction for fluorescence measuerment. The final concentration of the probes in the solutions was 1.0×10^{-5} M with pH = 10.1. Figure 4.1 shows the fluorescence peak intensities of (*S*)-**4.2**@PEG-PLLA at λ_{em} = 560 nm in the presence of the enantiomers of 19 amino acids. The micelle solution (*S*)-**4.2**@PEG-PLLA showed very weak fluorescence upon excitation at 430 nm. When it was treated with most of the amino acids, only very small fluorescence enhancement was observed. However, D-histidine greatly enhanced the fluorescence with an enhancement of 31.32-fold, while L-histidine exhibited an enhancement of 3.70-fold. The fluorescence intensity with D-histidine was found to be much greater than that with its L-enantiomer, with an *enantioselective* fluorescence enhancement ratio [ef = $(I_D-I_0)/(I_L-I_0)$; I_D, I_L, and I_0 represent the fluorescence intensities at 560 nm with/without D-/L-histidine respectively] was calculated to be 11.22, meaning a very good *enantioselectivity* for D-histidine over L-histidine.

H_8-BINOLdicarbaldehyde (*S*)-**4.3** was also fabricated into the micelle probe (*S*)-**4.3**@PEG-PLLA. However, unlike (*S*)-**4.1**@PEG-PLLA which showed enantioselective fluorescent enahcement with lysine and (*S*)-**4.2**@PEG-PLLAwhich showed enantioselective fluorescent enhancement with histidine, (*S*)-**4.3**@PEG-PLLA remained fluorescence OFF when treated with all the amino acids. This is probably because of the non-radiative relaxation of its excited state back to the ground state via the aliphatic vibrations of its partially hydrogenated naphthalene rings.

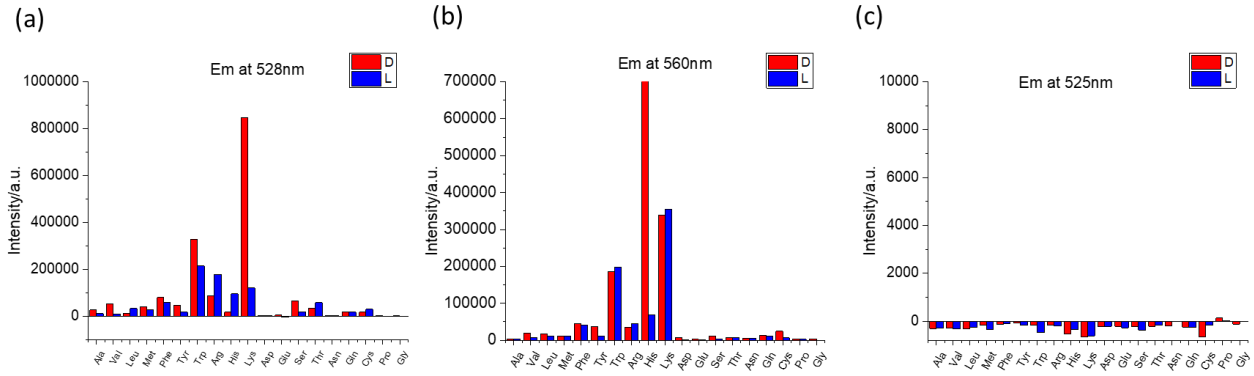

Figure 4. 1 Fluorescence intensities of (a) (*S*)-**4.1**@PEG-PLLA; (b) (*S*)-**4.2**@PEG-PLLA; (c) (*S*)-**4.3**@PEG-PLLA, with various amino acids including their both D- and L-enantiomers in CBS buffer solution. Emission at λ = 560nm, excitation at λ = 430nm, corresponding concentration of (*S*)-**4.2**= 10 μM, 2 equivalent $Zn(OAc)_2$, 4 equivalent amino acids. Reaction time = 3h at room temperature. Fluorescence measured at 5ºC, slit = 5/5nm, integration time = 0.1s.

4.2.2.2 Concentration Detection

We then studied the effect of the stoichiometry of histidine on the fluorescence responses of (*S*)-**4.2**@PEG-PLLA. As shown in Figure 4.2(a), the fluorescence intensities kept increasing with increasing concentrations of D-histidine until 4.0 equivalences (40 μM) after which the fluorescence intensities plateaued. Meanwhile, the fluorescence responses for L-histidine remains to be much weaker than those of D-histidine. Figure 4.2(b) featured the first-order linear fit of D-histidine reaction system in the range of 0.5-4.0 equivalences (5-40 μM). The R square value was

found to be 0.99. With a relatively sharp slope, the limit of detection (LOD = 3*SD/k. SD, standard deviation of noise; k, the slope of calibration curve) was then calculated to be 107 nM for D-histidine. The nano-molar scale value of LOD made (*S*)-**4.2@**PEG-PLLA superior over most other small molecule sensors, with common LOD in micro-molar scales, for histidine detection.[19]

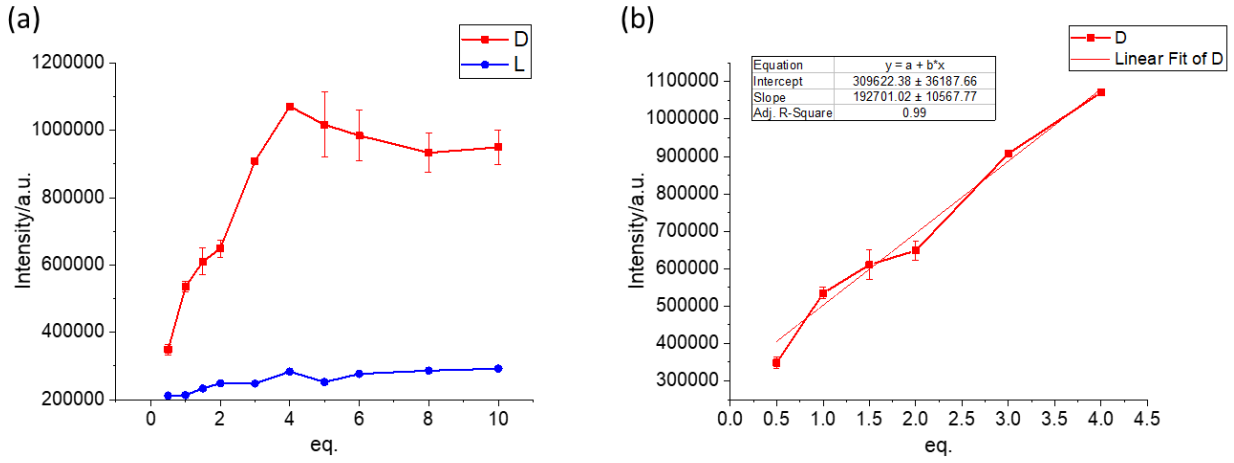

Figure 4. 2 (a) Stoichiometric studies of (*S*)-**4.2**@PEG-PLLA over D-/L-histidine in CBS buffer solution. (b) expanded view of 0.5 - 4.0 equivalences. Emission at λ = 560 nm, excitation at λ = 430 nm, corresponding concentration of (*S*)-**4.2** = 10 μM, 2 equivalent $Zn(OAc)_2$, with various equivalence of amino acids. Reaction time = 3 h at room temperature. Fluorescence measured at 5°C, slit = 5/5nm, integration time = 0.1s, error bars were obtained from 3 independent trials.

4.2.2.3 ee Detection

To further confirm the *enantioselective* recognition of this micelle probe. (*R*)-**4.2**, the enantiomer of (*S*)-**4.2**, was synthesized accordingly starting from (*R*)-H_4-BINOL. The diblock copolymer PEG-PDLA was also obtained from similar synthetic procedures for PEG-PLLA, from the D-lactide. (*R*)-**4.2**@PEG-PDLA, the enantiomeric analogue of (*S*)-**4.2**@PEG-PLLA was then prepared and studied for its fluorescence responses for histidine with varying enantiomeric excesses (ee = [D-L]/[D+L]). The ee studies were summarized in Figure 4.3a, the fluorescence responses of (*R*)-**4.2**@PEG-PDLA resembled a mirror image relationship with those of (*S*)-**4.2**@PEG-PLLA, which confirmed the observed *enantioselective* recognition of histidine. The

second-order fit relationships obtained gave very good R-square values, with 0.98 for (*S*)-**4.2**@PEG-PLLA, and 0.96 for (*R*)-**4.2**@PEG-PDLA. The imperfect matches of the fluorescence responses of two enantiomeric analogues are reasoned to be the results of intrinsic differences of the diblock copolymers such as differences in molecular weights and polydispersity (PDI), the random conformations of the polymers, and experimental errors. Utilizing the second-order fit calibration equations obtained, we tested the fluorescence responses of the micelle probes toward histidine samples of unknown ee values. The calculated ee values were found to be very close those measured with chiral HPLC techniques, as shown in Figure 4.3b.

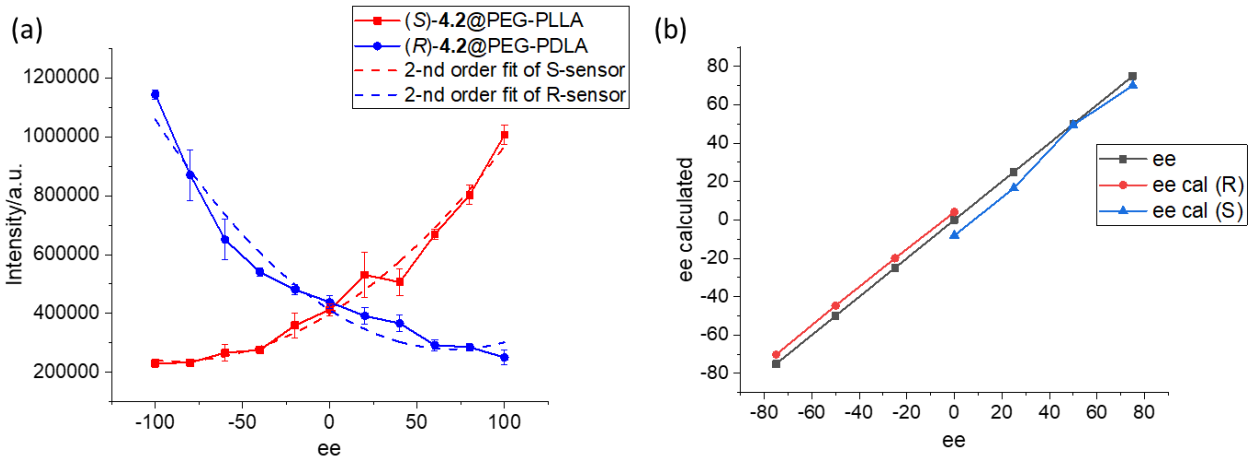

Figure 4. 3 (a) Fluorescence intensity of (*S*)-**4.2**@PEG-PLLA/(*R*)-**4.2**@PEG-PDLA with varying ee of histidine. (b) Unknown samples test results. Emission at λ=560nm, excitation at λ=430nm, corresponding concentration of (*S*)-**4.2** = 10 μM, 2 equivalent $Zn(OAc)_2$, 5 equivalence of histidine. Reaction time = 3h at room temperature. Fluorescence measured at 5°C, slit = 5/5nm, integration time = 0.1s, error bars were obtained from 3 independent trials.

4.2.3 Characterization of the Micelles

We studied the UV-vis responses of (*S*)-**4.2**@PEG-PLLA toward D-/L-histidine, but, no obvious changes were observed (see Figure S4.10). Given the strong fluorescence enhancements, the UV-vis data indicate that, only a very small degree of reaction happened between the micelle probe and the amino acid analytes, but the resulted products are very fluorescent inside the micelle

cores. Meanwhile, the roles of micelles in the molecular recognition events besides water solubility was investigated. In the absence of PEG-PLLA and micelles, the interactions of organic probe (*S*)-**4.2** with histidine in an organic solvent methanol gave fluorescent enhancements for both D-/L-histidine (see Figure S4.3), but the *enantioselectivity* are much smaller than that of the micelle probes. While the organic reaction systems were allowed to react in micro-molar concentrations and then diluted for fluorescence measurements, the micelles were found to have provided water solubility, stronger fluorescence intensities and improved selectivity.

The sizes of (*S*)-**4.2**@PEG-PLLA and its reaction systems with D-/L-histidine were characterized by dynamic light scattering (DLS), as summarized in Figure 4.4. The initial micelles of (*S*)-**4.2**@PEG-PLLA exhibited a very fine and narrow distribution of its sizes centered at 20.9 nm. Upon interaction with $Zn(OAc)_2$, and followed by the interaction with either D-/L-histidine, the sizes were well maintained at around 20.9-26.5 nm. Those data demonstrated the stability of the micelles during the recognition events.

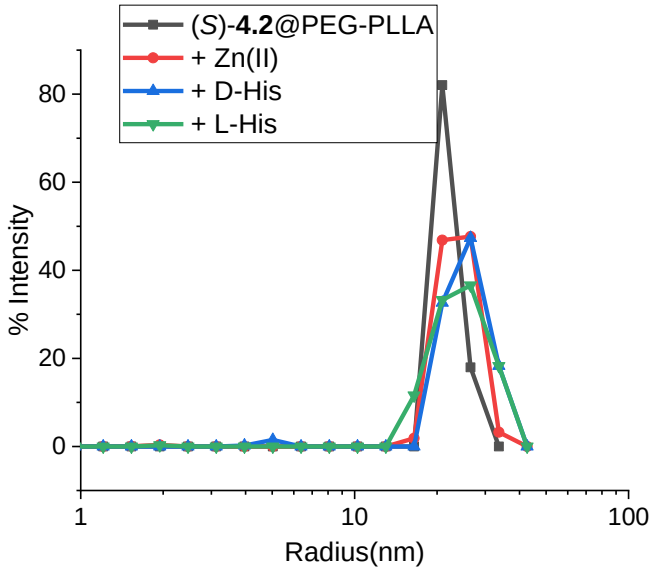

Figure 4. 4 DLS studies of (*S*)-**4.2**@PEG-PLLA and its interactions with histidine. Corresponding concentration of (*S*)-**4.2** = 10 μM, 2 equivalent $Zn(OAc)_2$, 5 equivalence of histidine. Reaction time = 3h at room temperature. DLS measuring temperature = 37 ^{o}C.

4.2.4 Mechanistic Studies

We conducted ^{1}HNMR experiments to study the reaction of (*S*)-**4.2** with histidine (TBA salt form) in DMSO-d_6 because of the difficulties to directly study the mechanism inside the micelles. When (*S*)-**4.2** was titrated with D-/L-histidine, both enantiomers turned the four downfield singlets (δ = 10.47, 10.28, 10.26, 10.03) first into two singlets (δ = 10.28 and 10.01) at 0.5 equivalences, then three singlets (δ = 10.64, 10.43, 10.01) at 1 equivalence, and two new singlets (δ = 10.65, 10.44) at above 2 equivalences (See Figure S4.6-S4.9). The immediate disappearance of the signals at δ = 10.47 & 10.26 indicated they belong to the -O<u>H</u> protons**.** The overall differences in the NMR spectra for the reaction of D-His with that of L-His are relatively small, but we can still observe the singlet at δ =8.58 was shifted to 8.57 in D-His case, and to 8.54 in L-His case.

4.3. Conclusion

In conclusion, a non-C_2 symmetric H_4-BINOL-based probe (*S*)-**4.2** has been synthesized, and encapsulated with PEG-PLLA to make the micelle-based fluorescent probe (*S*)-**4.2**@PEG-PLLA. The micelle sizes were characterized by DLS and were found to be stable in the interaction with histidine and Zn2+. (*S*)-**4.2**@PEG-PLLA allowed both *chemoselective* and *enantioselective* recognition of chiral histidine in water media in the presence of Zn(II). Besides its ability to detect different ee values of histidine, (*S*)-**4.2**@PEG-PLLA has extraordinarily low limit of detection at nano-molar scale. To our knowledge, (*S*)-**4.2**@PEG-PLLA is the most sensitive probe for histidine among the small molecular fluorescent probes. Another C_2 symmetric H_8-BINOLdicarbaldehyde (*S*)-**4.3** in its micelle form (*S*)-**4.3**@PEG-PLLA showed nearly no responses to all amino acids under the same conditions. The loss of fluorescence emission is attributed to more aliphatic substituents which allowed non-emissive energy relaxation. Unlike the C_2 symmetric BINOL-

based molecules, the H_4-BINOL-based molecules have not received much attention in the field of molecular recognition. This work shows that this class of non-C_2 symmetric materials are promising for application in fluorescent recognition.

4.4 Experimental

4.4.1. General experimental methods

All amino acids and other chemicals were purchased from Sigma Aldrich Chemical Co. or Alfa Aesar, and used without further purification. NMR spectra were recorded on Varian-600 MHz spectrometer. Chemical shifts for ^{1}H NMR were reported in parts per million relative to a singlet at 7.26 ppm for deuterated chloroform and 2.50 ppm for deuterated DMSO. Chemical shifts for ^{13}C NMR were reported in parts per million relative to a triplet at 77.16 ppm for deuterated chloroform. Steady-state fluorescence emission spectra were recorded on Horiba FluoroMax-4 spectrofluorometer. Low-temperature fluorescence emission spectra were recorded on Horiba FluoroMax-3 spectrofluorometer. Nanoparticle sizes and polydispersities were analyzed via dynamic light scattering (DLS, Wyatt, DynaPro). Deionized water was used for all the experiments.

Nano precipitation to prepare the micelle encapsulated probe 1.6 μmol of (*S*)-organic sensor cores (1.0 mg/mL in DMF) were added to 80 mg coblock polymer mPEG-PLLA (mPEG-PDLA for (*R*)-cores). More DMF was added to dissolve the coblock polymer and the volume was calibrated to 8 mL. The solution was sonicated for 10 minutes and added dropwise to a vortex of 72 mL water at a rate of 1 mL/min. The vortex was allowed to last 30 more minutes after the addition of DMF solution. The final mixture was dialyzed in DI water to form micelle solutions containing 20 μM corresponding organic cores.

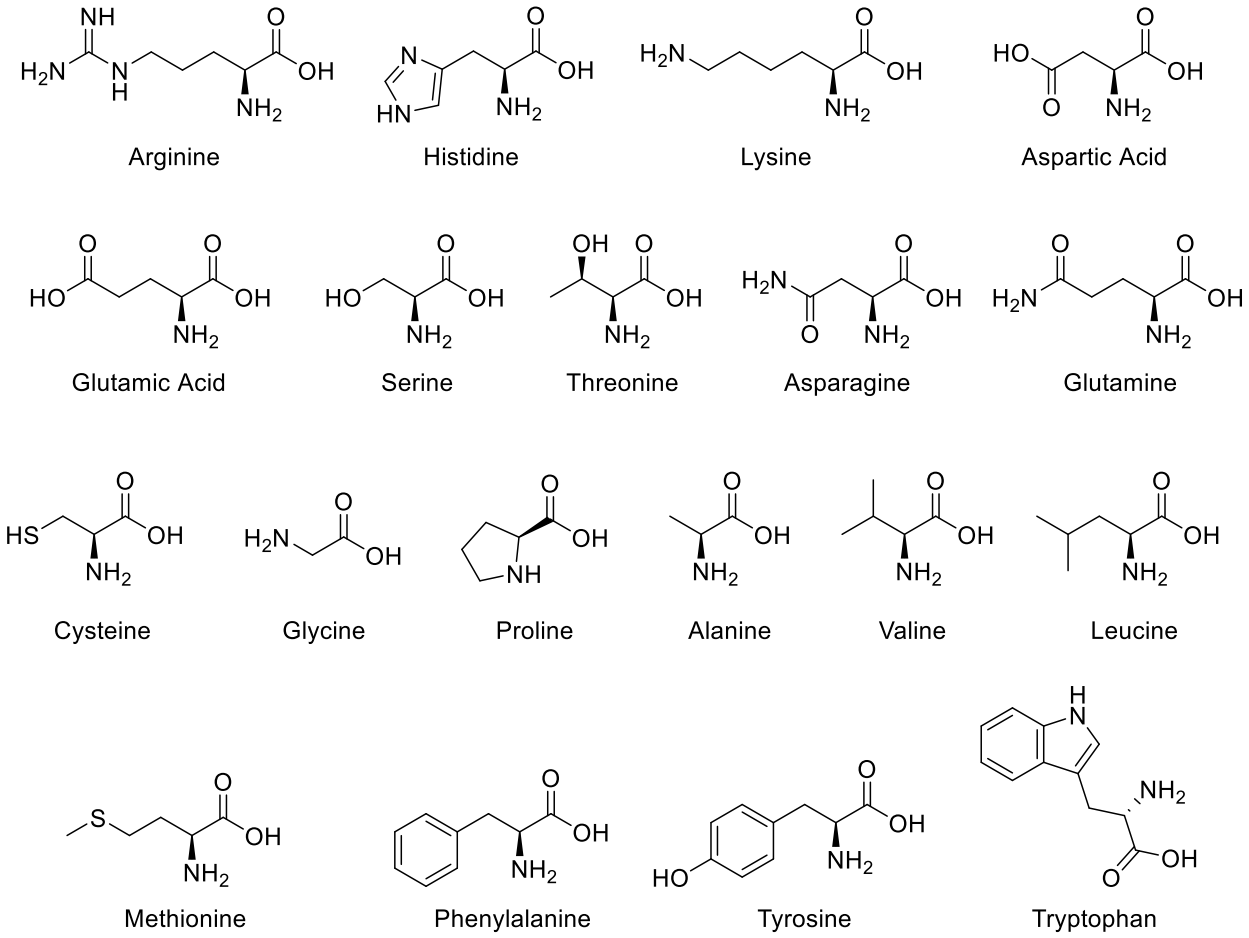

Figure S4. 1 Structure of Chiral Amino Acids

4.4.2. Synthesis and characterization data

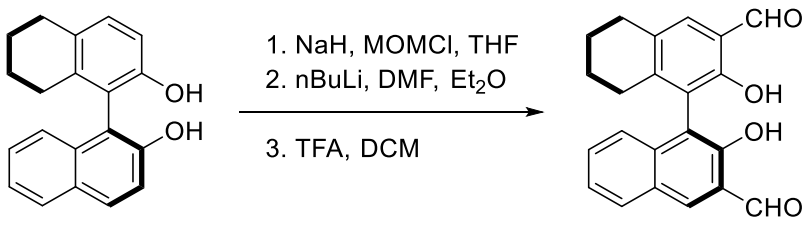

(*S*)-**4.2**
42%

Step 1: After pumping off air and refilling with nitrogen gas three times, (*S*)-H_4-BINOL (1.0 g, 3.44 mmol) was dissolved in dry-THF (30 mL), which was added dropwise to a slurry of sodium hydride (3.0 equiv, 10.32 mmol, 60% dispersed in mineral oil) in dry THF (20 mL) at 0 ^{o}C. The mixture was allowed to warm up to room temperature and react for one more hour. MOMCl (3.5 equiv, 12.04 mmol) was added dropwise at 0 ^{o}C, after which the reaction mixture was allowed to warm up to room temperature and react for four more hours. The reaction mixture was quenched by adding saturate ammonium chloride solution (5 mL). Diluted and extracted with ethyl acetate 3*50 mL), dried over sodium sulfate and concentrated for the next step.

Step 2: The mixture from the previous step was placed into a round-bottle flask, purged with nitrogen three times, and dissolved with dry ethyl ether (50 mL). n-Butyl lithium (4.0 equiv, 13.76 mmol, 2.5 M in hexane) was carefully added into the solution at -78 ^{o}C, and the mixture was allowed to warm up slowly and react at room temperature for two more hours. The reaction mixture was placed into an ice-water bath, and 5 eq. distilled DMF was added dropwise. After the addition, the reaction was allowed to warm up and react at room temperature for 12 h. The reaction was then quenched by carefully adding saturate ammonium chloride solution (20 mL), extracted with ethyl acetate (3*50 mL), dried over sodium sulfate, and concentrated for next step.

Step 3: The crude mixture from the last step was dissolved in DCM (10 mL) and cooled by an ice-water bath to which excess TFA (3.5mL) was added dropwise. The reaction mixture was

allowed to warm up to room temperature and react for another hour. It was then neutralized by sodium bicarbonate, extracted with DCM (3*15 mL), dried over sodium sulfate, concentrated, and eluted through column chromatography (ethyl acetate/hexanes) to afford (*S*)-2 as a yellow solid in 42% yield (500 mg) over three steps.

(S)-2,2'-dihydroxy-5,6,7,8-tetrahydro-[1,1'-binaphthalene]-3,3'-dicarbaldehyde, (*S*)-**4.2**.

^{1}H NMR (600 MHz, CDCl3), δ: 10.93(s, 1H), 10.55(s, 1H), 10.15(s, 1H), 9.90(s,1H), 8.26(s,1H), 7.96(d, J=8.4Hz, 1H), 7.50(ddd, J_1=1.4Hz, J_2=7.1Hz, J_3=8.4Hz, 1H), 7.41(s, 1H), 7.40(ddd, J_1=1.4Hz, J_2=7.1Hz, J_3=8.4Hz, 1H), 7.28(d, J=8.4Hz, 1H), 2.88(m, 2H), 2.50(m, 1H), 2.19(m, 1H), 1.78(m, 2H), 1.69(m, 1H), 1.62(m, 1H).

^{13}C NMR (151 MHz, $CDCl_3$) δ: 196.94, 196.25, 157.27, 152.93, 148.17, 138.29, 136.96, 134.25, 130.85, 130.18, 129.61, 127.76, 124.61, 124.38, 122.38, 122.23, 119.10, 117.80, 29.26, 27.98, 22.79, 22.64.

4.4.3. Fluorescence spectra

Fluorescent measurement at room temperature:

To a suspension of 1 mL of 2.0 x 10^{-5} M Probe and 1 mL carbonate buffer solution (CBS, 25 mM of sodium carbonate with 25 mM of sodium bicarbonate, pH = 10.1), were added with 5 μL of 20 mM amino acids (in CBS) and 10 μL of 4 mM $Zn(OAc)_2$ (in water). After let them stand for various hours, the fluorescence spectra of the mixtures weremeasured. Slit = 3/3 nm, int time = 0.1 s. Fluorescence emission spectra were recorded on Horiba FluoroMax-4 spectrofluorometer.

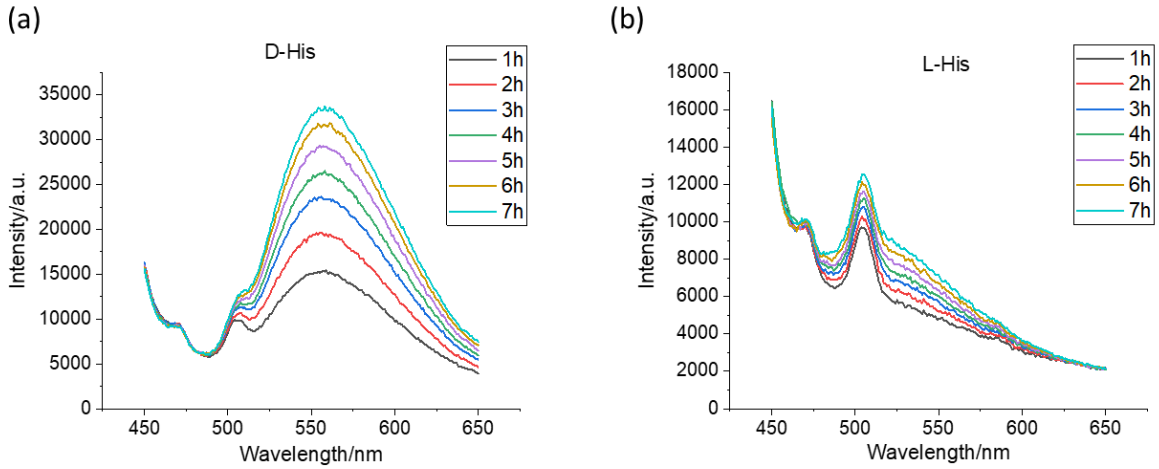

Figure S4. 2 (*S*)-**4.2**@PEG-PLLA's responses for (a) D-amino acids; (b) L-amino acids, in CBS buffer solution Corresponding organic sensor concentration = 10 μM, with 2 equiv zinc acetate, 5 equiv amino acids. Excited at 430 nm, slit=3/3nm, integration time=0.1s.

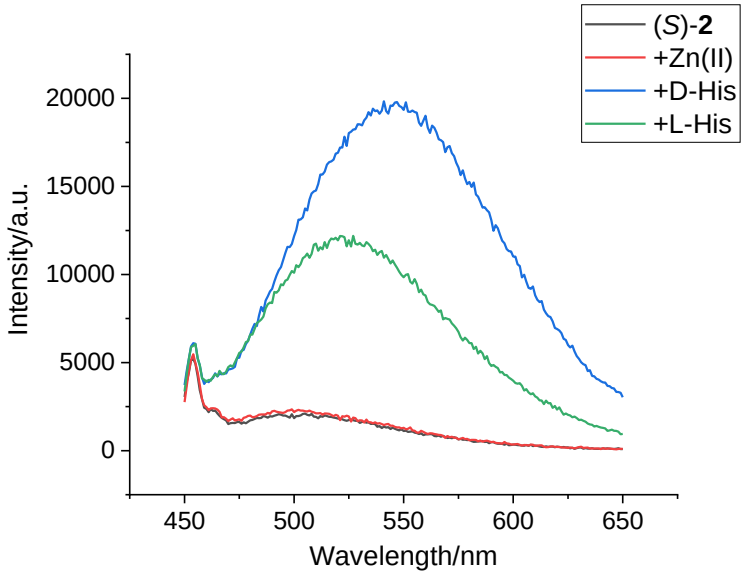

Figure S4. 3 Organic sensor (*S*)-**4.2's** responses in methanol solvent for D-/L-histidine. (*S*)-**4.2** concentration = 10 μM, with 2eq. zinc acetate, 5eq. amino acids. Excited at 430 nm, slit = 3/3 nm, integration time = 0.1 s.

Low-temperature fluorescence study:

To a suspension of 1 mL of 20 μM Probe and 1 mL CBS buffer, were added with 10 μL of 20 mM AA (in water) and 10 μL of 4 mM $Zn(OAc)_2$ (in water). After at rt for 3 h, the mixtures were chilled in an ice bath. The fluorescence spectra of the mixtures were measured with FluoroMax3 at 5 ^{o}Cs with a continuous nitrogen flow. Slit = 3/3 nm, int time = 0.3 s.

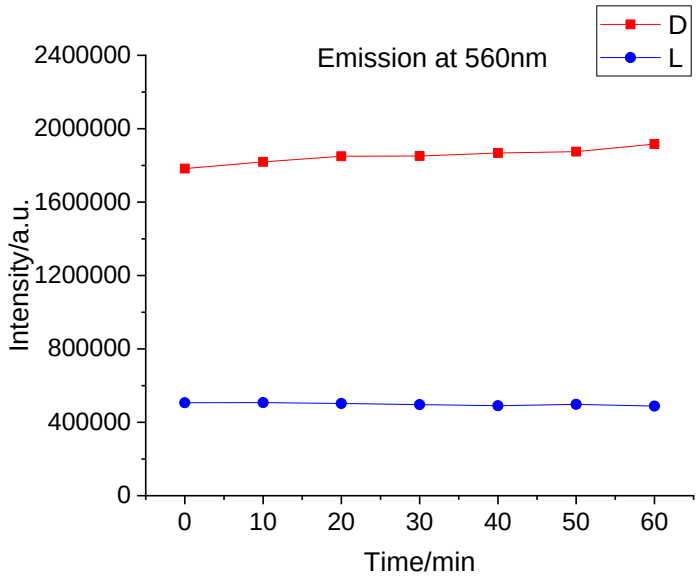

Figure S4. 4 The fluorescence intensity at 560 nm for the interaction of (*S*)-**4.2**@PEG-PLLA with 5 equiv D-/L-histidine in CBS buffer versus the time after quenched with ice-water bath. The intensity changed 7% within an hour with D-histidine. Corresponding organic sensor concentration = 10 μM, with 2 equiv zinc acetate, 5 equiv amino acids. Excited at 430nm, slit = 5/5 nm, integration time = 0.1s. give solvent

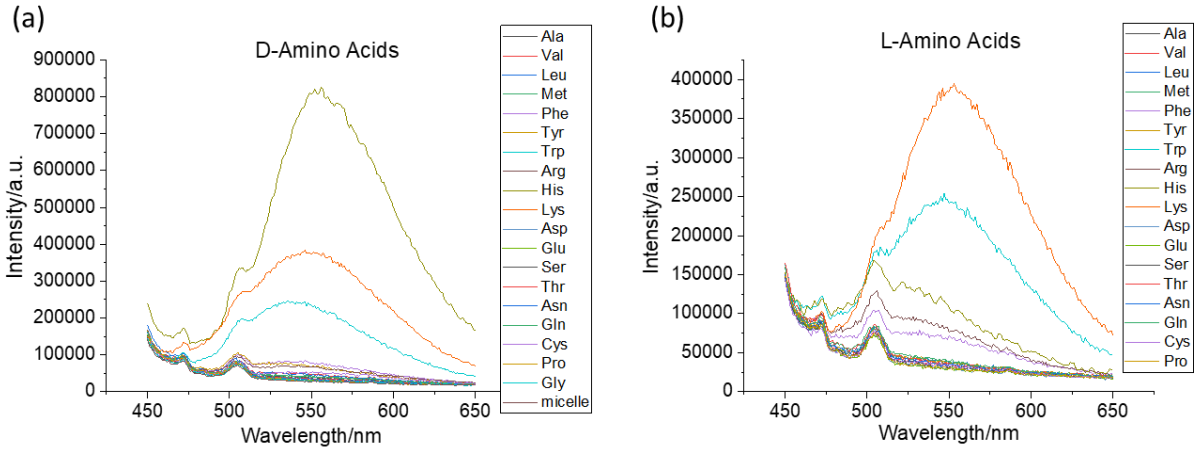

Figure S4. 5 Fluorescence spectra of (*S*)-**4.2**@PEG-PLLA's with (a) D-amino acids; (b) L-amino acids in CBS buffer. Corresponding organic sensor concentration = 10 μM, with 2 equiv zinc acetate, 5 equiv amino acids. Excited at 430 nm, slit = 5/5 nm, integration time = 0.1s.

4.4.4. NMR studies for the reaction of (*S*)-4.2 with histidine

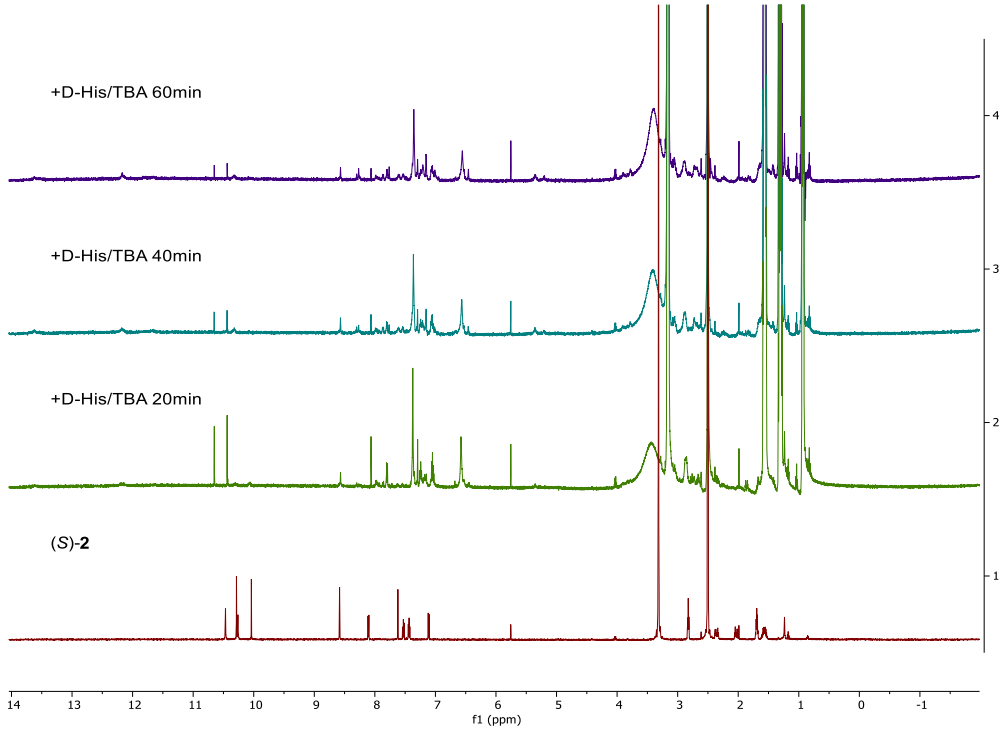

Figure S4. 6 ^{1}H NMR (600 MHz) spectra of the reaction between (*S*)-**4.2** and D-His over 20 – 60 min. (2.0 mM of (*S*)-**4.2,** 5 equiv. of His/TBA salt in DMSO-d_6.)

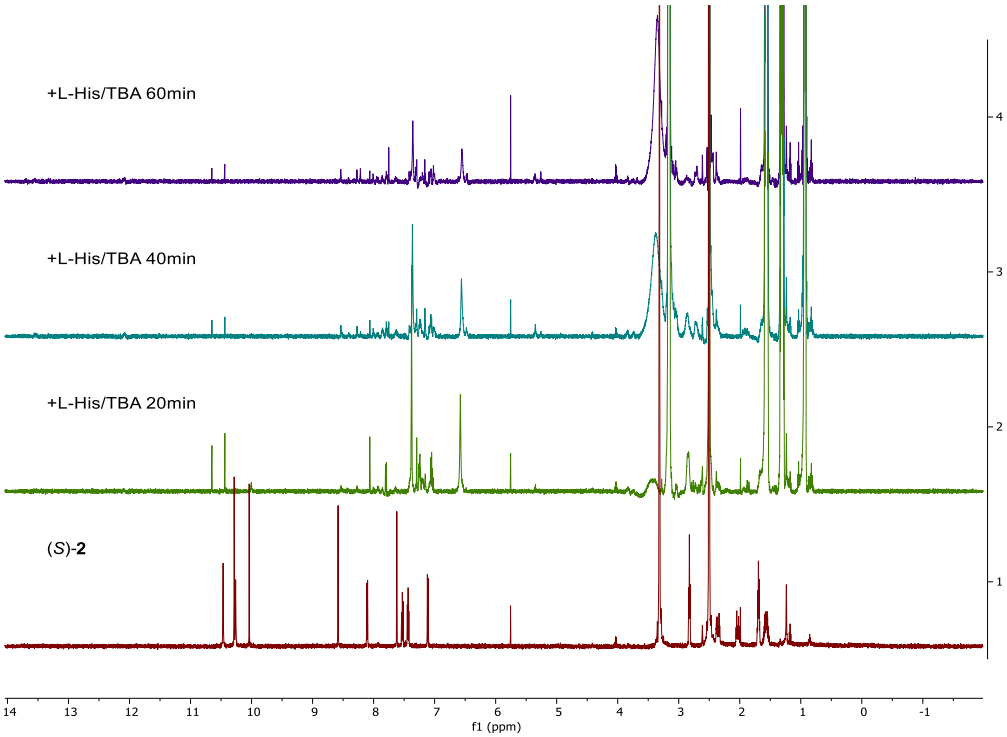

Figure S4. 7 ^{1}H NMR (600 MHz) spectra of the reaction between (*S*)-**4.2** and L-His over 20 – 60 min. (2.0 mM of (*S*)-**4.2,** 5 equiv of His/TBA salt in DMSO-d_6.)

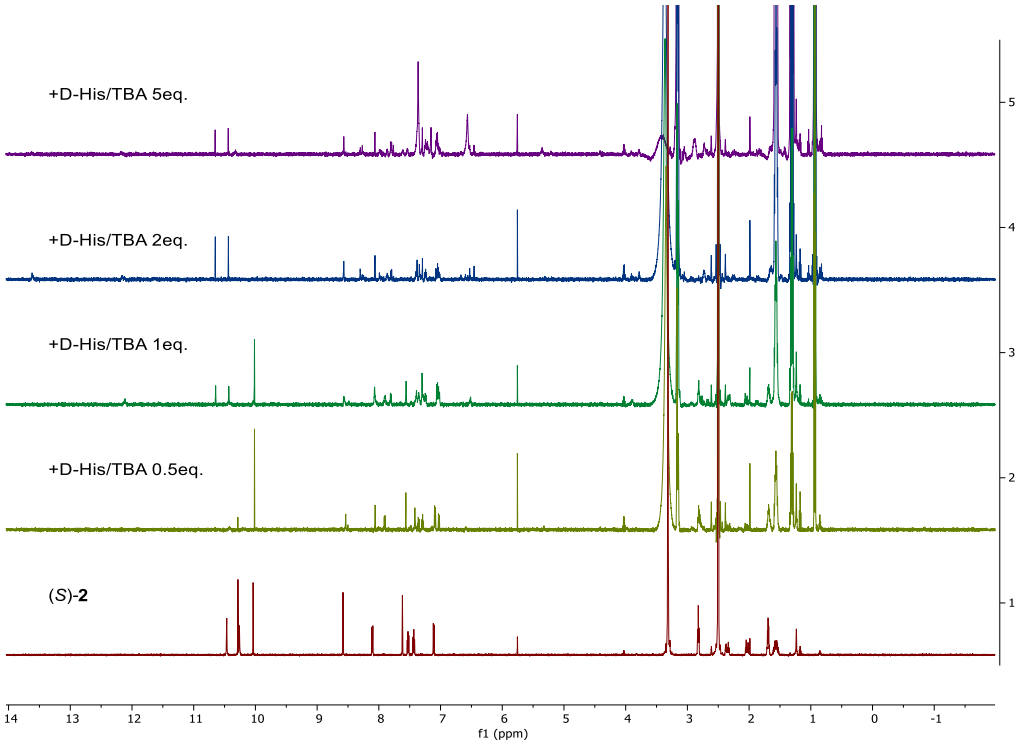

Figure S4. 8 ^{1}H NMR (600 MHz) spectra of the reaction between 2 mM (*S*)-**4.2** and 0.5 to 5 equiv of D-His/TBA in DMSO-d_6 after 40 minutes.

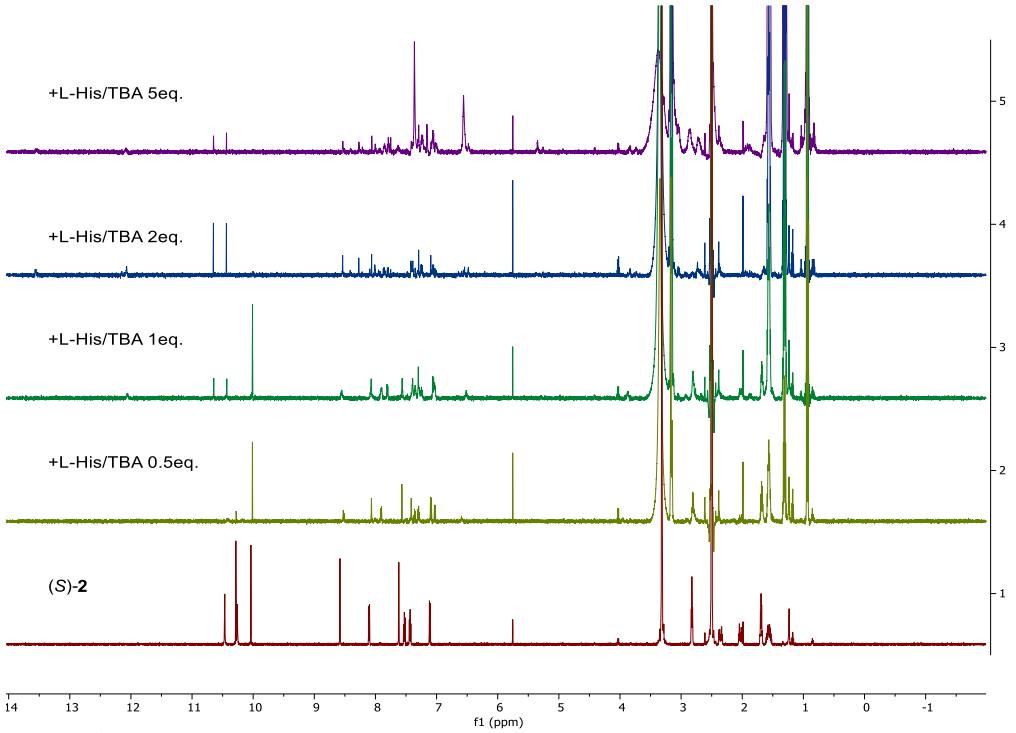

Figure S4. 9 ^{1}H NMR (600 MHz) spectra of the reaction between 2 mM (*S*)-**4.2** and 0.5 – 5 equiv of L-His/TBA in DMSO-d_6 after 40 minutes.

4.4.5. UV-vis spectra of (*S*)-4.2 with histidine

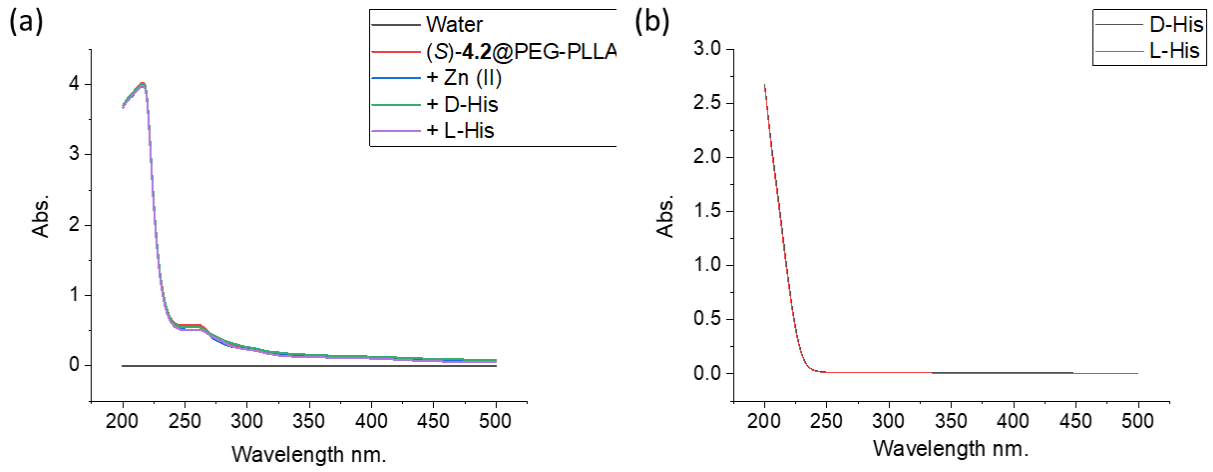

Figure S4. 10 UV-vis spectra of (a) (*S*)-**4.2**@PEG-PLLA with histidine and Zn2+; (b) D-/L-histidine. Corresponding (*S*)-**4.2** concentration = 10 µM, 2 equiv zinc acetate, 5 equiv His, in carbonate buffer solution (pH = 10.1).

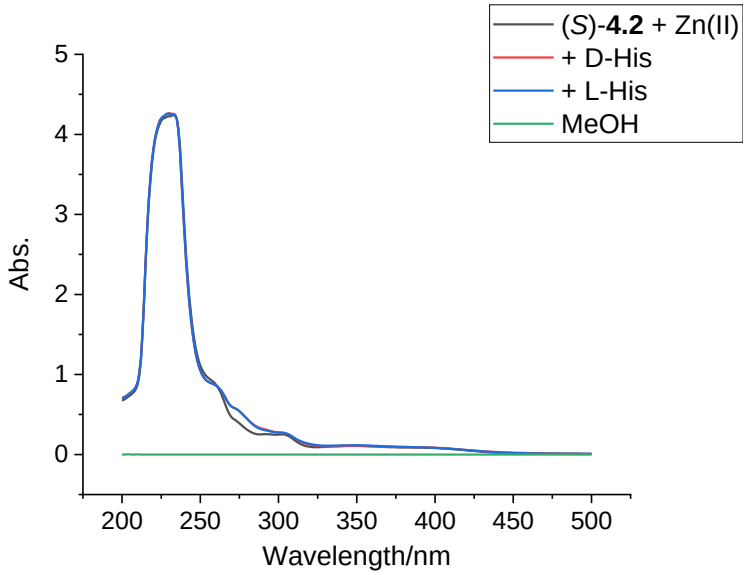

Figure S4. 11 UV-vis spectra of (*S*)-**4.2** with histidine and Zn^{2+} in methanol. (*S*)-**4.2** concentration = 10µM, 2 equiv zinc acetate, 5 equiv. His, in methanol.

4.4.6. NMR spectra

^{1}HNMR (600 MHz), $CDCl_3$

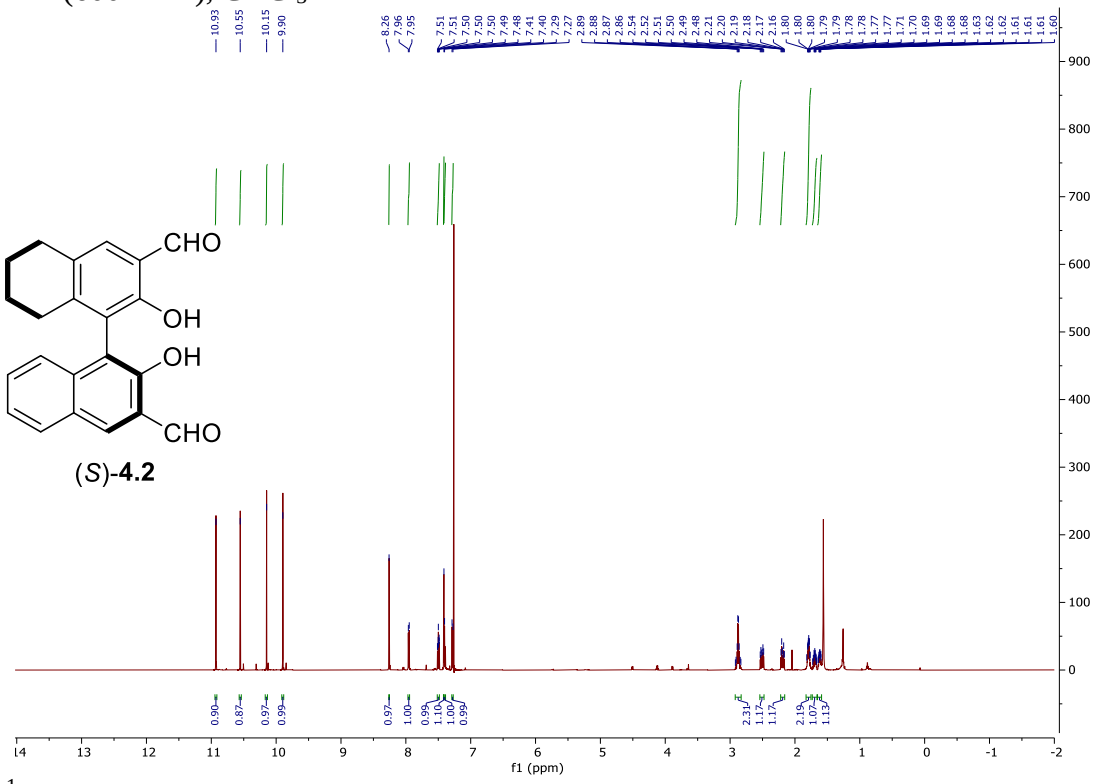

$^{13}C\{^{1}H\}$NMR (151MHz), $CDCl_3$

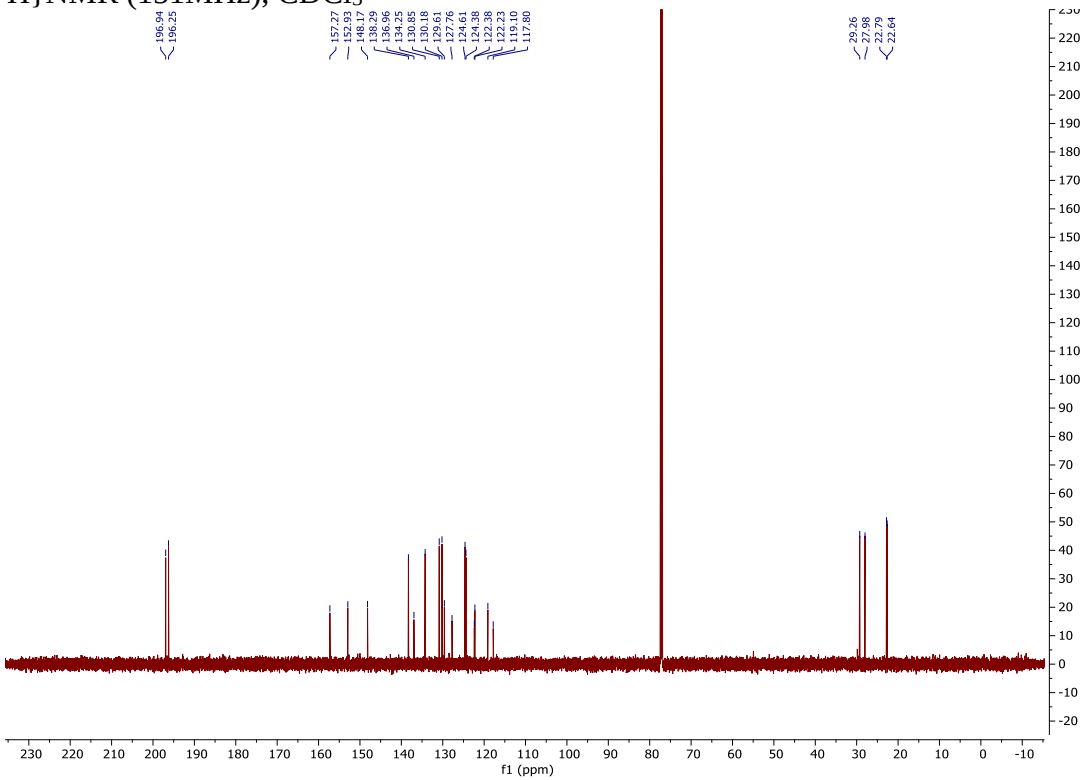

4.5 References

(1) Ramos-Montañez, S.; Winkler, M. E. Biosynthesis of Histidine. *EcoSal Plus* **2009**, *3* (2).

(2) Takayama, T.; Ogawa, T.; Hidaka, M; Shimizu, Y.; Ueda A.; Masaki, H. Esterification of Eschericia Coli TRNAs with D-Histidine and D-Lysine by Aminoacyl-TRNA Synthetases. *Biosci, Biotech, and Bioch* **2014**. *69:5*, 1040-1041.

(3) Marcone, G. L.; Rosini, E.; Crespi, E.; Pollegioni, L. D-Amino Acids in Foods. *Appl. Microbiol. and Biotechnol*. **2020**, *104*, pp 555–574.

(4) Grishin, D. V.; Zhdanov, D. D.; Pokrovskaya, M. V.; Sokolov, N. N. D-Amino Acids in Nature, Agriculture and Biomedicine. *All Life* **2020**, *13* (1), 11–22.

(5) Adachi, M.; Shimizu, · Rumi; Kato, S.; Oikawa, T. The First Identification and Characterization of a Histidine-Specific Amino Acid Racemase, Histidine Racemase from a Lactic Acid Bacterium, Leuconostoc Mesenteroides Subsp. Sake NBRC 102480. *Amino Acids* **2019**, *51*, 331–343.

(6) Gerber, D. A. Low Free Serum Histidine Concentration in Rheumatoid Arthritis. A Measure of Disease Activity. *J Clin Invest*. **1975**, *55(6)*, 1164-1173.

(7) Pinals, R. S.; Harris, E. D.; Burnett, J. B.; Gerber, D. A. Treatment of Rheumatoid Arthritis with L-Histidine: A Randomized, Placebo-Controlled, Double-Blind Trial. *J. Rheumatol.* **1977**, *4* (4), 414–419.

(8) Helliwell, P. S.; Marchesoni, A.; Peters, M.; Platt, R.; Wright, V. Cytidine Deaminase Activity, C Reactive Protein, Histidine, and Erythrocyte Sedimentation Rate as Measures of Disease Activity in Psoriatic Arthritis. *Ann. Rheum. Dis.* **1991**, *50* (6), 362–365.

(9) Zabek, A.; Swierkot, J.; Malak, A.; Zawadzka, I.; Deja, S.; Bogunia-Kubik, K.; Mlynarz, P. Application of 1H NMR-Based Serum Metabolomic Studies for Monitoring Female

Patients with Rheumatoid Arthritis. *J. Pharm. Biomed. Anal.* **2016**, *117*, 544–550.

(10) Minami, T.; Esipenko, N. A.; Zhang, B.; Isaacs, L.; Anzenbacher, P. "'Turn-on'" Fluorescent Sensor Array for Basic Amino Acids in Water. *Chem. Commun* **2014**, *50*, 61.

(11) Li, C.; Ma, J.; Zhao, L.; Zhang, Y.; Yu, Y.; Shu, X.; Li, J.; Jia, X. Molecular Selective Binding of Basic Amino Acids by a Water-Soluble Pillar[5]Arene. *Chem. Commun* **1924**, *49*, 3.

(12) Bailey, D. M.; Hennig, A.; Uzunova, V. D.; Nau, W. M. Supramolecular Tandem Enzyme Assays for Multiparameter Sensor Arrays and Enantiomeric Excess Determination of Amino Acids. *Chem. - A Eur. J.* **2008**, *14* (20), 6069–6077.

(13) Liu, K.; He, L.; He, X.; Guo, Y.; Shao, S.; Jiang, S. Calix[4]Pyrrole-TCBQ Assembly: A Signal Magnifier of TCBQ for Colorimetric Determining Amino Acids and Amines. *Tetrahedron Lett.* **2007**, *48* (24), 4275–4279.

(14) Douteau-Guével, N.; Perret, F.; Coleman, A. W.; Morel, J.-P.; Morel-Desrosiers, N. Binding of Dipeptides and Tripeptides Containing Lysine or Arginine by P-Sulfonatocalixarenes in Water: NMR and Microcalorimetric Studies. *J. Chem. Sic., Perkin Tran. 2*, **2002**, 524-532.

(15) Mutihac, L.; Hong Lee, J.; Seung Kim, J.; Vicens, J. Recognition of Amino Acids by Functionalized Calixarenes. *Chem. Soc. Rev* **2011**, *40*, 2777–2796.

(16) Du, J.; Huang, Z.; Yu, X.-Q.; Pu, L. Cite This. *Chem. Commun* **2013**, *49*, 5399.

(17) Folmer-Andersen, J. F.; Lynch, V. M.; Anslyn, E. V. "Naked-Eye" Detection of Histidine by Regulation of CuII Coordination Modes. *Chem. - A Eur. J.* **2005**, *11* (18), 5319–5326.

(18) Du, J.; Yu, S.; Huang, Z.; Chen, L.; Xu, Y.; Zhang, G.; Chen, Q.; Yu, X.; Pu, L. Highly Selective Ratiometric Fluorescent Recognition of Histidine by Tetraphenylethene-

Terpyridine-Zn(II) Complexes. *RSC Adv.*, **2016**, *6*, 25319-25329.

(19) Wang, J.; Liu, H. B.; Tong, Z.; Ha, C. S. Fluorescent/Luminescent Detection of Natural Amino Acids by Organometallic Systems. *Coord. Chem. Rev.*, **2015**, *303*, pp. 139-184.

(20) Shen, R.; Zou, L.; Wu, S.; Li, T.; Wang, J.; Liu, J.; Ling, L. A Novel Label-Free Fluorescent Detection of Histidine Based upon Cu 2+ -Specific DNAzyme and Hybridization Chain Reaction. *Spectrochim. Acta - Part A Mol. Biomol. Spectrosc.* **2019**, *213*, 42–47.

(21) Du, G.; Pu, L. Micelle-Encapsulated Fluorescent Probe: Chemoselective and Enantioselective Recognition of Lysine in Aqueous Solution. *Org. Lett.*, **2019**. *21*, 12, 4777-4781.

(22) Heumann, L. V; Keck, G. E. A New Method for the Synthesis of H 4-BINOL. *Tetrahedron: Asymmetry* **1981**, *36* (4), 32.

(23) Shen, X.; Guo, H.; Ding, K. The Synthesis of a Novel Non-C2 Symmetric H4-BINOL Ligand and Its Application to Titanium-Catalyzed Enantioselective Addition of Diethylzinc to Aldehydes. *Tetrahedron Asymmetry* **2000**, *11* (21), 4321–4327.

(24) Yue, Y.; Turlington, M.; Yu, X.-Q.; Pu, L. 3,3 0-Anisyl-Substituted BINOL, H 4 BINOL, and H 8 BINOL Ligands: Asymmetric Synthesis of Diverse Propargylic Alcohols and Their Ring-Closing Metathesis to Chiral Cycloalkenes. *J. Org. Chem* **2009**, *74*, 8681–8689.

(25) Long, J.; Hu, J.; Shen, X.; Ji, B.; Ding, K. Discovery of Exceptionally Efficient Catalysts for Solvent-Free Enantioselective Hetero-Diels-Alder Reaction. *J. Am. Chem. Soc.* **2002**, *124*, 1, 10-11.

(26) Huang, Z.; Yu, S.; Wen, K.; Yu, X.; Pu, L. Zn(II) Promoted Dramatic Enhancement in the Enantioselective Fluorescent Recognition of Functional Chiral Amines by a Chiral Aldehyde. *Chem. Sci.*, **2014**, *5*, 3457-3462

Chapter 5. Copolymers Affect Selectivity and Sensitivity of Micelle Probes

5.1 Introduction

5.1.1 Importance of Tryptophan

As an essential amino acid, tryptophan (Trp) is a fundamental building blocks for numerous proteins. Besides that, the importance of Trp has been highlighted in central nervous system, immunology, metabolism and cancer research.[1–5] While most of the related studies focused on L-Trp, much fewer attention has been given to its enantiomer D-Trp due to the relatively lower natural abundance. In 1996, D-Trp residue was firstly found in a normally translated polypeptide contryphan, which existed in the venom of *Conus radiatus*, a fish-hunting snail.[6] D-amino acids have been considered as physiologically active compounds and markers of diseases in chemical biology.[7] Recently, D-Trp has been reported to have growth-inhibitory effect on Vibrio spp., a group of bacteria among which several species are pathogens.[8]

5.1.2. Relevant Probes

Conventional techniques including high performance liquid chromatography (HPLC) are often used for the detection of D-Trp.[6,9] Optic techniques, especially fluorescence techniques, have advantages and are favored due to high sensitivity, simple instrumentation, and rapid analysis.[10,11] Chemoselective detection of Trp have been achieved through many approaches.[12] He et al. reported a metal-organic cerium tetrahedron that gave chemoselective fluorescent enhancement for Trp.[13] The selectivity was proposed to be due to aromatic stacking, hydrogen bonding, and size selection constrained by the probe.

Covalent linking of water-soluble poly(N-isopropylacrylamide)s or polyethylene glycol oligomers at BINOL unit has achieved the enantioselective detection of amino acids in water

media.[14,15] However, despite their decent enantioselectivity and scope, none of the probes exhibited recognition for Trp. Zeng reported the use of a SPIROL-based probe (*S*)-**5.1** that could enantioselectively responded to several amino acids including Trp.[16] So far, the enantioselective and chemoselective probing for Trp is very limited and rather complicated probe design is needed.[17]

Previously we reported the use of block copolymer poly(ethylene glycol)-poly(L-lactide) (PEG-PLLA) to encapsulate diformylBINOL (*S*)-**5.2** to form micelle probe (*S*)-**5.2**@PEG-PLLA.[18] The micelle probe itself was non-fluorescent initially. In the presence of zinc(II), (*S*)-**5.2**@PEG-PLLA could recognize lysine (Lys) both enantioselectively (D-Lys over L-Lys) and chemoselectively (Lys over other amino acids) with greatly enhanced fluorescence intensities at λ_{em} = 528 nm.

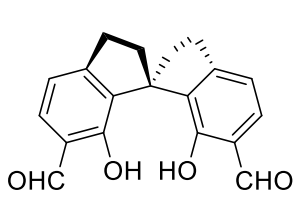

(*S*)-**5.1**

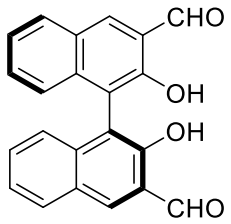

(*S*)-**5.2**

Compared with simple ionic surfactants, block copolymers have received mor attention as novel carriers for drug delivery.[19] PEG-PLLA and poly(ethylene glycol)-poly(ε-caprolactone) (PEG-PCL) have characteristics such as high biocompatibility and biodegradability. These two copolymers were reported as excellent micelle carriers to enhance the drug accumulation on the site of action and decrease off-target effect.[20–22] Poly(ethylene)-poly(ethylene-glycol) (PE-PEG) has a very simple hydrophobic block consisted of polyethylene. This cost efficient copolymer was reported to efficiently deliver amphotericin B to brain with limited toxicity to mammalian cells.[23] F68 is a member of Pluronic copolymer poly(ethylene oxide)-block-poly(propylene oxide)-block-

poly(ethylene oxide) (PEO-PPO-PEO).[24] These triblock copolymers have one centered hydrophobic part and two outstretching hydrophilic ends. They have been widely used for medical applications. A recent study used F68 for drug delivery with improved drug residence.[25] Among the four copolymers mentioned above, they share common hydrophilic block PEG, but with varying hydrophobic ends. In order to provide more understanding on micelle probes, we have studied how these micelle-forming copolymers could influence the fluorescent recognition of amino acids. And herein, we demonstrated that the selective recognition of amino acids can be tuned by the use of different micelle-forming copolymers.

PEG-PLLA 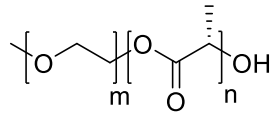

PEG-PCL 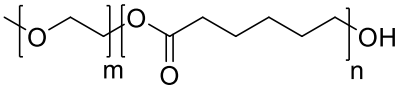

PE-PEG 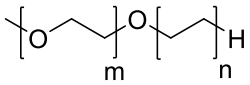

F68 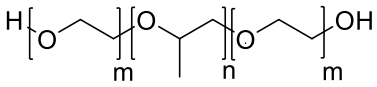

5.2 Results and Discussion

5.2.1 Fluorescence Studies

5.2.1.1 Amino Acids Screening

The micelle probes were prepared by nanoprecipitation method of (*S*)-**5.2** and copolymers to form (*S*)-**5.2**@PEG-PLLA, (*S*)-**5.2**@PEG-PCL, (*S*)-**5.2**@PE-PEG and (*S*)-**5.2**@F68 respectively with corresponding organic probe concentration of 2.0×10^{-5} M (See experimental for detailed experiments). All four micelle probes were non-fluorescent, and this meant that the photoinduced-electron-transfer (PET) quenching mechanism was preserved in water media. The

fluorescence responses of four micelle probes toward the two enantiomers of total 19 amino acids in the presence of $Zn(OAc)_2$ (2 equiv.) were investigated. For each measurement, 1 mL of micelle probe stock solution was mixed with 1 mL of carbonate buffer solution (CBS, 25 mM, pH = 10.1), 10 equiv. amino acid (10 µL of 20 mM stock solution in DI water). The reaction mixture was allowed to stand at room temperature for 3h and then tested for fluorescence either at room temperature or 5 °C. The final concentrations of the probes are 1.0×10^{-5} M. The fluorescence spectra of (*S*)-**5.2**@PEG-PLLA with amino acids are shown in Figure 5.1 as an example. Upon excitation at 407 nm, (*S*)-**5.2**@PEG-PLLA exhibited very strong fluorescence enhancement with D-Lys only, and medium strong enhancement with D-Trp and several L-amino acids. The fluorescence intensity differences allowed enantioselective and chemoselective detection of Lys as we discussed in Chapter 2.

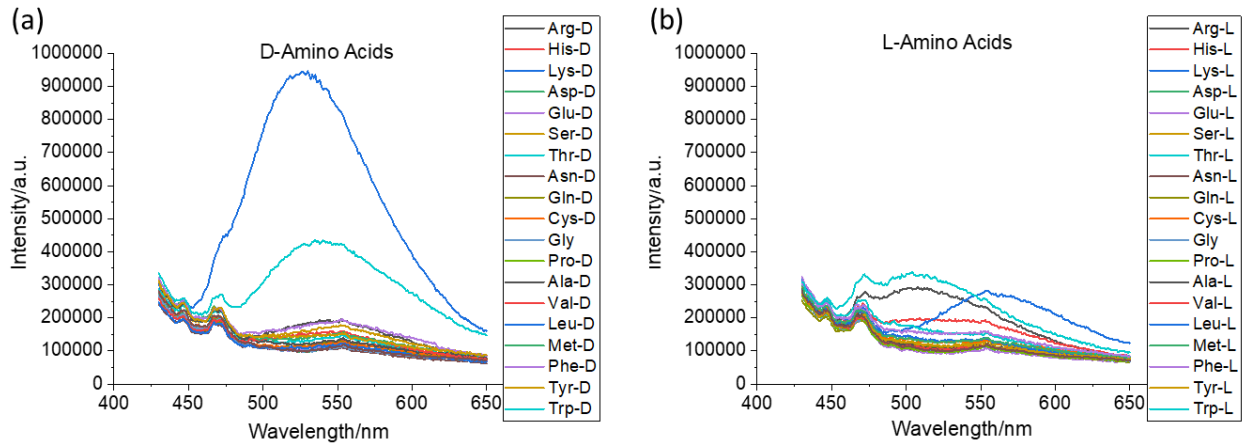

Figure 5. 1 (*S*)-**5.2**@PEG-PLLA responses for various (a) D-amino acids; (b) L-amino acids. (*S*)-**5.2** concentration = 10 µM, with 2 equiv $Zn(OAc)_2$, 10 equiv amino acids. Measured at 5 °C, excited at 407 nm, slit = 3/3 nm, integration time = 0.1 s.

All amino acids were tested by using the four micelle probes under the same conditions. The intensities at the emission maxima were summarized in Figure 5.2. While (*S*)-**5.2**@PEG-PLLA was both enantioselective and chemoselective for D-Lys, the observed selectivity changed when the probe was changed to (*S*)-**5.2**@PEG-PCL, (*S*)-**5.2**@PE-PEG, and (*S*)- **5.2**@F68. The

differences of the magnitude in Figure 5.2b and Figure 5.2c were due to the use of different fluorometer, since (*S*)-**5.2**@PEG-PCL and (*S*)-**5.2**@PE-PEG were less selective. We found that (*S*)-**5.2**@PEG-PCL gave similar strong responses for Trp and Lys, and medium strong responses for valine (Val), leucine (Leu) as well as phenylalanine (Phe) (Figure 5.2b). (*S*)-**5.2**@PE-PEG showed stronger fluorescence response with L-Trp than both enantiomers of Lys at λ_{em} = 520 nm (Figure 5.2c). In spite of its relatively low intensity, the enantioselectivity was expressed in

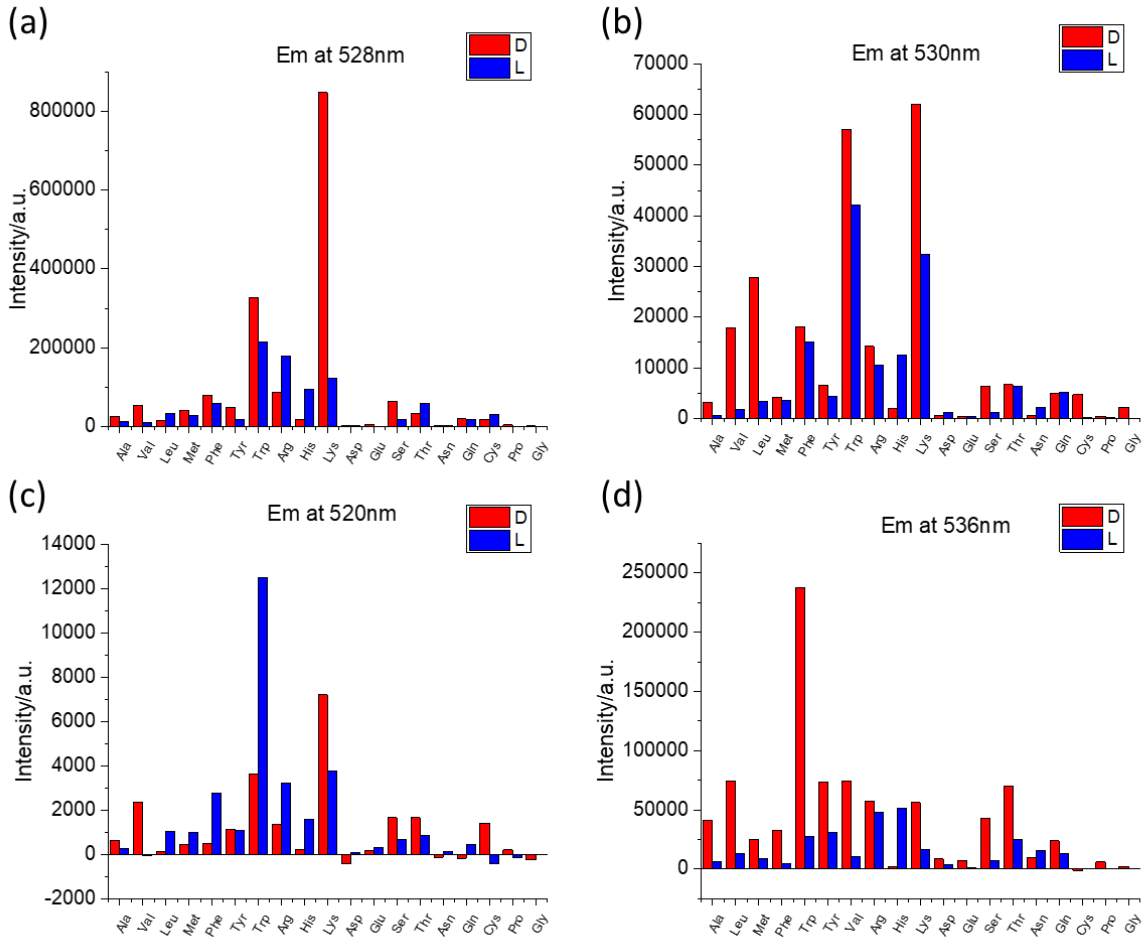

Figure 5. 2 Fluorescence response of the micelle probes (a) (*S*)-**5.2**@PEG-PLLA; (b) (*S*)-**5.2**@PEG-PCL; (c) (*S*)-**5.2**@PE-PEG; and (d) (*S*)-**5.2**@F68, towards various amino acids. Conditions: 10 μM micelle probe, 2 equiv $Zn(OAc)_2$, and 10 equiv amino acids in carbonate buffer solution. Spectra were taken after 3 h of reaction at rt. Peak intensities were used. Slit = 3/3 nm, integration time = 0.1 s. For (a) and (d), measured at 5 ^oC; for (b) and (c), measured at room temperature. Excited at 407 nm for (a), 430 nm for (b), (c), and 400 nm for (d).

enantioselective factor, *ef* = 0.29 favors L-Trp (*ef* = 3.5 in reverse) [*ef* = (I_D-I_0)/(I_L-I_0), where I_0 is the fluorescence of the probe without the amino acid]. The last micelle probe (*S*)-**5.2**@F68 was found to exhibit fluorescence enhancment at λ_{em} = 536 nm favoring D-Trp over all other amino acids (Figure 5.2d). It was surprising that the enantioselectivity was flipped by simply changing the micelle-forming polymer from PE-PEG to F68. The *ef* value was 9.2 favoring D-Trp. (*S*)-**5.2**@F68 also favored many other D-amino acids, and the *ef* values are listed below:, alanine (Ala) 6.5, Leu 5.6, methionine (Met) 2.9, Phe 7.8, tyrosine (Tyr) 2.4, Val 7.3, Lys 3.5, serine (Ser) 6.1, threonine (Thr) 2.8, with medium strong fluorescence intensities.

5.2.1.2 Concentration Detection

The concentration effect of Trp on the fluorescence responses of (*S*)-**5.2**@F68 was studied. As shown in Figure 5.3a, the fluorescence intensity at λ_{em} = 536 nm increased with increasing tryptophan concentration until 30 equiv. D-Trp at which the fluorescence enhancement was saturated. Meanwhile, the fluorescence signal remained very low with L-Trp. In the range of 1 to 25 equiv. of D-Trp, first-order linear fit was applied and R square value of 0.997 was found (Figure 5.3b). The limit of detection (LOD) was thus determined to be 962 nM for D-Trp (LOD = 3*SD/k. SD, standard deviation of noise. k, slope of calibration curve). With a tryptophan detection concentration range of 10 to 250 μM, (*S*)-**5.2**@F68 would be potentially useful to measure the tryptophan concentrations in biological systems such as human serum, where the concentration of tryptophan was found to be 67.2±10.2 μM.[26]

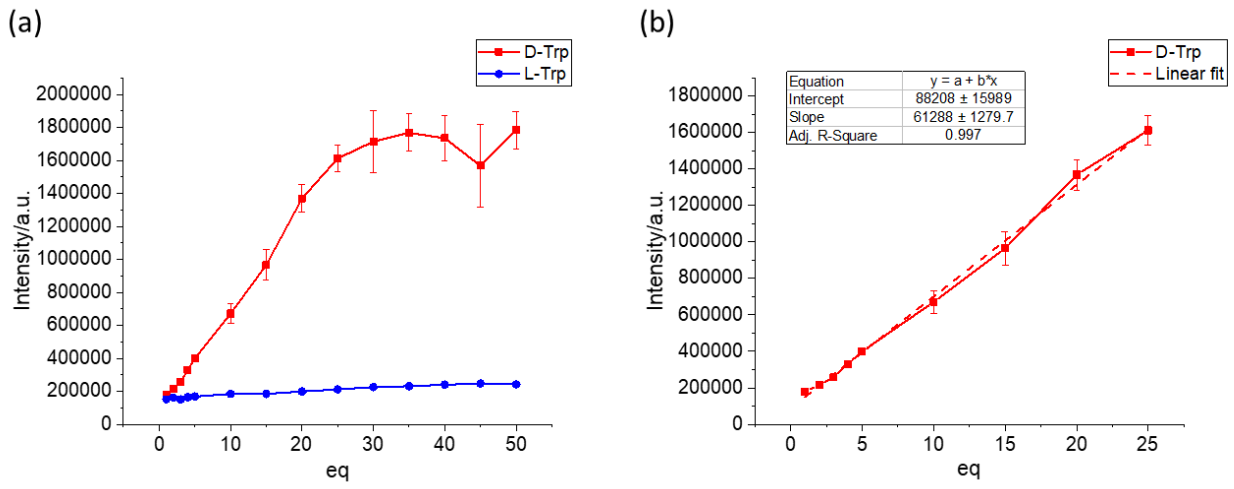

Figure 5. 3 (a) Fluorescence intensity of (*S*)-**5.2**@F68 (10 μM) and $Zn(OAc)_2$ (2 equiv.) at λ_{em} = 536 nm versus the stoichiometry of tryptophan. (b) Expanded view of 1 to 25 equiv. tryptophan. Error bars were made from 3 independent experiments. Measured at 5 ^{o}C, excited at 400 nm, slit = 5/5 nm, integration time = 0.1 s.

5.2.1.3 ee Detection

We then prepared the enantiomeric analog pairs of (*S*)-**5.2**@F68 and (*R*)-**5.2**@F68, and studied their fluorescence responses at various enantiomeric excesses of Trp (ee = [D-L]/[D+L]). As shown in Figure 5.4, the fluorescence responses of (*S*)-**5.2**@F68 and (*R*)-**5.2**@F68 resembled a mirror image relationship which confirmed the observed enantioselective recognition. The curve for (*S*)-**5.2**@F68 increased fast then slow, and finally fast again, indicating the existence of a pole in its derivative function. To our surprise, an unprecedented 3rd-order fit of the fluorescence intensity vs ee was observed with R square values of 0.998 and 0.994. A possible explanation was that, the product of (*S*)-**5.2** with one D-Trp and one L-Trp was also fluorescent but it would inhibit the fluorescence of the product of (*S*)-**5.2** with D-Trp in the micelles. The imperfect matches in Figure 5.4a were attributed to the intrinsic differences of the micelles, the random conformations of the polymers and their variable molecular weight distributions, and experimental errors. After letting the reaction mixture set for tens of hours, a new emission at λ_{em} = 490 nm appeared.

Although the intensity was fairly weak within most experiments time period of 3 hours, it allowed more accurate measurements of the ee by using the intensity ratio of I_{536}/I_{490}. This relationship was found to be in 2nd order with R square values of 0.997 and 0.998 for two enantiomeric probes respectively as seen in Figure 4b. The two calibration curves were perfectly matched, and the standard deviation for each single data point was extremely limited.

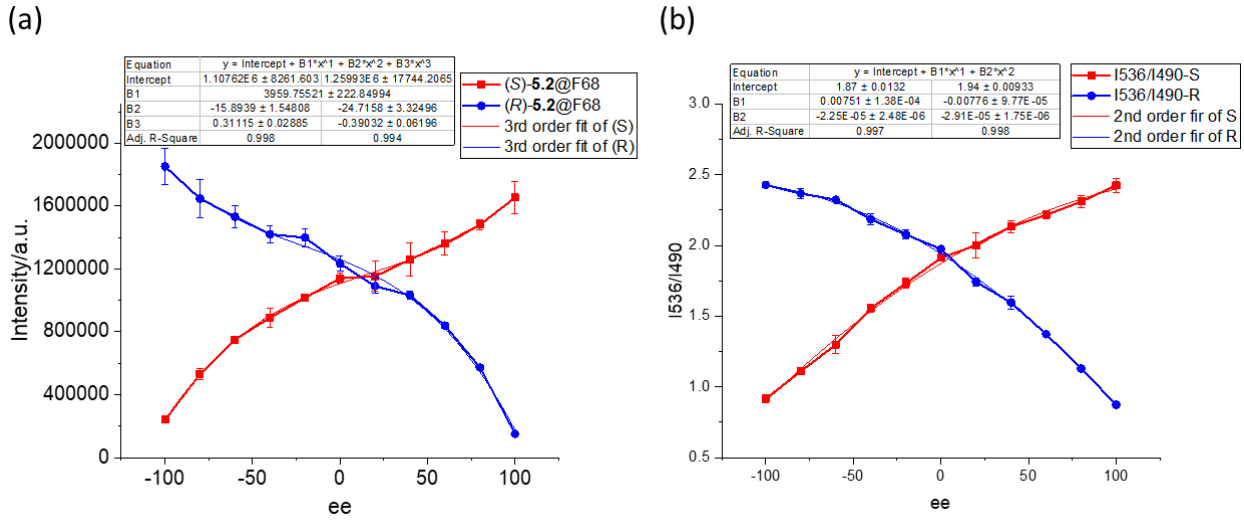

Figure 5. 4 (a) Fluorescence intensity of (*S*)-**5.2**@F68 / (*R*)-**5.2**@F68 (10 μM) and $Zn(OAc)_2$ (2 equiv.) at λ_{em} = 536 nm versus the ee of 40 equiv. Trp. (b) The ratio of fluorescence intensity at λ_{em} = 536 nm over that at λ_{em} = 490 nm. Error bars were made from 3 independent experiments. Measured at 5 °C, excited at 400 nm, slit = 5/5 nm, integration time = 0.1 s.

5.2.2 Characterization of Micelles

When (*S*)-**5.2**@F68 was treated with D- and L-Trp, the UV-vis spectra only showed the increased signals of the added tryptophan but no change in the absorption of the probe (See Figure S5.9) This indicates that there was only a very small degree of reaction between the probe and the amino acid under this condition which however has led to the dramatically enhanced fluorescence in aqueous solution. Without the copolymers in organic phase, the absorption at 400 nm for the reaction of D-Trp with the probe was slightly redshifted, while the UV-vis spectrum for the reaction of L-Trp resembled that of (*S*)-**5.2** in the 400 nm region. The fluorescence responses

without micelles in organic phase were also studied under the same conditions according to the reference.[27] Fluorescence enhancement was observed for both D-/L-Trp but with less enantioselectivity (See Figure S5.17). These data supported that the polymer-based micelles not only allowed the detection of tryptophan to be conducted in water, but also greatly enhanced the fluorescence sensitivity and selectivity. The sizes of all micelle probes were monitored by dynamic light scattering (DLS) (See Figure S5.13-5.16). They all had narrow distributions of radiuses in the range of 20-40 nm, which were properly maintained with the addition of Zn(II) and Trp analytes. It proved the stability of the micelles throughout this study.

5.2.3 Mechanistic Studies

^{1}H NMR studies on the reactions of (*S*)-**5.2** with Trp (in tetrabutylammonium salt form) were carried out in DMSO-d_6 in order to provide more insights into the mechanism. Fast conversion of the organic probe (*S*)-**5.2** to products was observed for the reactions with both D-/L-Trp. The signals of (*S*)-**5.2** quickly turned into a new set of peaks within 0.5 h (Figure 5.5). The two peaks at δ ~ 10.7 were the indole secondary amines -N<u>H</u>- of Trp and the corresponding reaction product. The two singlets at δ ~ 8.5, 8.0 were protons on 4,4'-positions of BINOL and the imine protons –CH=N. Newly formed aliphatic signals at δ ~ 3.9 were α-proton of Trp, and δ ~ 3.0 were β-protons of Trp. Slight difference in chemical shifts for the D-Trp reaction and L-Trp reaction confirmed the formation of diastereomeric products. The imine structures were further confirmed by ^{13}CNMR. The original aldehyde carbon -<u>C</u>HO at δ = 196.40 disappeared aftereach reaction, while the imine carbon -<u>C</u>H=N- signals showed up at δ =170.95 for the reactions of both D-/L-Trp.

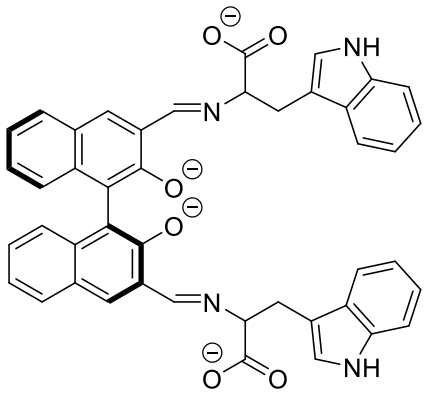

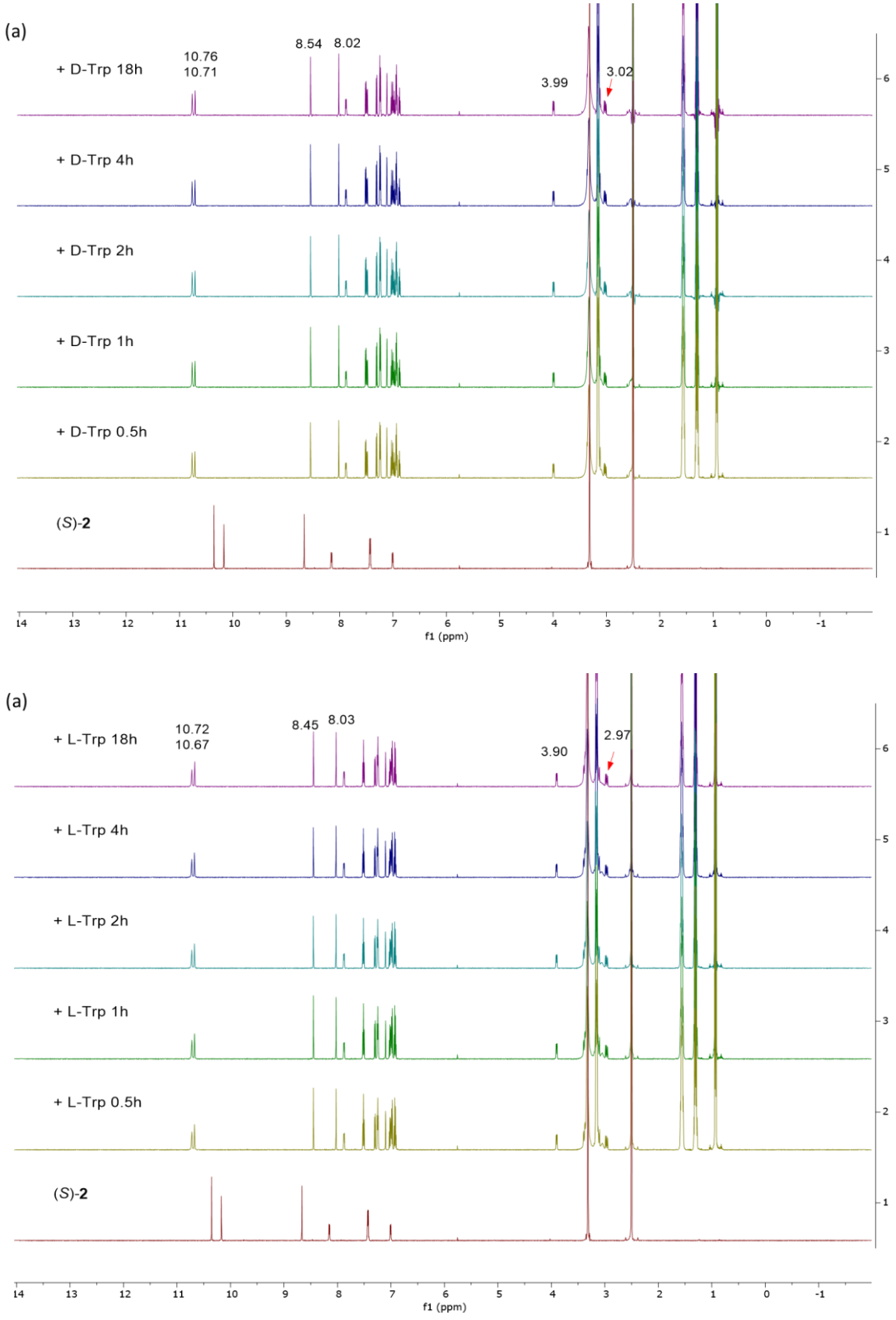

Figure 5. 5 ^{1}HNMR time course of (*S*)-**5.2** (2 mM in DMSO-d_6) with (a) D-Trp; (b) L-Trp. 5 equiv. Trp-TBA salts were used in DMSO-d_6. 600 MHz.

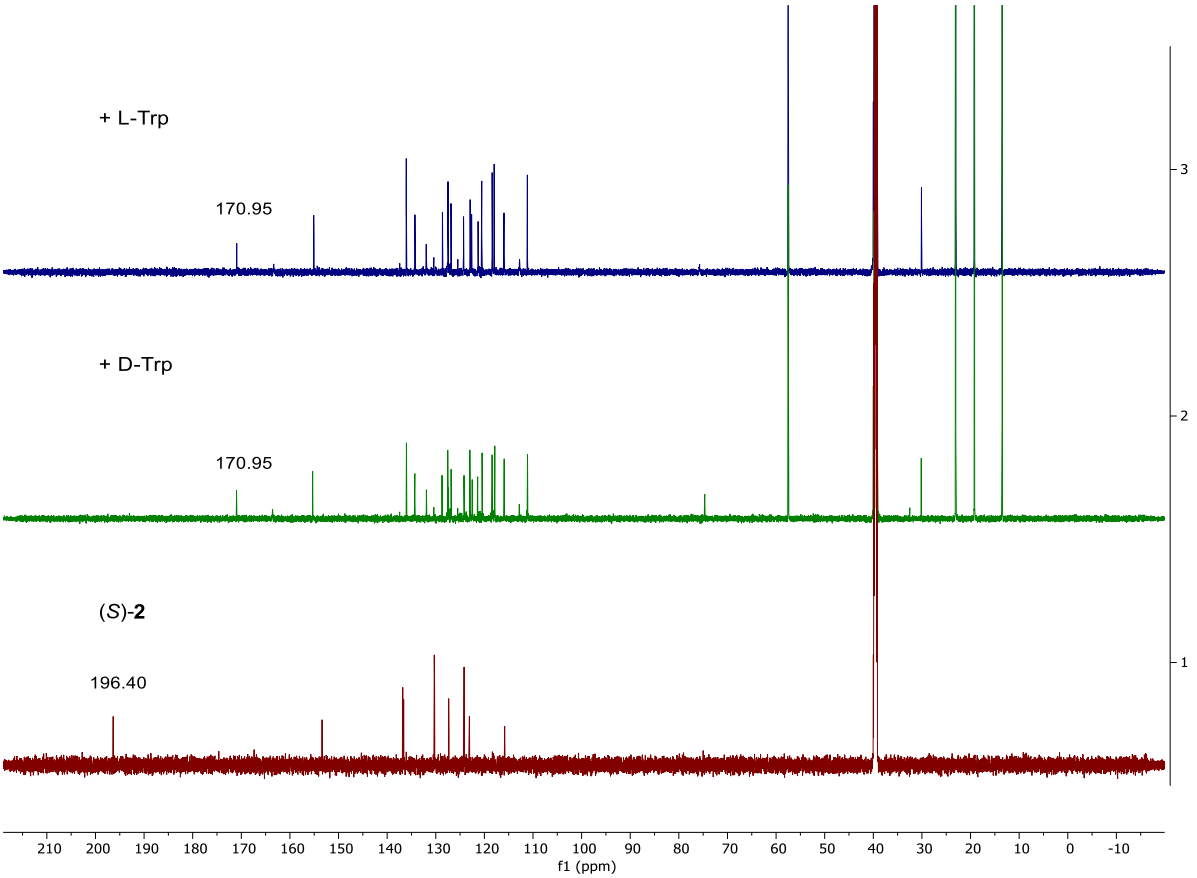

Figure 5. 6 ^{13}CNMR spectra of (*S*)-**5.2** (2 mM in DMSO-d_6) with (a) D-Trp; (b) L-Trp. 5 equiv. Trp-TBA salts were used in DMSO-d_6. 201 MHz.

5.3. Conclusion

In conclusion, four micelle probes (*S*)-**5.2**@PEG-PLLA, (*S*)-**5.2**@PEG-PCL, (*S*)-**5.2**@PE-PEG, and (*S*)-**5.2**@F68 had been fabricated with varying micelle-forming copolymers and the sizes were characterized by DLS. The interaction of these micelle probes with amino acids in the presence of Zn(II) has been investigated and it shows that the sensitivity and enantioselectivity of the fluorescent responses could be tuned by varying the copolymers while maintaining the same organic core. While (*S*)-**5.2**@PEG-PLLA was both chemoselective and enantioselective for D-Lys, (*S*)-**5.2**@PEG-PCL had compatible fluorescence responses for Trp and Lys, (*S*)-**5.2**@PE-PEG favored L-Trp, and (*S*)-**5.2**@F68 favored D-Trp. (*S*)-**5.2**@F68 had decent enantioselectivity

for Trp with *ef* value up to 9.2. The low LOD value of 962 nM and linear range of 10-250 μM were found for D-Trp. Unprecedented 3rd-order fit of calibration curve was observed in the ee study of D-Trp, and the accuracy could be even further improved by using intensity ratios of I_{536}/I_{490}. The imine forming reaction between the amino acid and the probe was supported by NMR studies. This work demonstrates that simply switching the copolymers can dramatically influence the outcome performances of micelle probes, and it provides a new strategy to develop fluorescent probes for the detection of biologically important molecules.

5.4 Experimental

5.4.1. General experimental methods

All amino acids and other chemicals were purchased from Sigma Aldrich Chemical Co. or Alfa Aesar, and used without further purification. ^{1}HNMR spectra were recorded on Varian-600 MHz spectrometer. ^{13}CNMR spectra were recorded on Bruker-800 MHz spectrometer. Chemical shifts for ^{1}H NMR were reported in parts per million relative to a singlet 2.50 ppm for deuterated DMSO. Chemical shifts for ^{13}C NMR were reported in parts per million relative to a septet at 39.52 ppm for deuterated DMSO. Steady-state fluorescence emission spectra were recorded on Horiba FluoroMax-4 spectrofluorometer. Low-temperature fluorescence emission spectra were recorded on Horiba FluoroMax-3 spectrofluorometer. Nanoparticle sizes and polydispersities were analyzed via dynamic light scattering (DLS, Wyatt, DynaPro). Deionized water was used for all the experiments.

Nano precipitation to prepare the micelle encapsulated probe 1.6 μmol of (*S*)-organic sensor cores (1mg/mL in DMF) were added to 80 mg coblock polymers. More DMF was added to dissolve the coblock polymer and the volume was calibrated to 8 mL. The solution was sonicated for 10 minutes and added dropwise to a vortex of 72 mL water at a rate of 1 mL/min. The vortex was allowed to last 30 more minutes after the addition of DMF solution. The final mixture was dialyzed in DI water to form micelle solutions containing 20 μM corresponding organic cores.

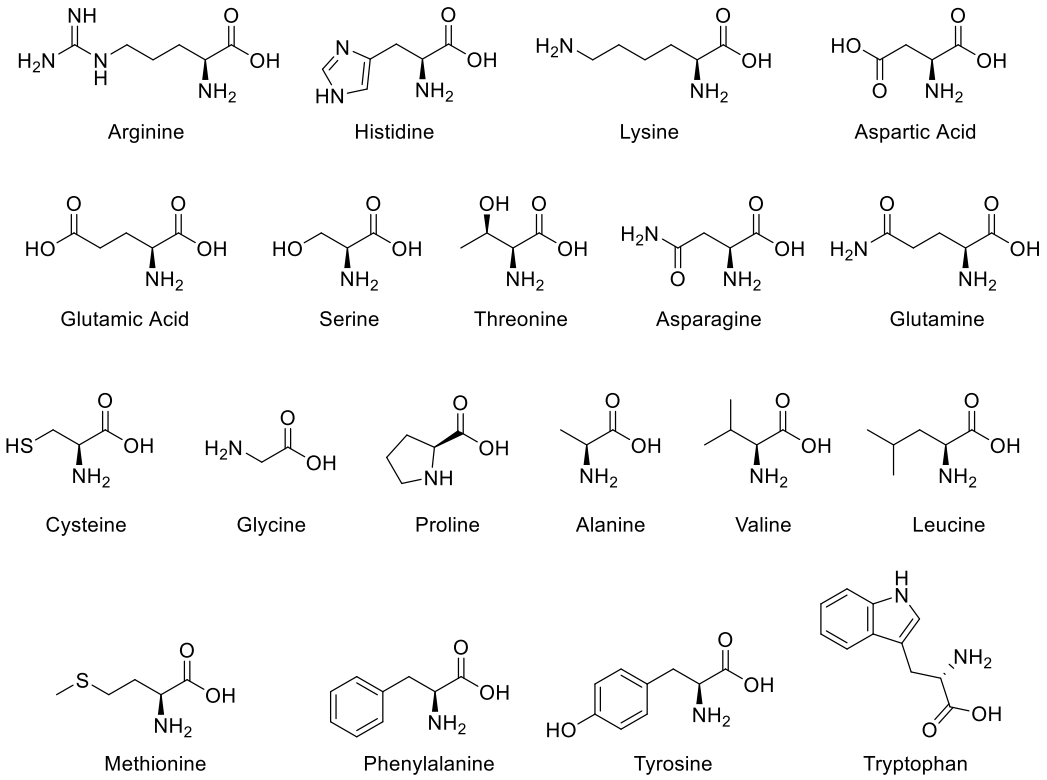

Figure S5. 1 Structure of Chiral Amino Acids

5.4.2. Fluorescence spectra

Fluorescent measurement at room temperature:

To a suspension of 1 mL of 2.0 x 10^{-5} M Probe and 1 mL carbonate buffer solution (CBS, 25mM of sodium carbonate with 25 mM of sodium bicarbonate, pH = 10.1), were added with 5 µL of 20 mM amino acids (in CBS) and 10 µL of 4 mM $Zn(OAc)_2$ (in water). After let them stand for various hours, the mixtures were tested for fluorescence. Slit = 3/3nm, int time =0.1s. Fluorescence emission spectra were recorded on Horiba FluoroMax-4 spectrofluorometer.

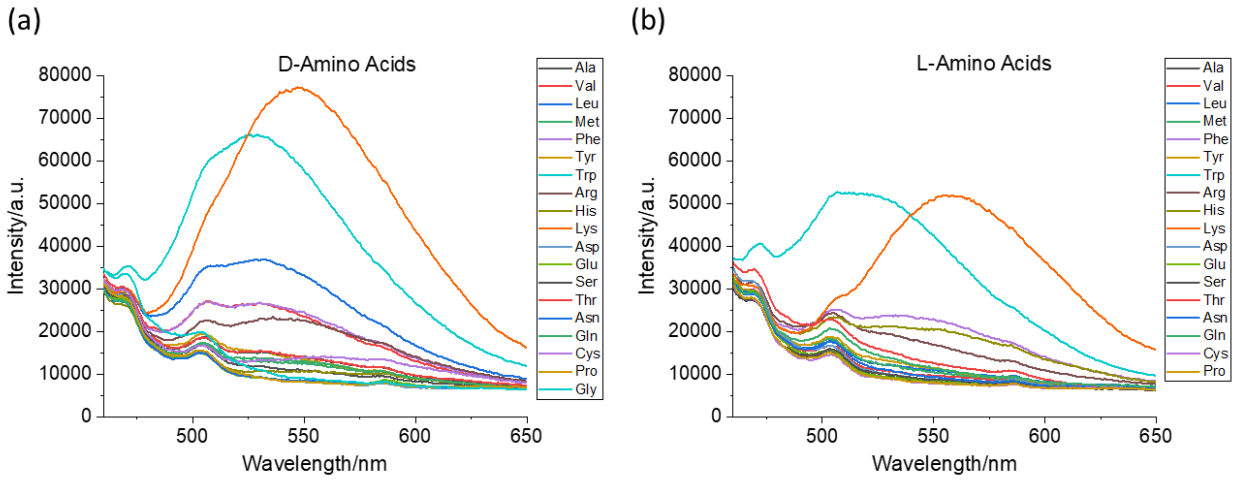

Figure S5. 2 (*S*)-**5.2**@PEG-PCL's fluorescence responses for (a) D-amino acids; (b) L-amino acids. Corresponding organic sensor concentration = 10 µM, with 2equiv. zinc acetate, 10eq. amino acids. Excited at 430nm, slit=3/3nm, integration time=0.1s.

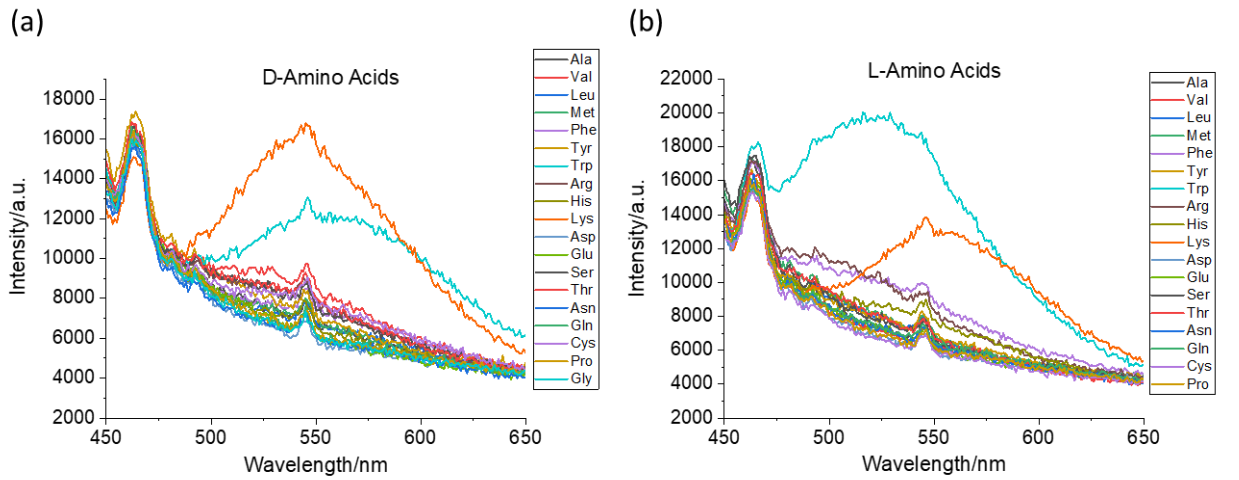

Figure S5. 3 (*S*)-**5.2**@PE-PEG's fluorescence responses for (a) D-amino acids; (b) L-amino acids. Corresponding organic sensor concentration = 10 μM, with 2equiv. zinc acetate, 10eq. amino acids. Excited at 430nm, slit=3/3nm, integration time=0.1s.

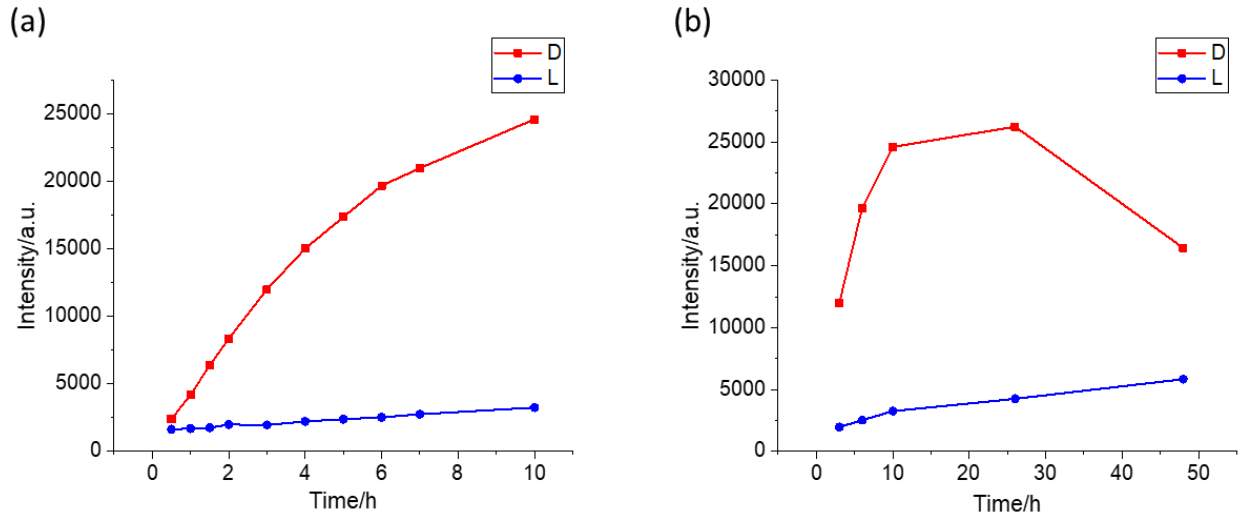

Figure S5. 4 (*S*)-**5.2**@F68's fluorescence intensity with D- and L-Trp at λ_{em} = 536 nm versus the reaction time. (a) 1-10 hours; (b) 4-48 hours. Corresponding organic sensor concentration = 10 μM, with 2 equiv. zinc acetate, 10 equiv. amino acids. Excited at 400nm, slit = 3/3nm, integration time = 0.1s.

Low-temperature fluorescence study:

To a suspension of 1 mL of 20 µM Probe and 1 mL CBS buffer, were added with 10 µL of 20mM AA (in water) and 10 µL of 4 mM $Zn(OAc)_2$ (in water). After let them stand for 3 hours, the mixtures were chilled in an ice bath, and tested for fluorescence with FluoroMax3 at a temperature of 5 degree Celsius with a continuous nitrogen flow. Slit = 3/3nm, int time = 0.3s.

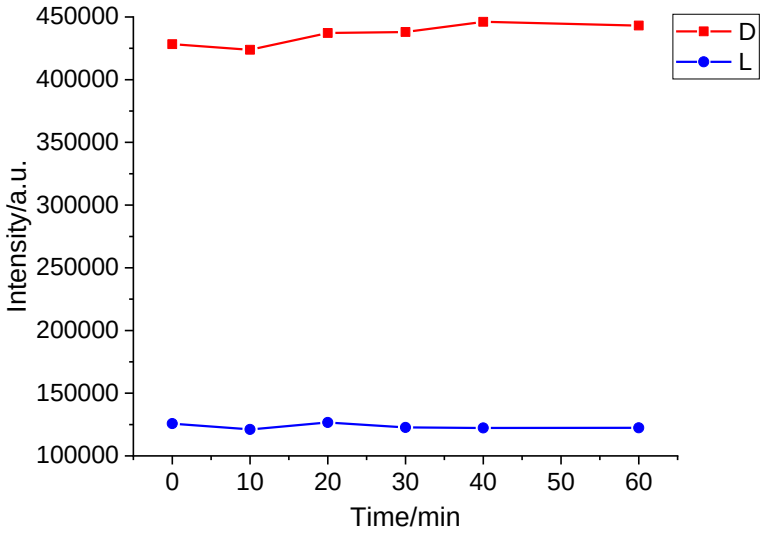

Figure S5. 5 Fluorescence intensity of the (*S*)-**5.2**@F68-Trp reaction mixtures at λ_{em} = 536 nm versus the time after the reaction was quenched with ice-bath. Corresponding organic sensor concentration = 10 µM, with 2equiv. zinc acetate, 10 equiv. amino acids. Excited at 400nm, slit = 3/3nm, integration time = 0.1s. The intensities were stable after quenched with ice bath.

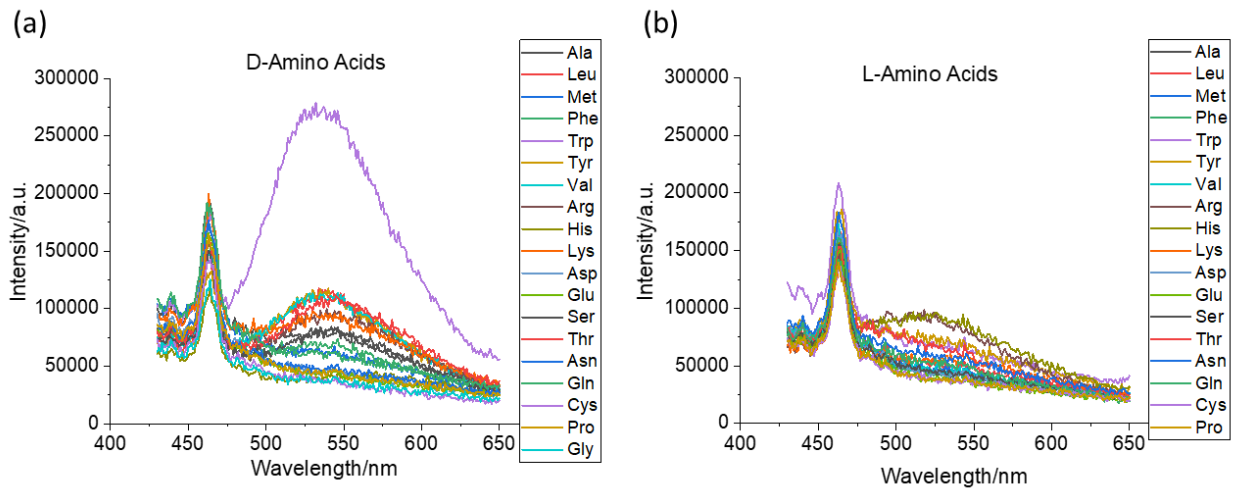

Figure S5. 6 (*S*)-**5.2**@F68's fluorescence responses with (a) D-amino acids; (b) L-amino acids. Corresponding organic sensor concentration = 10 μM, with 2 equiv. zinc acetate, 10 equiv. amino acids. Excited at 400 nm, slit = 3/3nm, integration time = 0.1s.

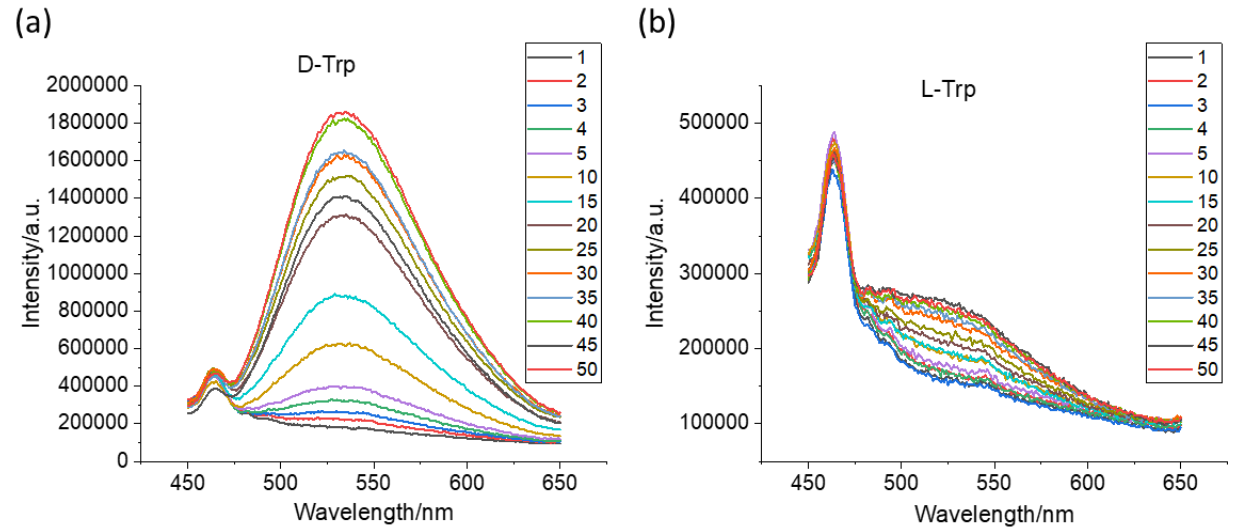

Figure S5. 7 (*S*)-**5.2**@F68's fluorescence responses with (a) D-Trp; (b) L-Trp at varying equivalences. Corresponding organic sensor concentration = 10 μM, with 2equiv. zinc acetate. Excited at 400 nm, slit = 5/5nm, integration time = 0.1s.

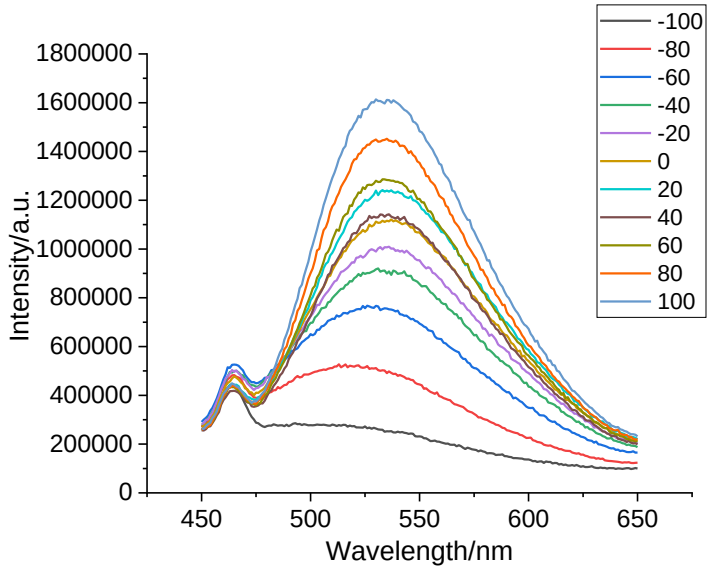

Figure S5. 8 (*S*)-**5.2**@PEG-PLLA's fluorescence responses with Trp at various ee. Corresponding organic sensor concentration = 10 μM, with 2 equiv. zinc acetate, 40 equiv. amino acids. Excited at 400 nm, slit = 5/5nm, integration time = 0.1s.

5.4.3. UV-vis Spectra

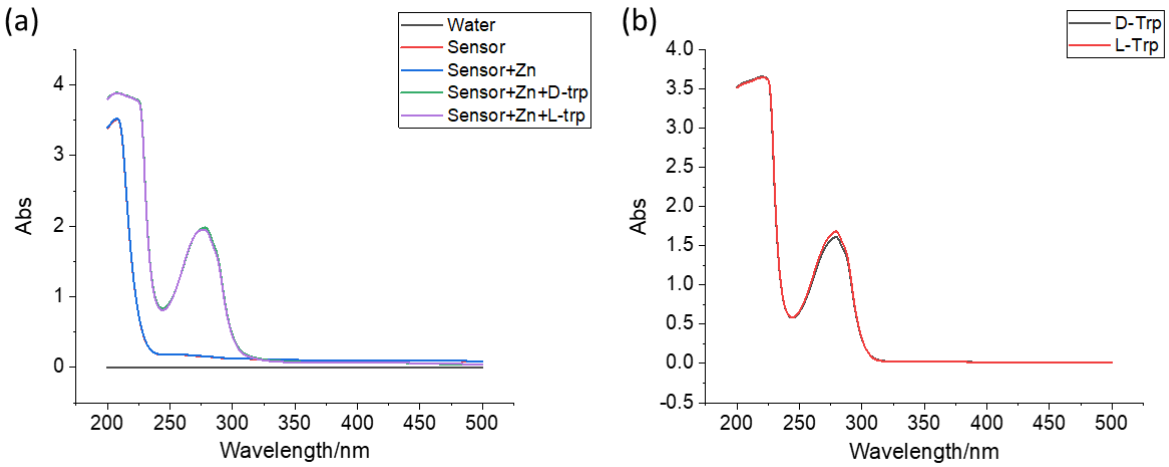

Figure S5. 9 UV-vis spectra of (a) (*S*)-**5.2**@F68 with Zn(II) and Trp; (b) D-/L-Trp. Corresponding (*S*)-**5.2** concentration = 10 µM, 2 equiv. zinc acetate, 40 equiv. Trp, in carbonate buffer solution.

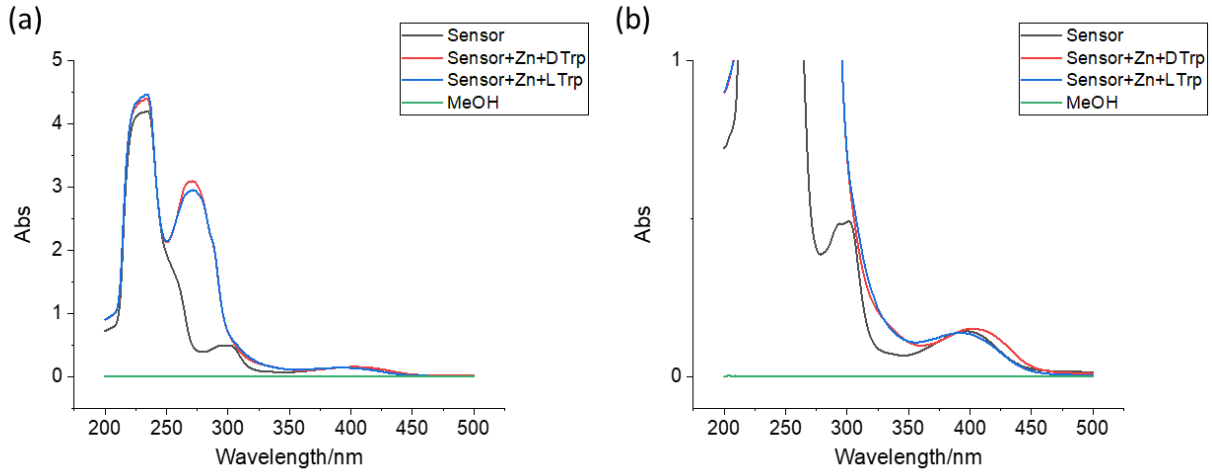

Figure S5. 10 (a) UV-vis spectra of (*S*)-**5.2** with Zn(II) and Trp; (b) The expanded view of (a). (*S*)-**5.2** concentration = 10 µM, 2 equiv. zinc acetate, 40 equiv. Trp/TBA, in methanol.

5.4.4. NMR studies for the reaction of (*S*)-5.2 with Trp

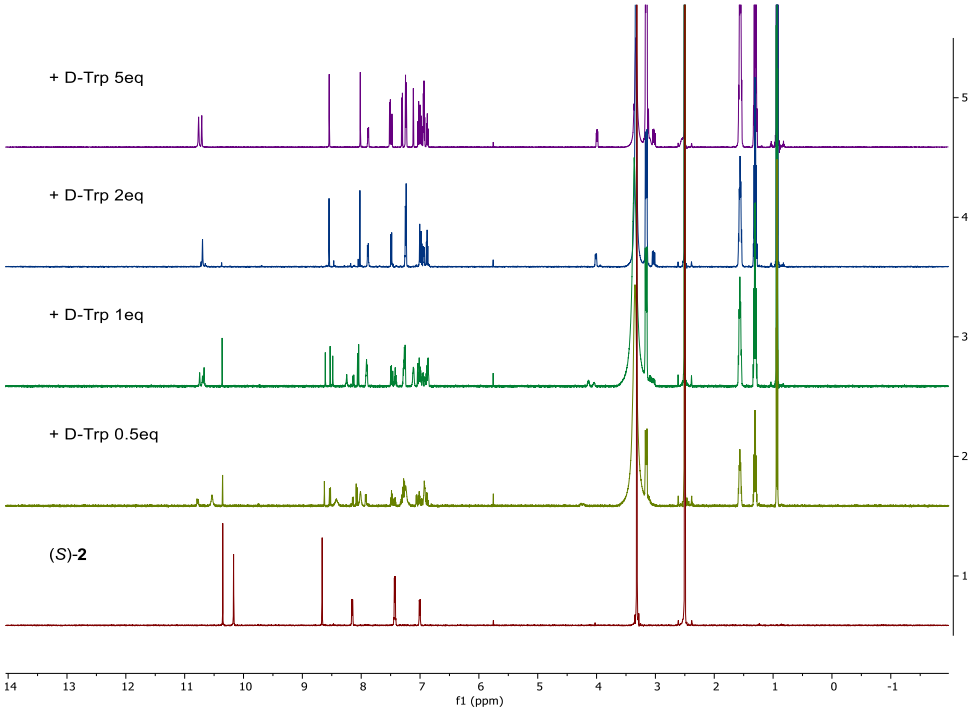

Figure S5. 11 ^{1}H (DMSO-d$_6$. 600 MHz) NMR spectra for the reaction of 2 mM (*S*)-**5.2** with varying amounts of D-Trp/TBA in DMSO-d$_6$.

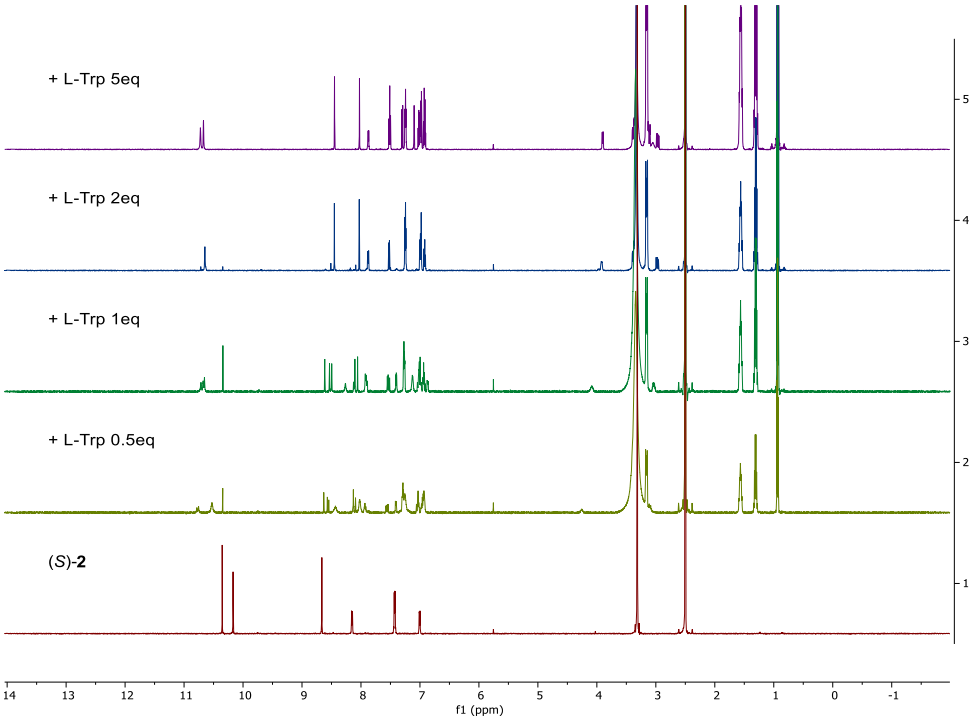

Figure S5. 12 ^{1}H (DMSO-d$_6$. 600 MHz) NMR spectra for the reaction of 2 mM (*S*)-**5.2** with varying amounts of L-Trp/TBA in DMSO-d$_6$.

5.4.5. DLS studies

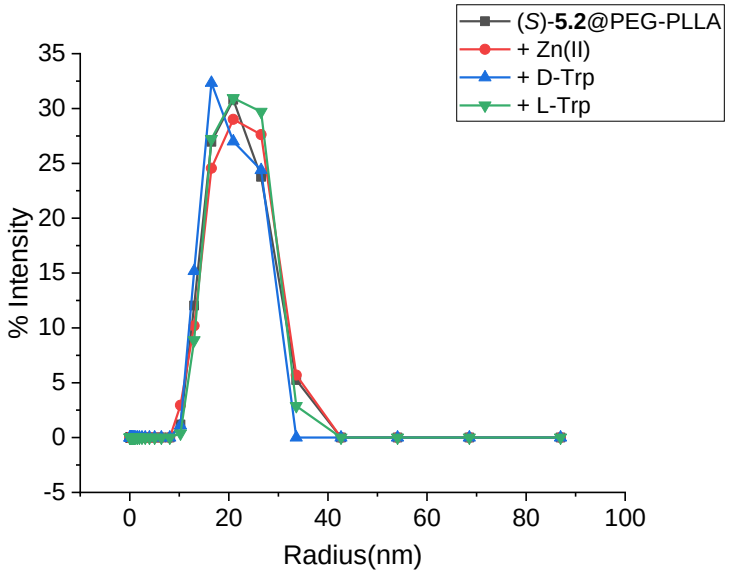

Figure S5. 13 DLS plots for the reactions of (*S*)-**5.2**@PEG-PLLA with Trp. Corresponding (S)-5.2 concentration = 10 µM, 2 equiv. zinc acetate, 40 equiv. Trp, in CBS buffer.

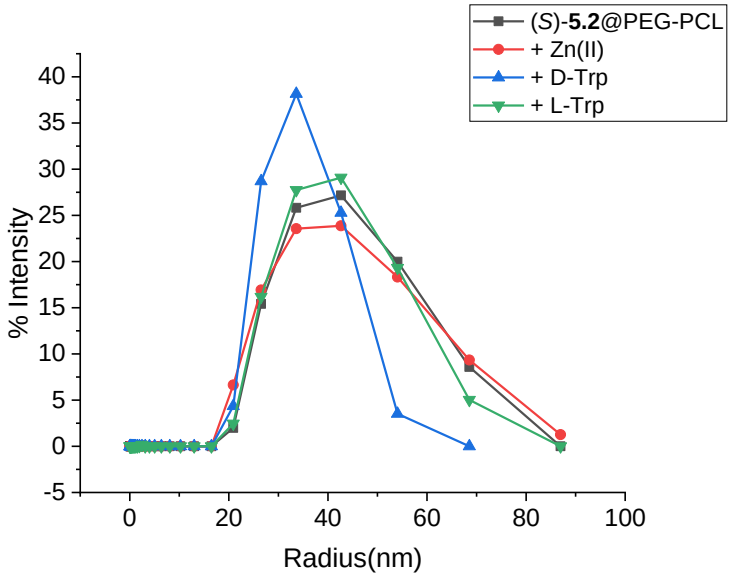

Figure S5. 14 DLS plots for the reactions of (*S*)-**5.2**@PEG-PCL with Trp. Corresponding (S)-5.2 concentration = 10 µM, 2 equiv. zinc acetate, 40 equiv. Trp, in CBS buffer.

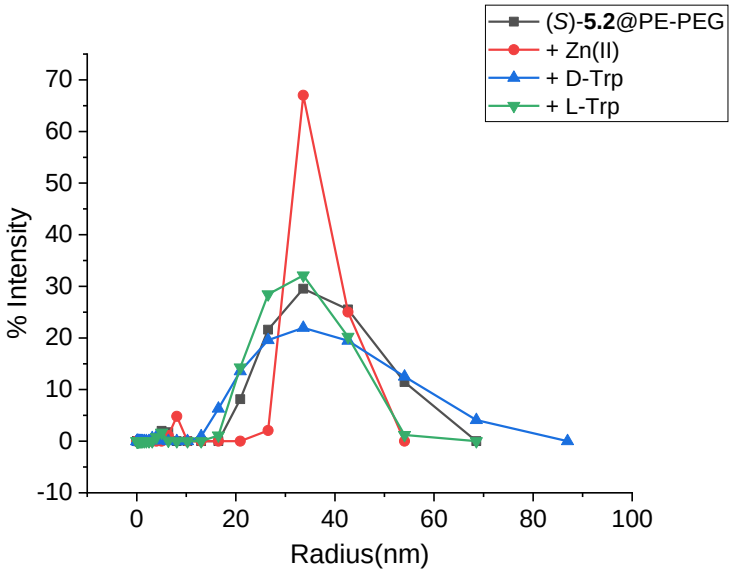

Figure S5. 15 DLS plots for the reactions of (*S*)-**5.2**@PE-PEG with Trp. Corresponding (S)-5.2 concentration = 10 μM, 2 equiv. zinc acetate, 40 equiv. Trp, in CBS buffer.

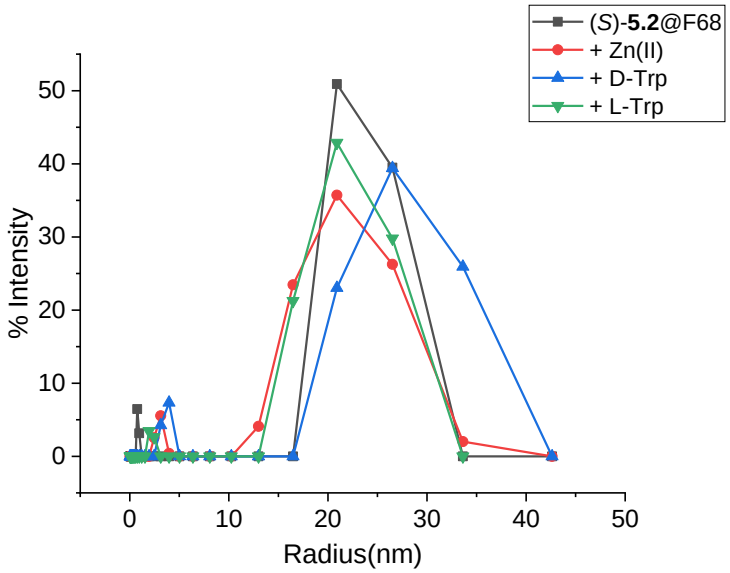

Figure S5. 16 DLS plots for the reactions of (*S*)-**5.2**@F68 with Trp. Corresponding (S)-5.2 concentration = 10 μM, 2 equiv. zinc acetate, 40 equiv. Trp, in CBS buffer.

5.4.6. Fluorescence spectra of organic probe (*S*)-5.2

Procedures were used according to reference (*Chem. Sci.* **2014**, *5* (9), 3457–3462). Stock solutions of 2 mM (*S*)-**5.2** in CH_2Cl_2, 2 mM $Zn(OAc)_2$ in CH_3OH and 6 mM Bu_4NOH in CH_3OH were freshly prepared for each measurement. A solution of (*S*)-**5.2** + Zn^{2+} (2 equiv.) + Bu_4NOH (10 equiv.) (2 mM) was mixed with 10 equiv. of the Trp solution (6 mM in H_2O). The resulting solution was allowed to stand at room temperature for 1.5 h before dilution and then tested for fluorescence.

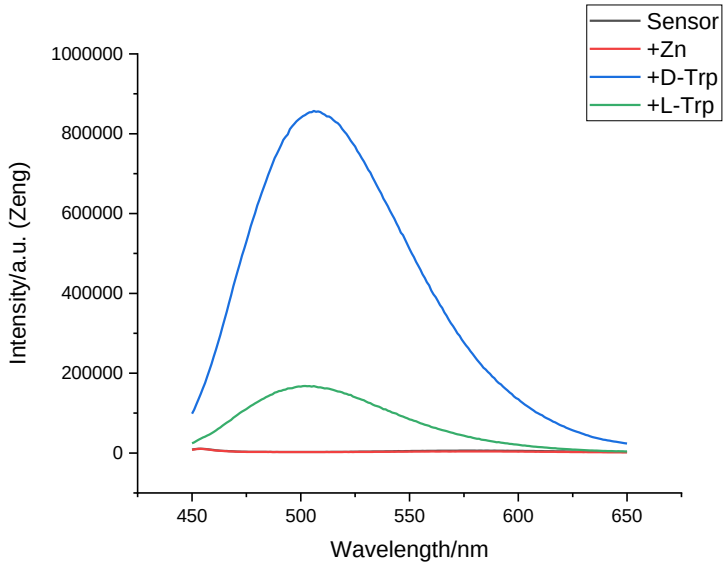

Figure S5. 17 (*S*)-**5.2**'s fluorescence interaction with Trp-TBA in methanol. (*S*)-**5.2** concentration = 10 µM, 2 equiv. zinc acetate, 10 equiv. Excited at 400 nm, slit = 5/5 nm, integration time = 0.1s.

5.5 References

(1) Knott, P. J.; Curzon, G. Free Tryptophan in Plasma and Brain Tryptophan Metabolism. *Nature* **1972**, *239* (5373), 452–453.

(2) Munn, D. H.; Zhou, M.; Attwood, J. T.; Bondarev, I.; Conway, S. J.; Marshall, B.; Brown, C.; Mellor, A. L. Prevention of Allogeneic Fetal Rejection by Tryptophan Catabolism. *Science* **1998**, *281* (5380), 1191–1193.

(3) Fallarino, F.; Grohmann, U.; Vacca, C.; Bianchi, R.; Orabona, C.; Spreca, A.; Fioretti, M. C.; Puccetti, P. T Cell Apoptosis by Tryptophan Catabolism. *Cell Death Differ.* **2002**, *9* (10), 1069–1077.

(4) Schröcksnadel, K.; Wirleitner, B.; Winkler, C.; Fuchs, D. Monitoring Tryptophan Metabolism in Chronic Immune Activation. *Clin Chim Acta*, **2006**, *364*, pp 82–90.

(5) Platten, M.; Wick, W.; Van Den Eynde, B. J. Tryptophan Catabolism in Cancer: Beyond IDO and Tryptophan Depletion. *Cancer Res.* **2012**, *80* (5), pp 5435–5440.

(6) Jimené Z ‡ §, E. C.; Olivera, B. M.; Gray, W. R.; Cruz, L. J. Contryphan Is a D-Tryptophan-Containing Conus Peptide. *J Biol. Chem.* **1996**, *271* (45), 28002-5.

(7) Genchi, G. An Overview on D-Amino Acids. *Amino Acids.* **2017**, *49*, 1521-1533.

(8) Chen, J.; Kudo, H.; Kan, K.; Kawamura, S.; Koseki, S. Growth-Inhibitory Effect of Dtryptophan on Vibrio Spp. in Shucked and Live Oysters. *Appl. Environ. Microbiol.* **2018**, *84* (19).

(9) Kobayashi, K.; Maezawa, T.; Tanaka, H.; Onuki, H.; Horiguchi, Y.; Hirota, H.; Ishida, T.; Horiike, K.; Agata, Y.; Aoki, M.; et al. The Identification of D-Tryptophan as a Bioactive Substance for Postembryonic Ovarian Development in the Planarian Dugesia Ryukyuensis. *Sci. Rep.* **2017**, *7*, 45175.

(10) Zhang, X.; Yin, J.; Yoon, J. Recent Advances in Development of Chiral Fluorescent and Colorimetric Sensors. *Chem. Rev.* **2014**, *114*, 9, 4918-4959.

(11) Pu, L. Simultaneous Determination of Concentration and Enantiomeric Composition in Fluorescent Sensing. *Acc. Chem. Res.* **2017**, *50*, 4, 1032-1040.

(12) Wang, J.; Liu, H. B.; Tong, Z.; Ha, C. S. Fluorescent/Luminescent Detection of Natural Amino Acids by Organometallic Systems. *Coord. Chem. Rev.* **2015**, *303*, pp 139–184.

(13) He, C.; Wang, J.; Wu, P.; Jia, L.; Bai, Y.; Zhang, Z.; Duan, C. Fluorescent Differentiation and Quantificational Detection of Free Tryptophan in Serum within a Confined Metal-Organic Tetrahedronw ChemComm. *Chem. Commun* **2012**, *48*, 11880–11882.

(14) Nian, S.; Pu, L. Amphiphilic Polymer-Based Fluorescent Probe for Enantioselective Recognition of Amino Acids in Immiscible Water and Organic Phases. *Chem. - A Eur. J.* **2017**, *23* (71), 18066–18073.

(15) Zhao, F.; Du, Y.; Tian, J.; Shi, D.; Wang, Y.; Hu, L.; Yu, S.; Yu, X.; Pu, L. Enantioselective Fluorescent Recognition of Amino Acids in Aqueous Solution by Using a Chiral Aldehyde Probe. *Eur J. Org. Chem.* **2018**, *16*, 1891–1895.

(16) Zeng, C.; Zhang, X.; Pu, L. Enantioselective Fluorescent Imaging of Free Amino Acids in Living Cells. *Chem. - A Eur. J.* **2017**, *23* (10), 2432–2438.

(17) Kaper, T.; Looger, L. L.; Takanaga, H.; Platten, M.; Steinman, L.; Frommer, W. B. Nanosensor Detection of an Immunoregulatory Tryptophan Influx/Kynurenine Efflux Cycle. *PLoS Biol.* **2007**, *5* (10), e257.

(18) Du, G.; Pu, L. Micelle-Encapsulated Fluorescent Probe: Chemoselective and Enantioselective Recognition of Lysine in Aqueous Solution. *Org. Lett.* **2019**, *21*,12, 4777-4781.

(19) Kataoka, K.; Harada, A.; Nagasaki, Y. Block Copolymer Micelles for Drug Delivery: Design, Characterization and Biological Significance. *Adv. Drug Deliv. Rev.* **2012**, *64*, 37–48.

(20) Wan, Y.; Chen, W.; Yang, J.; Bei, J.; Wang, S. Biodegradable Poly(l-Lactide)-Poly(Ethylene Glycol) Multiblock Copolymer: Synthesis and Evaluation of Cell Affinity. *Biomaterials* **2003**, *24*, 2195–2203.

(21) Kersey, F. R.; Zhang, G.; Palmer, G. M.; Dewhirst, M. W.; Fraser, C. L. Stereocomplexed Poly(Lactic Acid)−Poly(Ethylene Glycol) Nanoparticles with Dual-Emissive Boron Dyes for Tumor Accumulation. *ACS Nano* **2010**, *4* (9), 4989–4996.

(22) Grossen, P.; Witzigmann, D.; Sieber, S.; Huwyler, J. PEG-PCL-Based Nanomedicines: A Biodegradable Drug Delivery System and Its Application. *J Control Release*. 2017, *260*, pp 46–60.

(23) Shao, K.; Huang, R.; Li, J.; Han, L.; Ye, L.; Lou, J.; Jiang, C. Angiopep-2 Modified PE-PEG Based Polymeric Micelles for Amphotericin B Delivery Targeted to the Brain. *J. Control. Release* **2010**, *147* (1), 118–126.

(24) Alexandridis, P.; Hatton, T. A. Poly(Ethylene Oxide)-Poly(Propylene Oxide)-Poly (Ethylene Oxide) Block Copolymer Surfactants in Aqueous Solutions and at Interfaces: Thermodynamics, Structure, Dynamics, and Modeling. *Colloids Surfaces A: Physicochem. Eng. Aspects* **1995**, *96*, 1-46.

(25) Al Khateb, K.; Ozhmukhametova, E. K.; Mussin, M. N.; Seilkhanov, S. K.; Rakhypbekov, T. K.; Lau, W. M.; Khutoryanskiy, V. V. In Situ Gelling Systems Based on Pluronic F127/Pluronic F68 Formulations for Ocular Drug Delivery. *Int. J. Pharm.* **2016**, *502* (1–2), 70–79.

(26) Gostner, J. M.; Geisler, S.; Becker, K.; Fuchs, D.; Mayersbach, P.; Schennach, H. Serum Tryptophan, Kynurenine, Phenylalanine, Tyrosine and Neopterin Concentrations in 100 Healthy Blood Donors. *Pteridines* **2015**, *26* (1), 31–36.

(27) Huang, Z.; Yu, S.; Wen, K.; Yu, X.; Pu, L. Zn(ii) Promoted Dramatic Enhancement in the Enantioselective Fluorescent Recognition of Functional Chiral Amines by a Chiral Aldehyde. *Chem. Sci.* **2014**, *5* (9), 3457–3462.

Chapter 6. Future Directions

6.1 Introduction

We've demonstrated the micelle probes for achieving the detection of specific amino acids enantioselectively and chemoselectively. Some key results are summarized as follows. (*S*)-**6.1**@PEG-PLLA achieved the detection of chiral Lys both enantioselectively and chemoselectively, with LOD of 848 nM and 2nd order fit of the ee detection. (*S*)-**6.2**@PEG-PLLA achieved the detection of chiral Trp both enantioselectively and chemoselectively, with LOD of 2.6 μM and 1st order fit of the ee detection. (*S*)-**6.3**@PEG-PLLA achieved the detection of chiral His both enantioselectively and chemoselectively, with LOD of 107 nM and 2nd order fit of the ee detection. (*S*)-**6.1**@F68 achieved the detection of chiral Trp both enantioselectively and chemoselectively, with LOD of 962 nM and 3rd order fit of the ee detection.

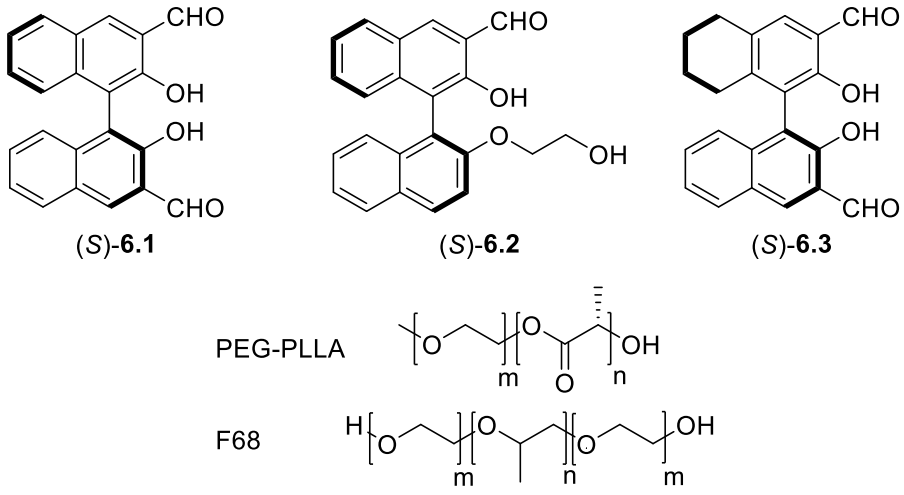

Figure 6. 1 Structures of the probe cores and the copolymers

All those studies were finished in water media. While other BINOL-based probes needed to be mixed with analytes at higher concentration of mM-scale, the micelle probes allowed easier processing by having the reaction happened at μM-scale.

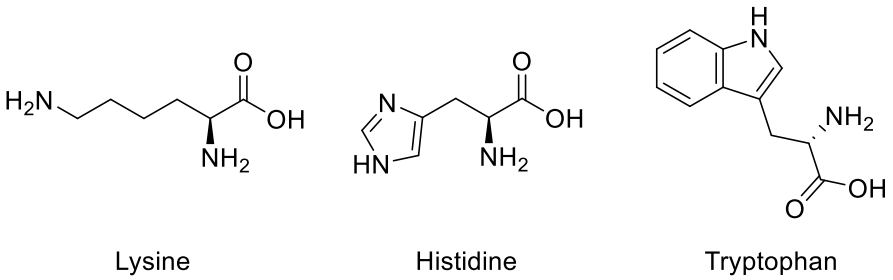

Lysine Histidine Tryptophan

Figure 6. 2 Structures of the analytes

6.2 Limitations and Future Directions

6.2.1 Mechanistic Studies

The selectivity of (*S*)-**6.1**@PEG-PLLA toward Lys came from the selective reaction of Lys's terminal amino groups as we mentioned in Chapter 2. For the rest studies, α-amino groups of amino acids are believed to form imine with the probe. However, given the structure similarity of the organic probes as well as the amino acids, it will be very useful to understand the reason of selective reaction in each case for future probe development.

NMR techniques were employed to provide more insights in the reaction process, but the studies were limited in organic phases only. The reason was that the concentrations of micelle probes were at μM-scale, even after concentrating with centrifuge (notice that at high concentration the micelles would aggregate). NMR study requires concentration at least around mM-scale and would not be able to directly monitor the reaction process within micelles. In order to answer those questions, novel techniques will be needed.

6.2.2 Limitations

The quite rare and interesting specific detections are limited to Trp, Lys and His. Considering the amino acids family of 20 members in total, only a limited part of them have been answered. Yet there are still blanks for other amino acids. Especially there are no answer for D-Ser, a key molecule in the neurotransmitter. D-Ser was found to be a co-agonist of the N-methyl

D-aspartate (NMDA), whose disorder is related to many diseases including schizophrenia.[1] Further study on the recognition of D-Ser will be of extreme importance regarding its biological functions.

Although other buffers had been tested, only basic buffer at pH = 10 allowed optimal results and was used throughout the entire study. The basic condition limited direct application of the micelle probes for biological applications, where cells won't survive such high pH value.

Other limitations include instrumentations and quantum yields. As we stated in the third chapter, (*S*)-**6.4**@PEG-PLLA exhibited good enantioselectivity for Phe. Further study on Phe was limited by the instrumentations, where the reaction was not able to be efficiently quenched at around 0 ^{o}C but with 17% increase per hour. It is promising that an even colder temperature can kinetically quench the reaction for stable data collection. In such a case, fluorometer and chilling bath will be placed under inert gas atmosphere to avoid condensation of water on cuvettes. The quantum yields of current probes are also very limited. Their fluorescence intensity is at the same level of other BINOL-based probes whose quantum yields are ~ 0.1 or lower. The low quantum yields are required for a fluorescence OFF-ON probe to improve sensitivity. Novel strategy to amplify quantum yields are required for *in vivo* imaging to avoid interferences of organelles' autofluorescence. Incorporating other fluorophores, redesigning the probes with better pull-push effect, and FRET will be potentially useful to solve the quantum yield issue.

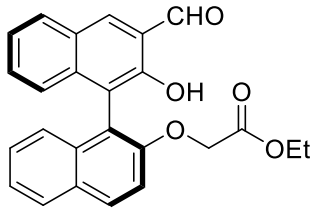

(*S*)-**6.4**

Figure 6. 3 Structures of the probe for Phe

6.2.3 Design of Organic Cores

In a field of experimental science, principles are rare at initial stages. A number of probes are needed to be reviewed for the summary of principles and guidelines for future probes. To address that, the library of micelle probes must be expanded.

One future direction is to synthesize more organic cores and engineer them into new micelle probes. Several Lewis base substituents have been discussed in Chapter 3. Future probe design could take more groups into considerations, such as aliphatic/aromatics, other functional groups, and more Lewis base for stronger chelation with Zn(II) or stronger hydrogen bonding interactions.

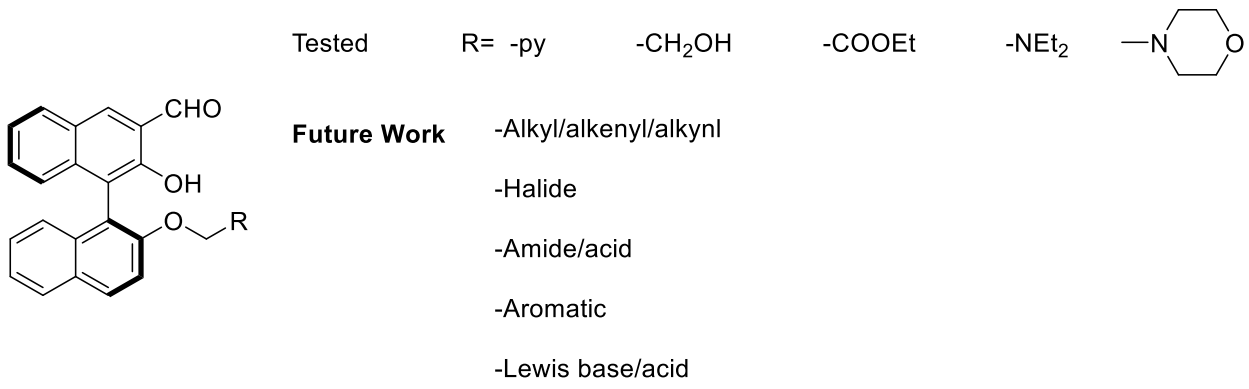

Figure 6. 4 New organic cores with different substituents

Another possible direction was to adjusting the length of aliphatic chain length to optimize fluorescent responses. We proposed the hydroxyl substituents assisted the coordination with Zn(II) complexes. The two naphthyl ring are in approximately perpendicular geometry with each other, and the structure is flexible in several tens of degrees of rotation. Thus, the length of aliphatic chains could have played an important role in the complexations. A detailed study will help isolate the most stable metal complexes, and allow the probing reaction happen at milder conditions.

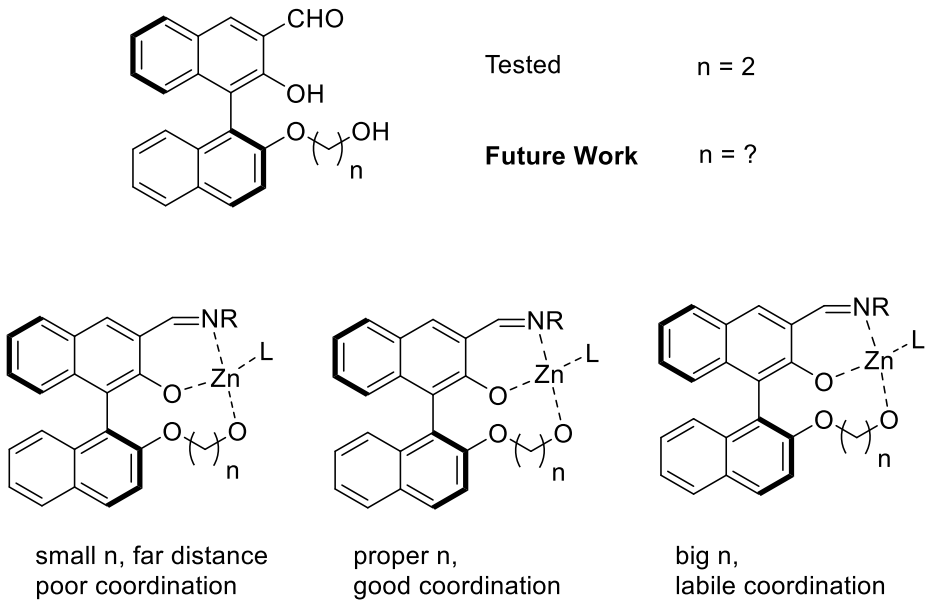

Figure 6. 5 New organic cores with different aliphatic chains

6.2.4 Screening of More Copolymers

As we stated in Chapter 5, copolymers have played a very important role in the selective detection of amino acids. With the same core, changing the copolymers from PEG-PLLA to F68 could switch the selectivity from Lys to Trp. This could be due to differences in hydrophobicity/hydrogen bonding/sizes of the copolymers. Given the limited amount of data, it is still not clear what type of interaction had dominated.

Besides, the reason that the fluorescence responses were only observed in carbonate buffer could be due to that the imine-Zinc complexes were stabilized at high pH condition. If that is true, modifying copolymers with more electron-rich units will help stabilize the product and allow the recognition event happen and milder pH. Poly(acrylic acid) (PAA) has a carboxylic acid in its monomer. The acid will be deprotonated in slightly basic solution and provide numerous basic spots. Utilizing PAA as a block in the copolymers could be an option to study later.

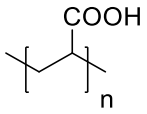

Figure 6. 6 Poly(acrylic acid)

The structures properties of Pluronic triblock copolymers, including Mw, PO unit length, hydrophilic-hydrophobic balance, could govern its hyperthermia sensitizing function in cancer therapy.[2] Given the big family sizes, the screening of the copolymers should provide many useful information.

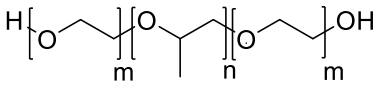

Figure 6. 7 Poloxamers

6.3 Other Applications

6.3.1 Probes on Metal Nanoparticles

Nanoparticles provides advantages such as large surface area, easily accessible surface chemistry, and energy communication enabled by the nano core.[3] We planned to incorporate FeNP's paramagnetic property our enantioselective probe (*S*)-**6.5** by covalently linking them together. This property was believed to be able to facilitate purification process by applying a magnetic field, which attracted the FeNP-sensor out from a mixture for fast fluorescence measurement and substrate tests.

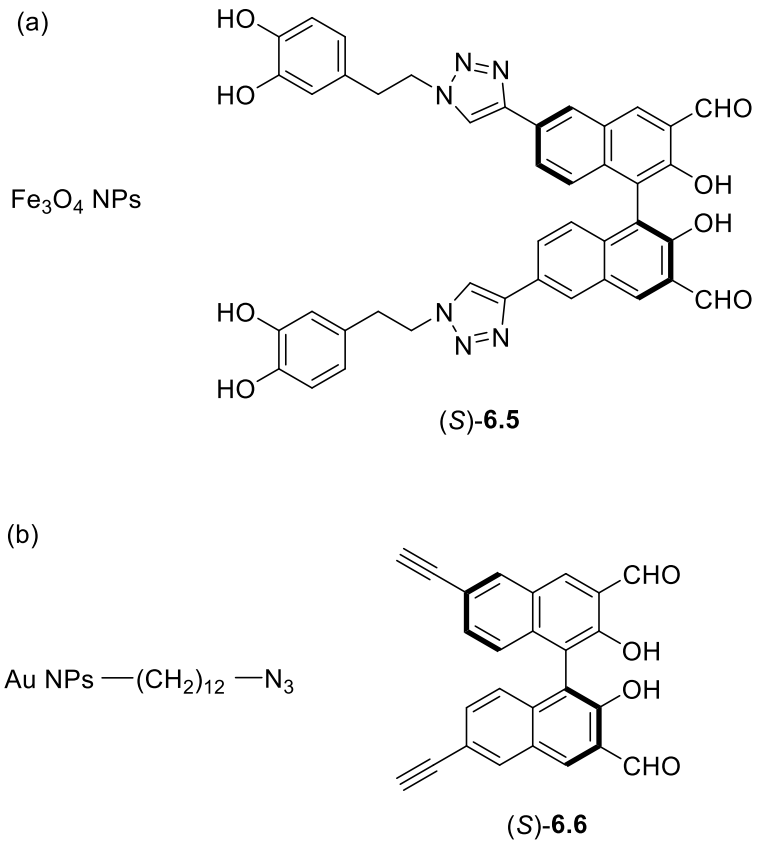

Figure 6. 8 Attempted binding with NPs

1,2-Benzenediol (catechol) has been reported to have strong binding affinity with FeNP.[4] Given that, an enantioselective probe (*S*)-**6.5** that has a catechol substituent (Catechol-Sensor) was synthesized. The binding experiments were performed in both heterogeneous and homogeneous conditions. However, UV-vis spectra did not support that Fe-NP and Catechol-Sensor were successfully bound together.

The gold nanoparticle (AuNP) was considered as an alternative solution, due to its strong binding with sulfur. In the attempt to synthesis a sensor that contains a thiol functionality (HS-Sensor), the sensor polymerized while being concentrated. Then, a thiol linker (HS-N_3) was bound on AuNP first, then a click reaction between Au-S-N_3 and alkyne-containing sensor was conducted to graft the sensor on AuNP. This binding was visualized by rapid color transfer between two solvent phases, and confirmed by UV-vis analysis of distinct Au-S SPR peak.

AuNP-based sensors have been reported to exhibit efficient fluorescence quenching ability.[3] It was assumed that this kind of energy quenching transfer could be avoided by extending the distance between AuNP core and fluorophore. Although the enantioselectivity was remained, the linear chain composed of more than ten carbons did not stop the energy transfer, and the fluorescence intensity was eventually decreased by magnitude.

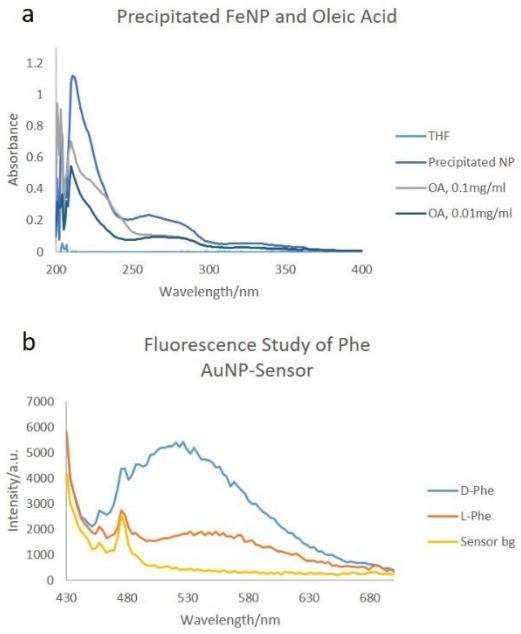

Figure 6. 9 (a) UV-vis spectra of FeNP precipitated from binding experiment and its comparison with Oleic Acid (OA) ligand. (b) Fluorescence Responses for both D- and L-Phenylalanine, detected by AuNP-Sensor.

Another strategy to stop the energy transfer is to coat nanoparticles with a thin layer of silica, as silica provides nanometer long distance, which is much longer than carbon chains.[5] Our collaborators at the Zhang lab studied how the thickness of silica can influence the energy communication. Future development of enantioselective probes on NP platforms are promising.

6.3.2 Probes on Optic Fibers

Optic fibers are versatile platforms. The easily modified surface can be used to link many useful molecules. Recent studies have utilized optic fibers for clinical applications.[6] One of their unique properties is that they avoided the light penetration issue of many fluorescent techniques for *in vivo* study. The excitation light will transport through optic fibers, excite probes at the tip areas, reflect back into the optic fiber, being filtered and detected by spectrometer.

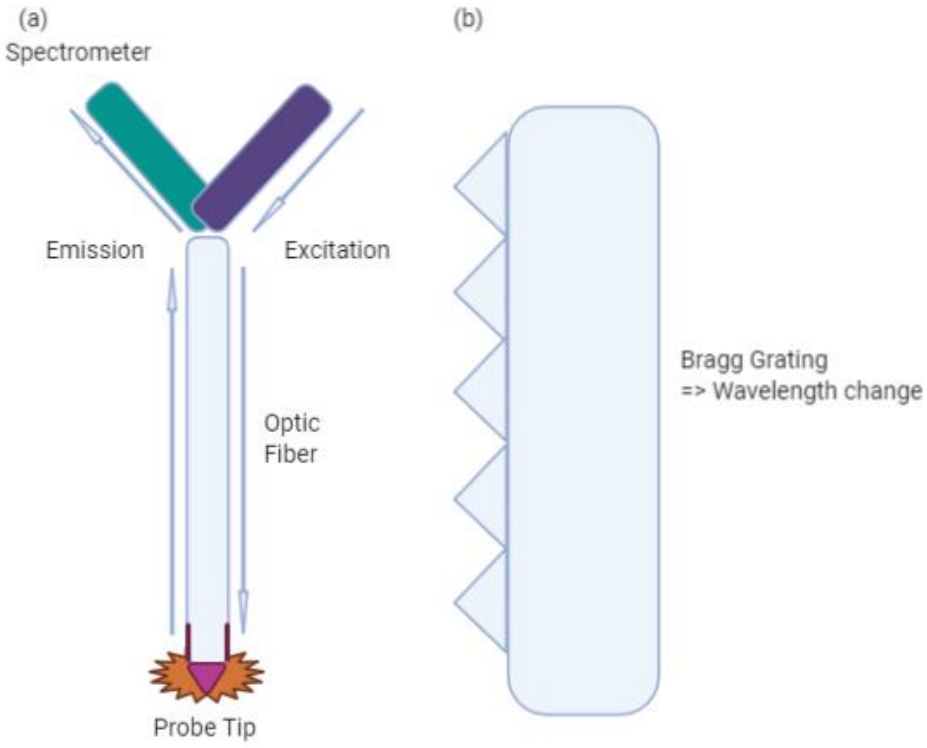

Figure 6. 10 Sketches of (a) an optic fiber probe; and (b) the application of Bragg's law

We have ongoing collaborations with Dr. Li's lab at Chongqing University of Technology for the covalent linking of enantioselective probe onto optic fibers. The linking is expected to go through silica coating and click chemistry with (*S*)-**6.6**. The enantioselective recognition is expected to be achieved through Bragg grating. After interaction with amino acids analytes, the sizes of products will vary because diastereomers were formed. Different sizes will lead to slightly

different radius, which will eventually lead to different wavelength based on the Bragg law. Utilizing the wavelength change for detections, optic fibers is expected to reach extremely low limit detection of nanomolar-scale.

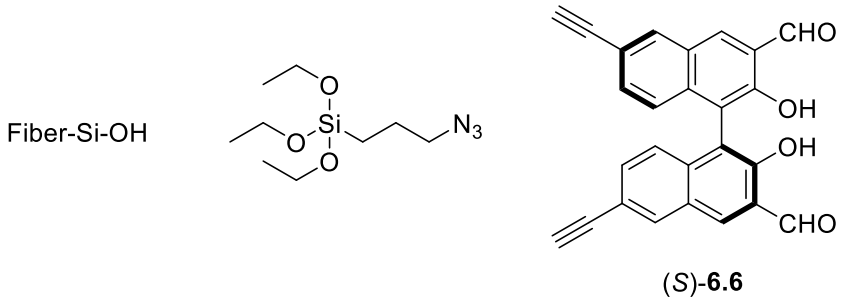

Figure 6. 11 Optic fiber linking materials

6.4 References

(1) Wolosker, H.; Dumin, E.; Balan, L.; Foltyn, V. N. D-Amino Acids in the Brain: D-Serine in Neurotransmission and Neurodegeneration. *FEBS Journal*. **2008**, *275* (14), pp 3514–3526.

(2) Krupka, T. M.; Exner, A. A. Structural Parameters Governing Activity of Pluronic Triblock Copolymers in Hyperthermia Cancer Therapy. *Int J Hyperther*, **2011**, *27* (7), 663-671.

(3) Zhou, W.; Gao, X.; Liu, D.; Chen, X. Gold Nanoparticles for in Vitro Diagnostics. *Chem. Rev.* **2015**, *115*, 19, 10575-10636.

(4) Rogers, H. J. Iron-Binding Catechols and Virulence in Escherichia Coli. *Infect. Immun.* **1973**, *7* (3), 438–444.

(5) Liu, Y.; Peng, S.; Ding, Y.; Rong, C.; Kim, J.; Liu, J. P.; Wang, Z. L.; Sun, S. Synthesis and Characterization of Ferroferriborate (Fe_3BO_5) Nanorods. *Adv. Funct. Mater.* **2009**, *19* (19), 3146–3150.

(6) Mallidi, S.; Anbil, S.; Bulin, A.-L.; Obaid, G.; Ichikawa, M.; Hasan, T. Beyond the Barriers

of Light Penetration: Strategies, Perspectives and Possibilities for Photodynamic Therapy. *Theranostics* **2016**, *6* (13), 2458–2487.